学位論文

Causal hydrodynamic fluctuations and their effects on high-energy nuclear collisions

(相対論的流体揺らぎと
高エネルギー原子核衝突反応への影響)

平成27年7月　博士 (理学) 申請

東京大学大学院理学系研究科
物理学専攻
村瀬　功一

Abstract

The system of quarks and gluons is described by quantum chromodynamics. Under sufficiently high temperature or high density, quarks and gluons are deconfined from hadrons and form a novel state of matter called quark-gluon plasma. It may be found in extreme conditions such as in the early universe and in compact stars. Also, quark-gluon plasma states can be created in experiments of high-energy nuclear collisions. Currently, understanding of the transport properties of the quark-gluon plasma are one of the major challenges. In particular the specific shear viscosity η/s of the quark-gluon plasma from the observed event-by-event fluctuations is actively discussed. The quantitative extraction of the transport properties needs integrated dynamical models with a proper treatment of all the sources of the event-by-event fluctuations. Among them the effects of the thermal fluctuations of hydrodynamics have not yet been studied within the integrated dynamical models so far. In this thesis, we consider the thermal fluctuations of the hydrodynamics, which are called hydrodynamic fluctuations, within second-order causal dissipative hydrodynamics to investigate the effects on the experimental observables of high-energy nuclear collisions.

We first consider the properties of the hydrodynamic fluctuations in the causal dissipative hydrodynamics. In relativistic systems the Navier-Stokes theory has problems of the acausality and instabilities. Therefore second-order causal theories with non-zero relaxation times are needed. We formulate the hydrodynamic fluctuations in the causal theories with non-uniform backgrounds and find an interesting property: The hydrodynamic fluctuations become always colored in the integral form of the constitutive equations while it turns out that they become white in the differential form of the constitutive equations. This property is proved using the fluctuation-dissipation relation, the causality, the relaxation and the retardation of the memory function, and the symmetries and structure of the constitutive equations written by the derivative expansion.

To consider the hydrodynamic fluctuations in numerical calculations, we develop a new conservative scheme of the causal dissipative hydrodynamics in curved coordinates which is robust against the large gradients caused by the fluctuations. In particular, by choosing the representation of the dissipative current fields to be the components in the local rest frame, we construct a scheme with no discretization errors in the transversality constraints of the dissipative currents.

We also consider the singular behavior of the fluctuating hydrodynamics with the hydrodynamic fluctuations. With the hydrodynamic fluctuations the hydrodynamic equations become stochastic partial differential equations which have a singular behavior in the limit of spatial resolution going to zero. We propose the necessity of coarse-graining scales in the framework. The stochastic integrals in the causal dissipative hydrodynamics are also studied.

Finally to investigate the effects of the hydrodynamic fluctuations in high-energy nuclear collisions, we implement the causal fluctuating hydrodynamics in our dynamical model with initial-state models and hadronic cascades, and perform a massive number of event-by-event numerical simulations. First we consider only the hydrodynamic fluctuations as the event-by-event fluctuations to see their qualitative effects. As a result, we find increase of the charged particle multiplicity, which is stronger in high-p_T hadrons. The elliptic flow v_2 is also increased by the fluctuations. Next we consider, in addition to the hydrodynamic fluctuations, the initial-state fluctuations which is considered to be the major part of the event-by-event fluctuations. As a result, we find that the relative increase of the multiplicity is larger in peripheral collisions. Also, the increase of the integrated v_2 by the hydrodynamic fluctuations turns out to be comparable to the decrease by the shear viscosity. Those results show that the hydrodynamic fluctuations are inevitable components in integrated dynamical models of the high-energy nuclear collisions for quantitative analyses of the transport properties of the quark-gluon plasma.

Table of Contents

Chapter 1

Introduction

The purpose of this thesis is to study the role of the thermal fluctuations of hydrodynamics in high-energy nuclear collisions and to obtain quantitative understanding of the properties of the created quark-gluon plasma. In this chapter we explain the basics of quantum chromodynamics that describes the dynamics of quarks and gluons in Section 1.1, and then recent topics of the high-energy nuclear collisions in Section 1.2. The outline of this thesis is given in Section 1.3.

1.1 Quantum chromodynamics and quark-gluon plasma

Quarks and *gluons* are elementary particles constituting the nucleons such as the protons and the neutrons. The dynamics of quarks and gluons is ruled by the strong interaction described by quantum chromodynamics (QCD). QCD is a non-Abelian gauge theory with $SU(3)$ group [1, 2]. The quarks are fermions with a "color" charge. The "color" has three degrees of freedom which are called red, green, and blue on the analogy of the three primary colors of the human visual perception. The gluons are gauge bosons which mediate the force between color charges. The quarks and the gluons can be compared to the electrons and the photons in quantum electrodynamics, respectively. However, unlike the photons the gluons have color charges, and can directly interact with other gluons. This is the characteristic nature of the gauge bosons in a non-Abelian gauge theory.

The quarks have flavor degrees of freedom too. There are six different flavors: Up, down, and strange quarks are the light flavors, and charm, bottom, and top quarks are the heavy flavors. The net quark number, i.e., the difference of the numbers of quarks and antiquarks, of each flavor is conserved under the strong interaction.

Hadrons are the compound particles made of quarks and gluons with color singlet states. The hadrons which consist of three valence quarks, such as the protons and the neutrons, are called *baryons* while the hadrons with a quark and an antiquark, such as pions, are called *mesons*. In the sense of quantum numbers, a proton is composed of two up quarks and one down quark, and a neutron is composed of one up quark and two down quarks.

The net baryon number is conserved in the interactions among the hadrons due to the net quark number conservation. The baryon chemical potential, namely the chemical potential associated with the baryon numbers, determines the net number density of the quarks in equilibrium states. Note that, the net baryon number density is sometimes referred to simply as the density in the present thesis.

One of the important characteristics of QCD is asymptotic freedom [3, 4]. At low temperature and density, the quarks and the gluons are confined in hadrons such as nucleons and pions, and their degrees of freedom do not have a significant effect on the dynamics of the system. However, the coupling constant of QCD becomes smaller at higher energy scales or smaller length scales due to the asymptotic freedom. Therefore at a sufficiently high temperature or a density, it is expected that the quarks and the gluons are deconfined from the hadrons, and the relevant degrees of freedom of the system become quarks and gluons instead of hadrons [5, 6]. This state of the matter consisting of weakly interacting quarks and gluons is named quark-gluon plasma (QGP) [7–9]. On the other hand, a phase where the quarks and the gluons are confined in hadrons is called hadronic phase.

Here let us consider the phase diagram of QCD (See the left panel of Fig. 1.1) [11]. The vertical axis of the phase diagram is the temperature T, and the horizontal axis is the baryon chemical potential μ_B. The hadronic phase are located in the lower left corner while the other region is the QGP in a broad

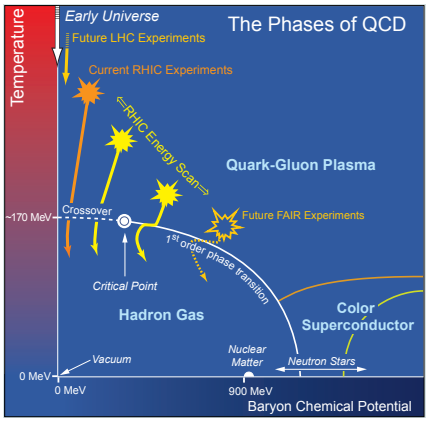

(a) Schematic QCD phase diagram

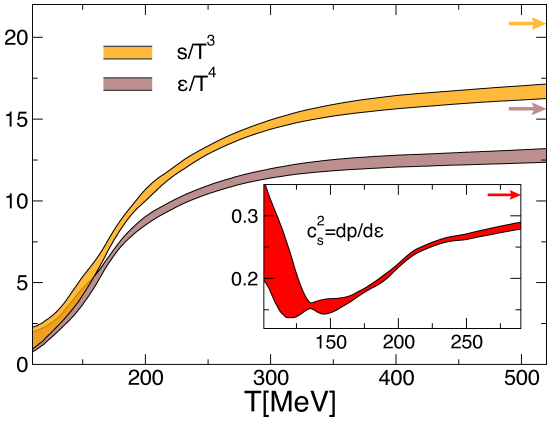

(b) EoS from lattice calculations

Figure 1.1: The left panel shows a schematic QCD phase diagram taken from the 2007 NSAC Long Range Plan [12]. The schematic trajectories of the matter states created in the high-energy nuclear collision experiments are overlaid as yellow and orange lines. The right panel, taken from Ref. [19], shows the entropy density s (yellow), the energy density e (brown), and the speed of sound c_s (red) as functions of temperature T from the lattice QCD simulations. The values indicated by arrows correspond to the Stefan-Boltzmann limit.

sense. On the T axis where the baryon chemical potential vanishes, the phase boundary of the hadronic phase and the QGP phase is known to be a crossover according to the 2+1 flavor lattice QCD calculations with the physical quark masses [13–17]. In the right panel of Fig. 1.1, the entropy density and the energy density are shown as a function of temperature which smoothly connect the low temperature region (hadronic phase) and the high temperature region (QGP phase). The latest calculations indicate that the pseudocritical temperature is around $T_c \sim 150$ MeV [18, 19]. The finite chemical potential region, where $\mu_B \neq 0$, is difficult to study using the lattice QCD calculations due to the sign problem [10, 11]. Results of various effective models suggest the existence of a critical point at a finite μ_B where the crossover changes to the first order phase transition [20–24]. The color superconductivity at high density region (large μ_B and $T \sim 0$) is also predicted [25–28].

Those QCD matters may be found in extreme conditions such as in the early universe [6] and in the compact stars [5]. In the early universe with the age of about ten micro seconds, the temperature of the universe is sufficiently large such that the universe was filled by QGP with a small μ_B. Such a QGP in the early universe is located on the top left corner of the phase diagram in Fig. 1.1 (left). While, QGP phase with color superconductivity is likely realized inside the compact stars such as neutron stars. These states are located at the lower right corner of the phase diagram near the baryon chemical potential axis. High temperature or high density states can be created artificially by the high-energy nuclear collision experiments. The QGP created in these experiments is cooled down to become the hadronic state. Considered evolution of the temperature and the density at each experiment is shown as trajectories in the phase diagram in Fig. 1.1 (left).

1.2 High-energy nuclear collisions

The high-energy nuclear collision experiments are currently operated mainly in Relativistic Heavy Ion Collider (RHIC) of Brookhaven National Laboratory (BNL) in the United States, and Large Hadron Collider (LHC) at European Laboratory for Particle Physics (CERN) (Fig. 1.2). In the experiments, two nuclei accelerated to almost the speed of light are collided with each other to create a fireball with extremely high temperature above 200 MeV. Such collision processes to reproduce the state of matter in the early universe are sometimes called “little bangs” as contrasted with the Big Bang.

The search for QGP with the high-energy nuclear collisions was initiated in Alternating Gradient Synchrotron (AGS) in BNL and Super Proton Synchrotron (SPS) in CERN. In the experiments at the top SPS energy in late 1990s, and at RHIC in early 2000s, various data suggested the creation of a new state of the matter in the experiments. One of the important signatures is the collective flows

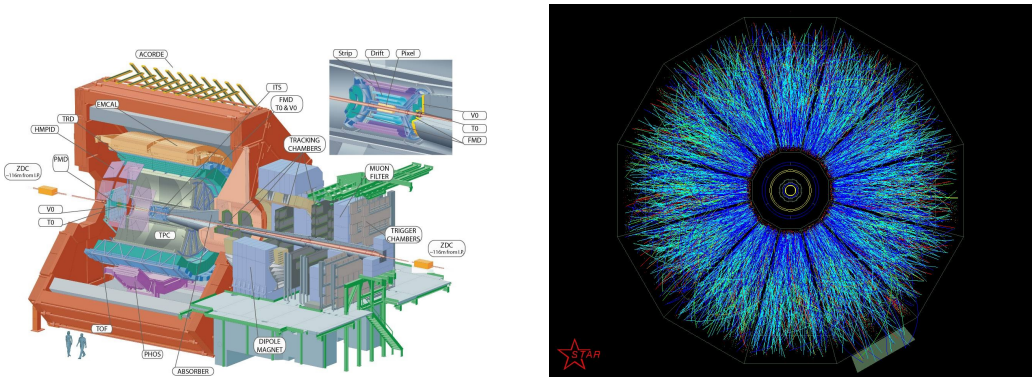

Figure 1.2: The left picture, taken from the paper [29], shows a detector design of the ALICE group at LHC. The right picture is the event display in the transverse plane of an event in STAR experiments at RHIC, taken from Ref. [30].

such as the radial flow and the elliptic flow [31, 32]. In particular large elliptic flows predicted by ideal hydrodynamic models [33–43] are observed at RHIC [44–50]. In the non-central high-energy nuclear collisions where the impact parameters are non-zero, the overlapping area of the nuclei has an almond shape. As the hydrodynamic flow is created by the pressure gradients, larger flow is created in the direction of the shorter axis of the almond shape than in the direction of the longer axis, which results in anisotropy of the final hadron momenta called elliptic flow v_2. Since the hydrodynamics is based on the local thermalization of the created matter, the success of the ideal hydrodynamics indicates that the matter reaches local equilibrium states in a sufficiently small time, and has small viscosity. This leads to the idea of strongly-coupled QGP (sQGP) [51–55]. Other signatures of the QGP include the contribution of thermalized matter to the direct photon spectra [56–61] and the invariant mass spectra of dielectron pairs [56, 58, 62, 63], J/ψ suppression [64–68], suppression of high-p_T hadrons [69–71], jet modification [72–77], and strangeness enhancement [78–82].

The ideal hydrodynamics means no dissipation such as viscosity and diffusion. However, any physical matter with non-zero length scale of the microscopic dynamics should have non-zero viscosity. The lower bound of the specific viscosity coefficient of the matter reads $\eta/s = 1/4\pi$ [83], where η and s are the shear viscosity coefficient and the entropy, due to the uncertainty relations of the quantum theory. This is called the Kovtun-Son-Starinets (KSS) bound [83]. One of the targets of this field is the quantitative understanding of the transport coefficients such as the bulk viscosity coefficient, and the relaxation times of the dissipative currents as well as the specific shear viscosity coefficient. In such studies the most important observables are the flow harmonics v_n which are explained by *event-by-event fluctuations* of the collisions.

The importance of the event-by-event fluctuations has been widely recognized in the interpretation of the elliptic flows from the Cu+Cu collisions [84]. In the Cu+Cu collisions, the measured elliptic flows are larger than expected from results of Au+Au collisions. Also non-zero elliptic flow is observed even in the most central collisions. While in the non-central collisions the almond shape of the created matter results in the momentum anisotropy through the hydrodynamic response, in the most central collisions the shape of the created matter has no geometric anisotropy, which is not compatible with the non-zero momentum anisotropy measured in the experiments. It turned out that this can be explained by taking into account the event-by-event fluctuations of the nucleon positions participating in the created matter. Even in the most central collisions, the shape of the created matter is not a true disk because it has fluctuations from event to event due to the finite number of the participant nucleons in the collided nuclei. The larger elliptic flow in Cu+Cu collisions and non-zero elliptic flow in the most central collisions can be well described by random elliptic components of the event-by-event initial shape of the matter.

More systematic studies of the event-by-event flow fluctuations are made with the higher harmonic flows v_n ($n \geq 3$) [85] as well as with the elliptic flow. The systematic measurements of the higher harmonics v_n are started around 2010 [88–91]. On the theoretical side, many groups [93, 121–127, 129–132, 138–157] have been performed event-by-event hydrodynamic simulations to investigate the relation between the experimental flow harmonics and the initial-state fluctuations.

A conventional source of the initial-state fluctuations is the nucleon distribution in the transverse

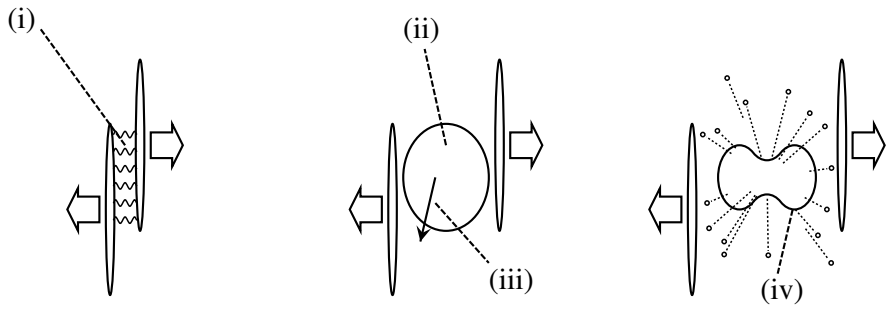

Figure 1.3: A schematic figure of the spacetime evolution of the matter is shown with the sources of the event-by-event fluctuations. The initial state of the collisions is two nuclei which is Lorentz-contracted due to the acceleration. The initial state of the created matter is the color electromagnetic fields in the longitudinal direction described by the color-glass condensate picture (the left figure). After the early thermalization, the hydrodynamic expansion of the created matter follows (the center figure). There are hard components passing through the medium such as jets. Finally, as the degrees of freedom becomes hadrons and then the mean free path becomes longer, the system is described with weakly interacting gas of the hadrons (the right figure). The symbols (i)-(iv) indicate the positions of sources of the event-by-event fluctuations. The details of each source is described in the text.

plane, and is investigated well using the Monte-Carlo version of the Glauber model and the color-glass condensate models to be explained in Chapter 2. However there are still other types of the sources of the event-by-event fluctuations during the spacetime evolution of the matter (See Fig. 1.3). To quantitatively determine the transport coefficients, we need to consider the effect of each source of the fluctuations quantitatively. Such sources of the fluctuations are listed below [92]. The index of each item (i)-(iv) corresponds to the labels in Fig. 1.3.

(i) Initial-state fluctuations of the gluon fields: The initial-state fluctuations include not only the fluctuations of the nucleon positions. Recently the quantum fluctuations of the gluon numbers with the negative binomial distribution are also studied actively. The IP-Glasma model [93,94] describes the initial stage classical Yang-Mills dynamics adopting the impact parameter dipole saturation (IP-Sat) model [95, 96] with the negative binomial distribution for the initial condition [97]. This model [94] well describes the experimental event-by-event distribution of the flow harmonics from ATLAS [98–100].

(ii) Thermal fluctuations of the hydrodynamics [92]: The shear viscosity turned out to have considerable effects on the observables such as the flow harmonics. According to the fluctuation-dissipation theorem, there should be thermal fluctuations if there is dissipation. The thermal fluctuations of hydrodynamics are called *hydrodynamic fluctuations*. If the local system is large enough that the thermodynamic limit can be justified, the thermal fluctuations can be neglected. However, in high-energy nuclear collisions, the microscopic length scale of the hydrodynamics is around $\tau \sim 0.1 - 1$ fm which is comparable to the size of the system itself around 1-10 fm. Also the effects of the critical fluctuations near the expected critical point in the QCD phase diagram are important phenomena to find a critical point and understand the phase diagram.

(iii) Disturbance by hard components: The hydrodynamic flow can be affected by the hard components, namely the large-momentum particles such as jets and mini-jets, which are not considered to be a part of the local equilibrium states [101].

(iv) Fluctuations from hadronization/freezeout process: The non-equilibrium dynamics near the crossover transition from QGP phase to hadronic phase is not considered in existing dynamical models. Those non-trivial dynamics can generated additional correlations to the final hadron distribution.

Among the above fluctuation sources, the effects of (ii) the hydrodynamic fluctuations are not yet studied in the full dynamical models of the high-energy nuclear collisions, and only the effects of the dissipation, such as the shear viscosity and the bulk viscosity, have been studied. The main purpose

of this thesis is to investigate the effect of the hydrodynamic fluctuations in the high-energy nuclear collisions. In particular we formulate the relativistic fluctuating hydrodynamics, which is the dissipative hydrodynamics with the hydrodynamic fluctuations, within the non-linear equations of the causal dissipative hydrodynamics. Then, to see the effects of the causal hydrodynamic fluctuations on the high-energy nuclear collisions, we implement the fluctuating hydrodynamics to perform event-by-event dynamical calculations.

1.3 Outline

This thesis is organized as in Fig. 1.4. First we see basic observables and current understanding of the collective dynamics of the high-energy nuclear collisions in Chapter 2, and set the languages of the relativistic hydrodynamics used later in Chapter 3. Next we consider the properties of the hydrodynamic fluctuations in the non-linear equations of the causal dissipative hydrodynamics in Chapter 4. To perform the numerical simulations with the hydrodynamic fluctuations we develop a new robust numerical scheme for the causal dissipative hydrodynamics in Chapter 5. Then we consider an apparent singularity of the stochastic partial differential equations which describe the hydrodynamics with the hydrodynamic fluctuations in Chapter 6. In Chapter 7 we implement the hydrodynamic fluctuations in our integrated dynamical model and perform massive number of the event-by-event dynamical simulations including the initialization models with the initial-state fluctuations, causal dissipative hydrodynamics with the hydrodynamic fluctuations, and hadronic cascades for the kinetic evolution of the hadron gas. Finally we analyze the obtained hadron distributions to investigate the effects of the hydrodynamic fluctuations.

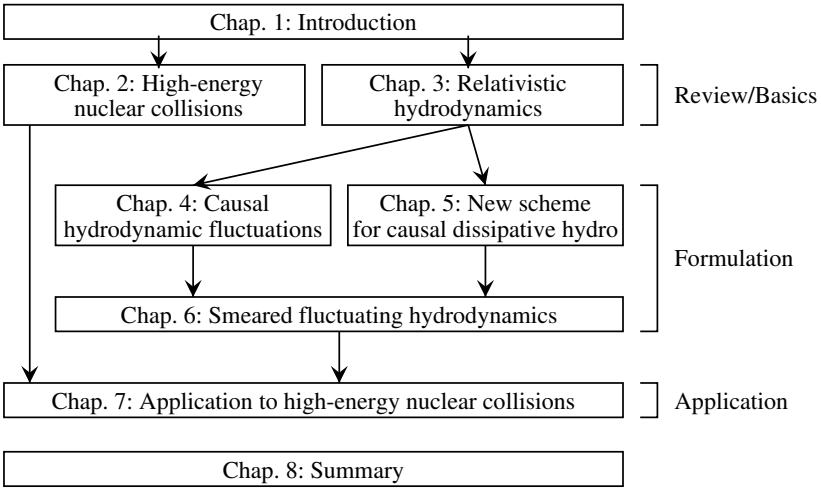

Figure 1.4: Outline of this thesis.

Chapter 2

High-energy nuclear collisions

Here we discuss the collective dynamics of the created matter in high-energy nuclear collisions by introducing the experimental observables in Section 2.1, and the current dynamical description of the collision process in Section 2.2. Finally the studies of the hydrodynamic fluctuations in the high-energy nuclear collisions are introduced in Section 2.3. Throughout this thesis, we adopt the natural unit such that $\hbar = c = 1$, and the Minkowski metric to be $g_{\mu\nu} = \mathrm{diag}(+,-,-,-)$. Also, the Einstein convension is applied to the repeated Lorentz indices. The symmetric part, and the antisymmetric part of a rank-2 tensor $A^{\mu\nu}$ are defined to be $A^{(\mu\nu)} \equiv (A^{\mu\nu} + A^{\nu\mu})/2$, and $A^{[\mu\nu]} \equiv (A^{\mu\nu} - A^{\nu\mu})/2$, respectively.

There are several experimental groups providing data of high-energy nuclear collisions at RHIC and LHC: STAR, PHENIX, PHOBOS, and BRAHMS from RHIC, and ALICE, ATLAS, and CMS from LHC. Also the experiments with various collision systems are operated in the two colliders. The collisions of two heavy ions (A+A) are the standard collisions to create the QGP. They include gold-gold collisions (Au+Au) and copper-copper collisions (Cu+Cu) at RHIC, and lead-lead collisions (Pb+Pb) at LHC. To further study the response to the initial-state geometry, uranium-uranium collisions (U+U) and copper-gold collisions (Cu+Au) have been operated at RHIC. The uranium nucleus has an ellipsoidal shape like a rugby ball, so that the initial states have more variety depending on the orientations of the colliding uranium nuclei. The Cu+Au collisions are asymmetric collisions where the observables, which vanish in symmetric collisions due to the symmetry, are measured. Recently results consistent with hydrodynamic models are obtained in the collisions of a heavy ion and a light nucleus. On the other hand, the results may also be explained within initial glasma pictures, i.e., pictures of strong longitudinal color electric/magnetic fields. The collective dynamics of such systems is one of the active topics of the recent few years. Such systems include proton-lead collisions (p+Pb) at LHC, and deuteron-gold collisions (d+Au). The run of helium-gold collisions (^{3}He+Au), expecting triangular components of the observables, are also performed in June 2014 at RHIC. In addition, the possibility of collectivity in high multiplicity events of p+p at LHC is also discussed.

2.1 Observables

In experiments, the observed quantities are basically related to spectra, or momentum distributions, of final particles emitted from the created matter. Among the final particles, hadrons carry important information on the collective dynamics of the matter. The hadron distributions reflect the final state of the thermalized matter since they emerge after the created hot matter is cooled down. This means that they have information on the final profile the collective flow induced in the created matter. On the other hand, photons and leptons, which are called electromagnetic probes, provide us information on the inside of the matter since they can pass through the matter as they weakly interact with the medium. Although there are still other important observables related to jets and the heavy flavors, we here focus on the distribution of light hadrons which is related to the collective dynamics. The distribution includes the number of the hadrons, the momentum, and the species of each hadron. Note that what actually be measured in experiments are rather indirect quantities such as the charge, the energy, the detected position, etc. of each track of a hadron in the detector. From this set of data, we reconstruct distributions of the hadrons and perform statistical analyses to obtain useful observables associated with the physics of the collision process.

The number of the hadrons measured by the detectors is called a multiplicity. In particular the

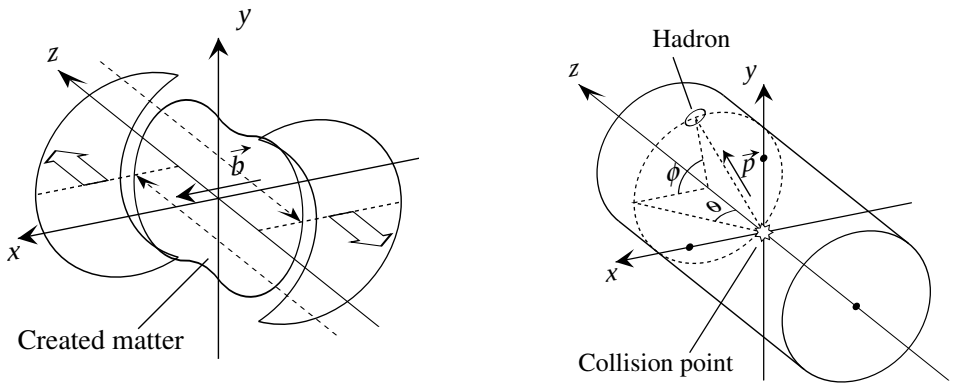

Figure 2.1: The left panel shows a schematic picture of the collision geometry after a collision occurred at a finite impact parameter vector $\vec{b}$. The two disks represent the Lorentz-contracted collided nuclei. The almond-shaped overlapping area turns into a hot matter, and the remaining crescent parts fly away to the beam directions. The right panel shows the angles of the observed hadron momentum. The polar angle θ is the angle of the momentum with respect to the beam axis, which is related to the pseudorapidity as $\eta_p = -\ln\tan(\theta/2)$. The azimuthal angle ϕ is the angle of the transverse momentum with respect to the x-z plane. Those angles are measured by the position in detectors where the hadron is detected.

charged particle multiplicity, namely the multiplicity of the charged hadrons is often used. To consider the momenta of hadrons we here introduce a particular coordinate system (see the right panel of Fig. 2.1). The line containing the impact parameter vector is defined to be the x-axis. The beam axis passing through the midpoint of the impact parameter vector is defined to be the z-axis. The x-z plane is called a reaction plane. The remaining axis normal to the reaction plane is the y-axis, and the x-y plane is called a transverse plane. The direction of the z-axis is called longitudinal direction. The momentum of each hadron can be expressed in this coordinates as $p^\mu = (E, p^x, p^y, p^z)$ where $E^2 = m_i^2 + \sum_{a=1}^{3}(p^a)^2$ with m_i being the mass of the hadron i. The momentum is usefully expressed by another set of the variables (p_T, y, ϕ):

$$E = m_T \cosh y, \tag{2.1}$$
$$p^z = m_T \sinh y, \tag{2.2}$$
$$p^x = p_T \cos\phi, \tag{2.3}$$
$$p^y = p_T \sin\phi, \tag{2.4}$$

where $p_T^2 \equiv (p^x)^2 + (p^y)^2$ is the transverse momentum, and $m_T^2 \equiv m_i^2 + p_T^2$ is the transverse mass. The symbol y, not to be confused with the coordinate y defined as $y = \tanh^{-1}(p^z/E) = (1/2)\ln[(E + p^z)/(E - p^z)]$. The symbol ϕ denotes the azimuthal angle measured with respect to the reaction plane. Those variables are essential to understand the collective dynamics of the system expanding in the z direction. However the measurement of m_T and y needs particle identification to determine the mass m_i. Instead yet another set of the variables (p_T, η_p, ϕ) which does not require the particle identification is often used:

$$|\boldsymbol{p}| = p_T \cosh\eta_p, \tag{2.5}$$
$$p^z = p_T \sinh\eta_p, \tag{2.6}$$

where $|\boldsymbol{p}|^2 = \sum_{a=1}^{3}(p^a)^2$. The new variable η_p, called pseudorapidity, can be obtained as $\eta_p = \tanh^{-1}(p^z/|\boldsymbol{p}|) = (1/2)\ln[(|\boldsymbol{p}| + p^z)/(|\boldsymbol{p}| - p^z)]$. While the symbol η is usually used for the pseudorapidity in experiments, we use the symbol η_p in this thesis to distinguish it from the symbol of the shear viscosity coefficient η. The pseudorapidity η_p can be simply related to the polar angle θ, which is the angle between the beam axis and the hadron momentum, by the relation $\tanh\eta_p = p^z/|\boldsymbol{p}| = \cos\theta$. See the right panel of Fig. 2.1 for the polar angle θ and the azimuthal angle ϕ. The rapidities y and η_p, and the polar angle θ also have the relation through p^z:

$$m_T \sinh y = p_T \sinh\eta_p = |\boldsymbol{p}|\cos\theta = p^z. \tag{2.7}$$

The Lorentz-invariant volume element in the momentum space is transformed as $d^3p/E = p_T dp_T d\phi dy = (p/E)p_T dp_T d\phi d\eta_p$, so that the invariant momentum spectra of the hadrons can be written as

$$E\frac{dN(\boldsymbol{p})}{d^3p} = \frac{dN(y, p_T, \phi)}{p_T dp_T d\phi dy} = \frac{E}{p}\frac{dN(\eta_p, p_T, \phi)}{p_T dp_T d\phi d\eta_p}. \tag{2.8}$$

2.1.1 Centrality

In the statistical analyses we first classify the events using the observables which are related to the collision geometry, and then consider averages of various quantities in each class. The most important geometry in the nucleus-nucleus collisions, which determines a global structure of the matter, is the impact parameter b of the collision. At the most central collision where impact parameter vanishes, almost all the nucleons in both nuclei participate in the created hot matter. On the other hand, in non-central collisions, only the nucleons in the overlapping area, with an almond shape in the transverse plane, participate in the created matter. The other nucleons pass through to the forward directions. The former nucleons are called participants or wounded nucleons, and the latter spectators. The impact parameter cannot be directly measured in the experiments, yet they have a strong correlation with the observables of the multiplicity of final hadrons $N_{\rm ch}$ or the total transverse energy E_T. The smaller the impact parameter is, the larger the multiplicity and the total energy become, so that they can be used as measures of the collision geometry associated with the impact parameter. The experimental observables used to determine centralities are summarized in Appendix A.1.

The centrality of an event is indicated by the percentage of more central events than that event in the whole events. The most central collision is indicated as 0%, and the most peripheral collision 100%. The centrality percentile is roughly proportional to the disk area of the smaller impact parameters, (centrality) $\sim b^2/b_{\rm max}^2 \propto \pi b^2$, except for the peripheral collisions where $b \gtrsim b_{\rm max}$. This is because the cross section is proportional to the transverse area in the space of the impact parameter vectors. The centrality is also associated with the number of the participant nucleons $N_{\rm part}$ through the Glauber Monte Carlo simulations [110–112], with the largest $N_{\rm part}$ corresponding to the most central collision.

2.1.2 Multiplicities and p_T spectra

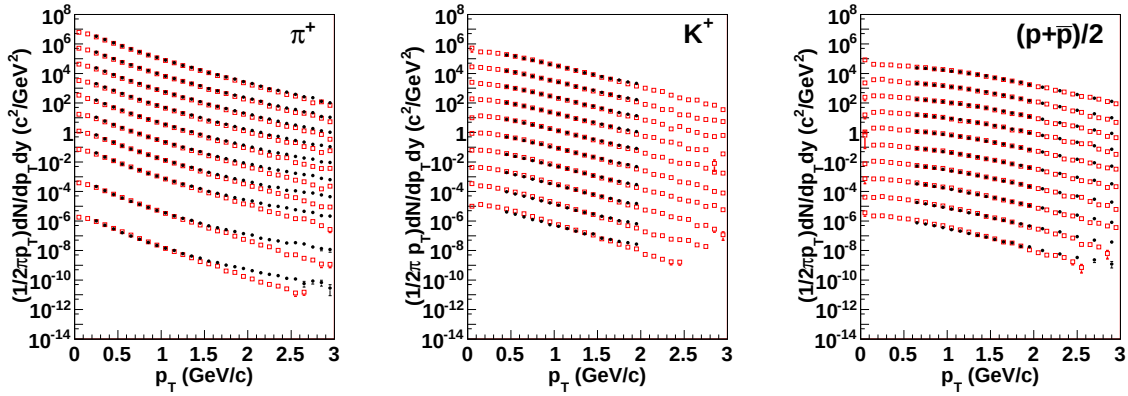

Figure 2.2: The identified hadron p_T spectra taken from Ref. [113] are shown for charged pions, charged kaons, and protons and antiprotons. The black filled circle shows the PHENIX data of Au+Au collisions of $\sqrt{s_{\rm NN}} = 200$ GeV [114]. The red open circles shows a results of model calculations with a color-glass condensate initial model combined with ideal hydrodynamics and hadronic cascades [113]. Each line corresponds to the centrality class 0-5, 5-10, 15-20, 20-30, 30-40, 40-50, 50-60, 60-70, and 70-80% from top to bottom. Each line is multiplied by 10^n with $n = 4, 3, 2, \ldots, -5$ for kaons and protons, and $n = 4, 3, 2, \ldots, -3$, -5 and -7 for pions.

The number of hadrons and its transverse-momentum distribution are also important observables. The charged particle multiplicity, whose main components are charged pions, charged kaons, protons, and anti-protons, can be used to estimate the total entropy produced in the whole collision processes.

The major part of the entropy is created in the initial stage since the entropy is not changed so much during the hydrodynamic evolution because of small viscosity. Therefore the entropy can be used to constrain the initial models of the entropy distribution. In particular the centrality dependence of the charged particle multiplicity, and its rapidity distribution are important observables for the constraints.

The p_T spectra of the identified hadrons are the transverse momentum distributions of each hadron species. In Fig. 2.2, examples of the spectra in Au+Au collisions are shown. The vertical axis is the invariant momentum distribution. The shape of each line can be explained by fitting a thermal distribution function $\sim \exp(-\sqrt{m_i^2 + p_T^2}/T_{\rm eff})$ with effective temperature $T_{\rm eff}$ being an inverse slope parameter. In high p_T region and peripheral collisions, the experimental yield of hadrons is larger than that in the hydrodynamic model since, in general, high p_T components of the system is not fully thermalized.

2.1.3 Azimuthal anisotropy

In the study of the collective dynamics of the high-energy nuclear collisions, the most important observables are called flow harmonics, which represent the azimuthal anisotropy of the momentum distribution of created hadrons. The flow harmonics v_n together with the event planes angles Ψ_n are defined as the Fourier coefficients of the azimuthal distribution of the observed hadron momenta $dN'(\phi)/d\phi$ [87, 89]:

$$\frac{dN'}{d\eta_p} = \frac{N'}{2\pi}\left[1 + 2\sum_{n=1}^{\infty} v_n \cos n(\phi - \Psi_n)\right], \tag{2.9}$$

where $N' = \int d\phi (dN'/d\phi)$. The symbol N' is the considered distribution of the hadrons with specific transverse-momentum and rapidity ranges, and particle species. The coefficients of the momentum anisotropy, v_n and Ψ_n, reflect the flow created in hydrodynamic evolutions. If the particles with isotropic momenta are created at the initial stage at each position in the transverse plane, and they do not interact with each other at all, the resulting azimuthal distribution would be isotropic and the flow harmonics would vanish. The non-zero value of the flow harmonics implies that collective flow is created by the interactions in the system.

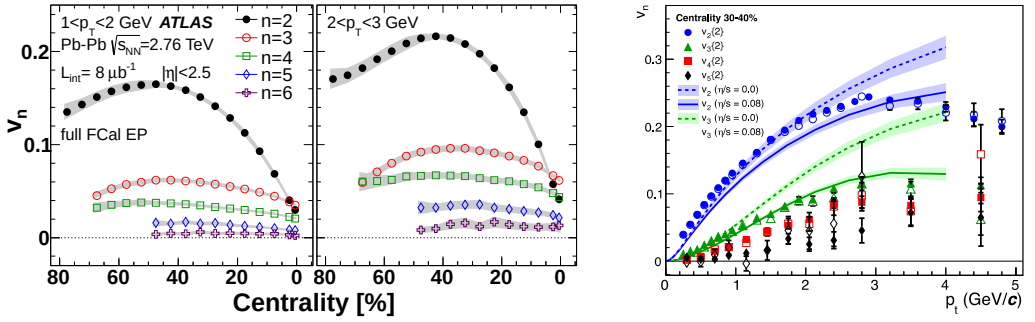

(a) Centrality dependence of integrated flow harmonics

(b) p_T-differential flow harmonics

Figure 2.3: In the figure (a) the centrality dependence of the higher harmonics of Pb+Pb collisions at $\sqrt{s_{\rm NN}} = 2.76$ TeV from ATLAS taken from Ref. [89] is shown. The event-plane method with subevents measured in FCal is used. The horizontal axis is the centrality where the right end corresponds to the most central collisions. The figure (b) taken from Ref. [88] shows p_T-differential v_n in non-central collisions 30-40%. The two-particle cumulant method is used to measure the harmonics. The points are the experimental data, and the lines indicate the results of hydrodynamic model calculations [115] with two different settings of shear viscosity η/s. The initial conditions for the hydrodynamic calculations are generated with the Glauber model.

The coefficients v_1, v_2, and v_3 are called directed flow, elliptic flow [31], and triangular flow [86], respectively. Finite v_1 means the hadrons are emitted in one direction. It is generally very small since the total transverse momentum of the system vanishes. The elliptic flow v_2 is the most important harmonics. It becomes large in non-central collisions because of the geometrical origin of the collided

nuclei. Since flow is generally created in the direction of the pressure gradient, the initial almond shape of the matter generates larger flow in the direction of the x-axis than in that of the y-axis. This results in quadruple azimuthal distributions of hadrons measured by v_2. The harmonics with the order $n \geq 3$ are called higher harmonics, and contain information on the event-by-event fluctuations of the collective dynamics. The higher harmonics of $n \leq 6$ are systematically measured in experiments. In Fig. 2.3 examples of the measured higher harmonics are shown. The centrality dependence is shown in the left panel. The flow harmonics v_n have smaller values with larger n. The elliptic flow v_2 has a larger values in non-central collisions because of the collision geometry. The higher harmonics v_n with $n \geq 3$ has less centrality dependence. In the right panel of Fig. 2.3, the p_T-differential v_n are shown. The flow harmonics v_n generally vanish at $p_T = 0$ because of the continuity of the thermal momentum distribution. The dashed line and the solid line correspond to the ideal hydrodynamics and the viscous hydrodynamics. Since the viscous hydrodynamics induces smaller radial velocity, the v_n becomes smaller with viscosity. With the non-zero shear viscosity near the lower bound $1/4\pi \sim 0.08$, the theoretical model produces the results close to the data. Note that the actual value of the viscosity depends on models of the hydrodynamic initial conditions, and the other sources of the event-by-event fluctuations including the hydrodynamic fluctuations.

In an actual event, the number of the observed hadrons is finite, so that the azimuthal distribution function $dN^{\rm raw}/d\phi$ is not smooth. Such event-by-event distribution contains the effect due to the finite number of the hadrons, which is a part of so-called non-flow effects. To focus on the physics of the collective dynamics, such a distribution contaminated by the non-flow effects is not useful. Instead we consider smooth azimuthal distribution $dN/d\phi$ defined by averaging the distribution over a specific set of "similar" events. For example, if the set of events with a fixed impact parameter is considered, the azimuthal distribution at midrapidity becomes

$$\frac{dN'}{d\eta_p} = \frac{N'}{2\pi}\left[1 + 2\sum_{k=1}^{\infty} v_{2k}\{\mathrm{RP}\}\cos 2k\phi\right], \tag{2.10}$$

where the origin $\phi = 0$ is the direction of the impact parameter vector. The flow harmonics in this definition is denoted by $v_{2k}\{\mathrm{RP}\}$. The odd orders of the flow harmonics $v_{2k+1}\{\mathrm{RP}\}$, and the event plane angles Ψ_n vanish due to the symmetry of the set of the events. However, this kind of azimuthal distribution cannot be measured in the experiments since impact parameter vectors defining the set of "similar" events cannot be measured.

In experiments, various methods to extract flow harmonics have been developed. The method of the harmonics is usually expressed in braces as $v_n\{\dots\}$. The major classes of the flow methods are the multi-particle cumulant methods and their derivatives: $v_n\{2\}, v_n\{4\}, \dots, v_n\{2m\}, v_n\{\mathrm{LYZ}\}$, and the event-plane methods: $v_n\{\mathrm{EP}\}, v_n\{\eta\text{-sub}\}, v_n\{\mathrm{SP}\}$, etc. The flow harmonics obtained in these methods are strongly related to the event-by-event fluctuations unlike the ideal ones in Eq. 2.10. First let us consider the event-by-event smooth azimuthal distributions by defining the ensemble of the "similar" events to be the set of events which share the same hydrodynamic initial conditions and the later evolution. This means that the single hydrodynamic event in terms of the fields of macroscopic variables corresponds to an ensemble of many microscopic states. Then the azimuthal distributions becomes a smooth probability density. In this way the event-by-event flow harmonics and angles, v_n and Ψ_n, can be defined for each hydrodynamic event using the Fourier decomposition 2.9. The experimentally obtained flow harmonics can be understood as the statistical moments of such event-by-event flow harmonics under ideal conditions. For example, the flow harmonics of the two particle cumulant method $v_n\{2\}$ can be understood as

$$v_n\{2\}^2 \sim \langle v_n^2 \rangle = \langle v_n \rangle^2 + \sigma_n^2, \tag{2.11}$$

where $\langle \cdots \rangle$ denotes the event average. The flow fluctuation is defined as $\sigma_n^2 = \langle (v_n - \langle v_n \rangle)^2 \rangle$. Similarly, the four-particle cumulant method $v_n\{4\}$ has the following relation when the flow fluctuation is sufficiently smaller than the flow itself, i.e., $\sigma_n^2 \ll \langle v_n \rangle^2$:

$$v_n\{4\}^2 \sim \langle v_n \rangle^2 - \sigma_n^2. \tag{2.12}$$

The flow harmonics with event-plane method $v_n\{\mathrm{EP}\}$ can be parametrized with α, $(1 < \alpha < 2)$, as

$$v_n\{\mathrm{EP}\} = \sqrt[\alpha]{\langle v_n^\alpha \rangle}. \tag{2.13}$$

If the resolutions of the event-plane angles Ψ_n are good enough, α reaches unity. Also, the two-particle moments with different p_T bins or different species, such as $\langle v_n(p_T^{\rm a})v_n(p_T^{\rm b})\rangle$, can also be measured. The event-plane correlations, such as $\langle\cos[n(\Psi_n-\Psi_m)]\rangle$, also contain abundant information on the initial-state models. Those various methods associated with the moments of the flow coefficients reflect some aspects of the original distribution of the coefficients. Instead of obtaining the moments, the event-by-event distribution of the flow coefficients can be reconstructed from the Fourier coefficients q_n with the finite number of particles using the recently developed unfolding technique by ATLAS [98–100].

2.2 Dynamical description of collision processes

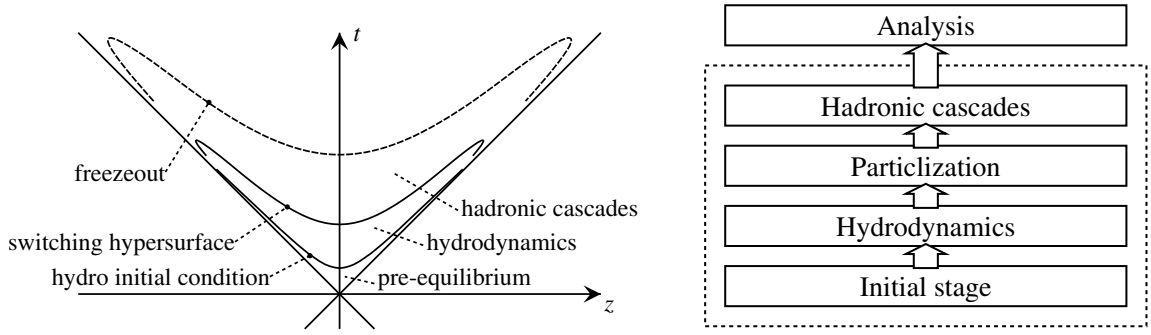

(a) The states of matter under the spacetime evolution

(b) Integrated theoretical framework to describe the whole process

Figure 2.4: In the left panel, a schematic spacetime evolution of the matter is shown. The horizontal axis, and the vertical axis are the longitudinal space coordinates z, and time t, respectively. The right panel shows a typical framework to describe the whole process of the collisions. It consists of several submodels of the initial stage, relativistic hydrodynamics, particlization, and hadronic cascades as well as the statistical analysis framework of the observables. The event-by-event calculations are performed using the models inside the dotted square, and analyses are applied after the event-by-event calculations.

There are several groups developing dynamical models to describe the whole processes of the high-energy nuclear collisions [35,36,41,113,116–137]. Along the process of the high-energy nuclear collisions, the state of the matter drastically changes from the initial color-glass condensate to the final non-interacting hadrons through the locally thermalized hydrodynamic stage and the hadronic gas stage. To describe such an evolution of the matter with quite different stages, modern dynamical models combine initial-state models, hydrodynamic models, and subsequent hadronic cascade models. Today the collective dynamics of the created matter is understood in the form of such models called hybrid models or integrated dynamical models. First let us outline the dynamics of the whole process of the collisions, and then discuss each stage of the collision process in separate subsections.

The created matter starts from a thin region due to the Lorentz contraction of the colliding nuclei. Then, it expands into the longitudinal direction at almost the light velocity. To capture the dynamics of such an expanding system in which the initial small structure grows into the later longitudinal structure, a useful coordinate system, the τ-η_s coordinates (τ,η_s,x,y) (Fig. 2.5), is defined by a coordinate transform to the laboratory system (t,x,y,z) as

$$t=\tau\cosh\eta_s, \tag{2.14}$$

$$z=\tau\sinh\eta_s. \tag{2.15}$$

The inverse transform can be written as $\tau=\sqrt{t^2-z^2}$, and $\eta_s=\tanh^{-1}(z/t)=(1/2)\ln[(t+z)/(t-z)]$. The coordinate τ is often called a "proper time" because it corresponds to the

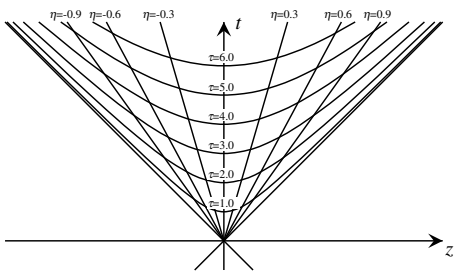

Figure 2.5: The τ-η_s coordinate mesh.

proper time of the fluid particle in the boost-invariant Bjorken flow described later in Subsection 2.2.2. The coordinate η_s is called a spacetime rapidity.

The very initial state of the collisions is described by two colliding nuclei with color-glass condensate picture described in Subsection 2.2.1. After the moment of the collision $\tau = 0$, a fast thermalization would be achieved with $\tau = \tau_0 \lesssim 1$ fm/c. There are various models to describe this initial state which will be described in Subsection 2.2.1.

The subsequent hydrodynamic evolution generates the collective flow of the created matter: The initial spatial distribution is converted into the final momentum anisotropy of the hadrons through this hydrodynamic stage. Although the ideal hydrodynamics had turned out to be well describe the behavior of the observed elliptic flow, small, but non-zero, viscosity has non-negligible effects on the quantitative feature of the flow harmonics. In fact one of the important quantities is the specific shear-viscosity coefficient η/s which affects the higher harmonics. The details of the hydrodynamic part are described in Subsection 2.2.2.

As the temperature of the matter becomes lower due to the expansion, the relevant microscopic degrees of freedom of the matter are gradually changed from quarks and gluons to hadrons. Then the mean free path of the constituent particles becomes longer than the system size, so that hydrodynamics is no more valid to describe the evolution of the system. In this stage the description of the system is switched from the hydrodynamics to the kinetic theory of hadron gases. The switching is performed on a three-dimensional hypersurface in the four-dimensional spacetime. This switching hypersurface is chosen, for example, to be the isothermal hypersurface with a fixed temperature $T_{\rm sw}$. The finite number of hadrons are sampled using the hydrodynamic fields on the hypersurface. This switching procedure is described in Subsection 2.2.3.

Subsequent dynamics of the hadrons is described with kinetic models where hadrons decay and scatter with each other to create resonances, etc. This process is called hadronic cascades, or hadronic afterburner, which shift the observed hadronic spectra such as the elliptic flow. This part is described in Subsection 2.2.4.

2.2.1 Initialization models

The initialization model provides the initial condition for the subsequent hydrodynamic stage. Most importantly, the initial entropy density or the energy density distribution, on the hypersurface at which hydrodynamics starts, is determined by the initialization model. In addition, the initial dissipative current fields and the flow velocity fields are dictated by the initialization models. There are several initialization models from simple phenomenological one to detailed one based on classical Yang-Mills dynamics. To fit into the later hydrodynamic calculations, the initial conditions are usually generated on a hypersurface at constant $\tau = \tau_0$ parametrized by three spatial coordinates (η_s, x, y). Here we give a brief overview of the two major models: the MC-Glauber model and the MC-KLN model. For the details of the initialization models, see Appendix A.2.

The basic model is the Glauber model [158, 159]. The experimental centrality dependence of the charged hadron multiplicity is fitted with the number of the participant nucleons and the number of binary collisions of nucleon pairs. In ideal hydrodynamic models, the final charged particle multiplicity directly corresponds to the entropy on the freezeout hypersurface where hydrodynamics ends. Since the total entropy is not increased by the ideal hydrodynamic evolution, the final entropy is just the initial entropy.

In the Glauber model, the initial entropy distribution in the transverse plane is generated by local densities of the nucleons. Those local densities are called thickness functions: $T^{\rm A}(\boldsymbol{x}_T)$ and $T^{\rm B}(\boldsymbol{x}_T)$ with $\boldsymbol{x}_T = (x, y)$ being the transverse coordinates. In the optical Glauber model, the thickness functions are calculated from the smooth Woods-Saxon distributions of the nucleons by integration with respect to the coordinate z. The participant densities $T^{\rm A/B}_{\rm part}(\boldsymbol{x}_T)$ are then calculated as the thickness $T^{\rm A/B}(\boldsymbol{x}_T)$ multiplied by the probability of the collisions at each transverse position. In the Monte-Carlo version of the Glauber model (MC-Glauber model), the positions of the finite number of the nucleons are sampled with the probability density of the Woods-Saxon distribution, and then the collision detection is applied for each pair of the nucleons from two nuclei. The resulting participant densities are calculated as the superpositions of the wounded nucleon profiles. It should be noticed here that, to reproduce the experimentally observed density of the Woods-Saxon distribution, one has to adjust the parameters of the Woods-Saxon distribution of the centers of the nucleons because experimental distribution corresponds

to the superposition of the nucleon profiles [160].

The Glauber model describes the profiles of the initial state in the transverse plane. In (2+1)-dimensional calculations, the Glauber model is sufficient to describe the hydrodynamic initial conditions. However in fully (3+1)-dimensional calculations, another model, which describe the longitudinal structure of the initial condition, is required. The effects of the longitudinal structure can be studied through asymmetric collisions such as Cu+Au and d+Au collisions. In the modified Brodsky-Gunion-Kuhn (modified BGK) model [119,161,162], the rapidity triangle shape observed in the charged particle multiplicity distribution of d+Au collisions [163] is used to extend the longitudinal profile of the Glauber model. The initial entropy density in the Glauber model combined with the modified BGK model is written in the following form:

$$\begin{aligned}\frac{dS(\boldsymbol{x}_T)}{\tau_0 d\eta_s d^2x_T} =& \frac{C}{\tau_0} f^{pp}(\eta_s)\theta(Y_b - |\eta_s|) \\ &\times \left\{(1-\delta)\left[\frac{Y_b+\eta_s}{2Y_b}T^{\rm A}_{\rm part}(\boldsymbol{x}_T) + \frac{Y_b-\eta_s}{2Y_b}T^{\rm B}_{\rm part}(\boldsymbol{x}_T)\right] + \delta\cdot T^{\rm AB}_{\rm coll}(\boldsymbol{x}_T)\right\},\end{aligned} \tag{2.16}$$

where the beam rapidity Y_b is defined so that $\cosh Y_b = \sqrt{s_{\rm NN}}/2m_N$ with the nucleon mass being $m_N = 0.939$ GeV. The overlap function $T^{\rm AB}_{\rm coll}(\boldsymbol{x}_T) \propto T^{\rm A}(\boldsymbol{x}_T)T^{\rm B}(\boldsymbol{x}_T)$ is the density of the number of the binary collisions of the nucleons. The function f^{pp} is a fitted function of the rapidity distribution of $p+p$ collisions. The Glauber model describes the shape of the created matter but does not provide the absolute value of the entropy, so that the overall scaling parameter C becomes a free parameter. This parameter is usually adjusted to reproduce the experimental charged particle multiplicity. Another free parameter δ is called a hard fraction parameter. The entropy produced by the participant nucleons is proportional to the thickness $T^{\rm A/B}$ while the entropy produced by the collisions is proportional to the square of the thickness functions. Since both contributions give different centrality dependence, the parameter δ can be adjusted to fit the centrality dependence of the charged particle multiplicity $dN_{\rm ch}/d\eta_p$ at midrapidity.

Another type of models which are often compared with the Glauber models is the color-glass condensate (CGC) model based on the CGC picture [166–168]. The CGC initial condition models include the Kharzeev-Levin-Nardi model (KLN model) [169] and its Monte-Carlo version (MC-KLN model) [170,171] which adopt the KLN approach [172–175]. In sufficiently high energy collisions, the matter of the initial stage is described by soft gluons. In the KLN approach, the rapidity distribution of the gluons is obtained by the k_T-factorization formula [176]. The initial entropy profile from the KLN model is calculated as the number density of the gluons:

$$\begin{aligned}\frac{dS(\eta_s,\boldsymbol{x}_T)}{\tau_0 d\eta_s d^2x_T} =& \, C\frac{2\pi^2}{C_{\rm F}}\int^{p_T^{\rm max}}\frac{d^2p_T}{p_T^2}\int^{p_T}\frac{d^2k_T}{4}\alpha_s(Q^2_{\rm max}(\boldsymbol{p}_T,\boldsymbol{k}_T)) \\ &\times \phi(x_+(p_T,\eta_s),(\boldsymbol{p}_T+\boldsymbol{k}_T)^2/4;Q^2_{s,{\rm A}}(\boldsymbol{x}_T)) \\ &\times \phi(x_-(p_T,\eta_s),(\boldsymbol{p}_T-\boldsymbol{k}_T)^2/4;Q^2_{s,{\rm B}}(\boldsymbol{x}_T)),\end{aligned} \tag{2.17}$$

where $\phi(x,kT^2;Q_s^2)$ is the unintegrated gluon distribution, and $Q^2_{s,{\rm A/B}}$ are the saturation scales calculated from the thickness functions $T^{\rm A/B}(\boldsymbol{x}_T)$. Like the Glauber model, the KLN model also has the overall scaling parameter to connect the entropy density and the gluon number density.

The indicators that characterize the profile of the initial conditions are the epsilons $\{\epsilon_n\}_n$ and the participant-plane angles $\{\Phi_n\}_n$ defined by the Fourier transform of the initial transverse density $\rho(\boldsymbol{x}_T) = (1/\tau_0)dS/d\eta_s d^2x_T$:

$$\epsilon_n e^{i\Phi_n} = -\int d^2x_T e^{in\phi_s} w_n(r_T)\rho(\boldsymbol{x}_T)\Big/\int d^2x_T w_n(r_T)\phi(\boldsymbol{x}_T), \tag{2.18}$$

where $\phi_s = \arg(x+iy)$ is the azimuthal angle in space. The radial weight function $w_n(r_T)$ is usually chosen as $w_n(r_T) = r_T^n$ or r_T^2. Like the flow harmonics of the momentum anisotropy, the epsilons and the participant-plane angles reflect the initial spatial anisotropy of the system. For example the eccentricity ϵ_2 measures the elliptic components of the initial conditions, and ϵ_3 the triangular components. It is known that, in the collisions at the fixed collision systems and the fixed centralities, the flow harmonics v_2 and v_3 are proportional to ϵ_2 and ϵ_3 in event-by-event models: $v_2/\epsilon_2 = $ const, and $v_3/\epsilon_3 = $ const. On the other hand, the harmonics v_n with the order greater than 3 are not proportional to the corresponding ϵ_n due to the contamination from the lower orders of the epsilons.

2.2.2 Hydrodynamic evolution

After the created matter forms a locally thermalized state of quarks and gluons (QGP), the hydrodynamic description can be applied to describe the spacetime evolution of the matter. The initial spatial density distribution is converted to the final momentum distribution mainly by the hydrodynamic response of the matter in this stage. The response depends on the bulk properties and the transport properties of the matter: the equation of state, and the constitutive equations with transport coefficients such as the shear viscosity, the bulk viscosity and the relaxation times. By analyzing the results of the hydrodynamic calculations with various equations of state, constitutive equations and transport coefficients, one can relate the matter properties to the final observables. The details of the framework of relativistic hydrodynamics will be summarized in Chapter 3.

The simplest hydrodynamic model of the high-energy nuclear collisions is the Bjorken's model [177]. In this model, the transverse dependence of the created matter is neglected, and the solution becomes boost invariant. This corresponds to the case that the colliding nuclei are sufficiently large such that the transverse profile of the created matter can be considered to be uniform, and the collision energy is high enough such that the matter has a boost invariant distribution in longitudinal direction. Under these ideal conditions, the flow velocity of the fluids vanishes in the τ-η_s coordinates: $u^{\eta_s} = u^x = u^y = 0$. Then the ideal hydrodynamic equation reduces to the following simple form:

$$\frac{de}{d\tau} = -\frac{e + p(e)}{\tau}, \tag{2.19}$$

where e is the internal energy density of the fluid, and $p = p(e)$ is the pressure as a function of the energy (i.e., the equation of state). With the equation of state of massless ideal gas: $p = (1/3)e$, the time evolution of the energy density can be solved as $e(\tau) \propto \tau^{-4/3}$, and the temperature becomes $T(\tau) \propto \tau^{-1/3}$. The solution of this model is called the Bjorken's flow or Bjorken's scaling solution. Since in this model a strong symmetry is imposed on the solution, the fluid fields is effectively (0+1)-dimensional with only the time dependence and no spatial dimensions.

In the actual nuclear collisions, the radial expansion in the transverse plane is induced due to the finite size of the colliding nuclei. Such expansion boosts the emitted hadrons and changes the spectra: e.g. it increases the observed mean transverse momentum $\langle p_T \rangle$. In addition the almond shape of the created matter due to the initial collision geometry produces the elliptic flow. To study such dynamics, we need to consider a (2+1)-dimensional dynamical model with the two transverse coordinates (x, y) and the time coordinate τ. The condition of Bjorken's flow u^{η_s} is imposed on the longitudinal direction. Those (2+1)-dimensional models successfully predicted the elliptic flow v_2 observed at RHIC in the early 2000s. To calculate the realistic hadron distributions which can be directly compared to the data through the observables, fully (3+1)-dimensional models are needed in the integrated dynamical models. With this complex situation with the event-by-event fluctuations, any analytic solutions like in the Bjorken's model are no longer available. The numerical calculations are needed to describe these hydrodynamics.

Recently, the equation of state has been almost fixed by the lattice QCD calculations [16, 178, 179]. It should be noticed here that the later stage of the hadronic cascades has its own equations of state to be calculated by simulations. To avoid discontinuity of the solution on the switching hypersurface, the equation of state in hydrodynamics should be smoothly connected to that of the adopted cascade model. In fact the parametrized equation of state based on the lattice calculations, but smoothly connected to each cascade models, are widely used: e.g. $s95p$-v1.1 for JAM, and $s95p$-v1.2 for UrQMD [180].

One of the current interests in the hydrodynamics is the extraction of the transport properties of the fluids [181]. By comparing the observed flow harmonics and those from viscous hydrodynamic models, the specific shear viscosity η/s turned out to be close to the lower bound $\eta/s \sim 1/4\pi$. The temperature dependence of the shear viscosity is discussed by comparing results with different collision energies $\sqrt{s_{\rm NN}}$ and centralities [182–184]. In comparison of the results of viscous hydrodynamics to the data, the viscosity observed at LHC is estimated to be larger than that of RHIC. This implies that the temperature of the created matter becomes higher with a higher collision energy. The effects of the bulk viscosity ζ are also investigated [185]. There are also many transport coefficients in the constitutive-equations of the second-order dissipative hydrodynamics. Constraints on such coefficients are also challenged [186].

The topics of the thermal fluctuations of hydrodynamics in the high-energy nuclear collisions are revisited in Section 2.3.

2.2.3 Particlization

The output of the hydrodynamics is the fluid fields on the switching hypersurface such as the velocity, the temperature, the shear stress tensor, and the bulk pressure. To calculate the observables using these results, the fluid fields should be first converted to the hadron distributions. In addition, to perform the subsequent rescattering of the hadrons in the cascade models, the distributions of the finite number of hadrons should be randomly sampled from the smooth probabilistic distribution function of the hadrons.

Given hydrodynamic fields on a switching hypersurface Σ, the spectrum of a resonance i can be expressed with Cooper-Frye formula [187]:

$$E\frac{d^3N_i}{d^3p} = \frac{g_i}{(2\pi)^3}\int_\Sigma d^3\sigma_\mu p^\mu f(p,x), \tag{2.20}$$

where g_i is the number of freedom degrees of the resonance i, and $d^3\sigma_\mu$ is a surface element on the switching hypersurface Σ. Here the hadron gas is considered to be a dilute gas and the interaction among hadrons can be neglected so that the distribution can be written with one particle distribution function. The correlations among the hadrons are neglected. The distribution function $f(p,x)$ gives the momentum distribution of particles at the position x of a surface element.

In the case of ideal hydrodynamics, the local momentum distribution is given by the Bose-Einstein distribution or the Fermi-Dirac distribution:

$$f(p,x) = f_0(p,x) \equiv \frac{1}{e^{\beta(p^\mu u_\mu - \mu_i)} - \epsilon}, \tag{2.21}$$

where $\beta = 1/T(x)$, and μ_i are the inverse temperature and the chemical potential of the particle at the position x, respectively. The four-velocity $u^\mu(x)$ is the flow velocity of the fluid at the position, which should not to be confused with the velocity of each particle. The statistical sign ϵ is $+1$ for bosons, and -1 for fermions. The above distribution of the particles in kinetic theories reproduces the local energy-momentum tensor of ideal hydrodynamics.

In the case of viscous hydrodynamics with the shear stress $\pi^{\mu\nu}$, the energy-momentum tensor has deviation from that of ideal hydrodynamics. The distribution function should be modified to reproduce the energy-momentum tensor including the viscous correction term such as the shear stress tensor and the bulk pressure. The distribution with the shear stress tensor $\pi^{\mu\nu}$ is known to have the following form to the first-order in the factor $\pi^{\mu\nu}$ [188, 189]:

$$f = f_0 + \delta f, \tag{2.22}$$

$$\delta f = f_0(1+\epsilon f_0)\frac{\pi^{\mu\nu}p_\mu p_\nu}{2(e+P)T^2}. \tag{2.23}$$

To determine the absolute number of the hadrons to be created, this procedure requires three dimensional integrations for each resonance i and at each three-dimensional hypersurface element. To reduce the time of the calculations, a special care should be paid for this step [113], or this stage takes the most part of the calculation time of the whole calculation of the process. The details of the procedure is described in Subsection 7.1.2 where the method in Ref. [113] is extended to support the viscous corrections.

2.2.4 Hadronic cascades

In hadronic cascades, the spacetime evolution of the hadron gas is calculated. The hadron gas is treated as a finite number of classical particles. In cascade models, hadrons and resonances decay or scatter with each other. The time evolution is performed as follows: For every pair of the hadrons, it is tested whether they scatter with each other. Then the scattering and the decay are performed in time order. Two hadrons scatter with each other if the impact parameter between them is smaller than the radius defined by the total cross section of the two hadrons. The impact parameter is calculated as the Lorentz-invariant distance of the classical trajectories of the two hadrons. For elastic scatterings, the momenta of the hadrons are just changed. The hadronic cascade models also contain inelastic scatterings, where the original hadrons are removed, and new hadrons are created. The decay can be simply performed by removing the particle and creating daughter particles at randomly sampled time with its decay rate.

In hadronic cascade models, many hadron/resonance species are considered. The list of hadrons and resonances, the cross sections of scattering processes, the decay rate, the branching ratios, etc. are inputs of the hadronic cascade models. There are several hadronic cascade models which have been used in high-energy nuclear collisions: RQMD [190–193], UrQMD [194–196], and JAM [197, 198].

The hadronic cascade is important to explain the dependence of observables on the hadron species. For example, let us consider the hadron mass dependence of the inverse slope parameter, $T_{\rm eff}$, of the identified hadron spectra. The hydrodynamic calculations without hadronic cascades predict a monotonic behavior of the slope parameter as a function of hadron mass. However experimentally measured spectra of multi-strange hadrons do not follow such a behavior [199, 200]. Indeed, the experimental behavior can be explained in the models with hadronic cascades [116–118]. Another example of the dependence on the hadron species is the identified p_T-differential elliptic flow. If all the hadrons are generated at a switching hypersurface and do not have interactions after that, the mass ordering of the elliptic flow v_2 is expected [37]. However, breaking of the ordering of the ϕ meson was predicted in hybrid calculations of hydrodynamics and the cascades, [119]. and was confirmed in experiments [201]. Those deviation from the pure hydrodynamic calculations comes from the fact that the effective freezeout time of each hadron species is different from each other. In actual interactions, the scattering processes are dependent on hadron species, and this leads to the different freezeout times of hadrons and breaking of the ordering. These effects are naturally taken into account in hadronic cascade models because each hadron species is distinguished from another, and has its own scattering processes and decay branch in the models.

Another importance of the cascades can be found in the dissipative effects of the hadronic phase on flows. To simultaneously fit the experimentally observed particle yields and the p_T-differential elliptic flows, models with hadronic cascades are necessary [202]. In particular, the rapidity dependence of the integrated elliptic flow v_2 was explained by the (3+1)-dimensional hydrodynamics with a cascade model [119,120]. In these calculations the flow generated in the hadronic cascades are essential to explain the observed rapidity dependence. If the hadronic phase is described with ideal hydrodynamics instead of the cascade models, the resulting rapidity dependence fails to fit the data.

2.3 Hydrodynamic fluctuations and high-energy nuclear collisions

In the equilibrium thermodynamics, we usually do not consider the thermal fluctuations. The reason is that the systems are sufficiently large compared to the microscopic scales, and the thermodynamic limit is approximately achieved. The typical magnitude of the thermodynamic fluctuations scales as the square root of the system size, i.e., $\delta \sim \sqrt{V}$ where δ denotes the fluctuations and V is the system size. In the thermodynamic limit relative fluctuations δ/V vanish because they are proportional to the inverse of the square root of the system size: $\delta/V \sim 1/\sqrt{V} \to 0\ (V \to \infty)$. As a consequence, the state of the system can be described with a finite small number of macroscopic variables, and we can forget the other microscopic degrees of freedom. In addition, the behavior of the system can be summarized with a thermodynamic function such as the entropy $S(E, N, V)$ with E, N, and V being extensive variables. The thermodynamic relations among the macroscopic variables are obtained from the thermodynamic function, and the relations of variables are closed with themselves, i.e., once a sufficient number of the macroscopic variables are given, the rest variables are obtained using the thermodynamic relations. This is the amazing characteristics of the thermodynamics which is a powerful tool for a wide variety of systems, including hydrodynamic systems where the gradient scale of the fluid fields is sufficiently larger than the microscopic scale of the system such as the mean free path.

We should still keep in mind that the thermodynamics can only be applied to systems in which the approximate thermodynamic limit can be justified. In high-energy nuclear collisions, the microscopic scale can be estimated with the relaxation time: τ_R = 0.1-0.5 fm, On the other hand, the matter structure of the scale of a femtometer is important especially in the higher harmonics in the event-by-event studies, Because those two scales are not well separated, we need to take the hydrodynamic fluctuations into account.

The first application of the hydrodynamic fluctuations to the high-energy nuclear collisions was made in Ref. [92, 235, 236], where the correlations of fluctuations of fluid fields are studied in the background of the boost invariant Bjorken expansion. They obtained interesting behaviors of two point correlations in rapidity distribution of created hadrons. In later works they also investigated the effect of the hy-

drodynamic fluctuations near the critical point focusing on the baryon diffusion current [237]. In their works they adopted the one-dimensional Bjorken model, and the transverse structures of the matter was not considered. Also, the effect of the fluctuations are considered up to the first order in the fluctuations. In Ref. [238], first dynamical simulations of the hydrodynamic fluctuations are performed for the high-energy nuclear collisions by treating the noises perturbatively.

To unveil the effects of the hydrodynamic fluctuations quantitatively, we need to consider the effects within the (3+1)-dimensional spacetime evolution of the matter using integrated dynamical models of the high-energy nuclear collisions. In such a dynamical model, the hydrodynamic equations cannot be linearized due to the strong expansion of the matter. Therefore, we need to investigate the treatment of the fluctuations in the non-linear hydrodynamic equations. In addition, in the numerical analyses, the causal dissipative hydrodynamics should be used to avoid the acausal propagation of signals and related numerical instabilities [216–218]. In such causal theories we also need to consider the causality of the noise correlations, which will be explained in Chapter 4.

Chapter 3

Relativistic hydrodynamics

In this chapter, we overview the basic notions of relativistic hydrodynamics focusing on the phenomenological structure of the equations. In both non-relativistic and relativistic systems, hydrodynamic equations are basically continuity equations of mass, momentum, energy and other conserved quantities.

The conservation laws in relativistic system are summarized in the following form:

$$\partial_\mu T^{\mu\nu} = 0, \tag{3.1}$$

$$\partial_\mu N_i^\mu = 0, \quad (i = 1, \ldots, n), \tag{3.2}$$

where the energy-momentum tensor $T^{\mu\nu}$ is the Noether current corresponding to the spacetime translational symmetry. The currents N_i^μ are the Noether currents corresponding to other internal symmetries of the system, with n being the number of the conserved currents.

Those conservation laws are not closed with themselves: the number of independent fields is 10 for the symmetric tensor $T^{\mu\nu}$ and $4n$ for the conserved currents N_i^μ, while the number of continuity equations, (3.1) and (3.2), is $n+4$. In hydrodynamics, we use the knowledge of thermodynamics to close the continuity equations and to solve the macroscopic dynamics. The input from the thermodynamics or statistical mechanics are given by the equation of state and the constitutive equations under the assumption that the system is close to a local-equilibrium state. Those equations give the macroscopic properties of the matter which encode the microscopic dynamics of the system.

3.1 Local rest frame

In order to introduce the equation of state and the constitutive equations, we first need to determine a local rest frame of matter to relate the conserved currents and thermodynamic quantities. The local rest frame is specified by a flow velocity field $u^\mu(x)$:

$$u^\mu(x) = \begin{pmatrix} \gamma(x) \\ \gamma(x)\boldsymbol{v}(x) \end{pmatrix}, \tag{3.3}$$

$$u^\mu(x)u_\mu(x) = 1, \tag{3.4}$$

where $\boldsymbol{v}(x)$ is the velocity of the local rest frame at a position x, and $\gamma(x) = 1/\sqrt{1-\boldsymbol{v}(x)^2}$ is the Lorentz factor at the position. The second line is the normalization of the velocity vector. Due to this normalization, the number of independent components of the velocity becomes three. In general the velocity field $u^\mu(x)$ can be an arbitrary time-like vector field normalized as (3.4). However, to properly describe the dynamics, it should be defined using the macroscopic state of the matter, i.e., the conserved currents such as $T^{\mu\nu}(x)$ and $N_i^\mu(x)$. In fact there are several ways to define the local rest frame of the matter using those conserved quantities.

In non-relativistic hydrodynamics, the velocity $\boldsymbol{v}(x)$ can be defined using the flow of mass density. Meanwhile, in relativistic systems such as the quark-gluon plasma, the mass density is not a well-defined quantity since the mass is no longer a conserved quantity. The number density of particles cannot be used as well, since what is conserved is the net charges, namely, the difference of the number of particles and antiparticles.

Instead of using the mass or the particle number, the energy-momentum density or the conserved charge density can be used to define the local rest frame in relativistic systems.

The frame of the energy density is called the Landau frame [203], where the velocity field u^μ can be defined as a normalized time-like eigenvector of the energy-momentum tensor:

$$T^\mu{}_\nu u^\nu = e u^\mu. \tag{3.5}$$

Here e is an eigenvalue which has the meaning of the energy density.

Note that the physical energy-momentum tensor has always one time-like eigenvector and three spacelike eigenvectors. This property comes from the fact that the physical energy-momentum tensor should be time-like[1] momentum densities $T^{0\mu}$ with $T^{0\mu}T^0{}_\mu > 0$. Such symmetric rank-2 tensor of four-dimensional Minkowski spacetime is known to have an eigensystem of Segre type "[1 1 1 1]" [204–206]. The tensor of this Segre type has four real eigenvalues. One eigenvalue corresponds to a time-like eigenvector, and the others correspond to three spacelike eigenvectors. The time-like eigenvector and its eigenvalue can be interpreted as a velocity of the energy and an energy density as in (3.5). The other three eigenvalues are principal stresses, and the corresponding eigenvectors are the principal axes of the stresses.

The frame of the charge density is called the Eckart frame [207]. where the velocity field is defined to be parallel to a specific charge current N_i^μ:

$$u^\mu = \frac{N_i^\mu}{\sqrt{N_{i\alpha}N_i^\alpha}}. \tag{3.6}$$

Here the factor $\sqrt{N_{i\alpha}N_i^\alpha}$ is the normalization.

In multi-component system ($n \geq 2$), one can also define the Eckart frame using a linear combination of the conserved currents. For example the Eckart frame can be defined with the sum of all the conserved currents [208]:

$$u^\mu = \frac{\sum_{i=1}^n N_i^\mu}{\sqrt{\left(\sum_{i=1}^n N_i^\alpha\right)^2}}. \tag{3.7}$$

Another version of the Eckart frame in multi-component system is the average particle frame [212] based on the kinetic theory. It is the frame of the energy flux caused by particle diffusion. The velocity fields is chosen to have the following equation:

$$u^\mu = \frac{1}{N}\sum_i^n \frac{N_i^\mu}{n_i}, \tag{3.8}$$

where $n_i = u_\mu N_i^\mu$.

In high-energy nuclear collisions, the Landau frame rather than the Eckart frame is commonly used for hydrodynamic models. One of the relevant conserved charges in the high-energy nuclear collisions is the baryon charge, so that one can define the Eckart frame of the baryon charge. However, the Eckart frame is not useful because the baryon charge density almost vanishes at the midrapidity in the reactions so that the direction of the charge current (3.6) cannot be normalized to determine its direction. On the other hand, the Landau frame can always be used since the energy density of the matter never vanishes.

3.2 Tensor decomposition and projectors

Once a local rest frame of the matter is given, the boost invariance of the local system is broken. As a result, the currents $(T^{\mu\nu}, N_i^\mu)$ are decomposed into several components [209]. Each component corresponds to an irreducible representation of the spatial rotation in the local rest frame. In addition, one can find a physical meaning of each component.

To decompose vectors and tensors, we consider the projectors onto each component constructed by the metric $g^{\mu\nu}$ and the velocity field u^μ. A four-vector is decomposed into a temporal component and a spatial

[1] Although the momentum density $T^{0\mu}$ can be light-like in some special system, such system cannot be described with hydrodynamics in general. For example, in a massless non-interacting gas such as the photon gas, the energy-momentum of the system becomes light-like if all the particles are moving to one direction. Such non-interacting system is not a subject of hydrodynamics.

component. The temporal component is defined to be parallel to the velocity vector u^μ and corresponds to the zeroth element of the vector in the local rest frame. The spatial component is defined to be transverse to the velocity vector. The projector onto the temporal components is $u^\mu(x)u_\nu(x)$. The projector onto the spatial component $\Delta^\mu{}_\nu(x)$ can be written as $\Delta^\mu{}_\nu(x) \equiv \delta^\mu{}_\nu - u^\mu(x)u_\nu(x) = g^\mu{}_\nu - u^\mu(x)u_\nu(x)$. These two components form a complete orthogonal system of the four-vector space:

$$\delta^\mu{}_\nu = u^\mu u_\nu + \Delta^\mu{}_\nu. \tag{3.9}$$

In addition, the spatial projector has the following properties:

$$\Delta^\mu{}_\alpha \Delta^\alpha{}_\nu = \Delta^\mu{}_\nu, \tag{3.10}$$

$$\Delta^{\mu\nu} = \Delta^{\nu\mu}, \tag{3.11}$$

$$u_\alpha \Delta^\alpha{}_\nu = 0. \tag{3.12}$$

The first two equations are the general relations for the projector P: $P^2 = P$ and $P^{\mathrm{T}} = P$. The third equation is the orthogonality between the temporal component and the spatial component.

In the local rest frame, the projectors are represented as

$$u^\mu u_\nu = \mathrm{diag}(1,0,0,0), \tag{3.13}$$

$$\Delta^\mu{}_\nu = \mathrm{diag}(0,1,1,1). \tag{3.14}$$

Now, we can decompose the conserved currents N_i^μ as

$$N_i^\mu = \delta^\mu{}_\nu N_i^\nu = u^\mu(u_\nu N_i^\nu) + \Delta^\mu{}_\nu N_i^\nu \tag{3.15}$$

$$= n_i u^\mu + \nu_i^\mu. \tag{3.16}$$

Here we defined $n_i \equiv u_\nu N_i^\nu$ and $\nu_i^\mu \equiv \Delta^\mu{}_\nu N_i^\nu$. The time component n_i is the density of i-th charge in the local rest frame of the matter, and the spatial component ν_i^μ is the charge diffusion. The first term $n_i u^\mu$ is interpreted as a motion of the charge carried by the matter, and the diffusion term ν_i^μ is the transport of the charge inside the matter. In the local rest frame, the current can be represented as

$$N_i^\mu = \begin{pmatrix} n_i & \nu_i^1 & \nu_i^2 & \nu_i^3 \end{pmatrix}^{\mathrm{T}}. \tag{3.17}$$

The charge densities n_i $(i = 1, \ldots, n)$ correspond to the spin-0 representation of the spatial rotation group $SO(3)$ in the local rest frame, so that they are not transformed under the spatial rotation. The diffusion currents ν_i^μ correspond to the spin-1 representation. Since they belong to the components orthogonal to the velocity field u^μ, an inner product of the diffusion current and the velocity vanishes:

$$u_\mu \nu_i^\mu = 0, \quad (i = 1, \ldots, n). \tag{3.18}$$

Therefore the number of independent elements of ν_i^μ is $3n$.

The gradient operator ∂_μ can also be decomposed:

$$\partial_\mu = \delta_\mu{}^\nu \partial_\nu = u_\mu(u^\nu \partial_\nu) + \Delta_\mu{}^\nu \partial_\nu \tag{3.19}$$

$$= u_\mu \mathrm{D} + \nabla_\mu. \tag{3.20}$$

Here we defined the temporal part $\mathrm{D} \equiv u^\mu \partial_\mu$ and the spatial part $\nabla_\mu \equiv \Delta_\mu{}^\nu \partial_\nu$. The time component of the gradient D implies the derivative with respect to the proper time of the fluid element. The term ∇_μ denotes a spatial derivative in the local rest frame where the gradient is written as

$$\partial_\mu = \begin{pmatrix} \mathrm{D} & \nabla_1 & \nabla_2 & \nabla_3 \end{pmatrix}. \tag{3.21}$$

The derivative D corresponds to the material derivative of the non-relativistic hydrodynamics $\mathrm{D}/\mathrm{D}t = \partial/\partial t + \boldsymbol{v} \cdot \nabla$, also known as the substantial derivative or the Lagrangian derivative:

$$\mathrm{D} = \gamma \frac{\partial}{\partial t} + \boldsymbol{u} \cdot \nabla \tag{3.22}$$

$$= \gamma \left(\frac{\partial}{\partial t} + \boldsymbol{v} \cdot \nabla \right) = \gamma \frac{\mathrm{D}}{\mathrm{D}t}. \tag{3.23}$$

The Lorentz factor γ represents a time dilation. The derivative can be formally written as $\mathrm{D} = d/d\tau$, where $\tau = \int dt/\gamma$ is the proper time of the fluid element.

Next, we consider the decomposition of the rank-2 tensor. The space of rank-2 tensor can be decomposed into six parts:

$$\begin{aligned}\delta^{\mu}{}_{\alpha}\delta^{\nu}{}_{\beta} =& u^{\mu}u^{\nu}u_{\alpha}u_{\beta} + 2u^{(\mu}u_{(\alpha}\Delta^{\nu)}{}_{\beta)} + 2u^{[\mu}u_{[\alpha}\Delta^{\nu]}{}_{\beta]} \\ &+ \frac{1}{3}\Delta^{\mu\nu}\Delta_{\alpha\beta} + \Delta^{\mu\nu}{}_{\alpha\beta} + \Delta^{[\mu}{}_{\alpha}\Delta^{\nu]}{}_{\beta},\end{aligned} \tag{3.24}$$

where $\Delta^{\mu\nu}{}_{\alpha\beta} \equiv \Delta^{(\mu}{}_{\alpha}\Delta^{\nu)}{}_{\beta} - \frac{1}{3}\Delta^{\mu\nu}\Delta_{\alpha\beta}$. The first term $u^{\mu}u^{\mu}u_{\alpha}u_{\beta}$ is the projector onto the time-time component. The second term $u^{(\mu}u_{(\alpha}\Delta^{\nu)}{}_{\beta)}$ and the third term $u^{[\mu}u_{[\alpha}\Delta^{\nu]}{}_{\beta]}$ are the projectors onto the symmetric and antisymmetric space-time component, respectively. The fourth term $\frac{1}{3}\Delta^{\mu\nu}\Delta_{\alpha\beta}$ is onto the trace of the space-space component, the fifth term $\Delta^{\mu\nu}{}_{\alpha\beta}$ is onto the symmetric traceless space-space component, and the last term $\Delta^{[\mu}{}_{\alpha}\Delta^{\nu]}{}_{\beta}$ is onto the antisymmetric space-space component.

The projector $\Delta^{\mu\nu}{}_{\alpha\beta}$ has the following properties:

$$\Delta^{\mu\nu}{}_{\alpha\beta}\Delta^{\alpha\beta}{}_{\kappa\lambda} = \Delta^{\mu\nu}{}_{\kappa\lambda}, \tag{3.25}$$

$$\Delta^{\mu\nu\alpha\beta} = \Delta^{\alpha\beta\mu\nu}, \tag{3.26}$$

$$\Delta^{\mu\nu\alpha\beta} = \Delta^{\nu\mu\alpha\beta}, \tag{3.27}$$

$$\Delta^{\mu}{}_{\kappa}\Delta^{\kappa\nu}{}_{\alpha\beta} = \Delta^{\mu\nu}{}_{\alpha\beta}, \tag{3.28}$$

$$u_{\mu}\Delta^{\mu\nu}{}_{\alpha\beta} = 0, \tag{3.29}$$

$$\Delta_{\mu\nu}\Delta^{\mu\nu}{}_{\alpha\beta} = \Delta^{\mu}{}_{\mu\alpha\beta} = 0. \tag{3.30}$$

The first and second equations are general relations of the projector. The other equations are obtained from the orthogonality with other projectors.

The energy-momentum tensor $T^{\mu\nu}$ of the fluid is symmetric if the angular momentum is locally conserved and are closed within the hydrodynamic system. Note that if the fluid is coupled to other systems such as the electromagnetic field, and the angular momentum can be exchanged between the systems, the energy-momentum tensor of the fluid can have asymmetric part. In this thesis we do not consider such special cases. Therefore, $T^{\mu\nu}$ is decomposed as follows:

$$T^{\mu\nu} = eu^{\mu}u^{\nu} + 2W^{(\mu}u^{\nu)} - \Delta^{\mu\nu}P_{\mathrm{tot}} + \pi^{\mu\nu}, \tag{3.31}$$

where $e \equiv u_{\alpha}u_{\beta}T^{\alpha\beta}$ is the time-time component, $W^{\mu} \equiv \Delta^{\mu}{}_{(\alpha}u_{\beta)}T^{\alpha\beta}$ is the symmetric space-time component, $P_{\mathrm{tot}} \equiv -\frac{1}{3}\Delta_{\alpha\beta}T^{\alpha\beta}$ is the trace of the space-space component, and $\pi^{\mu\nu} \equiv \Delta^{\mu\nu}{}_{\alpha\beta}T^{\alpha\beta}$ is the symmetric traceless part of space-space component. The antisymmetric components vanish due to the symmetry of the energy-momentum tensor $T^{\mu\nu}$. In the local rest frame, the energy-momentum tensor has the following form:

$$T^{\mu\nu} = \begin{pmatrix} e & W^1 & W^2 & W^3 \\ W^1 & P_{\mathrm{tot}} + \pi^{11} & \pi^{12} & \pi^{13} \\ W^2 & \pi^{21} & P_{\mathrm{tot}} + \pi^{22} & \pi^{23} \\ W^3 & \pi^{31} & \pi^{32} & P_{\mathrm{tot}} + \pi^{33} \end{pmatrix}. \tag{3.32}$$

The internal energy density e is the one observed in the local rest frame. The energy flux density W^{μ}, namely, the heat flux density observed in the local rest frame, implies the transport of the energy in the matter. The pressure P_{tot} is the isotropic part of the stress. We put the subscript $\cdot_{\mathrm{tot}}$ to distinguish the pressure from its equilibrium part P described by the equation of state. The shear-stress tensor $\pi^{\mu\nu}$ is the anisotropic part of the stress. The energy density e and the pressure P_{tot} correspond to the spin-0 representation of the spatial rotation group in the local rest frame, and the number of independent variables is 1. The energy flux density W^{μ} corresponds to the spin-1 representation, and the number of independent variables is 3. The shear stress $\pi^{\mu\nu}$ corresponds to the spin-2 representation, and the number of independent variables is 5. Those currents are transverse to the flow velocity:

$$u_{\mu}W^{\mu} = u_{\mu}\pi^{\mu\nu} = 0. \tag{3.33}$$

The velocity gradient tensor $\partial^\mu u^\nu$ is decomposed as follows:

$$\partial^\mu u^\nu = \frac{1}{2}\mathrm{D}(u^\mu u^\nu) + u^{[\mu}\mathrm{D}u^{\nu]} + \frac{1}{3}\Delta^{\mu\nu}\theta + \sigma^{\mu\nu} + \omega^{\mu\nu}, \tag{3.34}$$

$$\theta \equiv \partial_\alpha u^\alpha, \tag{3.35}$$

$$\sigma^{\mu\nu} \equiv \partial^{\langle\mu} u^{\nu\rangle} = \nabla^{(\mu} u^{\nu)} - \frac{1}{3}\Delta^{\mu\nu}\theta, \tag{3.36}$$

$$\omega^{\mu\nu} \equiv \nabla^{[\mu} u^{\nu]}. \tag{3.37}$$

The first and the second term in the equation (3.34) are the symmetric and the antisymmetric part of the space-time components, respectively. The third term is the trace of the space-space component. The fourth term and the fifth term are the symmetric and the antisymmetric part of the space-space components, respectively. The time-time component vanishes due to the normalization of the velocity vector (3.4): $u_\alpha u_\beta \partial^\alpha u^\beta = (1/2)\mathrm{D}(u_\beta u^\beta) = 0$. The factor in the third term, θ, is the expansion rate of the fluid element, which can be expressed as

$$\theta = \frac{\mathrm{D}(\gamma\delta V)}{\gamma\delta V}. \tag{3.38}$$

Here $\gamma\delta V$ is the volume of an infinitesimal fluid element observed in the local rest frame. The strain rate tensor $\sigma^{\mu\nu}$ implies the shear deformation rate, and the vorticity tensor $\omega^{\mu\nu}$ is the rate of the rotation of a fluid element.

It should be noticed here that some component of the currents $(T^{\mu\nu}, N_i^\mu)$ vanishes when a particular frame is chosen. In the Landau frame, the energy flux in the local rest frame vanishes: $W^\mu = u_\alpha \Delta^\mu{}_\beta T^{\alpha\beta} = e\Delta^\mu{}_\beta u^\beta = 0$. In the Eckart frame of the i-th charge, the charge diffusion current vanishes: $\nu_i^\mu = \Delta^\mu{}_\alpha N_i^\alpha = n_i \Delta^\mu{}_\alpha u^\alpha = 0$. If the Eckart frame with an linear combinations (3.7) is used, any of the diffusion currents does not vanish. Instead, a linear combination of the diffusion current vanishes: e.g., $\sum_{i=1}^n \nu_i^\mu = 0$. Therefore the diffusion currents are not linearly independent in such Eckart frame.

The quantities introduced so far are summarized in Table 3.1.

$e = u_\alpha u_\beta T^{\alpha\beta}$	energy density
$W^\mu = u_\alpha \Delta^\mu{}_\beta T^{\alpha\beta}$	energy flux density
$P_{\mathrm{tot}} = -\frac{1}{3}\Delta_{\alpha\beta} T^{\alpha\beta}$	pressure
$\pi^{\mu\nu} = \Delta^{\mu\nu}{}_{\alpha\beta} T^{\alpha\beta}$	shear stress
$n_i = u_\alpha N_i^\mu$	charge density
$\nu_i^\mu = \Delta^\mu{}_\alpha N_i^\mu$	charge diffusion current
$\mathrm{D} = u^\alpha \partial_\alpha$	material derivative
$\nabla_\mu = \Delta_\mu{}^\alpha \partial_\alpha$	spatial derivative
$\theta = \nabla_\alpha u^\alpha$	expansion rate
$\sigma^{\mu\nu} = \partial_{\langle\mu} u^{\nu\rangle}$	strain rate tensor
$\omega^{\mu\nu} = \nabla^{[\mu} u^{\nu]}$	vorticity tensor

Table 3.1: Tensor components

3.3 Tensor decomposition of the conservation laws

The conservation law of the energy-momentum tensor (3.1) can be decomposed into following two equations:

$$u_\beta \partial_\mu T^{\mu\beta} = 0, \tag{3.39}$$

$$\Delta^\mu{}_\beta \partial_\mu T^{\mu\beta} = 0. \tag{3.40}$$

These two equations and the conservation law of the conserved currents (3.2) can be rewritten in terms of the quantities introduced so far:

$$\begin{aligned}
\mathrm{D}e + (e + P_{\mathrm{tot}})\theta &= W^\mu \mathrm{D}u_\mu - \partial_\mu W^\mu + \pi^{\mu\nu}\sigma_{\mu\nu} && (3.41)\\
&= 2W^\mu \mathrm{D}u_\mu - \nabla_\mu W^\mu + \pi^{\mu\nu}\sigma_{\mu\nu}, && (3.42)\\
(e + P_{\mathrm{tot}})\mathrm{D}u^\mu &= \nabla^\mu P_{\mathrm{tot}} - \Delta^\mu{}_\alpha \partial_\beta \pi^{\alpha\beta} - 2\Delta^\mu{}_\alpha \partial_\beta u^{(\alpha} W^{\beta)} && (3.43)\\
&= -\nabla_\beta(\pi^{\beta\mu} - g^{\beta\mu}P_{\mathrm{tot}}) - u^\mu(W^\alpha \mathrm{D}u_\alpha + \pi^{\alpha\beta}\sigma_{\alpha\beta}) && (3.44)\\
&\quad - \mathrm{D}W^\mu - \frac{4}{3}\theta W^\mu - (\sigma^{\mu\beta} + \omega^{\mu\beta})W_\beta + \pi^{\mu\beta}\mathrm{D}u_\beta,\\
\mathrm{D}n_i + n_i\theta &= -\partial_\mu \nu_i^\mu && (3.45)\\
&= \nu_i^\mu \mathrm{D}u_\mu - \nabla_\mu \nu_i^\mu, \quad (i = 1, \ldots, n). && (3.46)
\end{aligned}$$

The first equation (3.41) describes the time evolution of the energy density, and the second equation (3.43) describes the time evolution of the velocity field. The third equation (3.45) describes the time evolution of a charge density. In the Landau frame, the equations of the energy density and the velocity, (3.42) and (3.44), reduce to simpler forms:

$$\begin{aligned}
\mathrm{D}e + (e + P_{\mathrm{tot}})\theta &= \pi^{\mu\nu}\sigma_{\mu\nu}, && (3.47)\\
(e + P_{\mathrm{tot}})\mathrm{D}u^\mu &= -\nabla_\beta(\pi^{\beta\mu} - g^{\beta\mu}P_{\mathrm{tot}}) - u^\mu(\pi^{\alpha\beta}\sigma_{\alpha\beta}) + \pi^{\mu\beta}\mathrm{D}u_\beta. && (3.48)
\end{aligned}$$

In the Eckart frame of the j-th charge, the right hand side of the equation of the j-th charge vanishes:

$$\mathrm{D}n_i + n_i\theta = 0, \quad (i = j). \tag{3.49}$$

Note that the equations of the other charges j $(i \neq j)$ still have non-zero right hand sides.

3.4 Ideal hydrodynamics

In this section, we consider the system close enough to an equilibrium state, and the local value of the currents $(T^{\mu\nu}, N_i^\mu)$ can be written by the equilibrium values. The hydrodynamics derived with such assumptions is called ideal hydrodynamics.

In the local-equilibrium state, macroscopic quantities which have *a specific direction* vanish since the system is isotropic in the local rest frame: $W^\mu = \pi^{\mu\nu} = \nu_i^\mu = 0$. Thus only the components of the trivial representation remain:

$$\begin{aligned}
T^{\mu\nu} &= eu^\mu u^\nu + P_{\mathrm{tot}}\Delta^{\mu\nu}, && (3.50)\\
N_i^\mu &= n_i u^\mu. && (3.51)
\end{aligned}$$

The independent fields of the energy-momentum tensor and the conserved currents are $e(x)$, $P_{\mathrm{tot}}(x)$, $u^\mu(x)$, and $n_i(x)$. The number of the fields is $1 + 1 + 3 + n = n + 5$. On the other hand, the number of the equations (3.42), (3.44), and (3.46) is $1 + 3 + n = n + 4$ which is smaller than the number of the fields. Therefore we need an additional equation to solve the dynamics. Here we use knowledge of the thermodynamics to close the equations. In the equilibrium state, the pressure can be given by the equation of state:

$$P_{\mathrm{tot}} = P(e, \{n_i\}). \tag{3.52}$$

At the same time, we can define other thermodynamic quantities using the energy density and the charge densities:

$$\begin{aligned}
T &= T(e, \{n_i\}), && (3.53)\\
\mu_j &= \mu_j(e, \{n_i\}), \quad (j = 1, \ldots, n), && (3.54)\\
s &= s(e, \{n_i\}). && (3.55)
\end{aligned}$$

where T is the temperature of the local-equilibrium state, and μ_j is the chemical potential of the j-th charge. The equilibrium entropy density s can also be defined.

With the conserved currents of the form (3.50) and (3.51), the hydrodynamic equations (3.42), (3.44), and (3.46) have simple forms:

$$\mathrm{D}e + (e+P)\theta = 0, \tag{3.56}$$
$$(e+P)\mathrm{D}u^\mu = \nabla^\mu P, \tag{3.57}$$
$$\mathrm{D}n_i + n_i\theta = 0. \tag{3.58}$$

These are the equations of relativistic ideal hydrodynamics. The term $e\theta$ in Eq. (3.56) and the term $n_i\theta$ in Eq. (3.58) denote changes of the energy density and the charge densities due to the change of the volume of a fluid element. The term $P\theta$ in Eq. (3.56) is the change of the energy density due to the work of the volume change by adjacent fluid elements. The right hand side in Eq. (3.57) is the pressure gradient which accelerates the fluid element.

Here let us consider the non-relativistic limit. In the limit, major part of the energy density e comes from the mass energy density $\rho_m c^2$ where ρ_m is the mass density. Then we can replace $e+P$ in (3.57) with $\rho_m = \rho_m c^2$ because the remaining internal energy density $u = e - \rho_m c^2$ and the pressure P are negligible compared with $\rho_m c^2$. The material derivative, the spatial derivative, and expansion rate also become $\mathrm{D} \to \frac{\partial}{\partial t} + \boldsymbol{v}\cdot\nabla$, $\nabla^\alpha \to -\nabla$, and $\theta \to \operatorname{div}\boldsymbol{v}$, respectively. As a result, the hydrodynamic equations reduce to:

$$\left(\frac{\partial}{\partial t} + \boldsymbol{v}\cdot\nabla\right)(\rho_m + u) + (\rho_m + u + P)\operatorname{div}\boldsymbol{v} = 0, \tag{3.59}$$
$$\rho_m\left(\frac{\partial}{\partial t} + \boldsymbol{v}\cdot\nabla\right)\boldsymbol{v} = -\nabla P, \tag{3.60}$$
$$\left(\frac{\partial}{\partial t} + \boldsymbol{v}\cdot\nabla\right)n_i + n_i\operatorname{div}\boldsymbol{v} = 0. \tag{3.61}$$

Using the mass conservation:

$$\frac{\partial\rho_m}{\partial t} + \operatorname{div}(\rho_m\boldsymbol{v}) = 0, \tag{3.62}$$

these equations can be reorganized as follows:

$$\frac{\partial n_i}{\partial t} = -\operatorname{div}(n_i\boldsymbol{v}), \tag{3.63}$$
$$\rho_m\left(\frac{\partial}{\partial t} + \boldsymbol{v}\cdot\nabla\right)\boldsymbol{v} = -\nabla P, \tag{3.64}$$
$$\frac{\partial}{\partial t}(u + \rho_m\boldsymbol{v}^2/2) = -\operatorname{div}[(u + \rho_m\boldsymbol{v}^2/2 + P)\boldsymbol{v}]. \tag{3.65}$$

They are nothing but the Euler equations known in non-relativistic ideal hydrodynamics.

3.5 First-order dissipative hydrodynamics

In the previous section, we assumed that the conserved currents can be written by their equilibrium values. In actual systems, however, the conserved currents can deviate from the equilibrium values due to the gradients of the fluid fields. Dissipative hydrodynamics is derived by taking the effect of such deviation into account.

In this section we consider the case that the deviation of the currents from its equilibrium value can be written in terms of first-order derivatives of fluid fields. Such dissipative hydrodynamics is called first-order dissipative hydrodynamics also known as the Navier-Stokes theory. Historically, the first-order dissipative hydrodynamics for relativistic fluid was first introduced by Eckart [207], and later by Landau [203].

3.5.1 Diffusion and thermodynamic force

In the static equilibrium, any quantities do not have macroscopic flow in its rest frame. While, in hydrodynamics in which thermodynamic quantities change dynamically, a macroscopic flow can occur in

the local rest frame. Such flow is generally called diffusion. For example, if the temperature of a fluid element is higher than the surroundings, the heat flow will occur toward the outer direction. This is the diffusion of heat. Another example is the momentum diffusion where a part of the fluid starts to move in the same direction as the neighboring fluid elements. This is the diffusion of the momentum.

The diffusion is generally created by gradients of the temperature, the chemical potentials and the velocity fields. Such gradients that cause the diffusion are called thermodynamic forces. The gradients of the temperature, the chemical potentials, and the velocity are decomposed as in Section 3.2:

$$\partial_\mu u_\nu = u_\mu \mathrm{D} u_\nu + \frac{1}{3}\Delta_{\mu\nu}\theta + \sigma_{\mu\nu} + \omega_{\mu\nu}, \tag{3.66}$$

$$\partial_\mu T = u_\mu \mathrm{D} T + \nabla_\mu T, \tag{3.67}$$

$$\partial_\mu \mu_i = u_\mu \mathrm{D}\mu_i + \nabla_\mu \mu_i, \quad (i = 1, \ldots, n). \tag{3.68}$$

Each term θ, $\sigma_{\mu\nu}$, $\omega_{\mu\nu}$, $\nabla_\mu T$, and $\nabla_\mu \mu_i$ $(i = 1, \ldots, n)$ is the thermodynamic force. The substantial derivatives $\mathrm{D}u^\mu$, $\mathrm{D}T$, $\mathrm{D}\mu_i$ $(i = 1, \ldots, n)$ are also thermodynamics forces. It should be noticed here that the substantial derivatives can be replaced by spatial derivatives using the hydrodynamic equations (3.42), (3.44), and (3.46) along with the thermodynamic relations $dT = (\partial T/\partial e)_{n_k} de + \sum_{j=1}^{n} (\partial T/\partial n_j)_{e, n_{k\neq j}} dn_j$, $d\mu_i = (\partial \mu_i/\partial e)_{n_k} de + \sum_{j=1}^{n} (\partial \mu_i/\partial n_j)_{e, n_{k\neq j}} dn_j$.

3.5.2 Dissipative current and constitutive equation

Any tensor components can have non-zero values when the thermodynamic forces exist because the existence of the gradient vector and tensor $\nabla_\mu T, \nabla_\mu \mu_i, \sigma_{\mu\nu}, \omega_{\mu\nu}$ breaks the isotropy in the local rest frame. Therefore the currents $(T^{\mu\nu}, N_i^\mu)$ in the system with diffusion have the following form:

$$T^{\mu\nu} = (e_{\mathrm{eq}} + \delta e) u^\mu u^\nu - \Delta^{\mu\nu}(P(e_{\mathrm{eq}}) + \Pi) + 2W^{(\mu} u^{\nu)} + \pi^{\mu\nu}, \tag{3.69}$$

$$N_i^\mu = (n_{i,\mathrm{eq}} + \delta n_i) u^\mu + \nu_i^\mu. \tag{3.70}$$

where e_{eq}, $n_{i,\mathrm{eq}}$, and $P(e_{\mathrm{eq}})$ are the equilibrium part of the energy density, the charge densities, and the pressure, respectively. The non-equilibrium parts δe, δn_i, and Π can arise due to the deviation of the state from the local-equilibrium state. The non-equilibrium part of the pressure $\Pi \equiv P_{\mathrm{tot}} - P(e_{\mathrm{eq}})$ is called bulk pressure.

Since the local state with diffusion is not a local-equilibrium state unlike the case of ideal hydrodynamics, a particular local-equilibrium state $(e_{\mathrm{eq}}, \{n_{i,\mathrm{eq}}\})$ close to the actual state should be picked up to define thermodynamic quantities. However, the choice of such local-equilibrium state is not unique. A corresponding local-equilibrium state cannot be determined only using thermodynamic considerations such as the second law. To determine the local-equilibrium state, an additional condition, called a matching condition, should be assumed.

In this thesis we adopt a local-equilibrium state in which the deviations of the energy and charge densities vanish [203]:

$$\delta e = \delta n_i = 0. \tag{3.71}$$

This condition is called the Landau matching condition and is commonly used in relativistic dissipative hydrodynamics. Under these conditions, the equilibrium part of the energy and charge densities are directly given by the actual energy and charge densities:

$$e_{\mathrm{eq}} = e = u_\alpha u_\beta T^{\alpha\beta}, \tag{3.72}$$

$$n_{i,\mathrm{eq}} = n_i = u_\alpha N_i^\alpha. \tag{3.73}$$

Hereafter, we use the symbols e and n_i for the equilibrium part instead of e_{eq} and $n_{i,\mathrm{eq}}$ because they are identical under the present matching condition. For further studies on frames and other matching conditions, see Ref. [210–214].

The currents (3.69) and (3.70) can be written in the form of the equilibrium parts plus the other

parts:

$$T^{\mu\nu} = T^{\mu\nu}_{\rm id} + \tau^{\mu\nu}, \tag{3.74}$$
$$N^{\mu}_{i} = N^{\mu}_{i\,\rm id} + \nu^{\mu}_{i}, \tag{3.75}$$
$$T^{\mu\nu}_{\rm id} \equiv eu^{\mu}u^{\nu} - \Delta^{\mu\nu}P(e), \tag{3.76}$$
$$N^{\mu}_{i\,\rm id} \equiv n_i u^{\mu}, \tag{3.77}$$
$$\tau^{\mu\nu} \equiv -\Delta^{\mu\nu}\Pi + 2W^{(\mu}u^{\nu)} + \pi^{\mu\nu}, \tag{3.78}$$

where $T^{\mu\nu}_{\rm id}, N_{i,\rm id}$ are the equilibrium part of the currents and have the same form with the currents in ideal hydrodynamics. The rest terms $\tau^{\mu\nu}, \nu^{\mu}_{i}$ are the dissipative part of the currents. Each term of dissipative parts $\Pi, W^{\mu}, \pi^{\mu\nu}, \nu^{\mu}_{i}$ is called dissipative current.

Then the hydrodynamic equations are rewritten as

$$\mathrm{D}e + (e + P + \Pi)\theta = 2W^{\mu}\mathrm{D}u_{\mu} - \nabla_{\mu}W^{\mu} + \pi^{\mu\nu}\sigma_{\mu\nu}, \tag{3.79}$$
$$\begin{aligned}(e + P + \Pi)\mathrm{D}u^{\mu} =& -\nabla_{\beta}[\pi^{\beta\mu} - g^{\beta\mu}(P + \Pi)] - u^{\mu}(W^{\alpha}\mathrm{D}u_{\alpha} + \pi^{\alpha\beta}\sigma_{\alpha\beta}) \\ & - \mathrm{D}W^{\mu} - \frac{4}{3}\theta W^{\mu} - (\sigma^{\mu\beta} + \omega^{\mu\beta})W_{\beta} + \pi^{\mu\beta}\mathrm{D}u_{\beta},\end{aligned} \tag{3.80}$$
$$\mathrm{D}n_i + n_i\theta = \nu^{\mu}_{i}\mathrm{D}u_{\mu} - \nabla_{\mu}\nu^{\mu}_{i}, \quad (i = 1, \ldots, n). \tag{3.81}$$

Here the independent fields are the equilibrium quantities: e, P, u^{μ}, and n_i, and the dissipative part: $W^{\mu}, \Pi, \pi^{\mu\nu}$, and ν^{μ}_{i}. The number of independent fields is $n+5$ for the equilibrium part while $3n+9$ for the dissipative part, so that $4n+14$ in total. On the other hand, the number of the equations is $n+5$ for the conservation laws and the equation of state, which is smaller than the number of fields. Thus, some additional equations are required. The number of the required equations is $3n+9$ which is the same as the number of fields of the dissipative currents.

Here we again borrow the knowledge of thermodynamics or statistical mechanics to close the hydrodynamic equations. What are needed are the expressions of dissipative currents in terms of equilibrium quantities and their derivatives, which are called constitutive equations:

$$\Gamma_a = \Gamma_a(T, \{\mu_i\}, \{X_b\}_b), \tag{3.82}$$

where Γ_a denotes a component of the dissipative currents $(\Pi, W^{\mu}, \pi^{\mu\nu}, \nu^{\mu}_{i})$, and X_b denotes a component of the thermodynamic forces. Note that X_b may contain higher orders of the derivatives of the thermodynamic variables such as $\nabla_{\mu}\nabla^{\mu}T$.

If the system is sufficiently close to the local-equilibrium state, the thermodynamic forces are small enough to enable expansion of the dissipative current (3.82) in terms of the power of the thermodynamic forces X_b:

$$\Gamma_a = \sum_{k=1}^{\infty}\sum_{b_1\ldots b_k} M_{ab_1\ldots b_k}(T, \{\mu_i\})X_{b_1}\ldots X_{b_k}, \tag{3.83}$$

where $M_a{}^{b_1\ldots b_k} = M_a{}^{b_1\ldots b_k}(T, \{\mu_i\})$ are phenomenological coefficients and reflect transport properties of the system. Note that the lowest order of the thermodynamic forces is $k = 1$ because the dissipative currents Γ_a should vanish in the absence of the thermodynamic forces $X_b = 0$.

If the thermodynamic forces are sufficiently small, the expansion (3.83) can be truncated up to a finite order of the derivatives. In this section we consider the simplest first-order case:

$$\Gamma_a = M^{(1)}_{ab}X^{(1)}_{b}, \tag{3.84}$$

where the thermodynamic forces $X^{(1)}_{b}$ are the first-order derivatives of thermodynamic quantities: (θ, $\sigma_{\mu\nu}, \omega_{\mu\nu}, \nabla_{\mu}T, \nabla_{\mu}\mu_i, \mathrm{D}u_{\mu}, \mathrm{D}T, \mathrm{D}\mu_i$). The phenomenological coefficients of the first-order terms, $M_a{}^{b}$, are called the Onsager coefficients. The first-order constitutive equations (3.84) can be written down for

each of the dissipative currents:

$$\Pi = M_{\Pi\theta}\theta + M_{\Pi T}\mathrm{D}T + \sum_{i=1}^{n} M^i_{\Pi\mu}\mathrm{D}\mu_i, \tag{3.85}$$

$$\pi^{\mu\nu} = M_{\pi\sigma}\sigma^{\mu\nu}, \tag{3.86}$$

$$W^\mu = M_{qu}\mathrm{D}u^\mu + M_{qT}\nabla^\mu T + \sum_{i=1}^{n} M^i_{q\mu}\nabla^\mu\mu_i, \tag{3.87}$$

$$\nu^\mu_j = M_{\nu_j u}\mathrm{D}u^\mu + M_{\nu_j T}\nabla^\mu T + \sum_{i=1}^{n} M^i_{\nu_j\mu}\nabla^\mu\mu_i, \tag{3.88}$$

where M's are the Onsager coefficients. It should be noticed here that only the thermodynamic forces corresponding to the same representation with the dissipative currents can appear in the right hand sides of the constitutive equations. If other terms appear in the right hand side, the isotropy of the constitutive equation is broken. Such restriction coming from the symmetry of the system is called the Curie-Prigogine principle [215].

3.5.3 Second law of thermodynamics

By considering the second law of thermodynamics, we can make further constraints on the phenomenological relations (3.85)-(3.88).

According to the second law, the entropy of the whole system should not decrease. In relativistic hydrodynamics, the second law of the local states is expressed using the entropy current S^μ:

$$\Phi \equiv T\partial_\mu S^\mu \geq 0. \tag{3.89}$$

The divergence $\partial_\mu S^\mu$ represents the entropy production rate in a unit volume, and the dissipative function Φ is the energy dissipation rate in a unit volume. The function represents the heat transfer in a unit of time $\delta Q = TdS$, namely, the increase of the internal energy e coming from the kinetic energy and potential energies of the fluid fields. Using thermodynamic relations and hydrodynamic equations, the dissipative function and the entropy production rate can be written as a function of other fluid fields.

To apply thermodynamic relations we first decompose the entropy current:

$$S^\mu = (s + \delta s)u^\mu + \Delta^\mu{}_\alpha S^\alpha \tag{3.90}$$

$$= su^\mu + \sigma^\mu, \tag{3.91}$$

$$\sigma^\mu \equiv S^\mu - su^\mu = \delta s u^\mu + \Delta^\mu{}_\alpha S^\alpha, \tag{3.92}$$

where $s = s_{\mathrm{eq}}(e, \{n_i\})$ is the density of the equilibrium entropy, and $\delta s \equiv u_\mu S^\mu - s_{\mathrm{eq}}(e, \{n_i\})$ is the deviation of the entropy current from its equilibrium value. The first term in (3.91) su^μ is the equilibrium part of the entropy current, and the second term σ^μ is the non-equilibrium part. The dissipative function is then written as

$$\Phi = T(\mathrm{D}s + s\theta) + T\partial_\mu\sigma^\mu. \tag{3.93}$$

To find the expression of the contribution from the equilibrium entropy $\mathrm{D}s + s\theta$, the first law of thermodynamics can be used:

$$dE + PdV = TdS + \sum_{i=1}^{n} \mu_i dN_i, \tag{3.94}$$

where E, V, S, N_i are the energy, the volume in the local rest frame, the equilibrium entropy, and the charges, respectively. The first law can be rewritten in terms of the densities e, s, and n_i:

$$\mathrm{D}e + (e + P)\theta = T(\mathrm{D}s + s\theta) + \sum_{i=1}^{n} \mu_i(\mathrm{D}n_i + n_i\theta). \tag{3.95}$$

Here we replaced the differential d with the substantial derivative D and used the relation[2] $\mathrm{D}X/V = \mathrm{D}\chi + \chi\theta$ where X and $\chi \equiv X/V$ are the extensive variable and its density, respectively. Each term can be expressed by non-equilibrium counterparts using the hydrodynamic equations (3.41) and (3.45), and the dissipative function (3.93). Then, the first law becomes

$$-\Pi\theta + W^\mu \mathrm{D}u_\mu - \partial_\mu W^\mu + \pi^{\mu\nu}\sigma_{\mu\nu} = (\Phi - T\partial_\mu\sigma^\mu) - \sum_{i=1}^{n} \mu_i \partial_\mu \nu_i^\mu. \tag{3.96}$$

Finally, the dissipative function reads

$$\begin{aligned}\Phi = &-\Pi\theta + \pi^{\mu\nu}\sigma_{\mu\nu} + W^\mu\left(\mathrm{D}u_\mu - \frac{1}{T}\nabla_\mu T\right) - \sum_{i=1}^{n}\nu_i^\mu T\nabla_\mu\frac{\mu_i}{T} \\ &+ T\partial_\mu\left(\sigma^\mu - \frac{W^\mu - \sum_{i=1}^{n}\mu_i\nu_i^\mu}{T}\right).\end{aligned} \tag{3.97}$$

It should be noticed in the above derivation that the expression of the dissipative function (3.97) is actually the first law (3.94), which is the conservation of the total energy. It reflects the fact that the heat which the internal energy receives is the loss of the kinetic energy and potential energies of fluid fields.

In the first-order case, the dissipative currents and σ^μ are expressed in terms of the linear combinations of the first-order thermodynamic forces. Thus, the first line of Eq. (3.97) has a quadratic form with respect to the thermodynamic forces, and the second line is linear in the thermodynamic forces.

To ensure the second law: $\Phi \geq 0$ for arbitrary configuration of fluid fields, the linear term should vanish. As a result, it can be shown that (see B.1 for details):

$$\sigma^\mu = \frac{W^\mu - \sum_{i=1}^{n}\mu_i\nu_i^\mu}{T}, \tag{3.98}$$

In addition, the dissipative function becomes quadratic in the thermodynamic forces:

$$\Phi = \sum_a \Gamma_a X_{\Gamma_a}, \tag{3.99}$$

where Γ_a denotes a dissipative current, and X_{Γ_a} is the corresponding conjugate thermodynamic force. The explicit expression for those currents and forces are given in Table 3.2.

Dissipative current Γ_a	Conjugate thermodynamic force X_{Γ_a}	Independent components
Π	$-\theta$	1
$\pi^{\mu\nu}$	$\sigma_{\mu\nu}$	5
W^μ	$X_\mu^W \equiv \mathrm{D}u_\mu - \frac{1}{T}\nabla_\mu T$	3
ν_i^μ	$X_\mu^i \equiv -T\nabla_\mu\frac{\mu_i}{T}$	$3n$

Table 3.2: The dissipative currents and the corresponding conjugate thermodynamic forces are shown. The number of the independent components are shown in the right column. The total number of components is $3n+9$. Since, a local rest frame u^μ is always chosen using the currents, the total number of independent components is effectively $3n+6$ in practice.

Since the second law $\Phi \geq 0$ tells that the quadratic form (3.99) is positive semidefinite, the dissipative currents Γ_a can be written in terms of linear combinations of the conjugate thermodynamic forces X_{Γ_b}:

$$\Gamma_a = \sum_b M'_{ab} X_{\Gamma_b}, \tag{3.100}$$

$$\Phi = \sum_{a,b} M'_{ab} X_{\Gamma_a} X_{\Gamma_b}, \tag{3.101}$$

[2] Using Eq. (3.38): $\theta = \mathrm{D}V/V$ where V is the volume in the local rest frame, the relation can be obtained: $\mathrm{D}\chi = \mathrm{D}(X/V) = \mathrm{D}X/V - (X/V)(\mathrm{D}V/V) = \mathrm{D}X/V - \chi\theta$.

where M'_{ac} is the Onsager coefficients. The Onsager reciprocal relations tell that the coefficients are symmetric due to the time reversibility of the microscopic system: $M'_{ab} = M'_{ba}$. In addition, the coefficient matrix of the quadratic form M'_{ab} is positive semidefinite, i.e., the eigenvalues are not negative.

As a result the explicit form of the constitutive equations (3.100) can be written down:

$$\Pi = -\zeta\theta, \tag{3.102}$$
$$\pi^{\mu\nu} = 2\eta\sigma^{\mu\nu}, \tag{3.103}$$
$$W^\mu = -\lambda\Delta^{\mu\nu}X^W_\nu - \sum_{i=1}^{n}\lambda_i\Delta^{\mu\nu}X^i_\nu, \tag{3.104}$$
$$\nu^\mu_i = -\lambda_i\Delta^{\mu\nu}X^W_\mu - \sum_{i=1}^{n}\kappa_{ij}\Delta^{\mu\nu}X^j_\nu, \tag{3.105}$$

where ζ, 2η, $-\lambda\Delta^{\mu\nu}$, $-\lambda_i\Delta^{\mu\nu}$, and $-\kappa_{ij}\Delta^{\mu\nu}$ are Onsager coefficients corresponding to M'_{ab}. Note that $-\Delta^{\mu\nu} = \mathrm{diag}(0,1,1,1)_{\mathrm{LRF}}$ is used as a spatial Kronecker delta in the local rest frame. While the energy current (W^μ, X^W_μ) and the charge diffusion (ν^μ_i, X^i_μ) mix with each other, the shear stress $(\pi^{\mu\nu}, \sigma_{\mu\nu})$ and the bulk pressure $(\Pi, -\theta)$ do not mix with another part due to the Curie-Prigogine principle. The coefficient λ_i is shared by the energy current and the diffusion, and the coefficient matrix of the charge part κ_{ij} is symmetric: $\kappa_{ij} = \kappa_{ji}$ due to the Onsager reciprocal relations. Not to break the second law of thermodynamics, the coefficients ζ, and η should be non-negative, and the following matrix should have positive semidefinite eigenvalues:

$$\begin{pmatrix} \kappa & \kappa_1 & \cdots & \kappa_n \\ \kappa_1 & \kappa_{11} & \cdots & \kappa_{n1} \\ \vdots & \vdots & \ddots & \vdots \\ \kappa_n & \kappa_{1n} & \cdots & \kappa_{nn} \end{pmatrix}. \tag{3.106}$$

The coefficient $\zeta(e, \{n_i\})$ is the bulk viscosity coefficient, and $\eta(e, \{n_i\})$ is the shear viscosity coefficient. Those viscosity coefficients are interpreted as momentum diffusion in the parallel and perpendicular directions to the momentum, respectively. The coefficients $\kappa(e, \{n_i\})$ and $\kappa_{ij}(e, \{n_i\})$ are the energy conductivity and charge diffusion coefficients, respectively. The coefficient of the cross term κ_i is called a thermodiffusion coefficient. The thermodiffusion term in Eq. (3.105) implies the diffusion caused by the gradient of temperature, which is known as the Soret effect. The reciprocal term in Eq. (3.104) denotes the energy flux caused by gradient of charge densities known as the Dufour effect. All those coefficients are positive or positive semidefinite. As a result, the spatial gradients of fluid fields decrease, and the entropy is ensured to increase.

In the Landau frame, the constitutive equations have simple forms due to the vanishing energy flux W^μ:

$$\Pi = -\zeta\theta, \tag{3.107}$$
$$\pi^{\mu\nu} = 2\eta\sigma^{\mu\nu}, \tag{3.108}$$
$$\nu^\mu_i = \sum_{i=1}^{n}\kappa_{ij}T\nabla^\mu\frac{\mu_j}{T}. \tag{3.109}$$

While, in the Eckart frame for a single component case, the charge diffusion ν^μ_1 vanishes instead:

$$\Pi = -\zeta\theta, \tag{3.110}$$
$$\pi^{\mu\nu} = 2\eta\sigma^{\mu\nu}, \tag{3.111}$$
$$W^\mu = -\kappa\left(\mathrm{D}u^\mu - \frac{1}{T}\nabla^\mu T\right) \tag{3.112}$$
$$= \lambda\nabla^\mu T - \lambda T\mathrm{D}u^\mu \tag{3.113}$$
$$= -\lambda\frac{n_1T^2}{e+P}\nabla^\mu\frac{\mu_1}{T} + O(\partial^2). \tag{3.114}$$

Here we defined the thermal conductivity $\lambda \equiv \kappa/T$. To obtain the last line, we used the hydrodynamic equation (3.80). Note that the second-order terms $O(\partial^2)$ [3] in the last line cannot be neglected even in the first order case since the second law is broken without those terms.

3.6 Causal dissipative hydrodynamics

3.6.1 Causality of the first-order theory and relaxation time

In the previous section we obtained the first-order constitutive equations. However, the first-order relativistic theory has problems of acausality and related instabilities [216–218]. The equation has infinite propagating speed of signals, which is incompatible with the relativistic description of the system with the light velocity as an upperbound.

The same problem is already appeared in the non-relativistic hydrodynamic equations. The equation describing diffusion phenomena in non-relativistic system has typically a parabolic partial differential equation known as a heat equation or a diffusion equation:

$$\frac{\partial}{\partial t}\rho(x,t) = -\frac{\partial}{\partial x}\cdot j(x,t), \tag{3.115}$$

$$j(x,t) = -D\frac{\partial}{\partial x}\rho(x,t), \tag{3.116}$$

$$\left(\frac{\partial}{\partial t} - D\frac{\partial^2}{\partial x^2}\right)\rho(x,t) = 0, \tag{3.117}$$

where ρ is the density of a conserved quantity, and j is the corresponding dissipative current. Eq. (3.115) is the conservation law, and Eq. (3.116) is the Fick's law which is a constitutive equation describing the dissipative current. By combining these two equations, the diffusion equation in the last line is obtained. The above parabolic equation has a propagator of the Gaussian form:

$$G(x,t) = \frac{1}{\sqrt{4Dt}}\exp\left(-\frac{x^2}{4Dt}\right), \tag{3.118}$$

$$\rho(x,t) = \int dx' G(x-x',t)\rho(x',0). \tag{3.119}$$

For non-zero time $t > 0$, $G(t, x-x')$ is always positive. Consequently, the equation has infinite propagating speed of signals.

To overcome the problem of the infinite propagating speed, a relaxation time τ_R can be introduced in (3.116) [219–221]:

$$\tau_R\frac{\partial}{\partial t}j + j = -D\frac{\partial}{\partial x}\rho. \tag{3.120}$$

Note that the current $j(t,x)$ is now another dynamical variable unlike in (3.116) where the current can be written in terms of $\rho(t,x)$. The resulting equation has a form of the telegrapher's equation:

$$\left(\tau_R\frac{\partial^2}{\partial t^2} + \frac{\partial}{\partial t} + D\frac{\partial^2}{\partial x^2}\right)\rho(t,x) = 0. \tag{3.121}$$

The solution with the initial condition $j(x, t=0) = 0$ has the following form [222, 223]:

$$\rho = \int dx' G(x-x',t)\rho(x',0), \tag{3.122}$$

$$G(t,x) = e^{-t/2\tau_R}\left(\frac{1}{2}\delta(vt-|x|) + \frac{1}{4v\tau_R}\Theta(vt-|x|)\left[I_0(u) + \frac{t}{2u\tau_R}I_1(u)\right]\right), \tag{3.123}$$

$$u = \frac{\sqrt{v^2t^2-x^2}}{2v\tau_R}. \tag{3.124}$$

[3] The second-order terms have the following form:

$$\frac{1}{e+P+\Pi}\left(-\frac{\Pi\nabla^\mu P}{e+P} + \nabla^\mu\Pi - \Delta^\mu{}_\alpha\partial_\beta\pi^{\alpha\beta} - 2\Delta^\mu{}_\alpha\partial_\beta u^{(\alpha}W^{\beta)}\right).$$

where $v^2 \equiv D/\tau_R$ is the velocity of a wavefront. The functions $I_0(u)$ and $I_1(u)$ are the modified Bessel functions of first kind. We can see that the Green function $G(x,t)$ vanishes for a position $|x| > vt$. Consequently, the signal speed is finite $v = \sqrt{D/\tau_R}$. One can choose sufficiently small τ_R to make the signal speed slower than that of light.

Full relativistic hydrodynamic equations of the first-order theory has a similar structure and the same problem [216, 217]. In addition, the first-order equations have unstable modes related to the acausality [217]. Those problems can be solved similarly to the above case by adding relaxation times into the constitutive equations (3.102)-(3.105):

$$\tau_\Pi \mathrm{D}\Pi + \Pi = -\zeta\theta, \tag{3.125}$$

$$\tau_\pi \Delta^{\mu\nu}{}_{\alpha\beta}\mathrm{D}\pi^{\alpha\beta} + \pi^{\mu\nu} = 2\eta\sigma^{\mu\nu}, \tag{3.126}$$

$$\tau_W \Delta^\mu{}_\alpha \mathrm{D}W^\alpha + W^\mu = -\kappa\left(\mathrm{D}u^\mu - \frac{1}{T}\nabla T\right) + \sum_{i=1}^n \kappa_i T\nabla^\mu\frac{\mu_i}{T}, \tag{3.127}$$

$$\tau_i \Delta^\mu{}_\alpha \mathrm{D}\nu_i^\alpha + \nu_i^\mu = -\kappa_i\left(\mathrm{D}u^\mu - \frac{1}{T}\nabla T\right) + \sum_{j=1}^n \kappa_{ij} T\nabla^\mu\frac{\mu_j}{T}. \tag{3.128}$$

where $\tau_\Pi, \tau_\pi, \tau_W$, and τ_{ij} are the relaxation times of each dissipative current. Those constitutive equations are called the *simplified Israel-Stewart equations*. Here we added the relaxation terms by hand. The relaxation terms $\tau_\Pi \mathrm{D}\Pi$, etc. are a part of the second-order terms, and are naturally introduced in the second-order dissipative hydrodynamics.

3.6.2 Second-order hydrodynamics

The second-order relativistic hydrodynamics was first studied by Israel and Stewart [224, 225] by extending its non-relativistic version [226].

In second-order hydrodynamics, the dissipative currents can be written in terms of thermodynamic forces up to the second order in derivatives:

$$\Gamma_a = \sum_b M_{ab}^{(1)} X_b^{(1)} + \sum_b M_{ab}^{(2)} X_b^{(2)}, \tag{3.129}$$

The second order terms $X_a^{(2)}$ contain derivatives of first-order thermodynamic forces such as $\mathrm{D}\theta$, $\nabla_\mu\nabla^\mu T$, $\Delta^\mu{}_\alpha\nabla_\beta\sigma^{\alpha\beta}$, etc., and products of two first-order thermodynamic forces such as $\theta\sigma^{\alpha\beta}$, $(\nabla_\mu T)(\nabla^\mu\mu_i)$, $\sigma_\alpha{}^{\langle\mu}\sigma^{\nu\rangle\alpha}$, etc.

The non-equilibrium part of the entropy current can also be written in terms of those thermodynamic forces:

$$S^\mu = su^\mu + \sigma^\mu_{(1)} + Q^\mu, \tag{3.130}$$

$$\sigma^\mu_{(1)} = \frac{W^\mu - \sum_{i=1}^n \mu_i\nu_i^\mu}{T}, \tag{3.131}$$

$$Q^\mu = \sum_a M_a^{(2)S} X_a^{(2)\mu}, \tag{3.132}$$

where $\sigma^\mu_{(1)}$ is the first-order deviation of the entropy current obtained in the previous section (3.98). The last term Q^μ is the second-order part of the entropy current, and $M_a^{(2)S}$ are phenomenological coefficients. The dissipative function (3.97) can be expressed with those terms:

$$\Phi = -\Pi\theta + \pi^{\mu\nu}\sigma_{\mu\nu} + W^\mu\left(\mathrm{D}u_\mu - \frac{1}{T}\nabla_\mu T\right) - \sum_{i=1}^n \nu_i^\mu T\nabla_\mu\frac{\mu_i}{T} + T\partial_\mu Q^\mu. \tag{3.133}$$

The constitutive equations of the dissipative currents are constrained by the second law of thermodynamics similarly to the first-order case.

Israel and Stewart derived the second-order relativistic dissipative hydrodynamics in two ways: a phenomenological derivation and a derivation from a transport theory [224,225]. In the phenomenological derivation, they wrote the second-order part of the entropy current Q^μ as a quadratic form of dissipative

currents which are first-order in thermodynamic forces, and obtained constitutive equations using the second law.

In a single component case $n = 1$, the current Q^μ is written in the following quadratic form:

$$\begin{aligned} TQ^\mu =& \frac{1}{2}u^\mu(-\beta_0\Pi^2 + \beta_1 q_\mu q^\mu - \beta_2 \pi_{\alpha\beta}\pi^{\alpha\beta}) + \alpha_0 \Pi q^\mu - \alpha_1 \pi^\lambda{}_\mu q^\mu \\ &+ \frac{1}{2}u^\mu \gamma_1 T W^\alpha W_\alpha + \gamma_2 T(\pi^\mu{}_\alpha W^\alpha - \Pi W^\mu). \end{aligned} \tag{3.134}$$

where $q^\mu = W^\mu - \frac{e+P}{n_1}\nu_1^\mu$, and $\beta_i(e,n)$, $\alpha_i(e,n)$, and $\gamma_i(e,n)$ are phenomenological coefficients. The dissipative function becomes

$$\begin{aligned} \Phi =& \Pi\left[-\theta - \beta_0 \mathrm{D}\Pi + \alpha_0 \partial_\mu q^\mu - \gamma_2 T \partial_\mu W^\mu + \Pi T \partial_\mu \frac{\beta_0 u^\mu}{2T}\right] \\ &+ \pi^{\alpha\beta}\left[\sigma_{\alpha\beta} - \beta_2 \mathrm{D}\pi_{\alpha\beta} - \pi_{\alpha\beta} T\partial_\mu \frac{\beta_2 u^\mu}{2T} - \alpha_1 \partial_\alpha q_\beta + \gamma_2 T \partial_\alpha W_\beta\right] \\ &+ q^\alpha\left[\frac{n_1 T}{e+P}\partial_\alpha \frac{\mu_1}{T} + \beta_1 \mathrm{D}q_\alpha + q_\alpha T \partial_\mu \frac{\beta_1 u^\mu}{2T} + \partial_\alpha(\alpha_0\Pi) - \partial_\mu(\alpha_1 \pi^\mu{}_\alpha)\right] \\ &+ W^\alpha\left[\mathrm{D}u_\alpha - \frac{\nabla_\alpha P}{e+P} + \gamma_1 T \mathrm{D}W_\alpha + W_\alpha T\partial_\mu \frac{\gamma_1 u^\alpha}{2} + \partial_\mu(\gamma_2 T \pi^\mu{}_\alpha) - \partial_\alpha(\gamma_2 T \Pi)\right]. \end{aligned} \tag{3.135}$$

Note that W^μ vanishes in the Landau frame, and $W^\mu = q^\mu$ in the Eckart frame. Thus the current W^μ is not an independent current. The independent dissipative currents here are Π, $\pi^{\mu\nu}$, and q^μ. To fulfill the second law of thermodynamics $\Phi \geq 0$, the dissipative currents can be determined so that the dissipative function has the following form:

$$\Phi = \frac{\Pi^2}{\zeta} + \frac{\pi^{\alpha\beta}\pi_{\alpha\beta}}{2\eta} - \frac{q^\alpha q_\alpha}{\lambda T}. \tag{3.136}$$

In the Landau frame the resulting constitutive equations become

$$\tau_\Pi \mathrm{D}\Pi + \Pi = \zeta\left[-\theta + \alpha_0 \partial_\alpha q^\alpha + \Pi T \partial_\alpha \frac{\beta_0 u^\alpha}{2T}\right], \tag{3.137}$$

$$\tau_\pi \Delta^{\mu\nu}{}_{\alpha\beta}\mathrm{D}\pi^{\alpha\beta} + \pi^{\mu\nu} = 2\eta\left[\sigma^{\mu\nu} - \pi^{\mu\nu} T\partial_\alpha \frac{\beta_2 u^\alpha}{2T} - \alpha_1 \partial^{\langle\mu} q^{\nu\rangle}\right], \tag{3.138}$$

$$\tau_q \Delta^\mu{}_\alpha \mathrm{D}q^\alpha + q^\mu = -\lambda T\left[\frac{n_1 T}{e+P}\nabla^\mu \frac{\mu_1}{T} + q^\mu T \partial_\alpha \frac{\beta_1 u^\alpha}{2T} + \nabla^\mu(\alpha_0\Pi) - \Delta^\mu{}_\alpha \partial_\beta(\alpha_1 \pi^{\alpha\beta})\right], \tag{3.139}$$

where $\tau_\Pi = \zeta\beta_0$, $\tau_\pi = 2\eta\beta_2$ and $\tau_q = \lambda T \beta_1$ are relaxation times.

In the Eckart frame the dissipative currents become

$$\tau_\Pi \mathrm{D}\Pi + \Pi = \zeta\left[-\theta + \bar{\alpha}_0 \partial_\alpha q^\alpha + \Pi T \partial_\alpha \frac{\beta_0 u^\alpha}{2T}\right], \tag{3.140}$$

$$\tau_\pi \Delta^{\mu\nu}{}_{\alpha\beta}\mathrm{D}\pi^{\alpha\beta} + \pi^{\mu\nu} = 2\eta\left[\sigma^{\mu\nu} - \pi^{\mu\nu} T\partial_\alpha \frac{\beta_2 u^\alpha}{2T} - \bar{\alpha}_1 \partial^{\langle\mu} q^{\nu\rangle}\right], \tag{3.141}$$

$$\bar{\tau}_q \Delta^\mu{}_\alpha \mathrm{D}q^\alpha + q^\mu = -\lambda T\left[\mathrm{D}u^\mu - \nabla^\mu \ln T + q^\mu T \partial_\alpha \frac{\bar{\beta}_1 u^\alpha}{2T} + \nabla^\alpha(\bar{\alpha}_0\Pi) - \Delta^\mu{}_\alpha \partial_\beta(\bar{\alpha}_1 \pi^{\alpha\beta})\right], \tag{3.142}$$

where $\bar{\beta}_1 \equiv \beta_1 + \gamma_1 T$, $\bar{\alpha}_0 \equiv \alpha_0 - \gamma_2 T$, and $\bar{\alpha}_1 \equiv \alpha_1 - \gamma_2 T$. We here defined another relaxation time: $\bar{\tau}_q \equiv \lambda T \bar{\beta}_1$.

Those equations are dynamical equations since they contain the time derivative of dissipative currents. In other words the dissipative currents are now dynamical variables which evolve under the constitutive equations. This kind of treatment of irreversible processes is called extended thermodynamic theory, or extended irreversible thermodynamics [226–230]. The constitutive equations have the form of relaxation equation as in the simplified Israel-Stewart equations (3.125)-(3.128). They actually have finite signal speed and are causal for sufficiently large relaxation times [217].

3.7 Brief summary

The dynamical equations of relativistic hydrodynamics are the conservation law of the currents (T^μ, N_i^μ). To close the equations, the equation of state and the constitutive equations, which describe the properties of the matter, are needed. To apply the equation of state and the constitutive equations, one has to choose a local rest frame of the matter, or the flow velocity u^μ, and define thermodynamic quantities by the decomposition of (T^μ, N_i^μ) with u^μ.

By assuming the conserved currents $(T^{\mu\nu}, N_i^\mu)$ to have the value in static equilibrium, the equations of relativistic ideal hydrodynamics can be obtained. The deviation of currents from the equilibrium value can be taken into account by expanding them with thermodynamic forces, namely, gradients of fluid fields. Such hydrodynamics is called relativistic dissipative hydrodynamics. In the constitutive equations of the first-order dissipative hydrodynamics, the dissipative currents are assumed to be linear in derivatives of fluid fields. The structure of the constitutive equations is constrained by the second law of thermodynamics, and by the symmetry of the system including isotropy and the time reversibility of microscopic dynamics. The resulting equation is the relativistic version of the Navier-Stokes equation. However, the first-order theory has a problem: superluminal propagation of signals and instabilities. To overcome these problems, relaxation terms can be added to the constitutive equations. The relaxation terms are second-order in the derivatives, and thus causal dissipative hydrodynamics is second-order or higher.

In the following chapters, we adopt the Landau frame in which the energy current W^μ always vanishes.

Chapter 4

Causal hydrodynamic fluctuations

In this chapter we introduce thermal fluctuations to causal dissipative hydrodynamics. We discuss their interesting properties using the relations such as fluctuation-dissipation relations and properties of response functions specific to relativistic systems.

The thermal fluctuations during the spacetime evolution of fluids are called hydrodynamic fluctuations, which are first introduced by Landau and Lifshitz in non-relativistic hydrodynamic equations [232]. Such hydrodynamics with the hydrodynamic fluctuations are called fluctuating hydrodynamics. The hydrodynamic equations have terms representing the fluctuations which have random values as in the case of Langevin equation for the Brownian motion. The power spectra of the noise terms are determined by fluctuation-dissipation theorem. The hydrodynamic fluctuations in relativistic systems are studied by Calzetta using the divergence type theory of relativistic hydrodynamics [233]. He considered the fluctuating hydrodynamic equations in a causal second-order dissipative hydrodynamics as well as in the first-order relativistic dissipative hydrodynamics. In his work the hydrodynamic fluctuations are assumed to be white noise. However it turned out through our work [231] that the noise correlation in relativistic systems is not so trivial and contains interesting physics as we will show in this chapter.

We first introduce an integral form of constitutive equations as a counterpart of a commonly used differential form in section 4.1. Then we apply the fluctuation-dissipation relation to the integral form and find colored noise correlations in general causal hydrodynamics in section 4.2. In a relativistic hydrodynamic models for high-energy nuclear collisions, non-linear hydrodynamic equations should be solved to describe the highly non-uniform expansion of the matter. To treat the hydrodynamic fluctuations in the model, the tensor structure of the dissipative currents and the noise correlations should be taken into account, which is described in section 4.3. Finally we consider the condition for the noise terms in the differential form to be white in section 4.4 and find an interesting restriction of the constitutive equations in relativistic systems.

4.1 Integral form of constitutive equation and memory function

In order to consider the fluctuation-dissipation relation in a causal theory, we first have to rewrite the constitutive equations in an explicit form with respect to dissipative currents. In the first-order case, the dissipative currents can be written in the following form:

$$\Gamma(x) = \kappa F(x), \tag{4.1}$$

where $\Gamma(x)$ is a dissipative current, and $F(x)$ and κ are the corresponding first-order thermodynamic force and the Onsager coefficient, respectively.

In the simplified Israel-Stewart case (3.125)-(3.128), the constitutive equation has the following form:

$$\Gamma(x) + \tau_R(x)\mathrm{D}\Gamma(x) = \kappa(x)F(x). \tag{4.2}$$

The above equation is not an explicit form in the dissipative current Γ. However the dissipative current $\Gamma(x)$ can be formally solved as

$$\Gamma(x) = \int_{-\infty}^{\tau} \frac{d\tau'}{\tau_R(\tau')} \exp\left(-\int_{\tau'}^{\tau} \frac{d\tau''}{\tau_R(\tau'')}\right) \kappa(x')F(x'), \tag{4.3}$$

where $\tau_R = \tau_R(e, \{n_i\})$ is the relaxation time. Here we introduced the proper time of the fluid particle τ:

$$\tau(t, \boldsymbol{x}) \equiv \tau(t_0, \boldsymbol{x}) + \int_{t_0}^{t} \frac{dt'}{u^0}[1 - u^i \partial_i \tau(t', \boldsymbol{x})]. \tag{4.4}$$

A fluid particle can be specified with comoving spatial coordinates $\boldsymbol{\sigma}$:

$$\boldsymbol{\sigma}(t, \boldsymbol{x}) \equiv \boldsymbol{\sigma}(t_0, \boldsymbol{x}) - \int_{t_0}^{t} \frac{dt'}{u^0} u^i \partial_i \boldsymbol{\sigma}(t', \boldsymbol{x}). \tag{4.5}$$

The spacetime point x^μ and the comoving coordinates $\sigma^\mu = (\tau, \boldsymbol{\sigma})$ are in one-to-one correspondence, and the position x can be expressed as a function of the comoving coordinates: $x = x(\tau, \boldsymbol{\sigma})$. A fixed $\boldsymbol{\sigma} \equiv$ const defines the trajectory of a fluid particle which is called a pathline. The pathline of the fluid particle can be simply interpreted as the world line of the fluid particle. The integration in (4.3) is performed on the pathline which can be explicitly written as

$$\Gamma(x(\tau, \boldsymbol{\sigma})) = \int_{-\infty}^{\tau} \frac{d\tau'}{\tau_R(\tau', \boldsymbol{\sigma})} \exp\left(- \int_{\tau'}^{\tau} \frac{d\tau''}{\tau_R(\tau'', \boldsymbol{\sigma})} \right) \kappa(\tau', \boldsymbol{\sigma}) F(x(\tau', \boldsymbol{\sigma})). \tag{4.6}$$

Hereafter we use a simple notation like (4.3) for this kind of integration.

Here we notice that there are two representations of the constitutive equations which are equivalent to each other. One is *a differential form of the constitutive equation* like (4.2). The other is *an integral form of the constitutive equation* like (4.3).

In a linear-response regime, the dissipative currents can be written in terms of the first-order thermodynamic force and a linear-response function [239]:

$$\Gamma(x) = \int d^4x' G(x, x') \kappa(x') F(x'), \tag{4.7}$$

where $G(x, x')\kappa(x')$ is the linear-response function. We factored out the Onsager coefficient κ from the function G for simplicity of later discussions. The first-order constitutive equation (4.1) corresponds to the case $G(x, x') = \delta^{(4)}(x - x')$, and the simplified Israel-Stewart equation (4.3) corresponds to the case

$$G(x, x') = \frac{1}{\tau_R(\tau')} \exp\left(- \int_{\tau'}^{\tau} \frac{d\tau''}{\tau_R(\tau'')} \right) \theta^{(4)}(\sigma - \sigma'), \tag{4.8}$$

$$\theta^{(4)}(\sigma - \sigma') \equiv \Theta(\tau - \tau') \delta^{(3)}(\boldsymbol{\sigma} - \boldsymbol{\sigma}') \left| \frac{\partial \sigma'^\mu}{\partial x^\alpha} \right|, \tag{4.9}$$

where $|\frac{\partial \sigma^\mu}{\partial x^\alpha}|$ is a Jacobian. The information of the thermodynamic force of the past remains in a non-equilibrium state of the local system, and the effect appears in dissipative currents. The response function describes such effects of thermodynamic forces on dissipative currents. The response function is also called a *memory function* [239] which we will use in this thesis.

It is in order here to enumerate the general properties of the memory function $G(x, x')$:

- The function is retarded: $G(x, x') = 0$ for $x^0 < x'^0$, since the dissipative current is determined by the present and past values of the thermodynamic force.

- The function vanishes for spatially distant two points due to causality:

$$G(x, x') = 0, \quad \text{for } (x - x')^2 < 0. \tag{4.10}$$

- The function goes to zero in a finite time: $G(x, x') \to 0$ as $x^0 - x'^0 \to \infty$. The dissipative currents should not depend on a thermodynamic force of infinite past since the system near the equilibrium should forget the information of thermodynamic forces within a finite time.

- If the background fields are in a uniform global equilibrium, the memory function acquires a translational symmetry: $G(x, x') = G(x - x')$.

4.2 Fluctuation-dissipation relation and colored noise

In the previous section, we wrote down the integral form of the constitutive equation (4.7). However the equation describes merely an ensemble averaged behavior of the dissipative currents. In an actual system with finite size of fluid elements, finite deviations from the ensemble average can arise. That is the hydrodynamic fluctuations:

$$\delta\Gamma \equiv \Gamma - \int d^4x' G(x-x')\kappa F(x') \neq 0. \tag{4.11}$$

This fluctuation cannot be uniquely determined only with macroscopic information, so that it is treated as a random variable as in the case of the Langevin equation. The statistical behavior of the thermal fluctuations around the local-equilibrium state is related to the memory function $G(x,x')$ through fluctuation-dissipation theorem (FDT), which leads to the fluctuation-dissipation relation (FDR):

$$\langle \delta\Gamma(x)\delta\Gamma(x')\rangle = G(x,x')\kappa(x')T(x') + T(x)\kappa(x)G(x',x)^{\mathrm{T}}, \tag{4.12}$$

where G^{T} denotes a transpose of a matrix G. Note that, in the case of a multi-component dissipative current, the memory function G and the Onsager coefficients κ are matrices. The transpose of the Onsager coefficients can be omitted since they are symmetric due to the Onsager reciprocal relation: $\kappa^{\mathrm{T}} = \kappa$. An example of the FDR (4.12) is the generalized Green-Kubo formula [240, 241] (see Appendix C.1).

In the case of the first-order dissipative hydrodynamics, the FDR becomes a delta function:

$$\langle \Gamma(x)\Gamma(x')\rangle = 2T(x)\kappa(x)\delta^{(4)}(x-x'). \tag{4.13}$$

This kind of fluctuations are called white noise since the power spectrum of the delta function in Fourier space is constant. In the first-order theory, the hydrodynamic fluctuations do not have autocorrelation.

In the case of causal dissipative hydrodynamics, the FDR does not become a delta function since the memory function should have a non-zero relaxation time in causal theory. Therefore the fluctuations in different times can have non-zero correlation. Such fluctuations are called colored noise. In the simplified Israel-Stewart case (4.3), the FDR becomes

$$\langle \Gamma(x)\Gamma(x')\rangle = \left[\frac{T(\tau')\kappa(\tau')\theta^{(4)}(\sigma-\sigma')}{\tau_R(\tau')} + \frac{T(\tau)\kappa(\tau)\theta^{(4)}(\sigma'-\sigma)}{\tau_R(\tau)}\right] \exp\left(-\left|\int_{\tau'}^{\tau}\frac{d\tau''}{\tau_R(\tau'')}\right|\right). \tag{4.14}$$

If the background fields (e, u^μ, n_i) are uniform and constant, the above correlation reduces to a simple exponential form:

$$\langle \Gamma(x)\Gamma(x')\rangle = \frac{T\kappa}{\tau_R}\exp\left(-\frac{|\tau-\tau'|}{\tau_R}\right). \tag{4.15}$$

4.3 Tensor structure of memory function

So far, we have discussed a generic dissipative current Γ. The actual dissipative currents such as $\pi^{\mu\nu}$ and ν_i^μ have tensor structures, which makes the memory function and the noise correlation non-trivial. In particular, the transversality between the dissipative currents and the four-velocity, $u_\mu\pi^{\mu\nu} = u_\mu\nu_i^\mu = 0$, plays an important role.

To see the transversality let us here consider the simplified Israel-Stewart constitutive equations (3.126), (3.128). In the Landau frame, the constitutive equations have the following form:

$$\Pi + \tau_\Pi \mathrm{D}\Pi = -\zeta\theta, \tag{4.16}$$

$$\pi^{\mu\nu} + \tau_\pi \Delta^{\mu\nu}{}_{\alpha\beta}\mathrm{D}\pi^{\alpha\beta} = 2\eta\sigma^{\mu\nu}, \tag{4.17}$$

$$\nu_i^\mu + \sum_{j=1}^{n}\tau_{ij}\Delta^\mu{}_\alpha \mathrm{D}\nu_j^\alpha = \sum_{j=1}^{n}\kappa_{ij}T\nabla^\mu\frac{\mu_j}{T}. \tag{4.18}$$

Here we notice that the time derivatives $\mathrm{D}\pi^{\alpha\beta}$ and $\mathrm{D}\nu_i^\alpha$ are projected with $\Delta^{\mu\nu}{}_{\alpha\beta}$ and $\Delta^\mu{}_\alpha$. Those projections ensure that the transversality of the dissipative currents $u_\mu\pi^{\mu\nu} = u_\mu\nu_i^\mu = 0$ is not broken

under the time evolution. As an example, let us consider the projection of the time derivative of the shear stress $\pi^{\mu\nu}$. Without the projection, the constitutive equation would be $\mathrm{D}\pi^{\mu\nu} \approx (2\eta\sigma^{\mu\nu} - \pi^{\mu\nu})/\tau_\pi$, and thus the time derivative of the transversality would not vanish:

$$\mathrm{D}(u_\mu \pi^{\mu\nu}) \approx \pi^{\mu\nu}\mathrm{D}u_\mu + u_\mu \frac{1}{\tau_\pi}(2\eta\sigma^{\mu\nu} - \pi^{\mu\nu}) = \pi^{\mu\nu}\mathrm{D}u_\mu \neq 0. \tag{4.19}$$

On the other hand, the transversality is preserved if the projection is taken into account:

$$\begin{aligned}
\mathrm{D}(u_\mu \pi^{\mu\nu}) &= \mathrm{D}(u_\mu \Delta^{\mu\nu}{}_{\alpha\beta}\pi^{\alpha\beta}) && (4.20)\\
&= \mathrm{D}(u_\mu \Delta^{\mu\nu}{}_{\alpha\beta})\pi^{\alpha\beta} + u_\mu(\Delta^{\mu\nu}{}_{\alpha\beta}\mathrm{D}\pi^{\alpha\beta}) && (4.21)\\
&= \mathrm{D}(0)\pi^{\alpha\beta} + u_\mu \frac{1}{\tau_\pi}(2\eta\sigma^{\mu\nu} - \pi^{\mu\nu}) = \pi^{\mu\nu}\mathrm{D}u_\mu = 0. && (4.22)
\end{aligned}$$

Note that if we consider the case of a uniform and constant background and only take linear perturbations into account, the equation (4.19) vanishes since $\mathrm{D}u^\mu_{\mathrm{bg}} = 0$, and thus the projections can be ignored. On the other hand, in non-linear hydrodynamic equations, the breaking of the transversality causes a problem even if it is small.

Due to the projections, the integral form of the constitutive equations has a non-trivial structure. To obtain that, we need to solve the differential form of the constitutive equations (4.17) and (4.18) and to obtain an explicit formula with respect to the dissipative currents. If the projection is ignored, the equations can be easily solved for each component of dissipative currents. While, with the projections, the components of the dissipative currents mix with each other and generate complicated structure of the memory function.

4.3.1 Projectors along a pathline

To write down the memory function and the integral form of the constitutive equations, we here introduce new projectors $\Delta(\tau_\mathrm{f};\tau_\mathrm{i},\boldsymbol{\sigma})^\mu{}_\alpha$ and $\Delta(\tau_\mathrm{f};\tau_\mathrm{i},\boldsymbol{\sigma})^{\mu\nu}{}_{\alpha\beta}$. They perform projections at every moment in the specified time span:

$$\Delta(\tau_\mathrm{f};\tau_\mathrm{i})^{\mu\nu}{}_{\alpha\beta} \equiv \lim_{N\to\infty} \Delta(\tau_\mathrm{f})^{\mu\nu}{}_{\alpha_0\beta_0}\left[\prod_{k=0}^{N-1}\Delta(\tau_\mathrm{f} + \tfrac{\tau_\mathrm{i}-\tau_\mathrm{f}}{N}k)^{\alpha_k\beta_k}{}_{\alpha_{k+1}\beta_{k+1}}\right]\Delta(\tau_\mathrm{i})^{\alpha_N\beta_N}{}_{\alpha\beta}, \tag{4.23}$$

$$\Delta(\tau_\mathrm{f};\tau_\mathrm{i})^{\mu}{}_{\alpha} \equiv \lim_{N\to\infty} \Delta(\tau_\mathrm{f})^{\mu}{}_{\alpha_0}\left[\prod_{k=0}^{N-1}\Delta(\tau_\mathrm{f} + \tfrac{\tau_\mathrm{i}-\tau_\mathrm{f}}{N}k)^{\alpha_k}{}_{\alpha_{k+1}}\right]\Delta(\tau_\mathrm{i})^{\alpha_N}{}_{\alpha}. \tag{4.24}$$

Here, $\boldsymbol{\sigma}$ is the comoving coordinates which specify a fluid particle and its pathline. The symbols τ_f and τ_i are proper times of the fluid particle $\boldsymbol{\sigma}$, and a pair $(\tau,\boldsymbol{\sigma})$ corresponds to a spacetime position x^μ. The projections are performed along a single pathline $\boldsymbol{\sigma}$ at every moment. Hereafter let us call the projectors *pathline projectors*. Although we do not write the $\boldsymbol{\sigma}$ dependence explicitly, all the fields above and later in this section implicitly depend on a single common $\boldsymbol{\sigma}$. The projected spaces by $\Delta(\tau)^\mu{}_\alpha$ and $\Delta(\tau)^{\mu\nu}{}_{\alpha\beta}$ are dependent on spacetime position x since the local rest frame defined by $u(x)^\mu$ depends on the position. The pathline projectors perform projections into such time-dependent spaces for every time between τ_i and τ_f.

If the value of $u^\mu, \mathrm{D}u^\mu$, and D^2u^μ are bounded in a considered domain, the limits in the definition (4.23), (4.24) are convergent and the projectors have the following properties (see Appendix C.2 for the

proof):

$$\Delta(\tau_\mathrm{f};\tau_\mathrm{i})^\mu{}_\alpha = \Delta(\tau_\mathrm{f};\tau_\mathrm{i})^\mu{}_\kappa \Delta(\tau_\mathrm{i})^\kappa{}_\alpha = \Delta(\tau_\mathrm{f})^\mu{}_\kappa \Delta(\tau_\mathrm{f};\tau_\mathrm{i})^\kappa{}_\alpha, \tag{4.25}$$

$$\Delta(\tau_\mathrm{f};\tau_\mathrm{i})^{\mu\nu}{}_{\alpha\beta} = \Delta(\tau_\mathrm{f};\tau_\mathrm{i})^{\mu\nu}{}_{\kappa\lambda} \Delta(\tau_\mathrm{i})^{\kappa\lambda}{}_{\alpha\beta} = \Delta(\tau_\mathrm{f})^{\mu\nu}{}_{\kappa\lambda} \Delta(\tau_\mathrm{f};\tau_\mathrm{i})^{\kappa\lambda}{}_{\alpha\beta}, \tag{4.26}$$

$$\Delta(\tau_\mathrm{i};\tau_\mathrm{i})^\mu{}_\alpha = \Delta(\tau_\mathrm{i})^\mu{}_\alpha, \tag{4.27}$$

$$\Delta(\tau_\mathrm{i};\tau_\mathrm{i})^{\mu\nu}{}_{\alpha\beta} = \Delta(\tau_\mathrm{i})^{\mu\nu}{}_{\alpha\beta}, \tag{4.28}$$

$$\Delta(\tau_\mathrm{f};\tau_\mathrm{i})^\mu{}_\alpha = \Delta(\tau_\mathrm{i};\tau_\mathrm{f})_\alpha{}^\mu, \tag{4.29}$$

$$\Delta(\tau_\mathrm{f};\tau_\mathrm{i})^{\mu\nu}{}_{\alpha\beta} = \Delta(\tau_\mathrm{i};\tau_\mathrm{f})_{\alpha\beta}{}^{\mu\nu}, \tag{4.30}$$

$$\Delta(\tau_\mathrm{f};\tau')^\mu{}_\kappa \Delta(\tau';\tau_\mathrm{i})^\kappa{}_\alpha = \Delta(\tau_\mathrm{f};\tau_\mathrm{i})^\mu{}_\alpha, \tag{4.31}$$

$$\Delta(\tau_\mathrm{f};\tau')^{\mu\nu}{}_{\kappa\lambda} \Delta(\tau';\tau_\mathrm{i})^{\kappa\lambda}{}_{\alpha\beta} = \Delta(\tau_\mathrm{f};\tau_\mathrm{i})^{\mu\nu}{}_{\alpha\beta}, \tag{4.32}$$

$$\mathrm{D_f}\Delta(\tau_\mathrm{f};\tau_\mathrm{i})^\mu{}_\alpha = [\mathrm{D_f}\Delta(\tau_\mathrm{f})^\mu{}_\kappa]\Delta(\tau_\mathrm{f};\tau_\mathrm{i})^\kappa{}_\alpha, \tag{4.33}$$

$$\mathrm{D_f}\Delta(\tau_\mathrm{f};\tau_\mathrm{i})^{\mu\nu}{}_{\alpha\beta} = [\mathrm{D_f}\Delta(\tau_\mathrm{f})^{\mu\nu}{}_{\kappa\lambda}]\Delta(\tau_\mathrm{f};\tau_\mathrm{i})^{\kappa\lambda}{}_{\alpha\beta}, \tag{4.34}$$

$$= [\mathrm{D_f}\Delta(\tau_\mathrm{f})^\mu{}_\kappa + \mathrm{D_f}\Delta(\tau_\mathrm{f})^\nu{}_\lambda]\Delta(\tau_\mathrm{f};\tau_\mathrm{i})^{\kappa\lambda}{}_{\alpha\beta}. \tag{4.35}$$

where $\mathrm{D_f} \equiv \frac{\partial}{\partial \tau_\mathrm{f}}$ is the substantial derivative with respect to τ_f.

The following relations are immediate consequences of (4.25) and (4.26):

$$\Delta(\tau_\mathrm{f};\tau_\mathrm{i})^\mu{}_\alpha u(\tau_\mathrm{i})^\alpha = 0, \tag{4.36}$$

$$u(\tau_\mathrm{f})_\mu \Delta(\tau_\mathrm{f};\tau_\mathrm{i})^\mu{}_\alpha = 0, \tag{4.37}$$

$$\Delta(\tau_\mathrm{f};\tau_\mathrm{i})^{\nu\mu}{}_{\alpha\beta} = \Delta(\tau_\mathrm{f};\tau_\mathrm{i})^{\mu\nu}{}_{\beta\alpha} = \Delta(\tau_\mathrm{f};\tau_\mathrm{i})^{\mu\nu}{}_{\alpha\beta}, \tag{4.38}$$

$$\Delta(\tau_\mathrm{f};\tau_\mathrm{i})^{\mu\nu}{}_{\alpha\beta} u(\tau_\mathrm{i})^\alpha = 0, \tag{4.39}$$

$$u(\tau_\mathrm{f})_\mu \Delta(\tau_\mathrm{f};\tau_\mathrm{i})^{\mu\nu}{}_{\alpha\beta} = 0, \tag{4.40}$$

$$\Delta(\tau_\mathrm{f};\tau_\mathrm{i})^{\mu\nu}{}_\alpha{}^\alpha = \Delta(\tau_\mathrm{f};\tau_\mathrm{i})^{\mu\nu}{}_{\alpha\beta} \Delta(\tau_\mathrm{i})^{\alpha\beta} = 0, \tag{4.41}$$

$$\Delta(\tau_\mathrm{f};\tau_\mathrm{i})^\mu{}_{\mu\alpha\beta} = \Delta(\tau_\mathrm{f})_{\mu\nu} \Delta(\tau_\mathrm{f};\tau_\mathrm{i})^{\mu\nu}{}_{\alpha\beta} = 0. \tag{4.42}$$

As a consequence of (4.27)-(4.32), a pathline projection preserves the norms of a spatial vector and a spatial symmetric traceless tensor:

$$(\Delta(\tau_\mathrm{f};\tau_\mathrm{i})^\mu{}_\alpha A^\alpha)(\Delta(\tau_\mathrm{f};\tau_\mathrm{i})_\mu{}^\beta A_\beta) = A^\alpha A_\alpha, \tag{4.43}$$

$$(\Delta(\tau_\mathrm{f};\tau_\mathrm{i})^{\mu\nu}{}_{\alpha\beta} B^{\alpha\beta})(\Delta(\tau_\mathrm{f};\tau_\mathrm{i})_{\mu\nu}{}^{\gamma\delta} B_{\gamma\delta}) = B^{\alpha\beta} B_{\alpha\beta} \tag{4.44}$$

for any spatial vector A^μ such that $\Delta(\tau_\mathrm{i})^\mu{}_\alpha A^\alpha = A^\mu$ and any spatial symmetric traceless tensor $B^{\mu\nu}$ such that $\Delta(\tau_\mathrm{i})^{\mu\nu}{}_{\alpha\beta} B^{\alpha\beta} = B^{\mu\nu}$. In other words, the pathline projections serve as specific Lorentz transformations for spatial vectors and spatial symmetric traceless tensors. One may feel this property to be counterintuitive because projections generally decrease the norm of a vector when changing its direction. In fact, this property of the pathline projector only holds after the limits in the definitions, (4.23) and (4.24). This can be intuitively understood with a simple two-dimensional Euclidean case: Imagining a clock face as a two-dimensional space, let us consider a point on the face as a spatial vector, and the line defined by the minute hand as the time-dependent projected space (see Fig. 4.1). While the minute hand, or the transverse space, continuously changes with time, the pathline projector performs the projection of the point into the minute hand at each time. If the projections are performed at discrete times, the norms of the vector becomes shorter by each projection. However, in the limit where the number of the projections increases, the spatial point is locked in the minute hand by the pathline projection. As a result, the pathline-projected point just rotates around the center of the clock together with the minute hand, without changing its distance from the center.

By solving (4.33) and (4.34) with the initial conditions (4.27) and (4.28), other forms of the projectors are:

$$\Delta(\tau_\mathrm{f};\tau_\mathrm{i})^\mu{}_\alpha = \left[\mathrm{T}\exp\left(\int_{\tau_\mathrm{i}}^{\tau_\mathrm{f}} d\tau \mathrm{D}\Delta(\tau)^\mu{}_\kappa\right)\right]^\mu_\kappa \Delta(\tau_\mathrm{i})^\kappa{}_\alpha, \tag{4.45}$$

$$\Delta(\tau_\mathrm{f};\tau_\mathrm{i})^{\mu\nu}{}_{\alpha\beta} = \left[\mathrm{T}\exp\left(\int_{\tau_\mathrm{i}}^{\tau_\mathrm{f}} d\tau \mathrm{D}\Delta(\tau)^{\mu\nu}{}_{\kappa\lambda}\right)\right]^{\mu\nu}_{\kappa\lambda} \Delta(\tau_\mathrm{i})^{\kappa\lambda}{}_{\alpha\beta}. \tag{4.46}$$

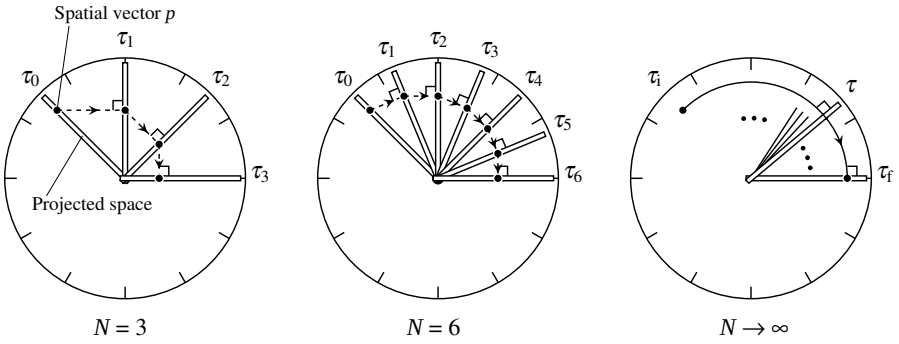

Figure 4.1: Illustration of the pathline projections by a clock. The time-dependent projected space corresponds to the hand of the clock. A spatial vector or a spatial symmetric traceless tensor corresponds to a point, p, on the minute hand. The symbol N denotes the number of the discretized times in the definitions (4.23) and (4.24), and $\tau_k \equiv \tau_{\rm i} + (\tau_{\rm f} - \tau_{\rm i})/N$ are the time points where $\tau_{\rm i}$ and $\tau_{\rm f}$ are the initial and the final time, respectively. The final norm $\|p(\tau_{\rm f})\| = [\cos(\Delta\theta/N)]^N \|p(\tau_{\rm i})\|$ goes to $\|p(\tau_{\rm i})\|$ as $N \to \infty$.

Here $\mathrm{T}\exp\int d\tau\cdot$ is a time-ordered exponential with respect to the proper time τ, i.e., the contractions of the Lorentz indices of $\Delta(\tau)^\mu{}_\lambda$ and $\Delta(\tau)^{\mu\nu}{}_{\kappa\lambda}$ are performed after the time ordering. These equations are less intuitive but more useful.

Using (4.35), another expression for $\Delta(\tau_{\rm f};\tau_{\rm i})^{\mu\nu}{}_{\alpha\beta}$ is found:

$$\Delta(\tau_{\rm f};\tau_{\rm i})^{\mu\nu}{}_{\alpha\beta} = \Delta(\tau_{\rm f};\tau_{\rm i})^\mu{}_\kappa \Delta(\tau_{\rm f};\tau_{\rm i})^\nu{}_\lambda \Delta(\tau_{\rm i})^{\kappa\lambda}{}_{\alpha\beta}. \tag{4.47}$$

This reflects the fact that the tracelessness and the symmetry of the tensor are independent from the local rest frame u^μ, and once the projection into the traceless symmetric space is made, there is no need of such projection in other times.

4.3.2 Integral form of constitutive equations with a tensor structure

Using the above pathline projectors, a class of the constitutive equations can be solved with respect to the dissipative currents.

The equations (4.33) and (4.34) can be rewritten in the following form:

$$\Delta(\tau_{\rm f})^\mu{}_\kappa \mathrm{D}_{\rm f} \Delta(\tau_{\rm f};\tau_{\rm i})^\kappa{}_\alpha = 0, \tag{4.48}$$

$$\Delta(\tau_{\rm f})^{\mu\nu}{}_{\kappa\lambda} \mathrm{D}_{\rm f} \Delta(\tau_{\rm f};\tau_{\rm i})^{\kappa\lambda}{}_{\alpha\beta} = \Delta(\tau_{\rm f})^\mu{}_\kappa \Delta(\tau_{\rm f})^\nu{}_\lambda \mathrm{D}_{\rm f} \Delta(\tau_{\rm f};\tau_{\rm i})^{\kappa\lambda}{}_{\alpha\beta} = 0. \tag{4.49}$$

The above equations mean that if a spatial vector A^μ and a traceless symmetric spatial tensor $B^{\mu\nu}$ obey the equation:

$$\Delta^\mu{}_\kappa \mathrm{D} A^\kappa = 0, \tag{4.50}$$

$$\Delta^{\mu\nu}{}_{\kappa\lambda} \mathrm{D} B^{\kappa\lambda} = 0, \tag{4.51}$$

they can be expressed as

$$A^\mu(\tau) = \Delta(\tau;\tau_{\rm i})^\mu{}_\kappa A^\kappa(\tau_{\rm i}), \tag{4.52}$$

$$B^{\mu\nu}(\tau) = \Delta(\tau;\tau_{\rm i})^{\mu\nu}{}_{\kappa\lambda} B^{\kappa\lambda}(\tau_{\rm i}). \tag{4.53}$$

In the case of the constitutive equations with relaxation times, the typical structures of the equations for shear-stress tensor and diffusion currents are:

$$\pi^{\mu\nu} + \tau_\pi \Delta^{\mu\nu}{}_{\kappa\lambda} \mathrm{D}\pi^{\kappa\lambda} = X^{\mu\nu}, \tag{4.54}$$

$$\nu_i^\mu + \sum_{j=1}^n \tau_{ij} \Delta^\mu{}_\kappa \mathrm{D}\nu_j^\kappa = X_i^\mu \tag{4.55}$$

where $X_\pi^{\mu\nu}$ and X_i^μ represent miscellaneous second-order terms. The constitutive equations with the above form can be formally solved with respect to the dissipative currents using pathline projectors:

$$\pi^{\mu\nu}(\tau) = \int_{-\infty}^{\tau} \frac{d\tau'}{\tau_\pi(\tau')} \exp\left(-\int_{\tau'}^{\tau} \frac{d\tau''}{\tau_\pi(\tau'')}\right) \Delta(\tau;\tau')^{\mu\nu}{}_{\alpha\beta} X^{\alpha\beta}(\tau'), \tag{4.56}$$

$$\nu_i^\mu(\tau) = \sum_{j,k=1}^{n} \int_{-\infty}^{\tau} d\tau' \tau_{ij}^{-1}(\tau') \left[\mathrm{T}\exp\left(-\int_{\tau'}^{\tau} d\tau'' \tau_{jk}^{-1}(\tau'')\right)\right]_{jk} \Delta(\tau;\tau')^\mu{}_\alpha X_k^\alpha(\tau'). \tag{4.57}$$

As a result, the integral forms of the constitutive equations for the simplified Israel-Stewart case (4.16)-(4.18) become

$$\Pi(\tau) = -\int_{-\infty}^{\tau} \frac{d\tau'}{\tau_\Pi(\tau')} \exp\left(-\int_{\tau'}^{\tau} \frac{d\tau''}{\tau_\Pi(\tau'')}\right) \zeta(\tau')\theta(\tau'), \tag{4.58}$$

$$\pi^{\mu\nu}(\tau) = \int_{-\infty}^{\tau} \frac{d\tau'}{\tau_\pi(\tau')} \exp\left(-\int_{\tau'}^{\tau} \frac{d\tau''}{\tau_\pi(\tau'')}\right) \Delta(\tau;\tau')^{\mu\nu}{}_{\alpha\beta} 2\eta(\tau')\sigma^{\alpha\beta}(\tau'), \tag{4.59}$$

$$\nu_i^\mu(\tau) = \sum_{j,k,l=1}^{n} \int_{-\infty}^{\tau} d\tau' \tau_{ij}^{-1}(\tau') \left[\mathrm{T}\exp\left(-\int_{\tau'}^{\tau} d\tau'' \tau_{jk}^{-1}(\tau'')\right)\right]_{jk} \Delta(\tau;\tau')^\mu{}_\alpha \kappa_{kl}(\tau') T(\tau') \nabla^\alpha \frac{\mu_l(\tau')}{T(\tau')}. \tag{4.60}$$

Then the memory functions for (4.17) and (4.18) are found to be

$$G_\Pi(x,x') = \frac{1}{\tau_\Pi(\tau')} \exp\left(-\int_{\tau'}^{\tau} \frac{d\tau''}{\tau_\Pi(\tau'')}\right) \theta^{(4)}(\sigma-\sigma'), \tag{4.61}$$

$$G_\pi{}^{\mu\nu}{}_{\alpha\beta}(x,x') = \frac{1}{\tau_\pi(\tau')} \exp\left(-\int_{\tau'}^{\tau} \frac{d\tau''}{\tau_\pi(\tau'')}\right) \Delta(\tau;\tau')^{\mu\nu}{}_{\alpha\beta} \theta^{(4)}(\sigma-\sigma'), \tag{4.62}$$

$$G_{ik}{}^\mu{}_\alpha(x,x') = \sum_{j=1}^{n} \tau_{ij}^{-1}(\tau') \left[\mathrm{T}\exp\left(-\int_{\tau'}^{\tau} d\tau'' \tau_{jk}^{-1}(\tau'')\right)\right]_{jk} \Delta(\tau;\tau')^\mu{}_\alpha \theta^{(4)}(\sigma-\sigma'). \tag{4.63}$$

4.4 White noise in differential form of constitutive equations

The autocorrelation of the hydrodynamic fluctuations in the integral form of the constitutive equations is directly given by the FDR. The autocorrelation of the counterpart noise term appearing in the differential form can be calculated using that of the noise in the integral form. To obtain the behavior of the noise term in the differential form, we first consider the simplified Israel-Stewart case. Then we discuss more general case under several conditions.

4.4.1 Hydrodynamic fluctuations in the simplified Israel-Stewart case

In the previous section we obtained the integral form of the constitutive equations (4.58)-(4.60) corresponding to the differential form of the simplified Israel-Stewart equation (4.16)-(4.18). Here we introduce hydrodynamic fluctuations $\delta\Pi$, $\delta\pi^{\mu\nu}$, and $\delta\nu_i^\mu$ into the integral form of the constitutive equations:

$$\Pi(\tau) = -\int d^4x' G_\Pi(x,x')\zeta(\tau')\theta(\tau') + \delta\Pi, \tag{4.64}$$

$$\pi^{\mu\nu}(\tau) = \int d^4x' G_\pi{}^{\mu\nu}{}_{\alpha\beta}(x,x') 2\eta(\tau')\sigma^{\alpha\beta}(\tau') + \delta\pi^{\mu\nu}, \tag{4.65}$$

$$\nu_i^\mu(\tau) = \sum_{j,k,l=1}^{n} \int d^4x' G_{ik}{}^\mu{}_\alpha(x,x') \kappa_{kl}(\tau') T(\tau') \nabla^\alpha \frac{\mu_l(\tau')}{T(\tau')} + \delta\nu_i^\mu. \tag{4.66}$$

The statistical behavior of the dissipative currents is given by the FDR (4.12):

$$\langle \delta\Pi(x)\rangle = \langle \delta\pi^{\mu\nu}(x)\rangle = \langle \delta\nu_i^\mu(x)\rangle = 0, \tag{4.67}$$

$$\langle \delta\Pi(x)\delta\Pi(x')\rangle = T(x')\zeta(x')G_\Pi(x,x') + T(x)\zeta(x)G_\Pi(x',x), \tag{4.68}$$

$$\langle \delta\pi^{\mu\nu}(x)\delta\pi^{\alpha\beta}(x')\rangle = 2T(x')\eta(x')G_\pi^{\mu\nu\alpha\beta}(x,x') + 2T(x)\eta(x)G_\pi^{\alpha\beta\mu\nu}(x',x), \tag{4.69}$$

$$\langle \delta\nu_i^\mu(x)\delta\nu_j^\alpha(x')\rangle = -\sum_{k=1}^n T(x')\kappa_{kj}(x')G_{ik}^{\alpha\mu}(x,x') - \sum_{k=1}^n T(x)\kappa_{ki}(x)G_{jk}^{\mu\alpha}(x',x). \tag{4.70}$$

Here the minus sign in the last term of (4.70) appears because a Lorentz index of $G^\mu{}_\alpha$ is raised with $-\Delta^{\alpha\beta} = \mathrm{diag}(0,1,1,1)_{\mathrm{LRF}}$, where $(\cdots)_{\mathrm{LRF}}$ is the components in the local rest frame.

Next we see the differential counterpart of the constitutive equations with fluctuations. Because of the introduction of the hydrodynamic fluctuations $\delta\Pi$, $\delta\pi^{\mu\nu}$, and $\delta\nu_i^\mu$, the corresponding differential forms (4.16)-(4.18) are also changed as

$$\Pi + \tau_\Pi \mathrm{D}\Pi = -\zeta\theta + \xi_\Pi, \tag{4.71}$$

$$\pi^{\mu\nu} + \tau_\pi \Delta^{\mu\nu}{}_{\alpha\beta}\mathrm{D}\pi^{\alpha\beta} = 2\eta\sigma^{\mu\nu} + \xi_\pi^{\mu\nu}, \tag{4.72}$$

$$\nu_i^\mu + \sum_{j=1}^n \tau_{ij}\Delta^\mu{}_\alpha \mathrm{D}\nu_j^\alpha = \sum_{j=1}^n \kappa_{ij} T\nabla^\mu \frac{\mu_j}{T} + \xi_i^\mu, \tag{4.73}$$

where ξ_Π, $\xi_\pi^{\mu\nu}$, and ξ_i^μ are the noise terms coming from the hydrodynamic fluctuations.

What characterize the behavior of the noise terms ξ_Π, $\xi_\pi^{\mu\nu}$, and ξ_i^μ are the noise autocorrelations. To obtain the autocorrelations we can use the relations between those noise terms in the differential form and the corresponding noise terms in the integral forms. By substituting the expression of dissipative currents in the integral forms (4.64)-(4.66) into the differential forms (4.71)-(4.73), we find expressions of the noise terms $(\xi_\Pi, \xi_\pi^{\mu\nu}, \xi_i^\mu)$ in terms of the hydrodynamic fluctuations in the integral form $(\delta\Pi, \delta\pi^{\mu\nu}, \delta\nu_i^\mu)$:

$$\xi_\Pi = \delta\Pi + \tau_\Pi \mathrm{D}\delta\Pi, \tag{4.74}$$

$$\xi_\pi^{\mu\nu} = \delta\pi^{\mu\nu} + \tau_\pi \Delta^{\mu\nu}{}_{\alpha\beta}\mathrm{D}\delta\pi^{\alpha\beta}, \tag{4.75}$$

$$\xi_i^\mu = \delta\nu_i^\mu + \sum_{j=1}^n \tau_{ij}\Delta^\mu{}_\alpha \mathrm{D}\delta\nu_j^\alpha. \tag{4.76}$$

The autocorrelations of those noise terms in the differential form can be calculated using the FDR for the integral form:

$$\langle \xi_\Pi(x)\xi_\Pi(x')\rangle = 2[T\zeta + \tau_\Pi \mathrm{D}(T\zeta)]\delta^{(4)}(x-x'), \tag{4.77}$$

$$\langle \xi_\pi^{\mu\nu}(x)\xi_\pi^{\alpha\beta}(x')\rangle = 4[T\eta\Delta^{\mu\nu\alpha\beta} + \tau_\Pi \mathrm{D}(T\eta\Delta^{\mu\nu\alpha\beta})]\delta^{(4)}(x-x'), \tag{4.78}$$

$$\langle \xi_i^\mu(x)\xi_j^\alpha(x')\rangle = -2[T\kappa_{ij}\Delta^{\mu\alpha} + \tau_\Pi \mathrm{D}(T\kappa_{ij}\Delta^{\mu\alpha})]\delta^{(4)}(x-x'). \tag{4.79}$$

The first line is obtained as

$$\langle \xi_\Pi(x)\xi_\Pi(x')\rangle = (1+\tau_\Pi \mathrm{D})(1+\tau_\Pi \mathrm{D}')\langle \delta\Pi(x)\delta\Pi(x')\rangle \tag{4.80}$$

$$= (1+\tau_\Pi \mathrm{D}')[T(x')\zeta(x')\delta^{(4)}(x-x')] + (1+\tau_\Pi \mathrm{D})[T(x)\zeta(x)\delta^{(4)}(x-x')] \tag{4.81}$$

$$= 2[T\zeta + \tau_\Pi \mathrm{D}(T\zeta)]\delta^{(4)}(x-x'), \tag{4.82}$$

where $\mathrm{D} = u^\mu(\partial/\partial x^\mu)$ and $\mathrm{D}' = u^\mu(\partial/\partial x'^\mu)$. Here we used a relation of the memory function (4.61) of the simplified Israel-Stewart case:

$$(1+\tau_\Pi \mathrm{D})G_\Pi(x,x') = \delta^{(4)}(x-x'). \tag{4.83}$$

In addition, we also used $\mathrm{D}'\delta^{(4)}(x-x') = -\mathrm{D}\delta^{(4)}(x-x')$. The autocorrelations of the other noise terms (4.78), (4.79) are obtained similarly:

$$\langle \xi_\pi^{\mu\nu}(x)\xi_\pi^{\alpha\beta}(x')\rangle = \Delta^{\mu\nu}{}_{\kappa\lambda}\Delta^{\alpha\beta}{}_{\gamma\delta}(1+\tau_\Pi \mathrm{D})(1+\tau_\pi \mathrm{D}')\langle \delta\pi^{\mu\nu}(x)\delta\pi^{\alpha\beta}(x')\rangle \tag{4.84}$$

$$= 4[T\eta\Delta^{\mu\nu\alpha\beta} + \tau_\Pi \mathrm{D}(T\eta\Delta^{\mu\nu\alpha\beta})]\delta^{(4)}(x-x'), \tag{4.85}$$

$$\langle \xi_i^\mu(x)\xi_j^\alpha(x')\rangle = \Delta^\mu{}_\kappa\Delta^\alpha{}_\gamma(1+\tau_\Pi \mathrm{D})(1+\tau_\pi \mathrm{D}')\langle \delta\nu_i^{\mu\nu}(x)\delta\nu_j^\alpha(x')\rangle \tag{4.86}$$

$$= -2[T\kappa_{ij}\Delta^{\mu\alpha} + \tau_\Pi \mathrm{D}(T\kappa_{ij}\Delta^{\mu\alpha})]\delta^{(4)}(x-x'). \tag{4.87}$$

We used the relations of the other memory functions (4.62), (4.63):

$$\Delta^{\mu\nu}{}_{\kappa\lambda}(1+\tau_\pi \mathrm{D}) G_\pi{}^{\kappa\lambda}{}_{\alpha\beta}(x,x') = \Delta^{\mu\nu}{}_{\alpha\beta}\delta^{(4)}(x-x'), \tag{4.88}$$

$$\Delta^{\mu}{}_{\kappa}(1+\tau_\pi \mathrm{D}) G_{ik}{}^{\mu}{}_{\alpha}(x,x') = \delta_{ij}\Delta^{\mu}{}_{\alpha}\delta^{(4)}(x-x'). \tag{4.89}$$

Finally we consider the case of a uniform background: $(e, n_i) = \text{const}$. The memory functions (4.61)-(4.63) reduce to simple forms:

$$G_\Pi(x-x') = \frac{1}{\tau_\Pi}\exp\left(-\tau-\tau'\tau_\Pi\right)\theta^{(4)}(\sigma-\sigma'), \tag{4.90}$$

$$G_\pi{}^{\mu\nu}{}_{\alpha\beta}(x-x') = \frac{1}{\tau_\pi}\exp\left(-\frac{\tau-\tau'}{\tau_\pi}\right)\Delta^{\mu\nu}{}_{\alpha\beta}\theta^{(4)}(\sigma-\sigma'), \tag{4.91}$$

$$G_{ik}{}^{\mu}{}_{\alpha}(x-x') = \sum_{j=1}^{n}\tau_{ij}^{-1}(\tau')\left[\exp(-(\tau-\tau')\tau_{jk}^{-1})\right]_{jk}\Delta^{\mu}{}_{\alpha}\theta^{(4)}(\sigma-\sigma'). \tag{4.92}$$

The noise autocorrelations in the differential form become

$$\langle \xi_\Pi(x)\xi_\Pi(x')\rangle = 2T\zeta\delta^{(4)}(x-x'), \tag{4.93}$$

$$\langle \xi_\pi^{\mu\nu}(x)\xi_\pi^{\alpha\beta}(x')\rangle = 4T\eta\Delta^{\mu\nu\alpha\beta}\delta^{(4)}(x-x'), \tag{4.94}$$

$$\langle \xi_i^{\mu}(x)\xi_j^{\alpha}(x')\rangle = -2T\kappa_{ij}\Delta^{\mu\alpha}\delta^{(4)}(x-x'). \tag{4.95}$$

4.4.2 Hydrodynamic fluctuations in general case

In the autocorrelations of the simplified Israel-Stewart case (4.77)-(4.79), we notice that all the correlations become delta functions, which means that the noise terms in the differential form become white noise. In the equation (4.81), we can see that the delta functions come from the relation:

$$(1+\tau_\pi \mathrm{D})\delta^{(4)}(x-x') + (1+\tau_\pi \mathrm{D}')\delta^{(4)}(x-x') = 2\delta^{(4)}(x-x'). \tag{4.96}$$

However this result depends on the structure of the linear operator $1+\tau_\Pi \mathrm{D}$ and cannot be applied to the general structure of the constitutive equations.

To discuss the nature of the noise in more general constitutive equations, we here consider the higher-order case in a linear-response regime with a uniform and constant background (e, u^μ, n_i). If the relaxation of the dissipative components $\Gamma = (\Pi, \pi^{\mu\nu}, \nu_i^\mu)$ is sufficiently faster than the variation of the local-equilibrium components (e, u^μ, n_i), thermodynamic quantities appearing in the constitutive equations, such as a relaxation time $\tau_\Pi = \tau_\Pi(e, \{n_i\})$, are constant. For simplicity, we choose a rest frame in which $u^\mu = (1\ 0\ 0\ 0)^{\mathrm{T}}$.

Let us first summarize the integral form and the differential form of the linear-response constitutive equations in the Fourier representation. Corresponding FDRs of the noise terms are also obtained in Fourier representation.

Under the condition of the uniform and constant backgrounds, the memory function has the translational symmetry, and thus the integral form of the constitutive equations (4.7) becomes

$$\Gamma(x) = \int d^4x' G(x-x')\kappa F(x'). \tag{4.97}$$

The above equation can be written in the Fourier space as

$$\Gamma_{\omega,\boldsymbol{k}} = G_{\omega,\boldsymbol{k}}\kappa F_{\omega,\boldsymbol{k}}. \tag{4.98}$$

Here we use the Fourier transform in the following convention:

$$f_{\omega,\boldsymbol{k}} = \int d^4x e^{ik^\mu x_\mu} f(x) = \int d^4x e^{i\omega t - i\boldsymbol{k}\cdot\boldsymbol{x}} f(x), \tag{4.99}$$

$$f(x) = \int \frac{d^4k}{(2\pi)^4} e^{-ik^\mu x_\mu} f_{\omega,\boldsymbol{k}} = \int \frac{d^4k}{(2\pi)^4} e^{-i\omega t + i\boldsymbol{k}\cdot\boldsymbol{x}} f_{\omega,\boldsymbol{k}}, \tag{4.100}$$

where $k^\mu = (\omega, \boldsymbol{k})$.

The differential form of the constitutive equations in the linear-response regime can generally be expressed in the following form [244, 245]:

$$L'(\mathrm{D}, \nabla^\mu)\Gamma(x) = M'(\mathrm{D}, \nabla^\mu)\kappa F(x), \tag{4.101}$$

where $L'(z, \boldsymbol{w})$ and $M'(z, \boldsymbol{w})$ are polynomials of z and $\boldsymbol{w}$.

The time derivative D in the polynomial M can be replaced by the spatial derivative acting on other dissipative currents or thermodynamic fields by substituting the hydrodynamic equations (3.79)-(3.81) to DF. Here we ignore the non-linear terms added by the substitution in the linear-response regime. As a result, the constitutive equations can be transformed into a form which does not contain the time derivative in the right-hand side:

$$L(\mathrm{D}, \nabla^\mu)\Gamma(x) = M(\nabla^\mu)\kappa F(x). \tag{4.102}$$

Several properties of the polynomials should be noted here:

- The coefficients of the polynomials $L(z, \boldsymbol{w})$ and $M(\boldsymbol{w})$ are real because they are the transport coefficients appearing in the constitutive equations.

- The polynomials $L(z, \boldsymbol{w})$ and $M(\boldsymbol{w})$ have finite degrees of z and $\boldsymbol{w}$ for practical purposes, i.e., the series are truncated to have a finite order of the derivatives.

- Because the lowest-order terms are $\Gamma = \kappa F(x)$, the constant term of each polynomial is unity:

$$L(z, w) = 1 + O(z, w), \tag{4.103}$$
$$M(w) = 1 + O(z). \tag{4.104}$$

  One can consider that the constant terms are factorized to the Onsager coefficients κ.

- The polynomials $L(z, \boldsymbol{w})$ and $M(\boldsymbol{w})$ contain only even orders of $\boldsymbol{w}$:

$$L(z, \boldsymbol{w}) = L''(z, \boldsymbol{w} \otimes \boldsymbol{w}), \tag{4.105}$$
$$M(\boldsymbol{w}) = M''(\boldsymbol{w} \otimes \boldsymbol{w}). \tag{4.106}$$

  To see this, we can consider the parity inversion $\boldsymbol{x} \to \boldsymbol{x}' = -\boldsymbol{x}$. Looking at the lowest order, we notice that the parity of the dissipative currents $\Gamma(x)$ and the thermodynamic force with the Onsager coefficients $\kappa F(x)$ are the same, and the parities of both of the polynomials $L(z, \boldsymbol{w})$ and $M(\boldsymbol{w})$ are $+1$. Therefore, the polynomials are even as a function of $\boldsymbol{w}$ and contain only even orders of spatial derivatives ∇^μ. Note that the even factor is not necessarily be the form of $\boldsymbol{w} \cdot \boldsymbol{w}$ because indices can be contracted with those of thermodynamic forces, e.g., $M(\nabla^\mu)\kappa\Gamma \sim 2\eta\nabla^\mu\nabla_\alpha\sigma^{\alpha\beta}$.

Next we consider the differential form in the Fourier space:

$$L(-i\omega, -i\boldsymbol{k})\Gamma_{\omega,\boldsymbol{k}} = M(-i\boldsymbol{k})\kappa F_{\omega,\boldsymbol{k}}. \tag{4.107}$$

Since we chose the rest frame, the substantial derivative $\mathrm{D} = u^\mu\partial_\mu$ and the spatial derivative $\nabla^\mu = \Delta^{\mu\alpha}\partial_\alpha$ were replaced by simple gradients: $\mathrm{D} = \partial_0 \to -i\omega$, and $\nabla^\mu = (0, \partial^i)^{\mathrm{T}} \to \partial^i = -\partial_i \to -i\boldsymbol{k}$.

By comparing the above Fourier representation of the differential form to that of the integral form (4.98), we find the relation of the polynomials and the memory function:

$$G_{\omega,\boldsymbol{x}} = L(-i\omega, -i\boldsymbol{k})^{-1}M(-i\boldsymbol{k}). \tag{4.108}$$

Next we introduce hydrodynamic fluctuations into the above integral and differential constitutive equations:

$$\Gamma_{\omega,\boldsymbol{k}} = G_{\omega,\boldsymbol{k}}\kappa F_{\omega,\boldsymbol{k}} + \delta\Gamma_{\omega,\boldsymbol{k}}, \tag{4.109}$$
$$L(-i\omega, -i\boldsymbol{k})\Gamma_{\omega,\boldsymbol{k}} = M(-i\boldsymbol{k})\kappa F_{\omega,\boldsymbol{k}} + \xi_{\omega,\boldsymbol{k}}, \tag{4.110}$$

where $\delta\Gamma_{\omega,\boldsymbol{k}}$ and $\xi_{\omega,\boldsymbol{k}}$ are the noise terms by the hydrodynamic fluctuations. By comparing these equations, we find that the relation between the noise terms in the differential form and the integral form:

$$\xi_{\omega,\boldsymbol{k}} = L(-i\omega, i\boldsymbol{k})\delta\Gamma_{\omega,\boldsymbol{k}}. \tag{4.111}$$

The FDR (4.12) is Fourier transformed into the following form:

$$\langle \delta\Gamma_{\omega,\boldsymbol{k}} \delta\Gamma^{\dagger}_{\omega',\boldsymbol{k}'} \rangle = T[G_{\omega,\boldsymbol{k}}\kappa + \kappa G^{\dagger}_{\omega,\boldsymbol{k}}](2\pi)^4\delta^{(4)}(k-k'), \tag{4.112}$$

where $\cdots^{\dagger}$ denotes the Hermitian conjugate of a matrix or a vector. The delta function in the right hand side comes from the translational symmetry of the memory function $G(x-x')$. The corresponding autocorrelation for the noise term in the differential form becomes

$$\begin{aligned}
\langle \xi_{\omega,\boldsymbol{k}} \xi^{\dagger}_{\omega',\boldsymbol{k}'} \rangle &= L(-i\omega, -i\boldsymbol{k}) \langle \delta\Gamma_{\omega,\boldsymbol{k}} \delta\Gamma^{\dagger}_{\omega',\boldsymbol{k}'} \rangle L(-i\omega', -i\boldsymbol{k}')^{\dagger} && (4.113)\\
&= I_{\omega,\boldsymbol{k}}(2\pi)^4\delta^{(4)}(k-k'), && (4.114)\\
I_{\omega,\boldsymbol{k}} &= T[M(-i\boldsymbol{k})\kappa L(-i\omega, -i\boldsymbol{k})^{\dagger} + L(-i\omega, -i\boldsymbol{k})\kappa M(-i\boldsymbol{k})^{\dagger}]. && (4.115)
\end{aligned}$$

Finally we mention a condition for the noise to be white. The autocorrelation in the real time becomes a delta function $\delta(t-t')$ when the factor of the power spectrum $I_{\omega,\boldsymbol{k}}$ does not have frequency dependence:

$$I_{\omega,\boldsymbol{k}} = I'_{\boldsymbol{k}}. \tag{4.116}$$

4.4.3 White noise in differential form of the general case

The power spectrum of the noise term in the general case was obtained in the equations (4.112), (4.115). Using the properties of the memory function, the FDR, and the polynomials of the constitutive equations, we can further study the hydrodynamic fluctuations in detail.

In this subsection we consider the case that the components of the dissipative current Γ_a do not mix with each other for simplicity. Then, the matrices κ_{ab}, $[G_{\omega,\boldsymbol{k}}]_{ab}$, $[L(-i\omega, -i\boldsymbol{k})]_{ab}$, $[M(-i\omega, -i\boldsymbol{k})]_{ab}$ are all diagonal. In the following discussion, we focus on a component of the dissipative current Γ without loss of generality, and treat $\kappa, G_{\omega,\boldsymbol{k}}, L$, and M as scalars.

First we consider the eigenvalues of the noise autocorrelation. Since the noise autocorrelation $\langle \xi(x)\xi^{\dagger}(x') \rangle$ is a covariance matrix when spatial dependence x and x' are seen as matrix indices, they are positive semidefinite due to the general property of the covariance matrix. This means that the eigenvalues of the correlation corresponding to a variance cannot be negative. The autocorrelation is already diagonalized in the Fourier space (4.114) due to the translational symmetry, and therefore the eigenvalues are nothing but the power spectra $I_{\omega,\boldsymbol{k}}$. The positive semidefiniteness can be written as

$$I_{\omega,\boldsymbol{k}} = 2T\kappa\Re[M(-i\boldsymbol{k})L(-i\omega, i\boldsymbol{k})] \geq 0. \tag{4.117}$$

Here we used the properties of the polynomial M: $M(-i\boldsymbol{k})$ is a real-valued function since the coefficients of $M(-i\boldsymbol{k})$ are real, and the polynomial contains only even degrees of $-i\boldsymbol{k}$ (4.106). The above inequality gives a strong restriction to the structure of the linear-response constitutive equations. Then the main results of this section can be summarized as follows:

- The polynomials $L(\mathrm{D}, \nabla^{\mu})$ and $M(\nabla^{\mu})$ have the following form:

$$\begin{aligned}
L(\mathrm{D}, \nabla^{\mu}) &= 1 + \tau_R \mathrm{D}, && (4.118)\\
M(\nabla^{\mu}) &= M''(\nabla_{\mu}\nabla^{\mu}) && (4.119)\\
&= 1 + m_{2p}\nabla_{\mu}\nabla^{\mu} + \cdots, && (4.120)
\end{aligned}$$

  where τ_R and m_2 are transport coefficients.

- The polynomial $M(-i\boldsymbol{k})$ is non-negative for all real $\boldsymbol{k}$:

$$M(-i\boldsymbol{k}) \geq 0. \tag{4.121}$$

- Even if the noise term in the integral form is colored, the noise term in the differential form always becomes white:

$$I_{\omega,\boldsymbol{k}} = 2T\kappa M(-i\boldsymbol{k}). \tag{4.122}$$

- The autocorrelation in the real space is written as

$$\langle \xi(x)\xi(x')\rangle = 2T\kappa M(\nabla^\mu)\delta^{(4)}(x-x'). \tag{4.123}$$

Now we prove the above results. First, to see the sign of the polynomial $L(-i\omega,-i\boldsymbol{k})$, we factorize the polynomial with respect to $i\omega$:

$$L(-i\omega,-i\boldsymbol{k}) = (-1)^N A_{\boldsymbol{k}} \prod_{p=1}^{N} i(\omega-\omega_p(\boldsymbol{k})), \tag{4.124}$$

where $N = \deg_\omega L$ is the degree of ω in the polynomial $L(-i\omega,-i\boldsymbol{k})$. The factor $A_{\boldsymbol{k}}$ is the coefficient of the term with the highest degree of $-i\omega$. The factor $A_{\boldsymbol{k}}$ is real due to the spatial inversion symmetry of the polynomial $L(-i\omega,-i\boldsymbol{k})$, (4.105). The wave number $\boldsymbol{k}$ is chosen such that $A_{\boldsymbol{k}} \neq 0$. The zeroes $\{\omega_p(\boldsymbol{k})\}_{p=1}^N$ of the polynomial $L(-i\omega,-i\boldsymbol{k})$ correspond to the poles of the memory function $G = M(-i\boldsymbol{k})/L(-i\omega,-i\boldsymbol{k})$. Therefore the imaginary part of the zeroes $\Im\omega_p(\boldsymbol{k})$ should be negative to ensure the retardation and relaxation of the memory function $G(x-x')$:

$$\Im\omega_p(\boldsymbol{k}) < 0, \quad (1 \le p \le N). \tag{4.125}$$

Let us consider the complex argument of the polynomials:

$$\arg[M(-i\boldsymbol{k})L(-i\omega,-i\boldsymbol{k})] = \arg M(-i\boldsymbol{k}) + \arg A_{\boldsymbol{k}} - \frac{N\pi}{2} + \sum_{p=1}^{N} \arg[\omega-\omega_p(\boldsymbol{k})]. \tag{4.126}$$

As the frequency ω goes from the negative infinity $-\infty$ to the positive infinity ∞, the argument of the factor $\omega-\omega_p(\boldsymbol{k})$ is continuously changed from 0 to $-\pi$ because $\Im\omega_p(\boldsymbol{k}) < 0$. Therefore the whole argument decreases continuously by $N\pi$:

$$\lim_{\omega\to\infty} \arg[M(-i\boldsymbol{k})L(-i\omega,-i\boldsymbol{k})] = \lim_{\omega\to-\infty} \arg[M(-i\boldsymbol{k})L(-i\omega,-i\boldsymbol{k})] - N\pi. \tag{4.127}$$

The positive semidefiniteness (4.117) is expressed in terms of the complex argument as

$$\arg[M(-i\boldsymbol{k})L(-i\omega,-i\boldsymbol{k})] \in \left(2m\pi - \frac{\pi}{2}, 2m\pi + \frac{\pi}{2}\right), \tag{4.128}$$

where m is an integer. We can see that the argument cannot be continuously changed by more than π, and therefore the degree of the polynomial should be $N = 0$, or 1.

Consequently, the polynomial $L(-i\omega,-i\boldsymbol{k})$ becomes

$$L(-i\omega,-i\boldsymbol{k}) = -i\omega A_{\boldsymbol{k}} + B_{\boldsymbol{k}}, \tag{4.129}$$

where $A_{\boldsymbol{k}}$ and $B_{\boldsymbol{k}}$ are even functions of the wave number $\boldsymbol{k}$, and real due to the spatial inversion symmetry of the polynomial $L(-i\omega,-i\boldsymbol{k})$ (4.105). In addition, the polynomial $M(-i\boldsymbol{k})$ should be non-negative:

$$M(-i\boldsymbol{k}) \ge 0. \tag{4.130}$$

Now we consider the causality of the memory function (4.10). The general conditions of the causality for the derivative expansion of a response function are given in Ref. [246]:

- The coefficient of the highest degree of ω, $A_{\boldsymbol{k}}$, should not contain $\boldsymbol{k}$. Therefore the coefficient becomes a constant $A_{\boldsymbol{k}} = \tau_R = \text{const}$, which is nothing but the relaxation time.

- The pole of the memory function $\omega_1(\boldsymbol{k}) = -iB_{\boldsymbol{k}}$ should follow the equations:

$$\lim_{|\boldsymbol{k}|\to\infty} \left| \frac{\Re\omega_1(\boldsymbol{k})}{|\boldsymbol{k}|} \right| < 1, \tag{4.131}$$

$$\lim_{|\boldsymbol{k}|\to\infty} \left| \frac{\Im\omega_1(\boldsymbol{k})}{|\boldsymbol{k}|} \right| < \infty. \tag{4.132}$$

  The first equation is trivially fulfilled since the pole is a pure imaginary number. The second equation means that the degree of $\boldsymbol{k}$ in $B_{\boldsymbol{k}}$ should not be larger than one. Since $B_{\boldsymbol{k}}$ is an even function of $\boldsymbol{k}$, $B_{\boldsymbol{k}}$ is a constant, and in fact $B_{\boldsymbol{k}} = 1$ due to the equation (4.103).

As a result the polynomial $L(-i\omega, -i\boldsymbol{k})$ has a simpler form:

$$L(-i\omega, -i\boldsymbol{k}) = 1 - i\omega\tau_R. \tag{4.133}$$

The noise spectrum becomes

$$I_{\omega,\boldsymbol{k}} = 2T\kappa M(-i\boldsymbol{k}), \tag{4.134}$$

which does not have frequency dependence. Thus the noise in the differential form is white noise as in the condition (4.116). The autocorrelation in the real space becomes

$$\langle \xi(x)\xi(x') \rangle = 2T\kappa M(\nabla^\mu)\delta^{(4)}(x - x') \tag{4.135}$$

$$= 2T\kappa[1 + m_2\nabla_\mu\nabla^\mu + \cdots]\delta^{(4)}(x - x'), \tag{4.136}$$

where m_2 is a transport coefficient contained in $M(\nabla^\mu)$. Note that the derivatives of the delta function are justified under some smearing procedure of the fluctuating hydrodynamics. Details of the smearing and the delta function are explained in the later sections 6.1 and 6.3.

4.5 Brief summary

In high-energy nuclear collisions, the event-by-event fluctuations are intensively studied using the dynamical model which consists of initial-state models and relativistic dissipative hydrodynamics combined with subsequent particlization process and hadronic cascades. To estimate the fluctuation effects in such dynamical models, the hydrodynamic fluctuations should be considered within full (3+1)-dimensional causal dissipative hydrodynamics using non-linear hydrodynamic equations.

We first defined the integral form of the constitutive equations as the counterpart of the differential form. In the integral form of the constitutive equations, the dissipative currents can be written down as a convolution of the thermodynamic forces and the memory functions. Using the fluctuation-dissipation relations, we have shown that the noise autocorrelations are written by the memory functions and are colored in general.

To consider the tensor structure of the memory functions under non-uniform backgrounds, we introduced new projectors along a pathline of hydrodynamics, by which the projection onto the transverse space to the four-velocity is performed at each time on the pathline. Using those projectors along the pathline, the explicit form of the memory function can be formally written down. We also studied several properties of the projectors.

Finally we investigated the characteristics of the hydrodynamic fluctuations in relativistic system using the constitutive equations, the general properties of the memory functions including causality, and the fluctuation-dissipation relation. To study the characteristics, we considered an ideal case of the linear-response regime in which the gradients and modulation of the background fields can be neglected. It turned out that the structure of the linear-response constitutive equations is constrained. As a consequence, the noise term in the differential form of the constitutive equations becomes always white even if the corresponding noise term in integral form is colored.

Chapter 5

New numerical scheme for causal dissipative hydrodynamics

In this chapter, we introduce a new numerical scheme to solve the causal dissipative hydrodynamics under large gradients caused by hydrodynamic fluctuations.

In the previous chapter, we discussed the two forms of constitutive equations: the integral form and the differential form. In Section 5.1 we compare pros and cons of using each form and adopt the differential form for our calculations. Subsequently, we present the whole set of the equations to solve in the numerical calculations. Then, in Section 5.2, we examine the constraints on the fluid fields in the causal dissipative hydrodynamics. The constraints may be violated by the discretization errors when the fluid fields have large gradients due to the hydrodynamic fluctuations. In Sections 5.3-5.5, we develop a new scheme which explicitly preserves the constraints. First we compare the choices of the dynamical variables in Section 5.3, and adopt the dissipative currents with their components in the local rest frame. After defining the tensor bases in Section 5.4, we show the time evolution equation of the dissipative currents in Section 5.5.

5.1 Integral form and differential form

There are two choices of the constitutive equations: the integral form and the differential form. In conventional relativistic dissipative hydrodynamics, the differential form is widely used. While, we have introduced the integral form in Section 4.1 to apply the FDR to the hydrodynamic fluctuations.

In the integral form, any memory function can be treated in the numerical simulation even if the derivative expansion of the memory function or the corresponding differential form is not known. The integral form, however, has several disadvantages compared to the differential forms:

- The integral form of the constitutive equations is non-Markovian, i.e., the dissipative currents depend on the thermodynamic forces of the past. Therefore to perform numerical calculations with the integral form, all the thermodynamic forces of the past should be memorized. This requires a large memory space. Since the memory function vanishes at a longer time compared to the relaxation time scale, the contribution of the thermodynamic forces of sufficiently past is negligible. Thus instead of the whole history of the thermodynamic forces, only those in a recent span of the relaxation time scale can be memorized to reduce the memory usage. Nevertheless, this still requires a large memory space to memorize the thermodynamic forces of multiple time steps.

- The integral form also requires large computational time. In the integral form, the four-dimensional numerical integration of the constitutive equations should be performed at each cell and each time step. Thus in a direct implementation of such integration, the depth of the nested loops becomes eight, which implies that the numerical integration of the integral form is almost unrealistic from the point of view of the numerical cost. In addition, to calculate the memory function on non-uniform fluid fields, complicated integration and tensor structures (4.58)-(4.63) should be taken into account. They make the numerical integration even complicated, and the cost increases much more.

- To calculate the dissipative currents at the initial step, the history of the thermodynamic forces before the initial time should be given as an initial condition. Since the thermodynamic forces before

the initial time cannot be described within hydrodynamics itself, this requires another model for the thermodynamic forces of the past. In the differential form, an initial condition is much simpler. The thermodynamic forces of the past are not needed as an initial condition. Instead the initial values of the dissipative currents are needed since the dissipative currents become new dynamical variables in the differential form. The degrees of freedom to describe such thermodynamic forces at an initial time are much less than those of a history of the thermodynamics forces. This means that testing the initialization model is much easier in the differential form than in the integral form.

- To compare the results with those of conventional dissipative hydrodynamics calculated with the differential form, the differential form is more useful than the integral form. Even if the integral form and the differential form are mathematically equivalent, using the integral form requires a control of the numerical errors of two different approaches.

- In the integral form, we have to generate the colored noise (4.12) while we can use the white noise in the differential form (4.123). The white noise can be simply generated independently at each time step. On the other hand, generating colored noise with a given time correlation requires additional memories and procedures.

With these considerations, we adopt the differential form of the constitutive equations for the relativistic fluctuating hydrodynamics. Here we summarize the whole set of the equations of the relativistic dissipative hydrodynamics to be considered in this chapter.

The conservation laws are written as

$$\bar{\partial}_\mu T^{\mu\nu} = 0, \tag{5.1}$$
$$\bar{\partial}_\mu N_i^\mu = 0. \tag{5.2}$$

We here used the symbol $\bar{\partial}_\mu$ for the covariant derivative rather than the standard notation ∇_μ since the symbol ∇_μ is already used for the spatial derivative. So far we have made discussions under the flat coordinates of the Minkowski space. However, in high-energy nuclear collisions, *curved coordinates* called the τ-η_s coordinates are widely used. Due to the Lorentz contraction of the colliding nuclei, the hydrodynamics of heavy-ion processes is started from a thin region with the order of a femtometer, and expanding into large region about the size of ten femtometer. Therefore a coordinate system expanding along with the matter is convenient to capture the essential details of the evolution, e.g., how initial small structures are growing into large structures. In the curved coordinates, we have to distinguish the covariant derivative from the naive partial differentiation. It should be noticed here that, even if the coordinates are curved, the spacetime itself is not curved in high-energy nuclear collisions, i.e., there is no curvature.

We adopted the Landau frame, so that the Noether currents $(T^{\mu\nu}, N_i^\mu)$ are decomposed as

$$T^{\mu\nu} = eu^\mu u^\nu - (P + \Pi)\Delta^{\mu\nu} + \pi^{\mu\nu}, \tag{5.3}$$
$$N_i^\mu = n_i u^\mu + \nu_i^\mu. \tag{5.4}$$

For the constitutive equations, we choose the following differential forms:

$$\tau_\Pi \bar{\mathrm{D}}\Pi + \sigma_\Pi \theta \Pi + \Pi = -\zeta\theta + \xi_\Pi, \tag{5.5}$$
$$\tau_\pi \Delta^{\mu\nu}{}_{\alpha\beta} \bar{\mathrm{D}}\pi^{\alpha\beta} + \sigma_\pi \theta \pi^{\mu\nu} + \pi^{\mu\nu} = 2\eta\sigma^{\mu\nu} + \xi_\pi^{\mu\nu}, \tag{5.6}$$
$$\tau_{ij} \Delta^\mu{}_\alpha \bar{\mathrm{D}}\nu_j^\alpha + \sigma_{ij}\theta\nu_j^\mu + \nu_i^\mu = \kappa_{ij} T \bar{\nabla}^\mu \frac{\mu_j}{T} + \xi_i^\mu. \tag{5.7}$$

Note that all the derivatives in the constitutive equations should also be written with the covariant derivatives: $\bar{\mathrm{D}} \equiv u^\mu \bar{\partial}_\mu$, $\bar{\nabla}^\mu \equiv \Delta^{\mu\nu}\bar{\partial}_\nu$, and $\theta \equiv \bar{\partial}_\mu u^\mu$. The non-linear terms, $\sigma_\Pi \theta \Pi$, $\sigma_\pi \theta \pi^{\mu\nu}$ and $\sigma_{ij}\theta\nu_j^\mu$, are added to be consistent with existing calculations.

The information of the matter properties enters the equation of state and the other transport coefficients: $P(e, \{n_i\})$, $T(e, \{n_i\})$, $\mu_j(e, \{n_i\})$, $\zeta(e, \{n_i\})$, $\eta(e, \{n_i\})$, $\kappa_{ij}(e, \{n_i\})$, $\tau_\Pi(e, \{n_i\})$, $\tau_\pi(e, \{n_i\})$, $\tau_{ij}(e, \{n_i\})$, $\sigma_\Pi(e, \{n_i\})$, $\sigma_\pi(e, \{n_i\})$, and $\sigma_{ij}(e, \{n_i\})$.

5.2 Conservation and transversality

In relativistic fluctuating hydrodynamics, fluid fields have large gradients because hydrodynamic fluctuations occur independently at each spatial point and contain short-wavelength components. With such large gradients, naive hydrodynamic calculations in the discretized grids suffer from problems. Here we introduce a new numerical scheme of causal dissipative hydrodynamics which is robust over the large gradients.

We especially focus on constraints on the fluid fields such as the transversality of the dissipative currents (3.18) and (3.33) as well as the conservations of the energy-momentum and the charges. In the continuum description of hydrodynamics, such constraints trivially hold within the hydrodynamic equations while we have to discretize the spacetime to represent the fluid fields in the numerical calculations. Small discretization errors of the constraints, which have the order of the grid spacing Δx and the time step Δt, can be accumulated during the time integration of the hydrodynamics to cause inaccurate results or even a crash of the calculation due to an instability caused by the errors.

The numerical schemes can be explicitly constructed so that the constraints are not broken by the discretization error. A numerical scheme without the discretization errors in the conservation laws is called a conservative scheme. The conservative schemes have been studied for a long time in the field of computational fluid dynamics for non-relativistic hydrodynamics. A major class of the conservative schemes is the finite volume method (FVM). In FVM, the dynamics of the system is described as the transfer of the conserved quantities from a cell to the adjacent cells, and thus the conservation laws hold explicitly. Note that even in the conservative scheme, there are still rounding errors of floating-point representation of the field values. However they are very small compared to the discretization errors and do not matter in the calculation of high-energy nuclear collisions. In relativistic hydrodynamics with curved coordinates, naive application of the FVM developed for non-relativistic systems breaks the conservation laws. Therefore we have developed a new conservative scheme for the relativistic hydrodynamics with curved coordinates in collaboration with Y. Tachibana. See appendix D.1 for the basic idea.

Another discretization errors specific to the causal dissipative hydrodynamics are the errors in transversality of the dissipative currents. The dissipative currents are defined as the spatial components of the conserved currents, and thus they are always transverse to the four-velocity which determines a specific direction of the time. It is not surprising that the constitutive equations describing the dissipative currents preserve the transversality of the dissipative currents along their time evolution. However, a naive discretization of the constitutive equations in time breaks the transversality. In non-relativistic systems, the transversality is trivially preserved because the spatial components and temporal components are explicitly separated, so that there is no room to mix even in discretized calculations. On the other hand, in relativistic systems, the direction of the time defined with the four-velocity of the medium is different at each spacetime point. This causes errors in the discretized constitutive equations when the quantities in different points, separated with a finite distance Δx and Δt, appear in the same expression.

In later sections we focus on constructing a new scheme preserving the transversality of the dissipative currents by considering a natural discretization of the constitutive equations.

5.3 Representation of fluid fields

Starting point of constructing a scheme is to choose the representation of the fluid fields or, in other words, to determine the set of the dynamical variables in the calculations. We here propose a new set of the variables: the dissipative currents represented in the local rest frame $(\Pi, \pi^{\mu\nu}_{\rm LRF}, \nu^{\mu}_{i\,\rm LRF})$ and the conserved densities $(T^{\mu 0}, N^0_i)$. This new choice is useful to construct the conservative scheme where the conservation law and the transversality are free from discretization errors.

5.3.1 Conservation laws and densities

First let us discuss the representation of the conserved densities. One choice of the variable set is the ideal part of the conserved density $(T^{\mu 0}_{\rm id}, N^0_{i\,\rm id})$ combined with the dissipative currents $(\Pi, \pi^{\mu\nu}, \nu^{\mu}_i)$. Another choice is the whole conserved density $(T^{\mu 0}, N^0_i)$ with the dissipative currents.

The former choice can be naturally obtained by extending the scheme for ideal hydrodynamics. In this representation, the conservation laws, (5.3) and (5.4), can be treated as the continuity equation of

the ideal part with source terms coming from the dissipation:

$$\bar{\partial}_\mu T^{\mu\nu}_{\rm id} = -\bar{\partial}_\mu \tau^{\mu\nu}, \tag{5.8}$$
$$\bar{\partial}_\mu N^{\mu}_{i\,{\rm id}} = -\bar{\partial}_\mu \nu^{\mu}_i. \tag{5.9}$$

The constitutive equations are solved as a dynamical equation for the dissipative currents. However, this representation has a problem: The conserved density of the system is not the densities of the ideal part $(T^{\mu 0}_{\rm id}, N^0_{i\,{\rm id}})$ but the whole density $(T^{\mu 0}, N^0_i) = (T^{\mu 0}_{\rm id} + \tau^{\mu 0}, N^0_{i\,{\rm id}} + \nu^0_i)$. Constructing a conservative scheme using this variable set is complicated because the ideal part and the dissipative part are independently solved by the conservation law and the constitutive equations, respectively. The constraints on the sum of these two parts should be applied to both of the conservation law and the constitutive equations in a consistent way.

In this thesis we adopt the other variable set with the whole conserved density $(T^{\mu 0}, N^0_i)$. In this choice, the conservation law can be simply solved using a conservative scheme. In addition, taking care of the curved coordinates as in Appendix D.1, the conservation law becomes free from the discretization errors.

5.3.2 Transversality and dissipative currents

We here discuss the representation of the dissipative currents by considering the transversality between the dissipative currents and the flow velocity, (3.18) and (3.33). As already noted, naively discretized constitutive equations break the transversality. There are two types of strategy to force the transversality: A and B as follows.

The first strategy A is to modify the dissipative currents to be transverse to the flow velocity after the time step. The strategy A is widely used in the existing calculations. In particular, (A1) the time components of the dissipative currents $(\pi^{0\mu}, \nu^0_i)$ can be reconstructed from the spatial components (π^{kl}, ν^k_i) using the transversality. Another way of the strategy A is (A2) to perform the projection of the dissipative currents after the time step.

The second strategy B is to adopt the representation of the dissipative part where transversality is trivially fulfilled. The reason why the constraints are needed in the strategy A is that the representation of the dissipative currents has redundant degrees of freedom. The intrinsic degrees of freedom of the shear-stress tensor $\pi^{\mu\nu}$ and each diffusion current ν^μ_i are 5 and 3, respectively. However, the apparent degrees of freedom of the diffusion currents are 10 and 4, respectively. In the strategy B, we consider the representations without redundant degrees, so that the constraints are not needed. In particular we consider the following two methods: (B1) a method with the full conserved currents $(T^{\mu\nu}, N^\mu_i)$, and (B2) a method the dissipative currents in the local rest frame $(\Pi, \pi^{\mu\nu}_{\rm LRF}, \nu^\mu_{i\,{\rm LRF}})$.

We adopt the method (B2) with $(\Pi, \pi^{\mu\nu}_{\rm LRF}, \nu^\mu_{i\,{\rm LRF}})$ in our scheme. To see the advantages of this method (B2), let us compare these methods with each other:

(A1) In the method to reconstruct the time components, the evolution of the spatial components is first solved with the constitutive equations, and then the time components are solved as

$$\nu^0_i = \sum_{j=1}^{3} u_j \nu^j_i / u_0, \tag{5.10}$$
$$\pi^{\mu 0} = \sum_{j=1}^{3} u_j \pi_{\mu j} / u_0. \tag{5.11}$$

However this method still has subtleties. In this method, specific components of the dissipative currents are chosen to be solved with the constitutive equations, and the other components are not solved with the constitutive equations. Although the choice of the spatial components seems the most natural, the definition of the spatial components depends on the choice of the spacetime coordinates of the calculation.

Another problem can be found in the following simple toy equation:

$$\Delta^\mu{}_\alpha \bar{\rm D} \nu^\alpha_i = 0, \tag{5.12}$$
$$\Delta^{\mu\nu}{}_{\alpha\beta} \bar{\rm D} \pi^{\mu\nu} = 0. \tag{5.13}$$

This equation preserves the transversality of the dissipative currents, and the solution is given by (4.52), (4.53):

$$\nu_i^\mu(\tau) = \Delta(\tau;\tau_{\rm i})^\mu{}_\kappa \nu_i^\kappa(\tau_{\rm i}), \tag{5.14}$$

$$\pi^{\mu\nu}(\tau) = \Delta(\tau;\tau_{\rm i})^{\mu\nu}{}_{\kappa\lambda} \pi^{\kappa\lambda}(\tau_{\rm i}). \tag{5.15}$$

According to the properties of the pathline projectors (4.43) and (4.44), the norm of the dissipative currents should not change along the time evolution:

$$\nu_i^\mu \nu_{i\,\mu} = \text{const}, \tag{5.16}$$

$$\pi^{\mu\nu}\pi_{\mu\nu} = \text{const}. \tag{5.17}$$

$$\tag{5.18}$$

However when the time components are reconstructed from the spatial components, the norms are not ensured to be preserved. The norms become unstable with large velocity gradients, and can have unphysically large values.

(A2) Another way of forcing the transversality is the projection. First all the components of the dissipative currents can be solved with the constitutive equations, and then they are projected onto their proper space. This method seems more natural than the previous method since specific components are not chosen explicitly. Also, this method is more stable than the previous one since the dissipative currents always decrease with the projection. However, in this method the norms become much smaller than the desired values when the velocity gradients are large.

(B1) One possibility of the strategy B, the representation without redundant degrees of the dissipative currents, is choosing the Noether currents $(T^{\mu\nu}, N_i^\mu)$ as the dynamical variables of the calculations. The Noether currents have just enough information to describe the system because the local rest frame is defined with the Noether currents, and all the quantities are defined by the decomposition under the frame. Thus the Noether currents are the most basic quantities of hydrodynamics. In this choice, the evolution equation of the Noether currents is obtained by combining the conservation law and the constitutive equations. We implemented a code with this scheme and tested. However, it turned out that this scheme has fatal instability in determination of the fluid velocity when the fluid velocity have large values.

(B2) As the second choice of the strategy B, we consider the dissipative currents $(\pi^{\mu\nu}_{\rm LRF}, \nu^\mu_{i\,\rm LRF})$ represented in the local rest frame at each spacetime point, combined with the conserved densities $(T^{\mu 0}, N_i^0)$. In this representation, the time components of the dissipative currents always vanish, and only the spatial components are solved in calculations. The degrees of the freedom reduce to the intrinsic number of each dissipative current, and there are no need to consider the constraints explicitly. In addition, in this representation the evolution by the pathline projector can be expressed with a spatial rotation which trivially preserves the norms. In this thesis we adopt this representation for relativistic dissipative hydrodynamics.

5.4 Tensor bases

Before giving explicit definitions of the dissipative currents in the local rest frame $(\pi^{\mu\nu}_{\rm LRF}, \nu^\mu_{i\,\rm LRF})$, we introduce several tensor bases and discuss mathematical treatments under these bases.

5.4.1 Laboratory basis

The most fundamental basis is the one associated with the flat coordinates (t, x, y, z) in the laboratory. In this coordinate system, the associated basis of tangent space and its dual basis are $\partial_{\bar\alpha} = (\partial_t, \partial_z, \partial_x, \partial_y)$ and $dx^{\bar\alpha} = (dt, dz, dx, dy)$, respectively. We use the tensor indices of lower Greek alphabets with the bar $\bar\alpha, \bar\beta, \ldots$ to denote the tensor components expressed in this basis.

5.4.2 Grid basis

In numerical calculations with curved coordinates, it is useful to consider the basis associated with the coordinate system of the grids. Let us call this basis the *grid basis*. In high-energy nuclear collisions, the τ-η_s coordinates (τ, η_s, x, y) are commonly used. The spatial derivatives of the quantities are evaluated along the spatial coordinates of this coordinate system. Also, the time evolution of the system is performed on the temporal coordinate of this coordinate system. Thus this basis is important in considering the spacetime evolution of the system. We use the tensor indices of lower Greek alphabets without bars for this basis: $\mu, \nu, \ldots$, and we write the bases as ∂_μ and dx^μ.

The basis transformations between the grid basis and the laboratory basis are given by $e^{\bar{\alpha}}{}_{\mu} \equiv \partial x^{\bar{\alpha}}/\partial x^\mu$ and $e^{\mu}{}_{\bar{\alpha}} \equiv (e^{\bar{\alpha}}{}_{\mu})^{-1}$. The transformation of the vector fields $V(= V^{\bar{\alpha}}\partial_{\bar{\alpha}} = V^\mu \partial_\mu)$ can be expressed as

$$V^{\bar{\alpha}} = e^{\bar{\alpha}}{}_{\mu} V^\mu, \tag{5.19}$$
$$V^\mu = e^{\mu}{}_{\bar{\alpha}} V^{\bar{\alpha}}. \tag{5.20}$$

In the τ-η_s coordinates, the metric tensor is $g_{\mu\nu} = \mathrm{diag}(1, -\tau^2, -1, -1)$. The basis transformations become the followings:

$$e^{\bar{\alpha}}{}_{\mu} = \begin{pmatrix} \cosh\eta_s & \tau\sinh\eta_s & 0 & 0 \\ \sinh\eta_s & \tau\cosh\eta_s & 0 & 0 \\ 0 & 0 & 1 & 0 \\ 0 & 0 & 0 & 1 \end{pmatrix}, \tag{5.21}$$

$$e^{\mu}{}_{\bar{\alpha}} = \begin{pmatrix} \cosh\eta_s & -\sinh\eta_s & 0 & 0 \\ -\frac{1}{\tau}\sinh\eta_s & \frac{1}{\tau}\cosh\eta_s & 0 & 0 \\ 0 & 0 & 1 & 0 \\ 0 & 0 & 0 & 1 \end{pmatrix}. \tag{5.22}$$

The Christoffel symbols in the grid basis are $\Gamma^0{}_{11} = \tau, \Gamma^1{}_{01} = \Gamma^1{}_{10} = 1/\tau$, and otherwise $\Gamma^\mu{}_{\alpha\beta} = 0$.

5.4.3 Grid tetrad

Here we define an orthonormal basis whose direction of time is parallel to that of the grid basis. Let us call the basis the *grid tetrad*. In the grid basis, the metric tensor is not isotropic, which makes it complex to treat the local thermodynamic quantities in the grid basis. Instead, the quantities are usually scaled to cancel the metric tensor. We here generalize the treatment as a new basis where the metric tensor has the simple form: $\mathrm{diag}(1, -1, -1, -1)$, yet the direction of the time is parallel to that in the grid basis. This is the basis of the inertial frame of each grid point. We use lower Roman alphabets with tildes $\tilde{a}, \tilde{b}, \tilde{c}, \ldots$ for the tensor indices in this basis since the scaled quantities are historically expressed with tildes in high-energy nuclear collisions.

Note that such an orthonormal basis is not unique because there are freedom degrees of spatial rotation. If the grid coordinates are already orthogonal, one orthonormal basis can be easily obtained by normalizing the grid basis. In general, the grid tetrad can be defined as a local linear transformations, $e^{\tilde{a}}{}_{\mu}$, of the grid basis: $dx^{\tilde{a}} = e^{\tilde{a}}{}_{\mu} dx^\mu$, $\partial_{\tilde{a}} = e^{\mu}{}_{\tilde{a}}\partial_\mu$. It should be noticed here that the components of $dx^{\tilde{a}}$ are not necessarily the exact differential, and thus the notations $dx^{\tilde{a}}$ and $\partial_{\tilde{a}}$ are just symbolic ones. This means that the grid tetrad is not a holonomic basis in general, i.e., it is not necessarily the associated basis of some coordinates.

In the τ-η_s coordinates, the grid tetrad can be chosen as $dx^{\tilde{a}} = (d\tau, \tau d\eta_s, x, y)$, and $\partial_{\tilde{a}} = (\partial_\tau, (1/\tau)\partial_{\eta_s}, \partial_x, \partial_y)$. The basis transformations between this basis and the grid basis are

$$e^{\mu}{}_{\tilde{a}} = \mathrm{diag}(1, 1/\tau, 1, 1), \tag{5.23}$$
$$e^{\tilde{a}}{}_{\mu} = \mathrm{diag}(1, \tau, 1, 1). \tag{5.24}$$

The basis transformations between this basis and the laboratory basis are given as

$$e^{\bar{\alpha}}{}_{\mu} = \begin{pmatrix} \cosh\eta_s & \sinh\eta_s & 0 & 0 \\ \sinh\eta_s & \cosh\eta_s & 0 & 0 \\ 0 & 0 & 1 & 0 \\ 0 & 0 & 0 & 1 \end{pmatrix}, \tag{5.25}$$

$$e^{\mu}{}_{\bar{\alpha}} = \begin{pmatrix} \cosh\eta_s & -\sinh\eta_s & 0 & 0 \\ -\sinh\eta_s & \cosh\eta_s & 0 & 0 \\ 0 & 0 & 1 & 0 \\ 0 & 0 & 0 & 1 \end{pmatrix}. \tag{5.26}$$

Because the grid tetrad is a nonholonomic basis, a special care is needed when considering the covariant derivatives. The familiar expression of Christoffel symbols $\Gamma_{\gamma\alpha\beta} = \frac{1}{2}(g_{\gamma\alpha,\beta} + g_{\gamma\beta,\alpha} - g_{\alpha\beta,\gamma})$ is no longer valid in nonholonomic bases. In an orthonormal basis, the Ricci rotation coefficients can be used instead of the above expression:

$$\bar{\partial}_{\tilde{a}} V^{\tilde{b}} = \partial_{\tilde{a}} V^{\tilde{b}} + \Gamma^{\tilde{b}}{}_{\tilde{c}\tilde{a}} V^{\tilde{c}}, \tag{5.27}$$

$$\Gamma^{\tilde{a}}{}_{\tilde{b}\tilde{c}} = \frac{1}{2} g^{\tilde{a}\tilde{d}} (f_{\tilde{d}\tilde{b}\tilde{c}} + f_{\tilde{d}\tilde{c}\tilde{b}} - f_{\tilde{b}\tilde{c}\tilde{d}}), \tag{5.28}$$

where the structure coefficients $f_{\tilde{a}\tilde{b}\tilde{c}}$ are defined by the Lie bracket: $[\partial_{\tilde{a}}, \partial_{\tilde{b}}] = f_{\tilde{a}\tilde{b}}{}^{\tilde{c}} \partial_{\tilde{c}}$. Given the expression of the basis transformation $e^{\tilde{a}}{}_{\mu}$ or $e^{\tilde{a}}{}_{\bar{\alpha}}$, the Christoffel symbols can alternatively be obtained by the basis transformation of the connection coefficients:

$$\Gamma^{\tilde{a}}{}_{\tilde{b}\tilde{c}} = e^{\tilde{a}}{}_{\mu} \partial_{\tilde{c}} e^{\mu}{}_{\tilde{b}} + e^{\tilde{a}}{}_{\mu} e^{\nu}{}_{\tilde{b}} e^{\xi}{}_{\tilde{c}} \Gamma^{\mu}{}_{\nu\xi}, \tag{5.29}$$

$$\text{or} \quad \Gamma^{\tilde{a}}{}_{\tilde{b}\tilde{c}} = e^{\tilde{a}}{}_{\bar{\alpha}} \partial_{\tilde{c}} e^{\bar{\alpha}}{}_{\tilde{b}}. \tag{5.30}$$

Unlike the symmetric Christoffel symbols, the Ricci rotation coefficients are antisymmetric with their first two indices: $\Gamma_{(\tilde{a}\tilde{b})\tilde{c}} = 0$ where $\Gamma_{\tilde{a}\tilde{b}\tilde{c}} = g_{\tilde{a}\tilde{d}} \Gamma^{\tilde{d}}{}_{\tilde{b}\tilde{c}}$. Therefore they have the following form:

$$\Gamma^{\tilde{a}}{}_{\tilde{b}\tilde{c}} = \left[\begin{pmatrix} 0 & \tilde{\boldsymbol{\Gamma}}^{\mathrm{T}}_{\tilde{c}} \\ \tilde{\boldsymbol{\Gamma}}_{\tilde{c}} & (\tilde{\Omega}_{\tilde{c}})_{[ij]} \end{pmatrix} \right]^{\tilde{a}}{}_{\tilde{b}}. \tag{5.31}$$

In the τ-η_s coordinates, the Christoffel symbols of this basis are $\Gamma^{\tilde{0}}{}_{\tilde{1}\tilde{1}} = \Gamma^{\tilde{1}}{}_{\tilde{0}\tilde{1}} = 1/\tau$, otherwise $\Gamma^{\tilde{a}}{}_{\tilde{b}\tilde{c}} = 0$. Each component of the Ricci rotation coefficients can be given by $\tilde{\boldsymbol{\Gamma}}_{\tilde{0}} = \tilde{\boldsymbol{\Gamma}}_{\tilde{2}} = \tilde{\boldsymbol{\Gamma}}_{\tilde{3}} = 0$, and $\tilde{\Omega}_{\tilde{c}} = 0$.

5.4.4 Flow tetrad

To represent the dissipative currents $(\pi^{\mu\nu}_{\mathrm{LRF}}, \nu^{\mu}_{i\,\mathrm{LRF}})$, we define another orthonormal basis in the local rest frame of the fluid. Let us call this basis the *flow tetrad*. We use the uppercase Roman alphabets for the tensor indices of this basis: $I, J, \ldots$. This basis also has the degrees of freedom of the spacial rotation like the grid tetrad. We fix the flow tetrad so that it can be obtained from the grid tetrad with a single Lorentz boost:

$$e^{I}{}_{\tilde{a}} = \begin{pmatrix} \tilde{u}^0 & -\tilde{\boldsymbol{u}}^{\mathrm{T}} \\ -\tilde{\boldsymbol{u}} & 1 + \frac{\tilde{\boldsymbol{u}}\tilde{\boldsymbol{u}}^{\mathrm{T}}}{1+\tilde{u}^0} \end{pmatrix}, \tag{5.32}$$

$$e^{\tilde{a}}{}_{I} = \begin{pmatrix} \tilde{u}^0 & \tilde{\boldsymbol{u}}^{\mathrm{T}} \\ \tilde{\boldsymbol{u}} & 1 + \frac{\tilde{\boldsymbol{u}}\tilde{\boldsymbol{u}}^{\mathrm{T}}}{1+\tilde{u}^0} \end{pmatrix}, \tag{5.33}$$

where $(\tilde{u}^0, \tilde{\boldsymbol{u}}) \equiv u^{\tilde{a}}$ is the flow velocity in the grid tetrad. In this basis, the flow velocity becomes $u^I = (1, \mathbf{0})$ and the time components of the dissipative currents vanish as expected.

This basis is another nonholonomic orthonormal basis, and the Christoffel symbols can be given by the Ricci rotation coefficients as in the case of the grid tetrad:

$$\Gamma^I{}_{JK} = \begin{pmatrix} 0 & \hat{\mathbf{\Gamma}}^{\mathrm{T}}_K \\ \hat{\mathbf{\Gamma}}_K & \hat{\Omega}_K \end{pmatrix}, \tag{5.34}$$

$$\hat{\mathbf{\Gamma}}_K \equiv -\frac{\partial_K \tilde{u}^0 + \tilde{\mathbf{\Gamma}}_K \cdot \tilde{\boldsymbol{u}}}{1+\tilde{u}^0}\tilde{\boldsymbol{u}} + \partial_K \tilde{\boldsymbol{u}} + \tilde{u}^0 \tilde{\mathbf{\Gamma}}_K + \tilde{\Omega}_K \tilde{\boldsymbol{u}}, \tag{5.35}$$

$$\hat{\Omega}_K \equiv \tilde{\Omega}_K + \left(\frac{\partial_K \tilde{\boldsymbol{u}} + \tilde{\Omega}_K \tilde{\boldsymbol{u}}}{1+u^0} + \tilde{\mathbf{\Gamma}}_K \right) \tilde{\boldsymbol{u}}^{\mathrm{T}} - \tilde{\boldsymbol{u}} \left(\frac{\partial_K \tilde{\boldsymbol{u}} + \tilde{\Omega}_K \tilde{\boldsymbol{u}}}{1+u^0} + \tilde{\mathbf{\Gamma}}_K \right)^{\mathrm{T}}, \tag{5.36}$$

where $\tilde{\mathbf{\Gamma}}_K = g^{\tilde{a}}{}_K \tilde{\mathbf{\Gamma}}_{\tilde{a}}$ and $\tilde{\Omega}_K = g^{\tilde{a}}{}_K \tilde{\Omega}_{\tilde{a}}$. The quantities in the flow tetrad are marked with hats: $\hat{\cdot}$.

5.5 Constitutive equations

Now we can explicitly define the representation of the dissipative currents. In our new scheme, the dissipative currents are represented in the flow tetrad:

$$\nu^I_i = \begin{pmatrix} 0 \\ \hat{\boldsymbol{\nu}}_i \end{pmatrix}, \tag{5.37}$$

$$\pi^{IJ} = \begin{pmatrix} 0 & 0 \\ 0 & \hat{\pi} \end{pmatrix}. \tag{5.38}$$

The conservation law are solved with the modified conservative scheme for the constitutive equations as described in Appendix D.1. In this section we focus on the constitutive equations.

The time evolution of the dissipative currents is described by the constitutive equations in causal dissipative hydrodynamics. Even if they are represented in the flow tetrad, it is basically the same. Nevertheless, it is interesting to observe how the structure of the constitutive equations changes under this non-trivial basis. The constitutive equations for the shear-stress tensor and diffusion currents have the following structure:

$$\Delta^I{}_K \bar{\mathrm{D}} \nu^K_i = Y^J_i, \tag{5.39}$$

$$\Delta^{IJ}{}_{KL} \bar{\mathrm{D}} \pi^{KL} = Y^{IJ}, \tag{5.40}$$

where

$$Y^J_i = -\sum_{j=1}^n \tau^{-1}_{ij} \left[(\sigma_{ij}\theta + 1)\nu^J_j - \sum_{k=1}^n \kappa_{jk} T \bar{\nabla}^J \frac{\mu_k}{T} - \xi^J_j \right], \tag{5.41}$$

$$Y^{IJ} = -[(\sigma_\pi \theta + 1)\pi^{IJ} - 2\eta\sigma^{IJ} - \xi^{IJ}_\pi]/\tau_\pi, \tag{5.42}$$

Since we defined the dissipative currents in the local rest frame in terms of the basis, the non-trivial structure due to the choice of this representation is already contained in the covariant derivatives. What we need to do is only writing down the terms in the covariant derivatives $\bar{\mathrm{D}}$. Using the expression $u^I \equiv (1, \mathbf{0})$ and $\Delta^I{}_J \equiv \mathrm{diag}(0,1,1,1)$, the left-hand sides of the equations (5.39) and (5.40) is expanded as

$$\Delta^I{}_J \bar{\mathrm{D}} \nu^J_i = \mathrm{D}\nu^I_i + \hat{\Omega}^I{}_{Ju} \nu^J_i, \tag{5.43}$$

$$\Delta^{IJ}{}_{KL} \bar{\mathrm{D}} \pi^{KL} = \mathrm{D}\pi^{IJ} + \hat{\Omega}^I{}_{Ku} \pi^{KJ} + \hat{\Omega}^J{}_{Lu} \pi^{IL}, \tag{5.44}$$

where $\hat{\Omega}^I{}_{Ju} \equiv \Delta^I{}_K (u^M \Gamma^K{}_{LM}) \Delta^L{}_J$ is the spatial part of the Ricci rotation coefficients. The other components of the Ricci rotation coefficients vanish due to the projectors on the left-hand sides. The projectors are originally introduced not to break the transversality of the dissipative currents in (3.126) and (3.128). Now we can see that the projectors prevent the temporal components of the Ricci rotation coefficients to make the dissipative currents have the temporal components in the local rest frame.

Combining the equations (5.43), (5.44), (5.39), and (5.39), the dynamical equations of the dissipative currents in the local rest frame are obtained:

$$\mathrm{D}\pi^{KL} = -\hat{\Omega}^{I}{}_{Ku}\pi^{KJ} - \hat{\Omega}^{J}{}_{Lu}\pi^{IL} + Y^{IJ}, \tag{5.45}$$

$$\mathrm{D}\nu_i^K = -\hat{\Omega}^{I}{}_{Ju}\nu_i^J + Y_i{}^J. \tag{5.46}$$

The content of the matrix $\hat{\Omega}^{I}{}_{Ju}$ can be written down with the grid basis quantities as

$$\hat{\Omega}^{I}{}_{Ju} = \begin{pmatrix} 0 & 0 & 0 & 0 \\ 0 & 0 & a^3 & -a^2 \\ 0 & -a^2 & 0 & a^1 \\ 0 & a^3 & -a^1 & 0 \end{pmatrix}, \tag{5.47}$$

$$\boldsymbol{a} \equiv \tilde{\boldsymbol{\Omega}}^*_u + \left(\frac{\mathrm{D}\tilde{\boldsymbol{u}} + \tilde{\boldsymbol{\Omega}}^*_u \times \tilde{\boldsymbol{u}}}{1+\tilde{u}^0} + \tilde{\boldsymbol{\Gamma}}_u \right) \times \tilde{\boldsymbol{u}} \tag{5.48}$$

where $\tilde{\boldsymbol{\Gamma}}_u \equiv u^{\tilde{a}}\tilde{\boldsymbol{\Gamma}}_{\tilde{a}}$ and $\tilde{\boldsymbol{\Omega}}^*_u \equiv \frac{1}{2}\epsilon^{ijk}u^{\tilde{a}}[\tilde{\Omega}_{\tilde{a}}]_{jk}$. This particular form indicates that $-\hat{\Omega}^{I}{}_{Ju}$ is an infinitesimal generator of the spatial rotation along the axis $\boldsymbol{a}$. Therefore the dissipative currents evolve by the (Y_i^J, Y^{IJ}) and, at the same time, rotate by $\boldsymbol{a}$. If the right-hand sides of the constitutive equation vanish, the dissipative currents just rotate, and their norms are preserved as expected in (5.16) and (5.17). In numerical simulations, the effect can be implemented as real rotations so that the norms are explicitly preserved. The rotation of a vector $\boldsymbol{v}$ by the axis $\boldsymbol{a}$ can be performed with the following expression:

$$\boldsymbol{v}' = \boldsymbol{v}\cos\theta + \boldsymbol{v} \times \hat{\boldsymbol{a}} + \hat{\boldsymbol{a}}(\boldsymbol{v} \cdot \hat{\boldsymbol{a}})(1 - \cos\theta), \tag{5.49}$$

where $\hat{\boldsymbol{a}} = \boldsymbol{a}/|\boldsymbol{a}|$. The rotation angle θ is chosen as $\tau\theta = |\boldsymbol{a}|\Delta t/u^0$ in actual calculations. The rotation of the shear-stress tensor can be performed by applying the rotation to each index.

In the flat grid (t, x, y, z), the rotation axis becomes $\boldsymbol{a} = \frac{\mathrm{D}\boldsymbol{u}}{1+u^0} \times \boldsymbol{u}$. In the τ-η_s coordinates, the axis becomes $\boldsymbol{a} = (\frac{\mathrm{D}\tilde{\boldsymbol{u}}}{1+\tilde{u}^0} + \tilde{\boldsymbol{\Gamma}}_u) \times \tilde{\boldsymbol{u}}$ where $\tilde{\boldsymbol{\Gamma}}_u = (\tilde{u}^1/\tau, 0, 0)$. It should be noticed here that all those expressions of the rotation axis are the specific results under the definition of the flow tetrad (5.33). The expression of the axis actually depend on the way of fixing the spatial-rotation ambiguity of the flow tetrad.

.

5.6 Brief summary

In this chapter we first discussed the constraints of the causal dissipative hydrodynamics. There are two major constraints in the causal dissipative hydrodynamics. One is the conservation law, and the other is the transversality between the dissipative currents and the flow velocity. The latter is specific to the causal dissipative hydrodynamics. Those constraints on the fluid fields suffer from the discretization errors with large gradients caused by the hydrodynamic fluctuations. It turned out that the scheme designed to eliminate the discretization errors should be developed for a robust calculation with hydrodynamic fluctuations. For the conservation law, there are already many studies such as finite volume methods, and we modified the existing finite volume method to properly treat the conservation in the curved coordinates.

Next we compared the choices of the set of the dynamical variables. We showed that the commonly used sets, $(T^{\mu 0}_{\mathrm{id}}, N^0_{i\,\mathrm{id}}, \Pi, \pi^{\mu\nu}, \nu^\mu_i)$ and $(T^{\mu 0}, N^0_i, \Pi, \pi^{\mu\nu}, \nu^\mu_i)$, break the preservation of the norms under the trivial evolution of the dissipative currents. Instead we proposed a representation with the dissipative currents in the local rest frame $(T^{\mu 0}, N^0_i, \Pi, \pi^{\mu\nu}_{\mathrm{LRF}}, \nu^\mu_{i\,\mathrm{LRF}})$. Then we defined the four tensor bases for the simplicity of the later calculations. After explicitly defining the dissipative currents in the local rest frame, we finally provided evolution equations of the dissipative currents and examined their properties.

Chapter 6

Smeared fluctuating hydrodynamics

In the previous chapter, we introduced a new numerical scheme for the causal dissipative hydrodynamics. To take into account the hydrodynamic fluctuations in the dissipative hydrodynamics, additional cares in the numerical calculations are needed. With the hydrodynamic fluctuations as random variables, the hydrodynamic equations become stochastic differential equations like the Langevin equation. In this chapter, we discuss how to define such stochastic partial differential equations in the numerical calculations of the causal fluctuating hydrodynamics.

First, to avoid a singularity of the fluctuating hydrodynamics, we discuss the coarse-graining scales and the necessity of the smearing of the noise fields in section 6.1. After considering the generation of the noise with given autocorrelations in section 6.2. we define the smearing methods of the noise in section 6.3. Then, in section 6.4, we discuss the difference between the Itô integral and the Stratonovich integral to interpret the noise terms in the first-order fluctuating hydrodynamics and in the causal fluctuating hydrodynamics.

6.1 Coarse-graining scales

In ordinary hydrodynamic simulations without noise, one can take smaller grid spacing and smaller time steps for better solution. In fluctuating hydrodynamic simulations with white noise terms, however, taking the continuum limit is not a trivial procedure. The magnitude of the averaged noise in a cell (6.14)-(6.16) becomes larger as the cell volume and a time step become smaller. The noise diverges in the continuum limit, which is not physical. This problem still occurs even if one uses a colored noise instead of the white noise because the colored noise in different positions at an equal time do not have correlations due to the causality of the memory function.

Here we should recall the coarse-graining scales, namely, a length scale and a time scale which limit the applicability of hydrodynamics. For example, as the cell volume and the time step get smaller, the value of dissipative stress tensor $\tau^{\mu\nu} = -\Delta^{\mu\nu}\Pi + \pi^{\mu\nu}$ eventually becomes larger than equilibrium components $-\Delta^{\mu\nu}P$. The total pressure $P + \Pi$ can even be negative. In such a situation, the constitutive equations are no longer valid. In fact, in deriving constitutive equations, it is assumed that the deviation of the considered state from the corresponding local-equilibrium state is small enough, which is not compatible with large $|\tau^{\mu\nu}| \gtrsim P$.

The singularity of the fluctuating hydrodynamics comes from the delta functions in the FDR. However the actual thermal noise with scales shorter than the coarse-graining scales cannot be described with the FDR, so that the singularity is not physical. To avoid this apparent singularity, the coarse-graining scale should be explicitly introduced in the formulation of the fluctuating hydrodynamics.

6.1.1 Scales in ordinary hydrodynamics

In the ordinary hydrodynamics without noise, the cell size of the *numerical* calculations can be simply set to the coarse-graining scale of the *physical* system. However, in the fluctuating hydrodynamics, this naive treatment does not work. In order to avoid the singularity, we need to distinguish the numerical scales from the physical coarse-graining scales. In this subsection, we consider the relations between the numerical scales and the physical scales in the ordinary hydrodynamics.

First we have to be aware of two "gaps" between the actual physical system and numerical calculations. One is a gap between the actual system and hydrodynamics with continuum analytic thermody-

namic fields. Hydrodynamic equations are constructed with continuum fields and their derivatives. On the other hand, the physical system is not exactly described by the continuum fields within its microscopic length scale and time scale. The other is a gap between continuum hydrodynamics and hydrodynamic simulations on a discretized grid. In a proper limit of the grid spacing and time step vanishing, numerical calculations are expected to correspond to the solution of continuum hydrodynamics. However we have to do calculations with a finite size of the grid due to finite computational resources.

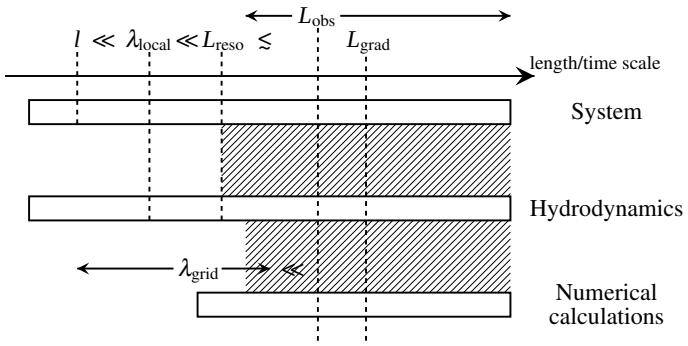

Figure 6.1: Scales in the ordinary hydrodynamics. The shaded regions indicate the ranges of the scales where the dynamics of the upper model can be described by the lower one.

To properly describe the physical system using discretized version of the hydrodynamics, we need to consider the scales of the calculations, the hydrodynamics, and the physical system, and discuss required relations among them (see Fig. 6.1).

In ordinary hydrodynamics without the hydrodynamic fluctuations, three separated scales of the system are assumed:

$$\ell \ll \lambda_{\rm local} \ll L. \tag{6.1}$$

A microscopic scale ℓ represents, for example, the mean free path in kinetic theories. The typical length and time of the macroscopic system, L, is the scale of the physics in the interests. An intermediate scale $\lambda_{\rm local}$ indicates the scale in which a thermodynamic limit can be justified approximately, and therefore a local-equilibrium state $(T, \{\mu_i\})$ can be defined. In order to achieve the approximate thermodynamic limit, the two scales ℓ and $\lambda_{\rm local}$ should be separated. In addition, to apply a differential ∂_μ to thermodynamic fields such as $T(x)$, the two scales $\lambda_{\rm local}$ and L should be separated as well.

To properly compare the macroscopic scale to the numerical scales, we have to introduce further three different macroscopic scales: $L_{\rm reso}$, $L_{\rm grad}$, and $L_{\rm obs}$. The first one $L_{\rm reso}$ is a resolution of the hydrodynamics which limits the applicability of the hydrodynamics to the actual system. Hydrodynamics is a framework with continuous fields and does not have any mathematical lower bound of length and time scales, apparently. Although, the actual microscopic system is not continuous thermodynamic fields. The physics with a shorter scale than $L_{\rm reso}$ cannot be described with the hydrodynamics while the dynamics of the system with a longer scale is described with hydrodynamics. The second scale $L_{\rm grad}$ is a typical length and a time scale of the field gradients, i.e., the scales of spatial and temporal variation of fluid fields. To describe the dynamics of the system with hydrodynamics, the scale of the field gradients should not be smaller than the resolution: $L_{\rm reso} \lesssim L_{\rm grad}$. The third one $L_{\rm obs}$ is the scale of the physics which we are interested in. To describe the physics of interests with hydrodynamics, this scale also should not be smaller than the resolution: $L_{\rm reso} \lesssim L_{\rm obs}$. It should be noticed here that those three macroscopic scales are not necessarily be the same order. For example, in a global-equilibrium state, the length scale of the gradients becomes very large: $L_{\rm grad} \to \infty$. However, this does not mean the resolution of the hydrodynamics gets worse: $L_{\rm reso} \not\to \infty$. The scales of interests $L_{\rm obs}$ can also be freely chosen as far as it is not smaller than the resolution scale. The relations among the scales then become

$$\ell \ll \lambda_{\rm local} \ll L_{\rm reso} \lesssim L_{\rm grad}, L_{\rm obs}. \tag{6.2}$$

In numerical simulations we solve the hydrodynamic equations with finite size of cells and time steps. Here another length scale $\lambda_{\rm grid}$ is defined as the scale of grid spacing and time steps. The grid scale should

be smaller than the scale of interests: $\lambda_{\rm grid} \ll L_{\rm obs}$. To obtain a reliable solution of the hydrodynamic equations, the scale of grid should be sufficiently—for example, a few times—smaller than the scale of the field gradients: $\lambda_{\rm grid} \ll L_{\rm grad}$. Otherwise the numerical solution is affected from the grid structure. For example, the solution would break isotropy of the system with too large gradients. Note that the grid spacing $\lambda_{\rm grid}$ can be smaller than the resolution of hydrodynamics $L_{\rm reso}$ when $L_{\rm reso} \sim L_{\rm grad} \gg \lambda_{\rm grid}$, or larger than the resolution when $L_{\rm reso} \ll L_{\rm grad}$. Consequently, a proper grid scale has the following relation:

$$\lambda_{\rm grid} \ll L_{\rm obs}, L_{\rm grad}. \tag{6.3}$$

The important point here is that the grid scale is not necessarily be the same order with the macroscopic scales.

6.1.2 Scales in fluctuating hydrodynamics

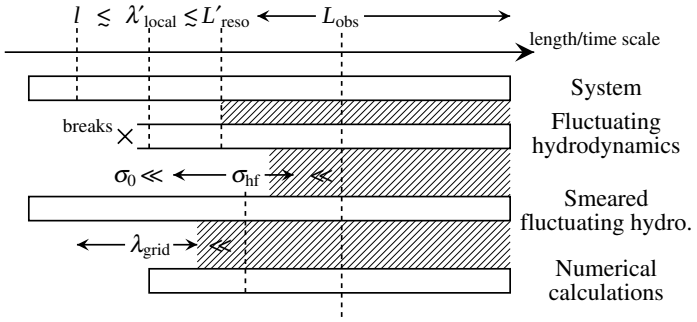

Figure 6.2: Scales in the fluctuating hydrodynamics

In the fluctuating hydrodynamics, the situation is somewhat different. We need to redefine all the scales appeared in the ordinary hydrodynamics (see Fig. 6.2). In this section, by considering scales of the physical system and the fluctuating hydrodynamics, we will introduce *smeared fluctuating hydrodynamics* to avoid the singularity, and discuss the grid spacing and the time step of the numerical calculations.

Let us first consider the scales of the fluctuating hydrodynamics for the system where the scale separations are not as good as in ordinary cases:

$$\ell \lesssim \lambda'_{\rm local} \lesssim L'_{\rm reso} \lesssim L_{\rm obs} \tag{6.4}$$

where $\lambda'_{\rm local}$ is a scale between the microscopic scale and the macroscopic scale. The scale $\lambda'_{\rm local}$ is not large enough to justify the thermodynamic limit, but still large enough that the deviation from the local-equilibrium state can be accounted with the dissipative currents and the hydrodynamic fluctuations. The symbol $L'_{\rm reso}$ denotes the resolution of fluctuating hydrodynamics. Note that the scales with the primes are different from those in the ordinary hydrodynamics even if we consider the same physical system. They depend on a description of the system.

The scale of the gradients $L'_{\rm grad}$ cannot be defined in the naive fluctuating hydrodynamics which contains any short scale of fluctuations. Such fields with large gradients cannot be handled with a finite size of grid. Moreover, with small length scales, the fluctuations become unphysically large. The problems occur totally due to hydrodynamic fluctuations of very short scales.

However, in obtaining the results for the scale of interests $L_{\rm obs}$, the fluctuations with a shorter scale are irrelevant. Therefore hydrodynamic fluctuations with shorter length scales can be switched off with some smearing procedure which will be described in Section 6.3. Here we define smeared fluctuating hydrodynamics by introducing a coarse-graining scale $\sigma_{\rm hf}$ or a cutoff scale of hydrodynamic fluctuations. The scale can be chosen to be sufficiently large so that hydrodynamics does not break down: $\sigma_{\rm hf} \gg \sigma_0$ where σ_0 is the scale in which the fluctuations become unphysically large. At the same time, the coarse-graining scale should be smaller than the scale of interests: $\sigma_{\rm hf} \ll L_{\rm obs}$. As a result, we should choose the smearing scale $\sigma_{\rm hf}$ so that

$$\sigma_0 \ll \sigma_{\rm hf} \ll L_{\rm obs}. \tag{6.5}$$

Finally to perform a numerical calculation of smeared fluctuating hydrodynamics, the grid scale should be smaller than the gradient scale. The gradient scale of the smeared fluctuating hydrodynamics becomes $\sigma_{\rm hf}$. Consequently, the grid spacing and time steps should be chosen so that

$$\lambda_{\rm grid} \ll \sigma_{\rm hf}. \tag{6.6}$$

6.2 Generating white noise

Let us show how to numerically generate the hydrodynamic fluctuations as Gaussian random numbers with the proper correlation. The noise fields can be independently generated in each cell since the noise term in the differential form of the constitutive equations is white. The noise of the shear-stress part and the diffusion part have non-trivial correlations, which can be taken into account by considering linear combinations of noise terms to find independent noise components.

The goal here is to generate the Gaussian random fields satisfying the following relations given in Chapter 4.

$$\langle \xi_\Pi(x)\rangle = 0, \qquad \langle \xi_\Pi(x)\xi_\Pi(x')\rangle = 2T\zeta\delta^{(4)}(x-x'), \tag{6.7}$$
$$\langle \xi_\pi^{IJ}(x)\rangle = 0, \qquad \langle \xi_\pi^{IJ}(x)\xi_\pi^{KL}(x')\rangle = 4T\eta\Delta^{IJKL}\delta^{(4)}(x-x'), \tag{6.8}$$
$$\langle \xi_i^{I}(x)\rangle = 0, \qquad \langle \xi_i^{I}(x)\xi_j^{K}(x')\rangle = 2T\kappa_{ij}\delta^{IJ}\delta^{(4)}(x-x'), \tag{6.9}$$

where $I, J, K, L = 1 \ldots 3$ are the indices in the local rest frame.

In numerical simulations, we cannot treat noise fields directly because of the delta functions. Instead we have to generate the cell-averaged values of the noise fields such as $\bar{\xi}_\Pi$:

$$\bar{\xi}_\Pi(V_{l,m}) = \frac{1}{V_{l,m}}\int_{V_{l,m}} dx^4 \xi_\Pi(x'), \tag{6.10}$$
$$\bar{\xi}_\pi^{IJ}(V_{l,m}) = \frac{1}{V_{l,m}}\int_{V_{l,m}} dx^4 \xi_\pi^{IJ}(x'), \tag{6.11}$$
$$\bar{\xi}_i^{I}(V_{l,m}) = \frac{1}{V_{l,m}}\int_{V_{l,m}} dx^4 \xi_i^{I}(x') \tag{6.12}$$

where $V_{l,m}$ is the (3+1)-dimensional volume of the given cell l at the time step m. The autocorrelation of the cell-averaged noise can be obtained by integrating the original correlations (6.7)-(6.9):

$$\langle \bar{\xi}_\Pi(V_{l,m})\bar{\xi}_\Pi(V_{l',m'})\rangle = \frac{1}{V_{l,m}V_{l',m'}}\int_{V_{l,m}}\int_{V_{l',m'}} dx^4 dx'^4 \langle \xi_\Pi(x)\xi_\Pi(x')\rangle \tag{6.13}$$
$$= 2T\zeta\delta_{ll'}\delta_{mm'}/V_{l,m}, \tag{6.14}$$
$$\langle \bar{\xi}_\pi^{IJ}(V_{l,m})\bar{\xi}_\pi^{KL}(V_{l',m'})\rangle = 4T\eta\Delta^{IJKL}\delta_{ll'}\delta_{mm'}/V_{l,m}, \tag{6.15}$$
$$\langle \bar{\xi}_i^{I}(V_{l,m})\bar{\xi}_j^{K}(V_{l',m'})\rangle = 2T\kappa_{ij}\delta^{IJ}\delta_{ll'}\delta_{mm'}/V_{l,m}. \tag{6.16}$$

The factor $\delta_{ll'}\delta_{mm'}$ means that noise terms in different two cells or in a cell with different times have no correlation, which is expected from the delta function in the original correlations (6.7)-(6.9). Therefore we can generate the noise independently in each cell and each time step. In the later part of this section, we will consider the noise generation in a cell and omitting the cell dependence $V_{l,m}$.

6.2.1 Bulk part

The autocorrelation of the bulk noise $\bar{\xi}_\Pi(x)$ is simple: $\langle \bar{\xi}_\Pi^2\rangle = 2T\eta/V_{\rm cell}$ where $V_{\rm cell}$ is the (3+1)-dimensional volume of the considered cell. Therefore, the bulk noise can be generated with

$$\bar{\xi}_\Pi = \sqrt{2T\zeta}\bar{w}_\Pi. \tag{6.17}$$

Here $\bar{w}_\Pi$ in each cell is an averaged white noise field which follows the Gaussian distribution of mean 0 and variance $1/V_{\rm cell}$.

6.2.2 Diffusion part

The autocorrelation of the diffusion noise $\bar{\xi}_i^I$ becomes non-trivial if the system has more than one conserved charge. The autocorrelation is diagonal with respect to the spatial index I due to the isotropy of the system. However, it is not necessarily diagonal with respect to the charge index i due to the cross terms κ_{ij} $(i \neq j)$ because the diffusion noise of a charge can have correlation with that of another charge.

In this case, the Onsager coefficient κ_{ij} can be diagonalized to find independent noise components ξ_i^*. Because of Onsager reciprocal relations, κ_{ij} is a symmetric matrix and can be diagonalized using an orthogonal matrix $O(\kappa)$:

$$O(\kappa)^{\mathrm{T}} \kappa O(\kappa) = \mathrm{diag}(\lambda_1(\kappa), \ldots, \lambda_n(\kappa)) \tag{6.18}$$

where $\lambda_i(\kappa)$ $(1 \leq i \leq n)$ are eigenvalues of the matrix κ_{ij}. Independent noise components are defined as $\xi_i^{*I} = O_{ij}^{\mathrm{T}} \bar{\xi}_j^I$, and their autocorrelation is diagonal:

$$\langle \xi_i^{*I} \xi_j^{*J} \rangle = O(\kappa)_{ik}^{\mathrm{T}} \langle \xi_k^{*I} \xi_l^{*J} \rangle O(\kappa)_{lj} \tag{6.19}$$

$$= 2T\lambda_i(\kappa)\delta_{ij}\delta^{IJ}/V_{\mathrm{cell}}. \tag{6.20}$$

As a result, the diffusion noise $\bar{\xi}_i^I$ can be generated by the following equation:

$$\bar{\xi}_i^I = O(\kappa)_{ij} \xi_i^{*I} \tag{6.21}$$

$$= \sum_{i=1}^{n} O(\kappa)_{ij} \sqrt{2T\lambda_i(\kappa)} \bar{w}_i^*, \tag{6.22}$$

where $\bar{w}_i^*$ are Gaussian random numbers with mean 0 and variance $1/V_{\mathrm{cell}}$. It should be noticed here that the orthogonal matrix $O(\kappa)_{ij}$ is determined from the Onsager coefficients κ_{ij}, and it generally depends on the temperature $T(x)$ and the chemical potentials $\mu_i(x)$. Therefore, the diagonalization should be performed for each cell at each time step unless κ_{ij} can be trivially diagonalized.

6.2.3 Shear-stress part

As for the noise in the shear-stress part $\bar{\xi}_\pi^{IJ}$, the autocorrelation can be diagonalized as well. However, we introduce more useful linear combinations which cannot be obtained by the diagonalization by a similarity transformation.

The autocorrelation matrix of shear-stress noise generally has the following form:

$$\langle \bar{\xi}_\pi^{IJ} \bar{\xi}_\pi^{KL} \rangle = \alpha \Delta^{IJKL} \tag{6.23}$$

$$= \alpha \left[\frac{1}{2}\delta^{IK}\delta^{JL} + \frac{1}{2}\delta^{IL}\delta^{JK} - \frac{1}{d}\delta^{IJ}\delta^{KL} \right] \tag{6.24}$$

where $\alpha = 4T\eta/V_{\mathrm{cell}}$, and $d = 3$ is the spatial dimension of the system. Because of the constraints on the shear-stress tensor, the number of the independent components of the shear-stress noise ξ^{IJ} is $d(d+1)/2 - 1$, same as a shear-stress tensor π^{IJ}. The autocorrelation matrix can be rewritten in terms of those independent components as

$$\langle \bar{\xi}_{\mathrm{d}}^i \bar{\xi}_{\mathrm{d}}^j \rangle = \alpha \left(\delta_{ij} - \frac{1}{d} \right), \quad (1 \leq i, j \leq d-1), \tag{6.25}$$

$$\langle \bar{\xi}_{\mathrm{nd}}^i \bar{\xi}_{\mathrm{nd}}^j \rangle = \frac{\alpha}{2}\delta_{ij}, \quad (1 \leq i, j \leq d(d-1)/2), \tag{6.26}$$

$$\langle \bar{\xi}_{\mathrm{d}}^i \bar{\xi}_{\mathrm{nd}}^j \rangle = \langle \bar{\xi}_{\mathrm{d}}^j \bar{\xi}_{\mathrm{nd}}^i \rangle = 0, \quad (1 \leq i \leq d-1, 1 \leq j \leq d(d-1)/2). \tag{6.27}$$

Here we defined the diagonal components $\bar{\xi}_{\mathrm{d}}^i = (\bar{\xi}^{11}, \ldots, \bar{\xi}^{d-1,d-1})$ $(i = 1, \ldots, d-1)$ and the nondiagonal components of the noise $\bar{\xi}_{\mathrm{nd}}^i = (\bar{\xi}^{12}, \bar{\xi}^{13}, \ldots, \bar{\xi}^{d-1,d})$ $(i = 1, \ldots, d(d-1)/2)$. The nondiagonal components have no correlations with the diagonal components and are diagonal in the autocorrelation matrix, so that each component can be determined independently:

$$\bar{\xi}_{\mathrm{nd}}^i = \sqrt{2T\eta}\, \bar{w}_{\mathrm{nd}}^i, \quad (1 \leq i \leq d(d-1)/2), \tag{6.28}$$

where $\bar{w}^i_{\rm nd}$ follows Gaussian distribution of mean 0 and variance $1/V_{\rm cell}$.

While, the autocorrelation matrix of the diagonal components $\bar{\xi}^i_{\rm d}$ is not diagonal. Although we can diagonalize the autocorrelation matrix such as the case of generating the diffusion noise, we introduce other useful linear combinations for independent noise components $\bar{\xi}^{*i}$:

$$\bar{\xi}^{*i}_{\rm d} = X^i{}_k \bar{\xi}^k_{\rm d} = \frac{1}{d-i}\left(\bar{\xi}^i_{\rm d} + \frac{1}{d-i+1}\sum_{k=1}^{i-1}\bar{\xi}^k_{\rm d}\right), \quad (1 \le i \le d-1), \tag{6.29}$$

$$\langle \bar{\xi}^{*i}_{\rm d}\bar{\xi}^{*j}_{\rm d}\rangle = X^i{}_k \langle \bar{\xi}^k_{\rm d}\bar{\xi}^l_{\rm d}\rangle X^{{\rm T}i}_l = \alpha\delta_{ij}\left(\frac{1}{d-i} - \frac{1}{d+1-i}\right), \quad (1 \le i,j \le d-1). \tag{6.30}$$

In this linear combinations, the autocorrelation matrix is "diagonalized". Note that this is not a similarity transformation with the form of $V^{-1}\langle \bar{\xi}^k_{\rm d}\bar{\xi}^l_{\rm d}\rangle V$ where V is a basis transformation, and hence it is not the ordinary diagonalization. This transformation is chosen to make the inverse transformation simple:

$$\bar{\xi}^i_{\rm d} = (X^{-1})^i{}_k \bar{\xi}^{*k}_{\rm d} = (d-i)\bar{\xi}^{*i} - \sum_{k=1}^{i-1}\bar{\xi}^{*k}, \quad (1 \le i \le d-1). \tag{6.31}$$

As a result, the diagonal components of the shear-stress noise are generated with the following equation:

$$\bar{\xi}^{i*}_{\rm d} = \sqrt{4\pi\eta\left(\frac{1}{d-i} - \frac{1}{d-i+1}\right)}\bar{w}^i_{\rm d}, \quad (1 \le i \le d-1), \tag{6.32}$$

$$\bar{\xi}^{ii}_{\pi} = (d-i)\bar{\xi}^{*i} - \sum_{k=1}^{i-1}\bar{\xi}^{*k}, \quad (1 \le i \le d-1), \tag{6.33}$$

$$\bar{\xi}^{dd}_{\pi} = -\sum_{k=1}^{d-1}\bar{\xi}^{*k}, \tag{6.34}$$

where $\bar{w}^i_{\rm d}$ follows Gaussian distribution of mean 0 and variance $1/V_{\rm cell}$.

6.3 Smearing the noise fields

In the last section, we discussed the necessity to introduce the coarse-graining scales. The singularity of the noise fields $\bar{w}_\Pi, \bar{w}^*_i, \bar{w}^i_{\rm nd}, \bar{w}^i_{\rm d}$ in (6.17), (6.22), (6.28), and (6.32) actually causes numerical problems in the relevant scales of the high-energy nuclear collisions. In this section, to solve this problem, we propose two different ways to generate a coarse-grained field of $\bar{w}(V_{l,m})$ where $V_{l,m}$ denotes the cell l at the time step m.

To save numerical costs, we particularly consider the smearing of the noise fields in space, and not in time. First we consider the fields averaged in a time step $t_m \to t_m + \Delta t$:

$$w(\boldsymbol{x}) = \frac{1}{\Delta t}\int_{t_m}^{t_m+\Delta t} dt' w(\boldsymbol{x}, t'), \tag{6.35}$$

$$\langle w(\boldsymbol{x})w(\boldsymbol{x}')\rangle = \delta^{(3)}(\boldsymbol{x}-\boldsymbol{x}')/\Delta t. \tag{6.36}$$

We then define how to spatially coarse-grain the random fields $w(\boldsymbol{x})$ given by the autocorrelation (6.36) in two ways: Gaussian smearing and wavenumber cutoff.

6.3.1 Gaussian smearing

In the applications to high-energy nuclear collisions, the coarse graining with the Gaussian kernel has been used for initial conditions. The fields generated with microscopic models are smeared so that the hydrodynamic description can be applied (see, for example, [124, 247]). Also, the effects of the coarse-graining within hydrodynamic evolution are discussed in Ref. [248] using the stochastic variational method based on Lagrangian specification of hydrodynamics.

Here we apply the Gaussian coarse-graining to the noise smearing of the fluctuating hydrodynamics. The idea of Gaussian smearing procedure is that (i) a normal white noise field $w(\boldsymbol{x})$ is generated, and then (ii) the generated field is smoothed by solving a diffusion equation:

$$w(\boldsymbol{x}; s=0) = w(\boldsymbol{x}), \tag{6.37}$$

$$\frac{\partial}{\partial s} w(\boldsymbol{x}; s) = D \sum_{i=1}^{3} \frac{\partial^2}{\partial x_i^2} w(\boldsymbol{x}; s). \tag{6.38}$$

The resulting smeared field reads

$$w(\boldsymbol{x})^\sigma \equiv w(\boldsymbol{x}; s = \sigma^2/2D) \tag{6.39}$$

$$= \frac{1}{(2\pi\sigma^2)^{3/2}} \int d^3x' \exp\left(-\frac{(\boldsymbol{x}-\boldsymbol{x}')^2}{2\sigma^2}\right) w(\boldsymbol{x}'). \tag{6.40}$$

The autocorrelation of the coarse-grained fields $w(\boldsymbol{x})^\sigma$ become

$$\langle w(\boldsymbol{x})^\sigma w(\boldsymbol{x}')^\sigma \rangle = \frac{1}{\Delta t} \frac{1}{(4\pi\sigma^2)^{3/2}} \exp\left(-\frac{(\boldsymbol{x}-\boldsymbol{x}')^2}{4\sigma^2}\right). \tag{6.41}$$

In numerical calculations, $\bar{w}(V_{l,m})$ is first generated in each cell with variance $1/V_{l,m}$, and the discretized version of the diffusion equation (6.38) is solved. Since the noise in each cell is already averaged in the cell volume, the initial *time* s_0 is set so that $\sqrt{2Ds_0} = \Delta x/2$, for example.

In this method, smeared fields can be quickly generated with a small numerical cost for relatively small coarse-graining length σ. While, this method is not economic for a large coarse-graining length σ since the cost increases in the order $O(\sigma^2)$ as σ becomes larger. To calculate the convolution of the fields with Gaussian kernel of large σ, discrete Fourier transforms (DFT) can be used with the fast Fourier transform (FFT) algorithm instead of solving the "diffusion" equation.

If one would like to take into account the temperature dependence of the coarse-graining scales, this method can be easily extended to allow the spacial dependence of the "diffusion" coefficient $D(x)$.

6.3.2 Wavenumber cutoff

In this method a cutoff wavelength λ, or equivalently a cutoff wavenumber $2\pi/\lambda$, is introduced in the Fourier space:

$$w(\boldsymbol{k})^\lambda = \Theta(2\pi/\lambda - |\boldsymbol{k}|) w(\boldsymbol{k}), \tag{6.42}$$

$$w(\boldsymbol{k})^\lambda \equiv \int d^3x e^{-i\boldsymbol{k}\cdot\boldsymbol{x}} w(\boldsymbol{x})^\lambda, \tag{6.43}$$

$$w(\boldsymbol{k}) \equiv \int d^3x e^{-i\boldsymbol{k}\cdot\boldsymbol{x}} w(\boldsymbol{x}). \tag{6.44}$$

In real space, the coarse-grained random fields $w(\boldsymbol{x})^\lambda$ can be expressed with a convolution of a kernel $\kappa(\boldsymbol{x})$ and the random fields $w(\boldsymbol{x})$:

$$w(\boldsymbol{x})^\lambda = \int d^3x' \kappa(\boldsymbol{x}-\boldsymbol{x}') w(\boldsymbol{x}'), \tag{6.45}$$

$$\kappa(\boldsymbol{x}) \equiv \int \frac{d^3\boldsymbol{k}}{(2\pi)^3} e^{i\boldsymbol{k}\cdot\boldsymbol{x}} \Theta(2\pi/\lambda - |\boldsymbol{k}|) \tag{6.46}$$

$$= \frac{4\pi}{\lambda^3} \frac{j_1(2\pi|\boldsymbol{x}|/\lambda)}{2\pi|\boldsymbol{x}|/\lambda}. \tag{6.47}$$

where $j_1(\alpha) = (\sin\alpha - \alpha\cos\alpha)/\alpha^2$ is the $n=1$ spherical Bessel function of the first kind. The radial dependence of the kernel is shown in Fig. 6.3. The smearing with this cutoff method approximately corresponds to the Gaussian smearing of $\sigma \simeq 0.24\lambda$ as shown in the figure. The autocorrelation of the coarse-grained fields becomes

$$\langle w(\boldsymbol{x})^\lambda w(\boldsymbol{x}')^\lambda \rangle = \frac{1}{\Delta t} \kappa(\boldsymbol{x}-\boldsymbol{x}'). \tag{6.48}$$

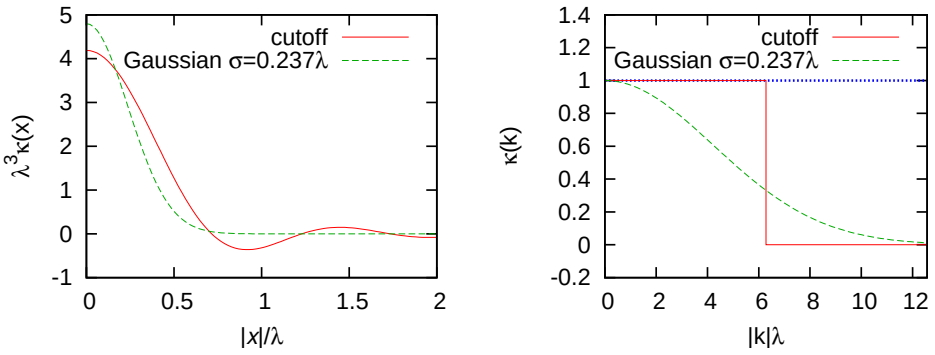

Figure 6.3: In the left panel, the red solid line shows the radial dependence of the cutoff kernel $\kappa(x)$ scaled by λ^3. The green dashed line shows a kernel of Gaussian smearing, $\lambda^3\kappa_G(x) = \lambda^3(1/\sqrt{2\pi\sigma^2})^3\exp(-x^2/2\sigma^2)$. The smearing length $\sigma = 0.237\lambda$ is determined to fit the cutoff kernel $\kappa(x)$ in the sphere $|x| < z_1$ where z_1 is the first zero of κ as a function of $|x|$. The kernels in the Fourier space are shown in the right panel. The blue dotted line shows the delta function kernel corresponding to the no-smearing case. With both of the smearing kernels, modes with large wavenumbers are suppressed.

The autocorrelation has exactly the same form with the kernel $\kappa(x)$ since $\Theta(2\pi/\lambda - |\boldsymbol{k}|)^2 = \Theta(2\pi/\lambda - |\boldsymbol{k}|)$.

In numerical calculations, the DFT is used instead of the ordinary Fourier transform:

$$\bar{w}(\boldsymbol{k}_{p,q,r}) = \sum_{l=0}^{N_x-1} e^{-2\pi i \frac{pl}{N_x}} \sum_{m=0}^{N_y-1} e^{-2\pi i \frac{qm}{N_y}} \sum_{n=0}^{N_z-1} e^{-2\pi i \frac{rn}{N_z}} \bar{w}(\boldsymbol{x}_{l,m,n}) \tag{6.49}$$

where $l, m, n \in \mathbb{N}_0$ are indices to specify the cell at $\boldsymbol{x}_{l,m,n} = (l\Delta x, m\Delta y, n\Delta z)$, and $\Delta x, \Delta y$ and Δz are the size of the cells. The integers $p, q, r \in \mathbb{Z}$ specify the wavenumber $\boldsymbol{k}_{p,q,r} = (2\pi p/N_x\Delta x, 2\pi q/N_y\Delta y, 2\pi r/N_z\Delta z)$.

First, the random fields in Fourier space, $\bar{w}(\boldsymbol{k}_{p,q,r})$, are directly generated instead of performing the DFT on $\bar{w}(\boldsymbol{x}_{l,m,n})$ because the autocorrelation of $w(\boldsymbol{k}_{p,q,r})$ is explicitly known:

$$\langle \bar{w}(\boldsymbol{k}_{p,q,r})^* \bar{w}(\boldsymbol{k}_{p',q',r'}) \rangle = \frac{N_x N_y N_z}{\Delta t \Delta x \Delta y \Delta z} \delta_{pp'}\delta_{qq'}\delta_{rr'}. \tag{6.50}$$

For (p, q, r) satisfying $2p \equiv 0 \pmod{N_x}$, $2q \equiv 0 \pmod{N_y}$, and $2r \equiv 0 \pmod{N_z}$, the imaginary part of the noise $\Im\bar{w}(\boldsymbol{k}_{p,q,r})$ always vanishes, and the real part $\Re\bar{w}(\boldsymbol{k}_{p,q,r})$ follows the Gaussian distribution of variance $N_xN_yN_z/\Delta t\Delta x\Delta y\Delta z$. For the other (p, q, r), the imaginary part and the real part are two independent random variables, and both follow the Gaussian distribution of variance $(1/2)(N_xN_yN_z/\Delta t\Delta x\Delta y\Delta z)$. The imaginary part and the real part of $\bar{w}(\boldsymbol{k}_{p,q,r})$ can be generated as Gaussian random numbers of each variance. Then, after applying the wavenumber cutoff, a coarse-grained random field $\bar{w}(\boldsymbol{x}_{l,m,n})^\lambda$ is obtained using the inverse DFT:

$$\bar{w}(\boldsymbol{k}_{p,q,r})^\lambda = \Theta(2\pi/\lambda - |\boldsymbol{k}_{p,q,r}|)\bar{w}(\boldsymbol{k}_{p,q,r}), \tag{6.51}$$

$$\bar{w}(\boldsymbol{x}_{l,m,n})^\lambda = \frac{1}{N_xN_yN_z} \sum_{p=0}^{N_x-1} e^{2\pi i \frac{pl}{N_x}} \sum_{q=0}^{N_y-1} e^{2\pi i \frac{qm}{N_y}} \sum_{r=0}^{N_z-1} e^{2\pi i \frac{rn}{N_z}} \bar{w}(\boldsymbol{k}_{p,q,r})^\lambda. \tag{6.52}$$

Note that, since the generated field $\bar{w}(\boldsymbol{x}_{l,m,n})^\lambda$ is a periodic function due to the definition of the DFT, a sufficient margin larger than the coarse-graining length should be taken for non-periodic systems.

If one uses an unstructured grid for the hydrodynamic simulation, a covering structured grid can be introduced to generate the random fields, and the noise $\bar{w}(V_{l,m})$ in a cell can be determined by interpolating the smeared field $\bar{w}(x_{l',m',n'})^\lambda$ on the covering grid.

In Fig. 6.4, examples of the generated fields are shown.

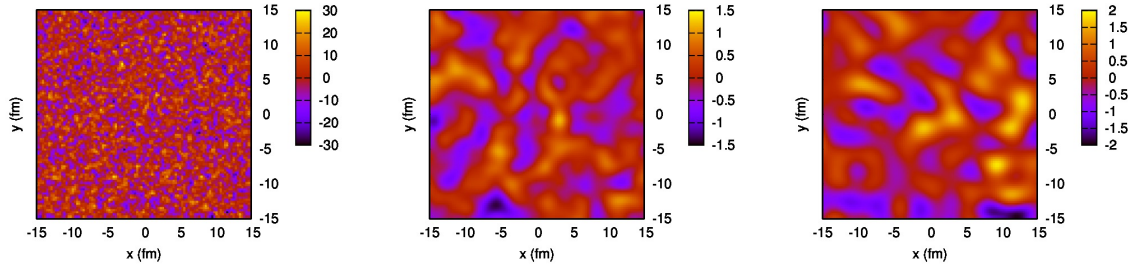

(a) no smearing (b) Gaussian ($\sigma = 1$fm) (c) cutoff ($\lambda = 4.2$fm)

Figure 6.4: Examples of the generated random fields are shown. The left panel (a) shows a field of no-smearing case $\bar{w}(x)$ in which the noise is independently generated in each cell. The center panel (b) shows a field $\bar{w}(x)^\sigma$ smeared with the Gaussian kernel of $\sigma = 1$ fm. The right panel (c) shows a field $\bar{w}(x)^\lambda$ with wavelength cutoff of $\lambda = 4.2$ fm. The cutoff λ is chosen to be $\sigma \simeq 0.24\lambda$. The volume of the cells is $(0.3\text{ fm})^3$ and the time step is $\Delta t = 0.15$ fm.

6.3.3 In curved coordinates

In curved coordinates, coordinate values do not necessarily correspond to physical lengths. Therefore the apparent coarse-graining length scale can depend on a spacetime position x and a direction ∂_α even if the coarse-graining scale is physically isotropic and uniform in space. In τ-η_s coordinates, the metric $g_{\alpha\beta} = \mathrm{diag}(1, -\tau^2, -1, -1)$ depends on the direction while it is invariant under translation. Thus the coarse-graining length σ_i or λ_i depend on a direction i, but not on position $\boldsymbol{x} = (x, y, \eta_s)$. In this case, the above two methods can be easily modified. For Gaussian smearing, the diffusion equation and the resulting expression can be modified as follows:

$$\frac{\partial}{\partial s} w(\boldsymbol{x}; s) = \sum_{i=1}^{3} D_i \frac{\partial^2}{\partial x_i^2} w(\boldsymbol{x}; s), \tag{6.53}$$

$$w(\boldsymbol{x})^{\boldsymbol{\sigma}} = w(\boldsymbol{x}; s = 1) \tag{6.54}$$

$$= \frac{1}{\prod_{i=1}^{3} \sqrt{2\pi\sigma_i^2}} \int d^3x' \exp\left(-\sum_{i=1}^{3} \frac{(x^i - x'^i)^2}{2\sigma_i^2} \right) w(\boldsymbol{x}'). \tag{6.55}$$

where $D_i = \sigma_i^2/2$. For wavenumber cutoff, the cutoff becomes $\Theta(2\pi - \sum_{i=1}^{3} k^i \lambda_i)$, and the kernel is modified as follows:

$$\kappa(\boldsymbol{x}) = \frac{4\pi}{\prod \lambda_i} \frac{j_1(2\pi\sqrt{\sum (x_i/\lambda_i)^2})}{2\pi\sqrt{\sum (x_i/\lambda_i)^2}}. \tag{6.56}$$

The Jacobian factor of the delta function should be noticed here:

$$\langle \bar{w}(x')\bar{w}(x) \rangle = \prod_{\mu=0}^{3} \delta(x^{\bar{\mu}} - x'^{\bar{\mu}}) \tag{6.57}$$

$$= \frac{1}{\sqrt{-g}} \prod_{\alpha=0}^{3} \delta(x^\alpha - x'^\alpha). \tag{6.58}$$

The autocorrelation (6.57) is defined in flat coordinates since the FDRs are written in the flat coordinates. Hence, it has the additional factor $1/\sqrt{-g}$ in general curved coordinates (6.58).

6.4 Stochastic integrals

In solving the Langevin equation which contains the noise term with delta function correlation, there are two different ways of defining the stochastic integrals: the Itô integral and the Stratonovich integral.

In both definitions of the integrals, the noise terms in the fluctuating hydrodynamic equations are interpreted using the Itô products, and Stratonovich products, respectively. In subsection 6.4.1, we see those definitions and adopt the Stratonovich integral to define the fluid fields of the fluctuating hydrodynamics. The Stratonovich integral in terms of the Stratonovich products is rewritten by the Itô products with additional terms, which is useful in the numerical simulation with the explicit Euler's method. In subsections 6.4.2 and 6.4.3, we discuss the explicit structure of the fluctuating hydrodynamic equations in the first-order theory and the causal theory, respectively.

6.4.1 Itô integral and Stratonovich integral

Let us consider a generalized form of the Langevin equation:

$$\frac{d}{dt}X_l = f_l(X,t) + \sum_m g_{lm}(X,t)\xi_m, \tag{6.59}$$

where $X = \{X_l\}$ is a set of dynamical variables to solve, and ξ_m are the noise terms which satisfy $\langle \xi_l(t)\xi_m(t')\rangle = \delta_{lm}\delta(t-t')$. The functions $f_l(X,t)$ and $g_{lm}(X,t)$ contain the details of the dynamics. In the case of the fluctuating hydrodynamics, X is the set of the fluid fields and ξ_m are the independent components of the hydrodynamic fluctuations.

There are mathematical uncertainties in the above equation due to the singular behavior of the noise terms. There are two different ways to define the above equation in a mathematically rigorous manner:

$$dX_l^{\mathrm{I}} = f_l(X^{\mathrm{I}},t)dt + \sum_m g_{lm}(X^{\mathrm{I}},t)\cdot dB_m, \tag{6.60}$$

$$dX_l^{\mathrm{S}} = f_l(X^{\mathrm{S}},t)dt + \sum_m g_{lm}(X^{\mathrm{S}},t)\circ dB_m, \tag{6.61}$$

where B_m are the Wiener processes, and $\cdot$ and $\circ$ denote the Itô product and the Stratonovich product, respectively. The Itô-type and the Stratonovich-type definition of the integrals, X^{I} and X^{S}, give two different solutions of the Langevin equation. The detailed definition of those integrals are given in Appendix E.1.

We adopt the Stratonovich-type definition of the hydrodynamic fields since, in physical system, it is known that Langevin equation has the form of the Stratonovich-type equation (Wong-Zakai theorem) [249–251] [1]. The fluctuations arising in an actual physical system have a non-zero correlation time in their microscopic time scale, and therefore they are colored noises. The Langevin equation is derived by approximating the colored noise with the short scale by white noise, and the noise term with such approximation becomes the Stratonovich-type form. Therefore, it is natural to adopt the Stratonovich-type definition in fluctuating hydrodynamics.

There is another practical benefit of choosing the Stratonovich-type. The ordinary differential rules, such as the Leibnitz rule, can be used in differentiating the Stratonovich integrals while they cannot be used in the Itô calculus. Since the Leibnitz rule and other differential rules appear in many places of hydrodynamic equations and thermodynamic relations, using the Itô-type integral makes treatment of physical quantities complex and non-trivial.

While the Itô-type definition has the form of the ordinary Euler method, the Stratonovich-type definition has the form of an implicit time-integration method which is not useful in numerical calculations. Here we can transform the Stratonovich-type definition into an explicit form. Supposing $g_{lm}(X)$ is an analytic function of X and therefore a C^2 function, the Stratonovich product can be written in terms of

[1] For stochastic partial differential equations which have the spatial dimension of the fields, the Wong-Zakai theorem has difficulties in the continuum limit with respect to the space [252]. However, we here do not get into the details of such mathematically rigorous discussion since we introduce a non-zero smearing scale to the equations and do not consider the limit of the smearing scale vanishing.

the Itô product:

$$g_{lm}(X,t)\circ dB_m = g_{lm}(X,t)\cdot dB_m + \frac{1}{2}dg_{lm}\cdot dB_m \tag{6.62}$$

$$= g_{lm}(X,t)\cdot dB_m + \frac{1}{2}\sum_{k,n}\frac{\partial g_{lm}}{\partial X_k}g_{kn}(X,t)dB_m\cdot dB_n + O(dt^{3/2}) \tag{6.63}$$

$$= g_{lm}(X,t)\cdot dB_m + \frac{1}{2}\sum_{k}\frac{\partial g_{lm}}{\partial X_k}g_{km}(X,t)dt. \tag{6.64}$$

As a result, an explicit form of the Stratonovich-type integral X^{S} is obtained:

$$dX_l^{\mathrm{S}} = f_l(X^{\mathrm{S}})d\tau + \sum_m g_{lm}(X^{\mathrm{S}})\cdot dB_m + \frac{1}{2}\sum_{m,k}\left.\frac{\partial g_{lm}}{\partial X_k}\right|_{X^{\mathrm{S}}} g_{km}(X^{\mathrm{S}})d\tau. \tag{6.65}$$

It should be noticed here that, although the Stratonovich-type integral is originally defined by applying the Stratonovich products to the naive Langevin equation (6.59), it can also be written by the Itô products with additional terms. The name of the "Stratonovich" integral does not mean that they can only be written by the Stratonovich products.

In later sections, we consider the Stratonovich integrals written by the Itô products with the additional terms.

6.4.2 In Navier-Stokes theory

The first-order relativistic hydrodynamics is already known to have infinite speed of propagation and instabilities, and therefore it is not compatible with relativity. Here we discuss the structure of the first-order fluctuating hydrodynamics and find another problem of the first-order theory.

In the Landau frame, the hydrodynamic equations (3.79), (3.80), (3.81) become

$$\mathrm{D}e + (e+P+\Pi)\theta = \pi^{\alpha\beta}\sigma_{\alpha\beta}, \tag{6.66}$$

$$(e+P+\Pi)\mathrm{D}u^\mu - \pi^\mu{}_\alpha \mathrm{D}u^\alpha = \nabla^\mu(P+\Pi) - \nabla_\alpha\pi^{\alpha\mu} - u^\mu(\pi^{\alpha\beta}\sigma_{\alpha\beta}), \tag{6.67}$$

$$\mathrm{D}n_i + n_i\theta = -\partial_\alpha\nu_i^\alpha, \quad (i=1,\dots,n). \tag{6.68}$$

The dissipative currents are given by the first-order constitutive equations with hydrodynamic fluctuations:

$$\Pi = \Pi_{\mathrm{avg}}(U) + \delta\Pi, \tag{6.69}$$

$$\pi^{\mu\nu} = \pi^{\mu\nu}_{\mathrm{avg}}(U) + \delta\pi^{\mu\nu}, \tag{6.70}$$

$$\nu_i^\mu = \nu^\mu_{i,\mathrm{avg}}(U) + \delta\nu_i^\mu, \tag{6.71}$$

where $U=(e,u^\mu,n_i)$ denotes a set of thermodynamic fields. The terms $\Pi_{\mathrm{avg}}(U)$, $\pi^{\mu\nu}_{\mathrm{avg}}(U)$, and $\nu^\mu_{i,\mathrm{avg}}(U)$ are the average part of the constitutive equations:

$$\Pi_{\mathrm{avg}}(U) = -\zeta\theta, \tag{6.72}$$

$$\pi^{\mu\nu}_{\mathrm{avg}}(U) = 2\eta\sigma^{\mu\nu}, \tag{6.73}$$

$$\nu^\mu_{i,\mathrm{avg}}(U) = \sum_{j=1}^{n}\kappa_{ij}T\nabla^\mu\frac{\mu_j}{T}. \tag{6.74}$$

The stochastic part $\delta\Pi$, $\pi^{\mu\nu}$, and $\delta\nu_i^\mu$ are given by Gaussian white noise fields with the following correlations:

$$\langle\delta\Pi(x)\delta\Pi(x')\rangle = 2T\zeta\delta^{(4)}(x-x'), \tag{6.75}$$

$$\langle\pi^{\mu\nu}(x)\pi^{\alpha\beta}(x')\rangle = 4T\eta\Delta^{\mu\nu\alpha\beta}\delta^{(4)}(x-x'), \tag{6.76}$$

$$\langle\delta\nu_i^\mu(x)\delta\nu_j^\alpha(x')\rangle = 2T\kappa_{ij}(-\Delta^{\mu\alpha})\delta^{(4)}(x-x'). \tag{6.77}$$

In integration of fluctuating hydrodynamics, those terms are expressed with the normal Gaussian noise $W_\Pi(x)$, $W_{\pi,a}(x)$, and $W_i(x)$:

$$\delta\Pi(x) = I_\Pi(U) w_\Pi, \qquad \langle w_\Pi(x) w_\Pi(x)\rangle = \delta^{(4)}(x-x'), \tag{6.78}$$

$$\pi^{\mu\nu}(x) = \sum_{a=1}^{5} I^{\mu\nu}_{\pi,a}(U) w_{\pi,a}, \qquad \langle w_{\pi,a}(x) w_{\pi,b}(x)\rangle = \delta_{ab}\delta^{(4)}(x-x'), \tag{6.79}$$

$$\delta\nu^\mu_i(x) = \sum_{j=1}^{n} I^\mu_{ij}(U) w_i, \qquad \langle w_i(x) w_j(x)\rangle = \delta_{ij}\delta^{(4)}(x-x'), \tag{6.80}$$

where $I_\Pi(U) = \sqrt{2T\zeta}$, $I^{\mu\nu}_{\pi,a}(U)$, and $I^\mu_{ij}(U)$ are the intensities of the noise. The explicit formula of $I^{\mu\nu}_{\pi,a}(U)$ and $I^\mu_{ij}(U)$ can be constructed as described in Section 6.2.

The hydrodynamic equations can be summarized in the following form:

$$[F(U) + G(U,w)]\mathrm{D}U = f(U) + g(U,w), \tag{6.81}$$

where $\mathrm{D}U \equiv (\mathrm{D}e\ \ \mathrm{D}u^\mu\ \ \mathrm{D}n_i)^{\mathrm{T}}$ is the vector of the time derivatives of dynamical fields, and $w = (w_\Pi, w_{\pi,a}, w_i)$ are independent noise terms. The coefficient matrices $F(U)$ and $G(U,w)$, and vectors $f(U)$ and $g(U,w)$ are defined as follows:

$$F = \begin{pmatrix} 1 & 0 & 0 \\ 0 & \Delta^\mu{}_\nu[e+P+\Pi_{\mathrm{avg}}(U)] + \pi_{\mathrm{avg}}{}^\mu{}_\nu(U) & 0 \\ 0 & \nu_{\mathrm{avg},i\nu} & -\delta_{ij} \end{pmatrix}, \tag{6.82}$$

$$G = \begin{pmatrix} 0 & 0 & 0 \\ 0 & \Delta^\mu{}_\nu\delta\Pi + \delta\pi^\mu{}_\alpha & 0 \\ 0 & \delta\nu^\mu_i & 0 \end{pmatrix}, \tag{6.83}$$

$$f(U) = \begin{pmatrix} -[e+P+\Pi_{\mathrm{avg}}(U)]\theta + \sigma_{\alpha\beta}\pi^{\alpha\beta}_{\mathrm{avg}}(U) \\ \nabla^\mu[P+\Pi_{\mathrm{avg}}(U)] - \nabla_\alpha\pi^{\alpha\mu}_{\mathrm{avg}} - u^\mu\sigma_{\alpha\beta}\pi^{\alpha\beta}_{\mathrm{avg}} \\ n_i\theta + \nabla_\alpha\nu^\alpha_{i,\mathrm{avg}} \end{pmatrix}, \tag{6.84}$$

$$g(U,w) = \begin{pmatrix} -\theta\delta\Pi + \sigma_{\alpha\beta}\delta\pi^{\alpha\beta} \\ \nabla^\mu\delta\Pi - \nabla_\alpha\delta\pi^{\alpha\mu} - u^\mu\sigma_{\alpha\beta}\delta\pi^{\alpha\beta} \\ -\nabla_\alpha\delta\nu^\alpha_i \end{pmatrix}. \tag{6.85}$$

The noise terms are contained in $G(U,w)$ and $g(U,w)$.

Although $g(U,w)$ contains the spatial derivatives of noise terms such as $\nabla^\mu\delta\Pi$, the derivatives can be interpreted as linear transformations of the noise terms. For example, in numerical calculations, the derivatives can be replaced by finite differences of noise variables of neighboring cells. In smeared fluctuating hydrodynamics described in Section 6.3, the derivatives can be expressed with the derivatives of smearing kernels. For bulk pressure fluctuations,

$$\delta\Pi(x) = I_\Pi(x) w^\lambda_\Pi(x) \tag{6.86}$$

$$= I_\Pi(x)\int d^4x\kappa(x-x')w_\Pi(x), \tag{6.87}$$

$$\nabla^\mu\delta\Pi = \int dx^4\nabla^\mu[I_\Pi(x)\kappa(x-x')]w_\Pi(x'). \tag{6.88}$$

The derivatives in fluctuating hydrodynamics without smearing can be defined as a limit of the smearing kernel going to the delta function: $\kappa(x-x') \to \delta^{(4)}(x-x')$. Therefore $g(U,w)$ can be rewritten in the form $g(U)\circ w$ where the Stratonovich product '$\circ$' includes the integral over space or the sum over cells. The matrix $G(U,w)$ can also be written in the form $G(U,w) = G(U)\circ w$.

As a result, the hydrodynamic equations for the first-order fluctuating hydrodynamics have the following structure:

$$F(U)\mathrm{D}U + G(U)\mathrm{D}U\circ w = f(U) + g(U)\circ w. \tag{6.89}$$

Unlike the ordinary Langevin equations, the first-order relativistic fluctuating hydrodynamics has a noise term in the coefficients of the time derivative: $G(U)\mathrm{D}U \circ w$. The term arises essentially due to the derivatives of time components of the dissipative currents, such as $\partial_0(-\Delta^{0\mu}\Pi + \pi^{0\mu})$. Note that such terms do not appear in non-relativistic fluctuating hydrodynamics because the dissipative currents do not have any time components in non-relativistic theory. This kind of stochastic equations cannot be mathematically defined in an ordinary way. This is a new problem of the first-order relativistic theory, which turns out in the fluctuating hydrodynamic equations.

6.4.3 In causal theory

In causal theory, the dissipative currents $\Gamma = (\Pi, \pi^{\mu\nu}, \nu_i^\mu)$ are dynamical variables. Therefore the conservation laws (6.66)-(6.68) are the dynamical equations independent from constitutive equations. Those conservation laws can be solved explicitly in terms of the time derivatives $\mathrm{D}U = (\mathrm{D}e\ \mathrm{D}u^\mu\ n_i)$:

$$\mathrm{D}U = f_1(U) \equiv \begin{pmatrix} -(e+P+\Pi)\theta + \pi^{\alpha\beta}\sigma_{\alpha\beta} \\ A^\mu(U) \\ -n_i\theta\nu_i^\alpha A_\alpha(U) - \nabla_\alpha \nu_i^\alpha \end{pmatrix}, \tag{6.90}$$

$$A^\mu(U) \equiv [\Delta^\mu{}_\alpha(e+P+\Pi) - \pi^\mu{}_\alpha]^{-1}{}_\alpha[\nabla^\alpha(P+\Pi) - \nabla_\beta\pi^{\beta\alpha} - u^\alpha(\pi^{\kappa\lambda}\sigma_{\kappa\lambda})]. \tag{6.91}$$

Note that the matrix $\pi^{IJ} - \Delta^{IJ}(e+P+\Pi)$ in the definition of $A^\mu(U)$ is always invertible in the subspace of the spatial projector $\Delta^{\mu\nu}$ because of the positivity of the pressure and the energy density. The physical stress $\pi^{IJ} - \Delta^{IJ}(P+\Pi)$ should have three positive eigenvalues being the principal stresses, and the tensor $-\Delta^{IJ}e = e\delta^{IJ}$ is the scalar matrix with the eigenvalue of the energy e with a positive value. Therefore the eigenvalues of $\pi^{IJ} - \Delta^{IJ}(e+P+\Pi)$ are positive, and thus the tensor is invertible.

The constitutive equations have the following form:

$$\Pi + \tau_\Pi \mathrm{D}\Pi^{\mu\nu} = -\zeta\theta + C_\Pi(U,\Gamma) + \xi_\Pi, \tag{6.92}$$

$$\pi^{\mu\nu} + \tau_\pi \Delta^{\mu\nu}{}_{\alpha\beta}\mathrm{D}\pi^{\alpha\beta} = 2\eta\sigma^{\mu\nu} + C_\pi^{\mu\nu}(U,\Gamma) + \xi_\pi^{\mu\nu}, \tag{6.93}$$

$$\nu_i^\mu + \sum_{j=1}^n \tau_{ij}\Delta^\mu{}_\alpha \mathrm{D}\nu_j^\alpha = \sum_{j=1}^n \kappa_{ij} T\nabla^\mu \frac{\mu_j}{T} + C_i^\mu(U,\Gamma) + \xi_i^\mu, \tag{6.94}$$

where $C_\Pi(U,\Gamma)$, $C_\pi^{\mu\nu}(U,\Gamma)$ and $C_i^\mu(U,\Gamma)$ include miscellaneous higher-order terms. The noise terms ξ_Π, $\xi_\pi^{\mu\nu}$ and ξ_Π are given as

$$\xi_\Pi = I_\Pi(U) w_\Pi, \tag{6.95}$$

$$\xi_\pi^{\mu\nu} = \sum_{a=1}^5 I_{\pi,a}^{\mu\nu}(U) w_{\pi,a}, \tag{6.96}$$

$$\xi_i^\mu = \sum_{j=1}^n I_{ij}^\mu(U) w_i, \tag{6.97}$$

where the intensities I_Π, I_π, I_{ij} and the noise terms w_Π, w_π, w_i are defined in (6.78)-(6.80). The time derivatives terms $\Delta^\mu{}_\alpha \mathrm{D}\nu_i^\alpha$ and $\Delta^{\mu\nu}{}_{\alpha\beta}\mathrm{D}\pi^{\alpha\beta}$ can be decomposed as

$$\Delta^\mu{}_\alpha \mathrm{D}\nu_i^\alpha = \mathrm{D}\nu_i^\mu + u^\mu \mathrm{D}u_\alpha \nu_i^\alpha = \mathrm{D}\nu_i^\mu + u^\mu A_\alpha(U)\nu_i^\alpha, \tag{6.98}$$

$$\Delta^{\mu\nu}{}_{\alpha\beta}\mathrm{D}\pi^{\alpha\beta} = \mathrm{D}\pi^{\mu\nu} + u^\mu \mathrm{D}u_\alpha \pi^{\alpha\nu} + u^\nu \mathrm{D}u_\beta \pi^{\mu\beta} \tag{6.99}$$

$$= \mathrm{D}\pi^{\mu\nu} + u^\mu A_\alpha(U)\pi^{\alpha\nu} + u^\nu A_\beta(U)\pi^{\mu\beta}. \tag{6.100}$$

By putting the equations (6.95)-(6.100) into the constitutive equations (6.92)-(6.94), the following equa-

tions for the dissipative currents are obtained:

$$\mathrm{D}\Gamma = f_2(U,\Gamma) + g_2(U)w, \tag{6.101}$$

$$f_2(U,\Gamma) \equiv \begin{pmatrix} \frac{1}{\tau_\Pi}[-\Pi - \zeta\theta + C_\Pi(U,\Gamma)] \\ \frac{1}{\tau_\pi}[-\pi^{\mu\nu} - 2A_\alpha(U)u^{(\mu}\pi^{\nu)\alpha} + C_\pi^{\mu\nu}(U,\Gamma)] \\ \sum_{j=1}^n \tau_{ij}^{-1}[-\nu_j^\mu - u^\mu A_\alpha(U)\nu_i^\alpha + C_j(U,\Gamma)] \end{pmatrix}, \tag{6.102}$$

$$g_2(U)w \equiv \begin{pmatrix} \frac{1}{\tau_\Pi} I_\Pi(U) w_\Pi \\ \frac{1}{\tau_\pi}\sum_{a=1}^5 I_{\pi,a}^{\mu\nu}(U) w_{\pi,a} \\ \sum_{j,k=1}^n \tau_{ij}^{-1} I_{jk}^\mu(U) w_k \end{pmatrix}. \tag{6.103}$$

As a result, the structure of the hydrodynamic equations (6.90), (6.101) becomes

$$dU = f_1(U,\Gamma)d\tau, \tag{6.104}$$

$$d\Gamma = f_2(U,\Gamma)d\tau + g_2(U)\circ dB, \tag{6.105}$$

where $U = (e, u^\mu, n_i)$, $\Gamma = (\Pi, \pi^{\mu\nu}, \nu_i^\alpha)$, $B = \int d\tau w$, and $\tau = \int dt/u^0$ is the proper time. The first equation is the conservation law, and the second equation is the constitutive equation. The equations have different structure from the first-order case (6.89). The dissipative currents Γ are dynamical variables now, and the constitutive equation becomes a dynamical equation. The noise term $g_2(U)\circ dB$ appears only in the second equation, and the first equation does not have a direct noise term. The thermodynamic quantities U experience effects of the hydrodynamic fluctuations indirectly through the evolution of Γ. Finally it should be noticed that the coefficient of the noise term $g_2(U)$ has no dependence on Γ since the coefficient $g_2(U)$ has a simple form $\sim \sqrt{2T\kappa}/\tau_\mathrm{R}$ where κ and τ_R are the Onsager coefficient and relaxation time, respectively.

In this specific structure of the causal hydrodynamic equations, the difference between the stochastic integrals vanishes. The Stratonovich product term can be rewritten by the Itô products using the relation (6.65):

$$g_2(U)\circ dB = g_2(U)\cdot dB + \frac{1}{2}dg_2\cdot dB \tag{6.106}$$

$$= g_2(U)\cdot dB + \frac{1}{2}\left[\frac{\partial g_2}{\partial U}dU + \frac{\partial g_2}{\partial \Gamma}d\Gamma\right]dB + O(d\tau^{3/2}) \tag{6.107}$$

$$= g_2(U)\cdot dB. \tag{6.108}$$

To obtain the last equation, we used the relations $dU\cdot dB = X d\tau\cdot dB = 0$, and $\partial g_2(U)/\partial\Gamma = 0$. Therefore there are no differences between the Stratonovich definition and the Itô definition of the fluid fields in causal theories. This reflects the simple fact that the hydrodynamic fluctuations in causal theories are inherently colored noise and do not have singular behavior like the white noise. Solving hydrodynamics using the differential form of the constitutive equations with white noise terms, instead of using the integral form with colored noise, is just a technical choice which does not change the physics.

Therefore it is justified to solve the hydrodynamic equations with the Itô integrals which actually have the same form as Euler's method:

$$dU = f_1(U,\Gamma)d\tau, \tag{6.109}$$

$$d\Gamma = f_2(U,\Gamma)d\tau + g_2(U)\cdot dB. \tag{6.110}$$

6.5 Brief summary

In this chapter, we first discussed the singularity of the fluctuating hydrodynamics and considered coarse-graining scales to avoid the singularity. We need to introduce the smearing length scale of the hydrodynamics, and the grid spacing and the time steps in the numerical calculations should be sufficiently smaller than the smearing scale. Next we considered the generation of the random noise with the desired autocorrelations. The noise autocorrelation can be diagonalized to find the independent noise components, and the noise terms can be expressed as the linear combinations of those independent components.

Then we introduced two methods of the noise smearing. One is the Gaussian smearing method using the diffusion equations. The other is the wavenumber cutoff method with the fast Fourier transforms. Finally we discussed the stochastic integrals and found that, in causal hydrodynamics with non-zero relaxation times, there is no difference between the Itô integrals and the Stratonovich integrals. This reflects the fact that the hydrodynamic fluctuations in the causal theory are inherently colored even if the noise terms are white in the differential form of the constitutive equations.

Chapter 7

Application to high-energy nuclear collisions

7.1 Integrated dynamical framework

Let us first summarize our integrated dynamical framework to describe the evolution of the heavy-ion processes. As described in Section 2.2, our framework is composed of the initialization model, hydrodynamics, particlization, and hadronic cascades combined with the analysis framework of the hadron distributions.

For the initialization model of this study, we adopt the MC-KLN model with existing implementation of the model: `mckln` [171,253]. In this thesis, to compare the results with that of the ideal hydrodynamics, the initial conditions for the dissipative currents are fixed to zero as in the ideal hydrodynamics.

For hydrodynamics, we developed new codes using the new scheme described in Sections 5 and 6. The codes are written in `C++11`. To support the flat coordinates and the τ-η_s coordinates, the metric and the coordinates are implemented as modules so that they can be easily switched from one to the other. The noise is also implemented as modules to support several types of smearings. Matter properties, advection schemes, boundary conditions, and freezeout hypersurface determinations are also implemented as modules, respectively. We adopt $s95p$-v1.1 [180] for the equation of state. In the dissipative hydrodynamics and the fluctuating hydrodynamics, the shear viscosity is chosen as $\eta/s = 1/4\pi$. For the advection scheme, we extended an existing scheme for ideal hydrodynamics based on the Piecewise Parabolic Method (PPM) [254, 255] combined with the HLLE scheme [256, 257].

Using the output of the hydrodynamics, the hadrons are sampled using the Cooper-Frye formula with viscous corrections. Because this procedure naively requires large computation costs, we developed a new method to effectively sample the hadrons with the viscous correction. For ideas of this effective sampling, see subsection 7.1.2.

The subsequent hadronic cascades are performed using an existing library, JAM [197,198]. The JAM is a transport model based on the test particle method of the Boltzmann equation.

Finally the resulting hadron distributions are analyzed adopting the same methods as in the experiments. To handle the massive number of the events, we developed analysis codes `hprism`. In `hprism`, the flow vectors q_n of the pseudorapidity windows corresponding to the experimental detectors are calculated and cached in advance. Then, the event classification by the centrality, calculations of the resolution parameter of the event-plane method are performed. Finally the spectra of the hadrons, and the higher harmonics, etc. are calculated.

7.1.1 Isotropy of the fluctuating hydrodynamics

We now consider the isotropy of the fluctuating hydrodynamics to check the effects of the smearing. We perform tests of a global equilibrium state. In usual hydrodynamics, the solution of a global equilibrium state is uniform and does not evolve. In fluctuating hydrodynamics, however, the fluid fields always fluctuate around the equilibrium value locally even in the "global equilibrium state".

In Fig. 7.1, the angular distributions of the flow velocity are shown. Without smearing, the isotropy of the velocity distribution is broken. The distribution reflects the fact that the grids are composed of cube cells. The anisotropy weekens with the Gaussian smearing. In the case of $\sigma = 0.5$ fm, a slight anisotropy remains while the anisotropy disappears in the case of $\sigma = 1.0$ fm. Therefore, to recover the isotropy of the numerical calculations, sufficiently large smearing scales should be taken.

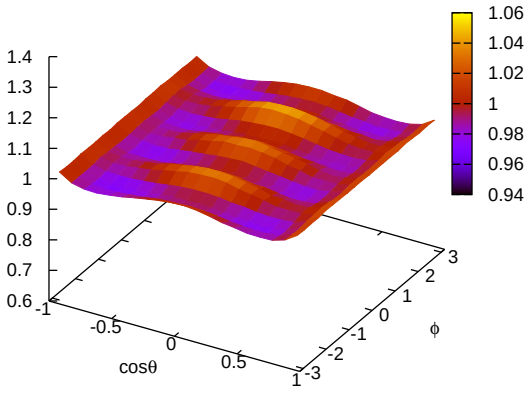

(a) no smearing

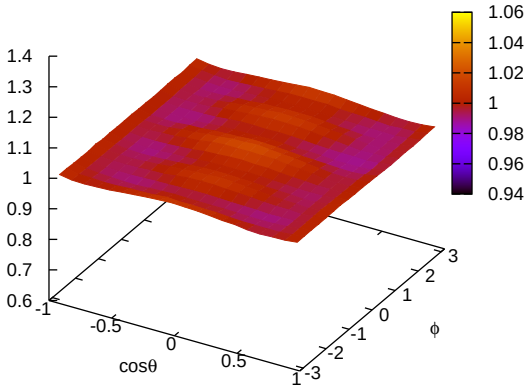

(b) $\sigma = 0.5$ fm

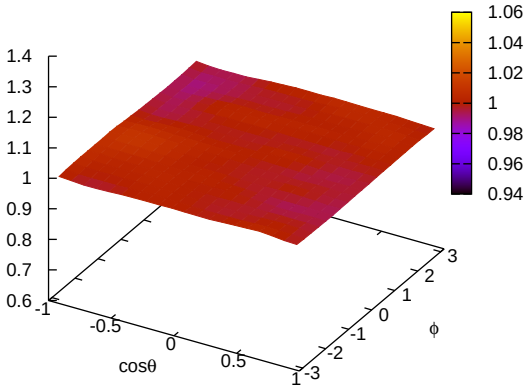

(c) $\sigma = 1.0$ fm

Figure 7.1: The angular distributions of the velocity are shown. The top panel (a) shows the result without smearing. The bottom two panel (b) and (c) show the results with the Gaussian smearing kernel of $\sigma = 0.5$ and 1.0 fm. The vertical axis is the probability density which is normalized to be unity in the isotropic case. The cell size of the calculations is $(0.3 \text{ fm})^3$. The time step is 0.15 fm.

7.1.2 Cooper-Frye sampling with viscous effect δf

We here present the key idea of an effective method of the particlization which enables the event-by-event calculations with a massive number of events. In a switching procedure, a complicated three-dimensional integration has to be numerically evaluated at each spacetime points on a hypersurface with a three-dimensional extension. This means that the depth of the nested loops becomes six in total for each species of hadrons and resonances. In addition there are 151 species of the resonances in the subsequent hadronic cascade model JAM. All of the resonances in JAM have to be sampled for a consistent description of the cascades. The direct calculation of such integration consumes enormous amount of time: around several hours with a core of recent CPUs for a single hydrodynamic event. In event-by-event calculations with a large event numbers around 10^4-10^6, such large numerical costs are not acceptable. This problem can be resolved by reducing the loop depth.

The sampling of the particles is performed for each hypersurface element. A naive procedure of the sampling is as follows: (1) the total number of the particles emitted from the hypersurface element is determined, and then (2) a momentum is assigned to each particle according to the given distribution. Let us see the above procedure in more detail:

(1) First we calculate the expected number of the particles emitted from a hypersurface element $\Delta^3\sigma_\mu$.

From the Cooper-Frye formula (2.20), the expected number of the particles is given by

$$\Delta N_i = g_i \int \frac{d^3p}{(2\pi)^3 E} [\Delta^3 \sigma_\mu p^\mu]^+ f(p,x)^+ \tag{7.1}$$

$$= g_i \int \frac{d^3p}{(2\pi)^3 E} [\Delta^3 \sigma_\mu p^\mu]^+ f_0 \left[1 + (1+\epsilon f_0) \frac{\pi^{\mu\nu} p_\mu p_\nu}{2(e+P)T^2}\right]^+, \tag{7.2}$$

where $F(x)^+ \equiv \max\{F(x), 0\}$ is the *positive part* of a function $F(x)$. The factor $[\Delta^3 \sigma_\mu p^\mu]^+$ extracts the positive contribution corresponding to the particles emitted from the fluid, and discards the negative contribution corresponding to the particles entering in the fluid.

The factor $f(p,x)^+$ means the positive part of the distribution $f(p,x)$ as well. The expression of the distribution $f(p,x)$ is not valid for large momentum p since it is the expansion in terms of the small parameter p. For large momentum p, the magnitude of the non-equilibrium part of the distribution δf becomes comparable to that of the equilibrium part f_0. The factor $f(p,x)$ can even have negative values although the physical $f(p,x)$ never has negative values. As the analytic form of the distribution of such non-equilibrium components is not known, we just discard the negative part of $f(p,x)$ and use the positive part $f(p,x)^+$. Next, the total number of the particles emitted n_i is determined by a Poisson random number of mean ΔN_i. The number of the particles follows the Poisson distribution because the particles are independent from one another in the description of Boltzmann equation for a rarefied gas.

(2) Finally, momenta are assigned to each of n_i particles randomly with the weight $[\Delta^3 \sigma_\mu p^\mu]^+ \times f(p,x)/E$.

As already noted, the above procedure has large numerical costs. Since the integrand of (7.2) is anisotropic in momentum space, it is difficult to reduce the dimension of the integrals by analytic transformation of the expression. Reducing the dimension of the integral (7.2) is the key to save the numerical costs. We here modify the procedure using the idea of *rejection sampling*, and reduce the dimension of a modified integral.

Let us consider the case that the integral (7.2) can be transformed into the following form:

$$\Delta N_i = g_i \int \frac{d^3p}{(2\pi)^3 E} [\Delta^3 \sigma_\mu p^\mu]^+ f_{\rm iso}(p,x) P_{\rm aniso}(p,x), \tag{7.3}$$

where $f_{\rm iso}(p,x)$ is a positive function and isotropic in the momentum p, and $P_{\rm aniso}(p,x)$ is a function satisfying $0 \le P_{\rm aniso}(p,x) \le 1$. In this case, we can first sample the particles using the isotropic distribution $f_{\max}(p,x)$ instead of using $f(p,x)^+$. The modified procedure is as follows:

(1) Obtain the total number of particles:

$$\Delta N_i' = g_i \int \frac{d^3p}{(2\pi)^3 E} [\Delta^3 \sigma_\mu p^\mu]^+ f_{\max}(p,x), \tag{7.4}$$

(2) Assign a momentum to each particle using the probability density function $f_{\max}(p,x)$.

(3) Accept each generated particle with the acceptance probability $P_{\rm aniso}(p,x)$ and remove rejected particles.

The integral (7.4) can be transformed into a one-dimensional integral since $f_{\max}(p,x)$ is isotropic, and the angular integration can be performed analytically. We can numerically integrate the one-dimensional integral with less costs. See Appendix F.1 for the details of the whole procedure of the integration and the momentum determination.

To obtain the explicit form of Eq. (7.3), we first move to the local rest frame of the fluid to make the integrand simpler. The apparent form of the integrand is not changed under the change of the frame because the integral measure $\int d^3p/E = \int d^4p \delta(p_\mu p^\mu)\Theta(p^0)$ is Lorentz invariant, and the other part of the integrand is a Lorentz scalar. A benefit of choosing the local rest frame is that the distribution f_0 becomes isotropic in the frame:

$$f_0(p) = f_0(E) = \frac{1}{e^{\beta(E-\mu_i)-\epsilon}}. \tag{7.5}$$

The remaining anisotropy of the distribution $f(p,x)$ comes from the term with $\pi^{\mu\nu}p_\mu p_\nu$. Another benefit of the local rest frame is that this factor also simplifies under the frame since the time components of dissipative currents vanish:

$$\pi^{\mu\nu}p_\mu p_\nu = \sum_{i,j=1}^{3} \pi^{ij}p^i p^j. \tag{7.6}$$

Then we separate the anisotropic part of the distribution $f(p,x)^+$:

$$f(x,p)^+ = f_{\rm max}(p,x)P_{\rm aniso}(p,x), \tag{7.7}$$

$$f_{\rm max}(p,x) \equiv \max\{f(p',x)^+ \mid \boldsymbol{p}' \in \mathbb{R}^3, \boldsymbol{p}'^2 = \boldsymbol{p}^2\} \tag{7.8}$$

$$= f_0\left[1 + (1+\epsilon f_0)\frac{\pi_{\rm max}\boldsymbol{p}^2}{2(e+P)T^2}\right], \tag{7.9}$$

$$P_{\rm aniso}(p,x) \equiv \frac{f(p,x)^+}{f_{\rm max}(p,x)} = \frac{\left[1 + (1+\epsilon f_0)\frac{\pi^{\mu\nu}p_\mu p_\nu}{2(e+P)T^2}\right]^+}{1 + (1+\epsilon f_0)\frac{\pi_{\rm max}\boldsymbol{p}^2}{2(e+P)T^2}}, \tag{7.10}$$

where $\pi_{\rm max}$ is the largest eigenvalue of the shear-stress tensor π^{IJ}. The eigenvalue $\pi_{\rm max}$ is always positive or zero due to the tracelessness $\pi^\mu_\mu = \sum_{i=1}^3 \pi_i = 0$, where π_i $(i = 1,\ldots,3)$ are the eigenvalues of the shear-stress tensor π^{IJ}. The isotropic part $f_{\rm max}(p,x)$ is the maximal value of $f(p,x)^+$ for a given $|\boldsymbol{p}|$. The function is obviously isotropic by definition, and $f_{\rm max}(p,x) \geq f(p,x)^+ \geq 0$. The function $P_{\rm aniso}(p,x)$ is the anisotropic part, and satisfies $0 \leq P_{\rm aniso}(p,x) \leq 1$.

7.2 Results with smooth initial condition

In this section, to investigate the effects of the hydrodynamic fluctuations, we perform simulations with a smooth initial condition without the initial-state fluctuations. We here consider Au+Au collisions with the energy of $\sqrt{s_{\rm NN}} = 200$ GeV.

To generate a single smooth initial condition, we fix the impact parameter of the collision to b =5.3 fm which roughly corresponds to the centrality percentile of 20%. Then we generate 1,000 fluctuating initial conditions, and average their entropy density distributions. The resulting initial condition in the transverse plane is shown in Fig. 7.2 (a). Since this is the non-central collision with a non-zero impact parameter, the generated density has an almond shape. The cell size is $\Delta x = \Delta y = 0.3$ fm and $\Delta\eta_s = 0.3$.

Subsequent hydrodynamic evolution is calculated using five types of hydrodynamics: the ideal hydrodynamics, the ordinary dissipative hydrodynamics without fluctuations, and the fluctuating hydrodynamics with three different smearing scales. For the smearing method, we adopted the Gaussian smearing of σ = 0.8, 1.0, and 1.2 fm. Note that the dissipative hydrodynamics corresponds to the infinite coarse-graining scale $\sigma \to \infty$. To see the unbiased effects of the hydrodynamic fluctuations, the scaling parameter of the initial entropy densities is common for all the hydrodynamics. The scaling parameter is a free parameter of the initialization model and is determined to reproduce the charged particle multiplicity of data in the ideal hydrodynamics. For each scale of the fluctuating hydrodynamics, we calculate 10^4 events. For the ideal hydrodynamics and the dissipative hydrodynamics, we calculate a single event.

Examples of the resulting energy profiles are shown in Fig. 7.2 (b), (c) and (d). As the flows are created by the pressure gradients, the matter expands into the radial direction. The energy density decreases due to two reasons: the energy is just diluted as the volume of the matter becomes larger, and the cells perform the work on the adjacent cells in the longitudinal directions. Since the ideal hydrodynamics and the dissipative hydrodynamics do not contain any fluctuations, the resulting profiles are smooth. On the other hand, starting from the smooth initial condition, the lumpy structure is created in the fluctuating hydrodynamics because of the hydrodynamic fluctuations. Unlike in the ideal and dissipative hydrodynamics, the results of the hydrodynamic evolutions differ from event to event in the fluctuating hydrodynamics.

After the sampling on the hypersurface at the switching temperature of $T_{\rm sw}$=155 MeV, we finally perform 10^4 hadronic cascades for each type of hydrodynamics, and analyze the obtained hadron distribution.

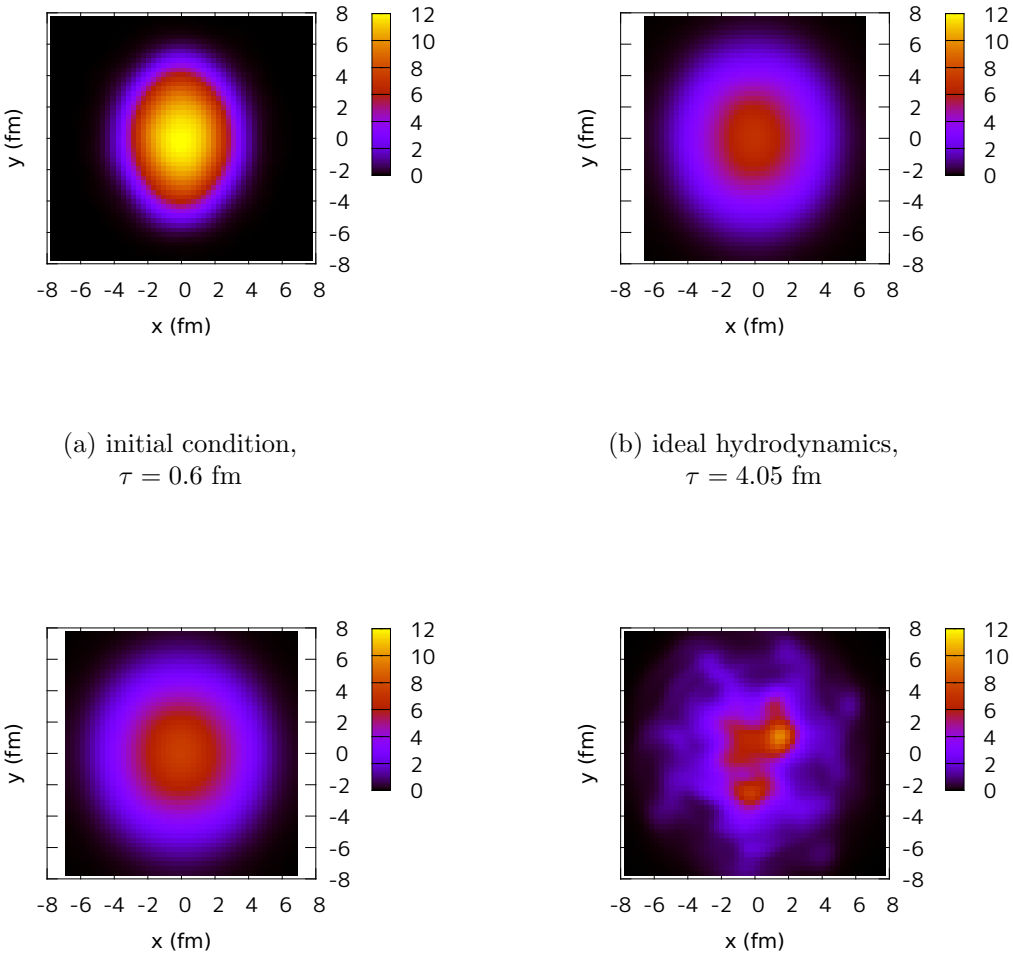

(a) initial condition, $\tau = 0.6$ fm

(b) ideal hydrodynamics, $\tau = 4.05$ fm

(c) dissipative hydrodynamics, $\tau = 4.05$ fm

(d) fluctuating hydrodynamics, $\tau = 4.05$ fm

Figure 7.2: Energy densities T^{00} [GeV/fm^2] in the transverse plane ($\eta_s = 0$). The top left panel shows the profile of the initial condition ($\tau = 0.6$ fm). The rest panels (b), (c), and (d) show the results of the ideal hydrodynamics ($\tau = 4.05$ fm), the dissipative hydrodynamics, and the fluctuating hydrodynamics, respectively.

In the left panel of Fig. 7.3, the charged particle multiplicities as functions of pseudorapidity are shown. We performed calculations using the fully (3+1)-dimensional model, so that the multiplicity distribution in a wide range of the pseudorapidity can be obtained. Because the matter density is largest at midrapidity and decreases with the rapidity, the multiplicity distribution also has a similar shape like a mountain. The flat region of the pseudorapidity $|\eta| \lesssim 1$ corresponds to the boost invariant part of the created matter as in the Bjorken's model [177]. At the midrapidity, the multiplicity is slightly smaller than in the neighboring rapidity, so that the multiplicity distribution has two peaks. This is due to the effect of the Jacobian $dy/d\eta = p/E$: while the rapidity distribution $dN_{\rm ch}/dy$ is flat, the pseudorapidity distribution decreases at midrapidity with the factor p/E. Now let us see the effects of the hydrodynamic fluctuations. While the multiplicity increases due to the viscosity, it further increases due to the hydrodynamic fluctuations. The increase is smaller with longer coarse-graining scales, which

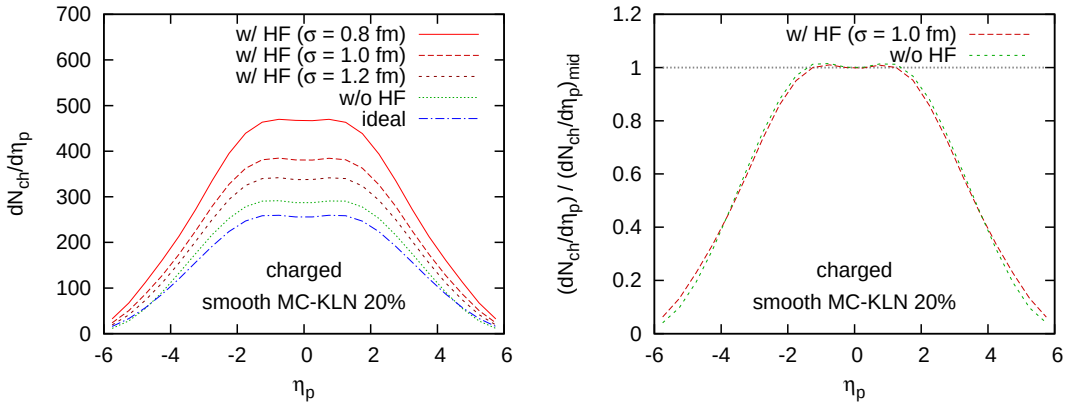

Figure 7.3: In the left panel, the charged particle multiplicities in each hydrodynamics are shown. Three red lines correspond to the results with hydrodynamic fluctuations. The green line corresponds to the results without hydrodynamic fluctuations. The blue line is the result of ideal hydrodynamics. In the right panel, the normalized multiplicities are shown to compare the shape of the multiplicity.

is consistent with the fact that the dissipative hydrodynamics corresponds to the infinite coarse-graining scale. This means that the scaling parameter of the initial entropy density should be tuned for each coarse-graining scales in actual event-by-event calculations.

In the right panel of Fig. 7.3, by normalizing the distributions to be unity at midrapidity, the shape of the charged particle multiplicities of the fluctuating hydrodynamics and that of the dissipative hydrodynamics are compared to each other. The charged particle multiplicity of the fluctuating hydrodynamics has broader tails than that of the dissipative hydrodynamics. This is because the flow velocity in the rapidity direction has dispersion due to the hydrodynamic fluctuations, and the hadron distribution is diffused by the dispersion. Nevertheless the effect is too small to be measured in experiments.

In Fig. 7.4, the transverse-momentum spectra of the identified hadrons are shown. The slopes of all the spectra are decreased by the hydrodynamic fluctuations, and the fluctuations of the shorter coarse-graining scales have stronger effects. In particular, the multiplicities in the higher transverse-momentum region around 2.5 GeV are multiplied by about 10 with the coarse-graining scale $\sigma = 0.8$ fm. This is because the flow velocities in the transverse plane are locally generated by the gradients caused by the hydrodynamic fluctuations. Note that this does not imply a strong radial flow because the generated flow velocities are random at each position and are not collective.

In Fig. 7.5, the integrated v_2 with the two particle cumulant method is shown for each hydrodynamics. The mountain shape of the elliptic flow comes from the initial density. Since the elliptic flow is gradually created by the hydrodynamic response of the matter, the size of the flow depends on the duration of the hydrodynamic stage. At larger rapidities, the elliptic flow is not fully developed because the duration of the hydrodynamics is shorter due to the smaller initial density of the created matter.

Let us compare the results of each hydrodynamics. Although the elliptic flow v_2 is decreased by the viscosity, the hydrodynamic fluctuations have opposite effects: the elliptic flow is increased by the fluctuations. The elliptic flows of the fluctuating hydrodynamics are even stronger than that of the ideal hydrodynamics. In Fig. 7.6, the differential v_2 as a function of transverse momentum is shown. The final differential v_2 is shown in the right panel, while those just after the hydrodynamics are shown in the left panel. By comparing them to each other, the flow v_2 created in the hydrodynamic stage, and that created in hadronic cascades can be studied. Unlike in the integrated v_2, the differential v_2 of the fluctuating hydrodynamics is smaller than that of the ideal hydrodynamics and almost the same as that of the dissipative hydrodynamics. This means that the increase of the elliptic flow in Fig. 7.5 is mainly due to the harder spectra of the fluctuating hydrodynamics seen in Fig. 7.4: Even if the differential p_T is not changed, the increase of the high-p_T hadrons pushes up the integrated v_2 because the high-p_T hadrons have larger differential v_2. Also, v_2 generated by the hadronic cascades are larger for the fluctuating hydrodynamics than for the dissipative hydrodynamics, which can be explained by the higher multiplicity in the case of the fluctuating hydrodynamics. The higher density leads to a larger flow created in the hadronic cascades.

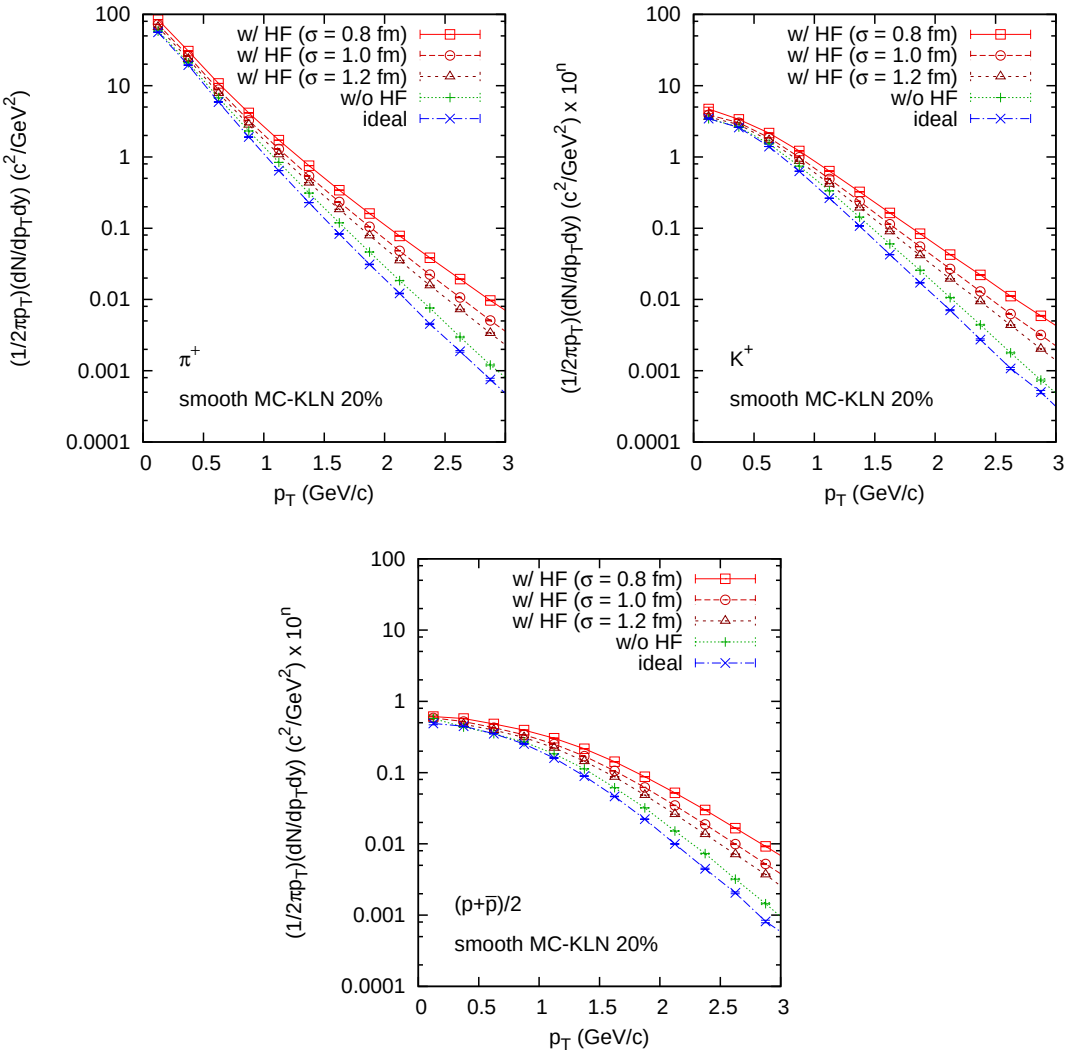

Figure 7.4: The transverse momentum spectra of identified hadrons are shown. The top left plot, the top right plot and the bottom plot show the p_T spectra of charged pions π^+, charged kaons K^+, and protons $(p+\bar{p})/2$, respectively. The red lines indicates the calculation with hydrodynamic fluctuations. The three lines from top to bottom correspond to the smearing length scale $\sigma = 0.8$ fm, 1.0 fm, and 1.2 fm, respectively. The green lines are the results of causal viscous hydrodynamics without hydrodynamic fluctuations, which corresponds to the limit $\sigma \to \infty$. The blue lines are the results of ideal hydrodynamics.

In Figs. 7.7 and 7.8, three methods of harmonics are compared to each other. Each method of the harmonics roughly corresponds to the different order of moments of the event-by-event anisotropic flows, so that the distribution of the flow fluctuations can be studied by comparing different methods to each other. In the dissipative hydrodynamics, all the three methods are consistent to have the same value, because there are no fluctuations. In the fluctuating hydrodynamics, three methods give systematically different values. This is because each method has different dependency on flow fluctuations. In the fluctuating hydrodynamics, the event-plane method $v_2\{\eta\text{-sub}\}$, and the elliptic flow with respect to the reaction plane $v_2\{\mathrm{RP}\}$ have the same value in most pseudorapidity region. This is because the hydrodynamic fluctuations are independent in forward and backward rapidity regions, and such fluctuation effects are canceled by the resolution correction of the event-plane method. The two-particle cumulant method has larger values than the other methods. This means the non-zero flow fluctuations in the fluctuating hydrodynamics. Note that the event-plane method has a slightly larger value than the $v_2\{\mathrm{RP}\}$ at mid-rapidity because of the correlation of the subevents and the flow fluctuations.

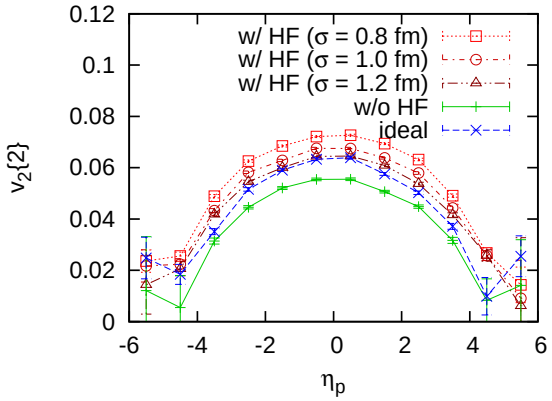

Figure 7.5: The integrated $v_2\{2\}$ as a function of pseudorapidity is shown.

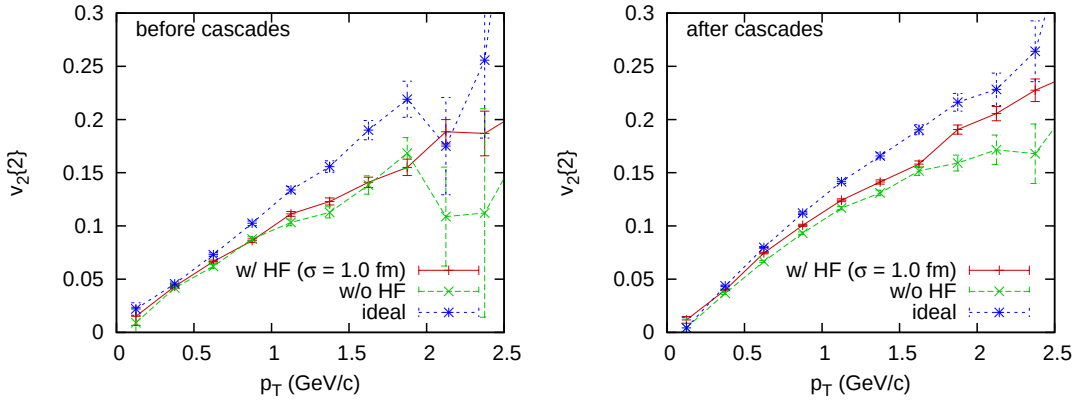

Figure 7.6: The differential $v_2\{2\}$ as functions of transverse momentum are shown. The left panel shows the results before cascades, which correspond to the hadron distribution on the switching hypersurface. The right panel shows the results after cascades.

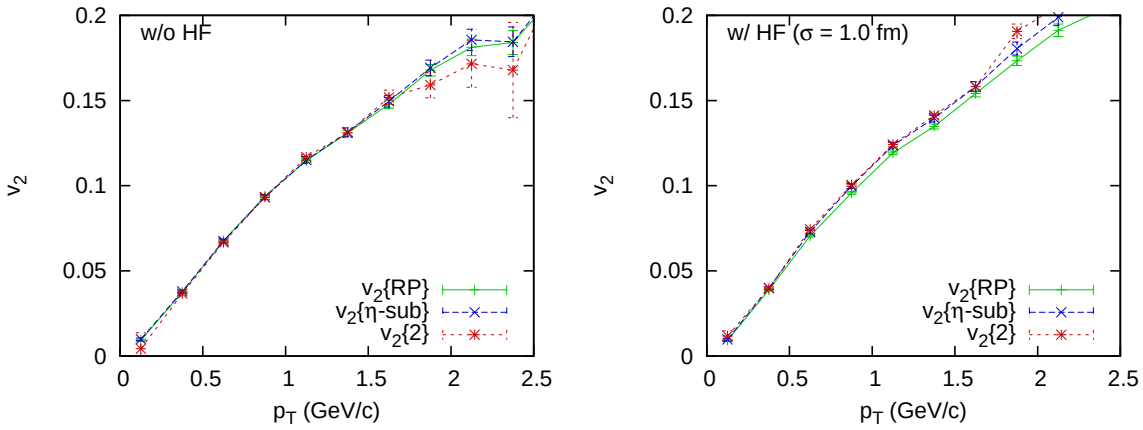

Figure 7.7: Three methods of harmonics are compared by the differential v_2. The left and the right panel correspond to the dissipative hydrodynamics and the fluctuating hydrodynamics.

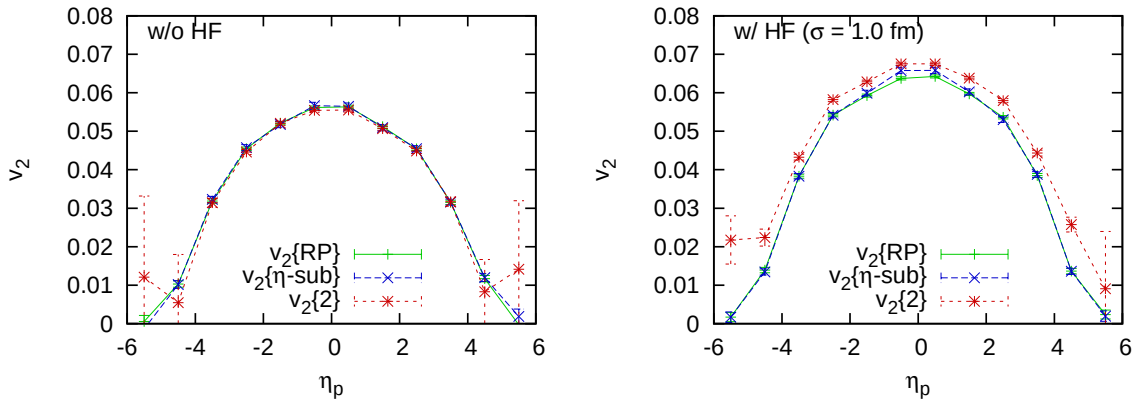

Figure 7.8: Three methods of harmonics are compared by the integrated v_2. The left and the right panel correspond to the dissipative hydrodynamics and the fluctuating hydrodynamics.

7.3 Results with initial-state fluctuations

In the actual processes of the high-energy nuclear collisions, the major source of the event-by-event fluctuations is the initial-state fluctuations. To compare the effects of the hydrodynamic fluctuations to those of the initial-state fluctuations, we should take into account both fluctuations in the same calculations.

In this section, we perform event-by-event calculations with fluctuating initial conditions. We consider three cases for the hydrodynamic stage: the ideal hydrodynamics, the dissipative hydrodynamics without noise, and the fluctuating hydrodynamics with the smearing scale of $\sigma = 1.0$ fm. For each hydrodynamics, we calculated 10^5 events of hydrodynamics and hadronic cascades.

The initial conditions are generated with MC-KLN model with the minimum bias, i.e., the impact parameter is not fixed. For each of the dissipative hydrodynamics and the fluctuating hydrodynamics, the entropy densities of the initial conditions are scaled to reproduce the final charged particle multiplicity of the ideal hydrodynamics. The scaling parameters are 8.5, 7.0, and 5.7 for the ideal, dissipative, and fluctuating hydrodynamics, respectively. In Fig. 7.9, the resulting charged particle multiplicities are shown.

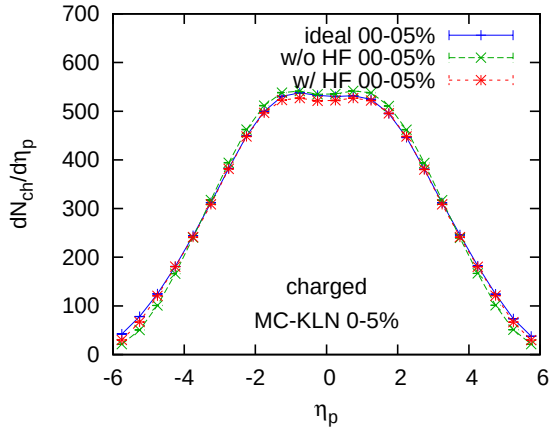

Figure 7.9: The charged particle multiplicity $dN/d\eta$ is shown for each hydrodynamics.

The hydrodynamic evolutions with the three types of the hydrodynamics are shown in Fig. 7.10. Note that the switching hypersurfaces shown in the top row are almost the same in all the three hydrodynamics even if the entropy scales of the initial conditions are different from each other. This is because the density profile of MC-KLN is steep at the edges of the matter so that the temperature largely changes at the edges.

In the ideal hydrodynamics, the matter is cooled down faster than the dissipative hydrodynamics. This is because the collective flow of the matter is generated faster in the ideal hydrodynamics, so that the internal energy e is quickly converted to the kinetic energy of the fluid, $K = T^{00} - e = (e + P)\boldsymbol{u}^2$. In the fluctuating hydrodynamics, the local flows in random directions are generated by the hydrodynamic fluctuations, and this causes the faster cool down like in the ideal hydrodynamics.

In the dissipative hydrodynamics, the initial lumpy structure is washed out quicker than the case of the ideal hydrodynamics due to the viscosity. In the fluctuating hydrodynamics, on the other hand, the lumpy structure is washed out by the viscosity and, at the same time, is newly created by the hydrodynamic fluctuations. As a result the matter distribution is lumpier in the fluctuating hydrodynamics. The shape of the matter is also largely changed due to the hydrodynamic fluctuations. The direction of the elliptic component of the matter distribution is remained at the last row of Fig. 7.10 in the ideal and dissipative hydrodynamics, but it changes in the fluctuating hydrodynamics.

In Fig. 7.11, the transverse momentum spectra of charged pions, charged kaons and protons are shown. We can see that the effect of the hydrodynamic fluctuations are qualitatively the same as in the calculations without initial-state fluctuations; High-p_T hadrons are increased even with the initial-state fluctuations. Here we can also investigate the centrality dependence of the spectra. The factor of the increase of the high-p_T hadrons is larger in peripheral collisions. This result can be explained by the

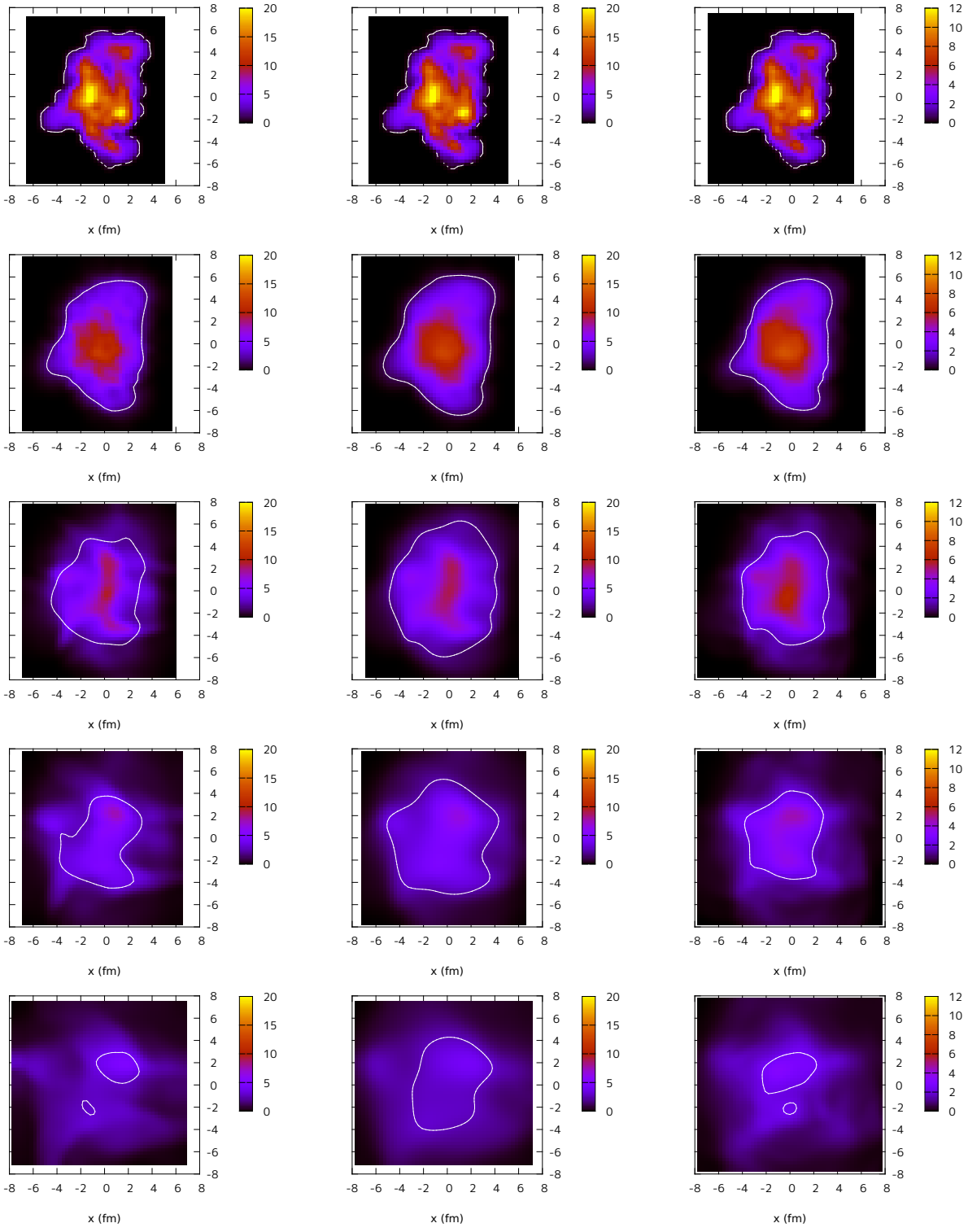

Figure 7.10: Examples of the evolution with the three types of the hydrodynamics are shown. The left, center, and right column correspond to the ideal hydrodynamics, the dissipative hydrodynamics, and the fluctuating hydrodynamics, respectively. The three evolutions share the same initial condition with their own entropy scales. The times of five rows are τ =0.6, 2.1, 3.6, 5.1, 6.6 fm from top to bottom. The colors indicate the energy densities T^{00} (GeV/fm^3). The white lines correspond to the switching hypersurface of $T_{\rm sw}$ =155 MeV.

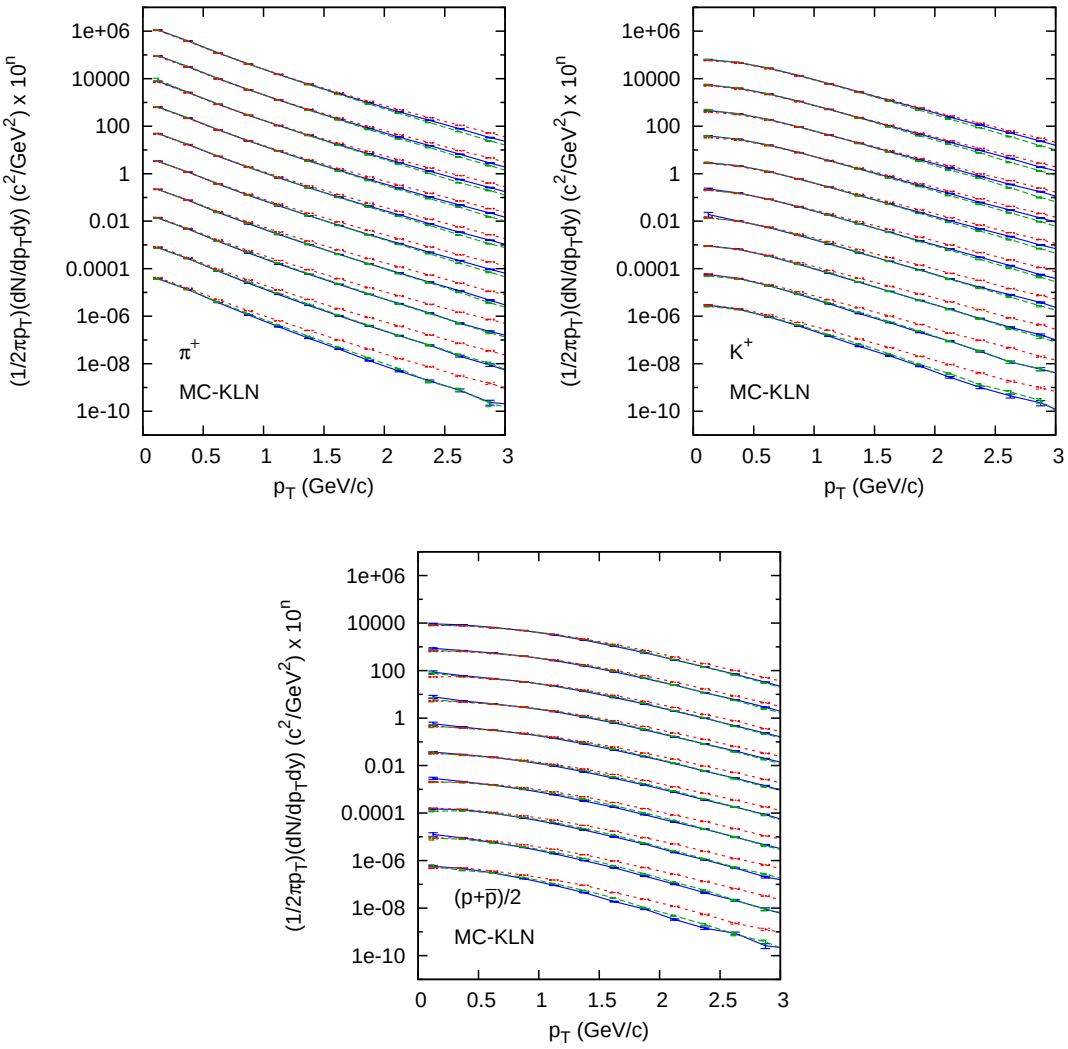

Figure 7.11: The transverse momentum spectra of identified hadrons are shown for each centralities. The top left, top right and bottom plot correspond to the spectra of charged pions, charged kaons, and protons, respectively. Centrality classes are 0-4% ($\times 10^4$), 5-10% ($\times 10^3$), 10-15% ($\times 10^2$), 15-20% ($\times 10^1$), 20-30%, 30-40% ($\times 10^{-1}$), 40-50% ($\times 10^{-2}$), 50-60% ($\times 10^{-3}$), 60-70% ($\times 10^{-4}$), and 70-80% ($\times 10^{-5}$) from top to bottom. The blue lines, green lines, and red lines correspond to the results of the ideal hydrodynamics, the dissipative hydrodynamics, and the fluctuating hydrodynamics, respectively.

properties of the thermal fluctuations: The relative fluctuations of the macroscopic quantities are larger in smaller systems. Because the system size of the created matter is smaller in the peripheral collisions, the effect of the hydrodynamic fluctuations becomes larger.

In Fig. 7.12, the integrated $v_2\{2\}$ as functions of the pseudorapidity are shown. For all centralities, we can see that the elliptic flows are decreased by the viscosity, but are increased by the hydrodynamic fluctuations. In the most central collisions, the effect of the hydrodynamic fluctuations surpasses that of the viscosity, so that v_2 of the fluctuating hydrodynamics are larger than that of the ideal hydrodynamics. In other centralities, v_2 of the fluctuating hydrodynamics and the ideal hydrodynamics are the same order. This can be understood as follows: In non-central collisions, the elliptic flow originated from the initial geometry is disordered by the hydrodynamic fluctuations to have smaller effects, which cancels the increase of the elliptic flow due to the hydrodynamic fluctuations. In the central collisions, on the other hand, there is no initial geometry origin, and the elliptic flow is simply created by the hydrodynamic fluctuations.

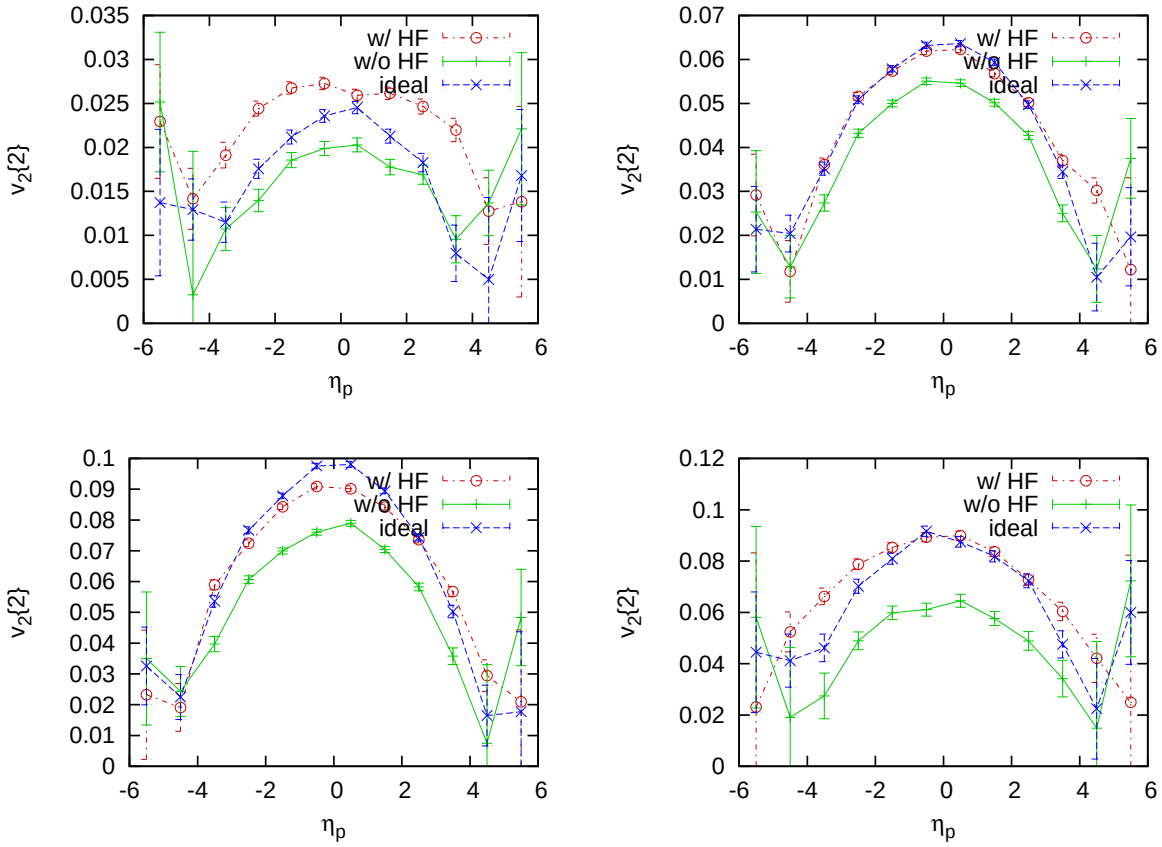

Figure 7.12: The integrated $v_2\{2\}$ as functions of the pseudorapidity are shown. Centralities are 0-5%, 15-20%, 40-50%, and 60-70% for the top left, the top right, the bottom left, and the bottom right panel, respectively.

In Fig. 7.13, the elliptic flows $v_2\{2\}$ as functions of the transverse momentum are shown. In the most peripheral collisions shown in the bottom right panel, the differential elliptic flow is increased by the hydrodynamic fluctuations. In other centralities, the result of the dissipative and fluctuating hydrodynamics are close to each other. This result again implies that the effect of the hydrodynamic fluctuations are relatively larger in smaller systems.

In the most central collisions where the geometry-origin elliptic flow is small, all the three hydrodynamics show similar results. In the non-central collisions, on the other hand, the result of the ideal hydrodynamics is always larger than that of the other hydrodynamics due to the geometry-origin elliptic flows. Note that the increase of the integrated $v_2\{2\}$ of the fluctuating hydrodynamics seen in Fig. 7.12 can be explained by the increase of high-p_T hadrons in Fig. 7.11. Therefore the orderings of the three lines are different in Fig. 7.12 and Fig. 7.13.

All the results of the integrated dynamical model are larger than the experimental data. This is because in this study we assumed the specific shear viscosity to be the lower bound $\eta/s = 1/4\pi$ [83]. With realistic shear viscosity larger than the bound, the decrease of the results of the dissipative and fluctuating hydrodynamics becomes stronger, which makes the results to be consistent with the experimental data. The shear viscosity coefficient is constrained by analyzing the dependence of the flow harmonics on shear viscosity and comparing the results with experimental data. In this procedure the change of the flow harmonics by the hydrodynamic fluctuations directly means the change of the extracted shear viscosity coefficient. Thus in the quantitative extraction of the transport properties of the created matter, the effects of the hydrodynamic fluctuations cannot be neglected in dynamical models.

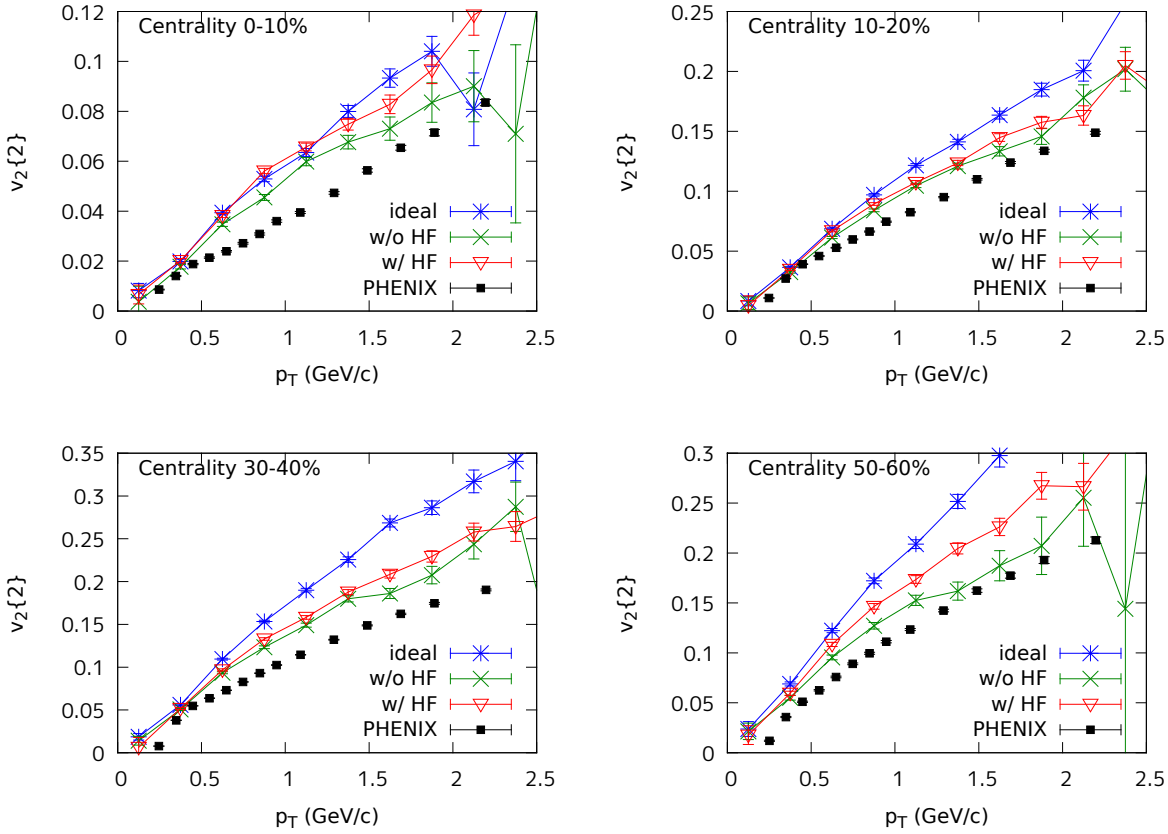

Figure 7.13: The elliptic flow $v_2\{2\}$ as functions of the transverse momentum are shown. The black points show the experimental results from PHENIX [258].

7.4 Brief summary

In this chapter, after introducing our dynamical model, we first performed the event-by-event calculations without the initial-state fluctuations. We compared the ideal hydrodynamics, the dissipative hydrodynamics, and the fluctuating hydrodynamics with three different smearing scales. As a result we found that the multiplicity of the charged hadrons is increased by the hydrodynamics fluctuations, and the effect is larger for a smaller smearing scale. This implies the necessity to retune the entropy scale of the initial condition in the fluctuating hydrodynamics. We also obtained the identified hadron spectra to find that the high-p_T hadrons are increased. The integrated elliptic flow is increased by the hydrodynamic fluctuations, which can be explained by the change of the spectra.

We also performed event-by-event calculations with the initial-state fluctuations for the minimum biased events. We considered the ideal, dissipative, and fluctuating hydrodynamics to compare the effects of the hydrodynamic fluctuations to that of the initial-state fluctuations. The similar behavior is obtained as in the calculations without the initial-state fluctuations. In particular, the change of the integrated elliptic flow due to the hydrodynamic fluctuations has the same order to the change due to the viscosity. This implies that the hydrodynamic fluctuations should be taken into account in the quantitative analysis of the viscosity of the QGP. We also found that the effects of the hydrodynamic fluctuations are larger in peripheral collisions in the hadron spectra and the elliptic flow.

Chapter 8

Summary

In this thesis, we investigated the properties of the hydrodynamic fluctuations in the causal dissipative hydrodynamics and applied them to the high-energy nuclear collisions. The hydrodynamic fluctuations are the thermal fluctuations of fluid fields arising in the space-time evolution of the matter. After the introduction of the high-energy nuclear collisions and the review on the relativistic hydrodynamics, we first investigated properties of the hydrodynamic fluctuations in relativistic systems. We then developed a new robust scheme of the causal dissipative hydrodynamics, and defined the smeared fluctuating hydrodynamics with an explicit coarse-graining scale. Finally, by performing a massive number of event-by-event dynamical simulations, we discussed the qualitative behavior of the effect of the hydrodynamic fluctuations on experimental observables. The hydrodynamic fluctuations have significant effects on the event-by-event fluctuations measured in the experimental observables such as higher harmonics, and thus they should be taken into account in the extraction of transport coefficients of the created matter.

In Chapter 1, we give a brief introduction to quantum chromodynamics, the quark-gluon plasma, and the high-energy nuclear collision experiments. Then we outlined the structure of this thesis.

After a brief introduction in Chapter 2, we introduced the related topics of the high-energy nuclear collisions. One of the major purposes of the high-energy nuclear collisions is the extraction of the transport properties of the quark-gluon plasma (QGP). The only way to experimentally create QGP is the high-energy nuclear collision experiments. In the experiment, two nuclei accelerated to nearly the light velocity are collided to each other to create high-temperature matter. Recent years, the event-by-event fluctuations are measured in the observables of the higher flow harmonics v_n. It turned out that the major origin of the event-by-event fluctuations is the initial-state fluctuations. The transport properties of the QGP, such as the specific shear viscosity η/s, can be extracted by comparing the results of the event-by-event simulations with the experimental data. In quantitative analysis of the transport properties, it is needed to consider all the sources of the event-by-event fluctuations including the initial-state fluctuations, the hydrodynamic fluctuations, freezeout processes of the hadron gas, and disturbance of the QGP fluids by jets. In particular, we have considered the effects of the hydrodynamic fluctuations in this thesis.

In Chapter 3, we reviewed the basic notions of the relativistic hydrodynamics. The dynamics of the relativistic hydrodynamics is basically written by the conservation law of the currents $(T^{\mu\nu}, N_i^\mu)$. In addition, the equation of state and the constitutive equations, where the properties of the matter are encoded, are needed to close the equations. To apply those equations, we need to define the thermodynamic quantities in terms of the conserved currents $(T^{\mu\nu}, N_i^\mu)$. In order to decompose the conserved currents into the thermodynamic fields, the flow velocity u^μ is introduced to define the local rest frame of the matter. The projectors $\Delta^{\mu\alpha}$ and $\Delta^{\mu\nu\alpha\beta}$ play important roles in the decomposition. The ideal hydrodynamics corresponds to the assumption that the conserved currents have the equilibrium values, which are written by the equilibrium pressure P, the internal energy density e, and the charge densities n_i. The relation among the quantities is given by the equation of state: $P = P(e, \{n_i\})$. The dissipative hydrodynamics can be obtained by considering the deviation of the conserved currents: the shear stress $\pi^{\mu\nu}$, the bulk pressure Π and the charge diffusion ν_i. Those dissipative currents are described by the constitutive equations in terms of the thermodynamic forces, i.e., the gradients of the thermodynamic fields. By expanding the dissipative currents to the first-order of the thermodynamic forces and imposing the second law of the thermodynamics, the Navier-Stokes theory of the relativistic dissipative hydrodynamics is obtained. However, this first-order theory has problems related to the acausal modes. The higher-order dissipative hydrodynamics can be constructed so that the causality is not broken, and it is

called causal dissipative hydrodynamics.

In Chapter 4, we investigated the nature of the hydrodynamic fluctuations in relativistic systems. The hydrodynamic fluctuations arise as the deviation of the dissipative currents from its ensemble averaged value specified by the ordinary constitutive equations. The constitutive equations are commonly written in terms of the thermodynamic forces and its derivatives, which we called the differential form of the constitutive equations. To define the constitutive equations with the hydrodynamic fluctuations, we considered the integral form of the constitutive equations in the linear-response regime. The integral form can be obtained by formally solving the differential form, and generally written as the convolution of the memory function and the thermodynamic force. The memory function is a retarded function which specifies the effect of the thermodynamic forces of past on the current dissipative currents. The power spectrum of the hydrodynamic fluctuations is written by the memory function according to the fluctuation-dissipation relation (FDR). The memory function in the causal dissipative hydrodynamics always has a non-zero relaxation time so that the hydrodynamic fluctuations in the integral form of the constitutive equations are always colored, i.e., the hydrodynamic fluctuations at different times have finite correlations. To find the explicit form of the spectrum in the non-linear hydrodynamic evolution, we solved the memory function on the non-uniform background by introducing the pathline projectors of the dissipative currents, $\Delta(\tau';\tau)^{\mu\alpha}$ and $\Delta(\tau';\tau)^{\mu\nu\alpha\beta}$, which perform the projections $\Delta^{\mu\nu}(\tau'')$ and $\Delta^{\mu\nu\alpha\beta}(\tau'')$ at every time $\tau'' \in [\tau', \tau]$ on the considered pathline. Then we considered the noise autocorrelations in the differential form of the constitutive equations using the causality, the FDR, the relaxation and the retardation of the memory function, and symmetries and the structure of the constitutive equations. As a result, we found that the structure of the differential form of the constitutive equations is constrained, and the noise terms in the differential form are always white, i.e., their autocorrelation is a delta function.

In Chapter 5 we developed a new conservative scheme of the causal dissipative hydrodynamics which is robust under the large gradients caused by the hydrodynamic fluctuations. First we considered two constraints of the causal dissipative hydrodynamics: the conservation law, and the transversality between the dissipative currents and the flow velocity. Although the original hydrodynamic equation preserves those constraints, naively discretized versions of the equation may suffer from the discretization errors of the constraints. The errors can be accumulated to cause wrong results or even a crash of the calculation due to instabilities triggered by the errors. Our scheme was explicitly constructed to be free from those discretization errors. For the conservation law, we extended the existing conservative scheme to correctly deal with curved coordinate systems. For the transversality, we considered the dissipative currents represented in the local rest frame. To find the constitutive equations in the representation in the local rest frame, we first defined four tensor bases and considered the basis transformations among them. The Christoffel symbols in the basis of the local rest frame become the Ricci rotation coefficients. As a result the constitutive equations in the local rest frame have an additional term which implies a spatial rotation of the dissipative currents, as well as the ordinary terms.

In Chapter 6, we considered the numerical implementation of the hydrodynamic fluctuations in the causal dissipative hydrodynamics. First we discussed the singularity of the fluctuating hydrodynamics to define the smeared fluctuating hydrodynamics. The autocorrelations of the noise terms at an equal time should be delta functions in space because of the causality of the memory function. These delta functions cause a singularity of the fluctuating hydrodynamics. In numerical calculations, we consider the averaged values of the fluid fields in a finite volume V of the fluid cells. In the continuum limit where the volume goes to zero, the noise terms diverge because they scale as $V^{-1/2}$. To avoid the singularity, a non-zero coarse-graining scale is needed. Although effective coarse graining is caused by the finite grid spacing of the calculation, the isotropy of such a kind of coarse graining is affected by the grid structure under large gradients by the hydrodynamic fluctuations. Therefore we explicitly introduced the physical coarse-graining scale and discussed the relations between the coarse-graining scale, the grid spacing, and the scale of interests for the reliable calculations. After giving the noise generation method with the proper autocorrelations, we considered the two different smearing procedures of the noise fields: the Gaussian smearing and the wavelength cutoff. Finally we discussed the stochastic integrals in the causal dissipative hydrodynamics. The fluctuating hydrodynamics containing random noise fields has stochastic differential equations like the Langevin-type equation. There are two different interpretations of such naive Langevin-type equations: the Itô integrals and the Stratonovich integrals. We adopt the Stratonovich integrals for the fluctuating hydrodynamics. However it turned out that in the causal fluctuating hydrodynamics, there are no differences between the Itô integrals and the Stratonovich integrals, which reflects the fact that the noise in the causal theory is not white but inherently colored.

In Chapter 7, we implemented our numerical scheme including the hydrodynamic fluctuations in the integrated dynamical model of the high-energy nuclear collisions to investigate the effects. We first performed event-by-event calculations without the initial-state fluctuations to clarify the qualitative effects caused by the hydrodynamic fluctuations. We found the increase of the charged particle multiplicity, whose rate is larger in the high-p_T hadrons in the identified hadron spectra. We also found the increase of the observable of the integrated v_2 which can be explained by the increase of the high-p_T hadrons which have larger differential v_2 values. The p_T integrated multiplicities are also increased by the hydrodynamic fluctuations. This implies the entropy density of the hydrodynamic initial conditions should be smaller than that used in conventional calculations. We then performed event-by-event calculations with both of the initial-state fluctuations and the hydrodynamic fluctuations to compare the effects of the two fluctuations to each other. It turned out that the effects of the hydrodynamic fluctuations are larger in the peripheral collisions, which reflects the fact that the relative thermal fluctuations are larger in smaller systems. We also found that the increase of the integrated v_2 by the hydrodynamic fluctuations is comparable to the decrease by the shear viscosity. In particular, in the central collisions where there are no geometrical origin of v_2, the hydrodynamic fluctuations have larger effects than the shear viscosity. Those results imply that, in the quantitative analysis of the shear viscosity, the hydrodynamic fluctuations should be taken into account in the dynamical models as well as the initial-state fluctuations and the shear viscosity.

For future works, we need to consider detailed and quantitative calculations and analyses to extract the information of the created matter and understand the dynamics caused by the hydrodynamic fluctuations. In particular, the following points should be considered:

- By performing the event-by-event calculations with the hydrodynamic fluctuations and comparing the results to experimental data, we should extract the information on the initial state, the dynamics of the high-energy nuclear collision processes, and the properties of the created QGP. Such information is expressed by the parameters of the existing models which include, for example, the initial entropy scale and other parameters in initial-state models, the transport coefficients of the matter in the hydrodynamic stage, and the switching temperature $T_{\rm sw}$ related to the freezeout process of the system. Those parameters can be tuned to reproduce the experimental observables. Since the hydrodynamic fluctuations change the observables used to tune each parameter, those parameters should also be modified by the hydrodynamic fluctuations. While we have already retuned the initial entropy scale in this thesis, other parameters have not yet been retuned. For example, the parameters in the initial conditions can be tuned to reproduce the charged particle multiplicity as a function of the pseudorapidity and the collision centrality. Then the transport coefficients such as the shear viscosity η/s should be extracted to reproduce the flow harmonics v_2. At the same time the difference of initial-state models, such as Monte-Carlo Glauber (MC-Glauber) model and Monte-Carlo Kharzeev-Levin-Nardi (MC-KLN) model, should be examined with the parameters tuned for each model. Each initial-state model has its own distributions of the initial anisotropies ϵ_n and the correlations of the anisotropy angles Φ_n, which can be investigated through distributions of the observed flow harmonics v_n and the correlations of the event-plane angles Ψ_n. Since the hydrodynamic fluctuations generate the flow fluctuations to modify the distributions of those flow coefficients, they become important in the study of the initial-state correlations.

- After the parameter retuning, we need to analyze in detail the hadron distributions from massive number of event-by-event calculations with the hydrodynamic fluctuations to find the quantitative effects which can be directly compared to the experimental data. It is important to investigate the experimental observables sensitive to the hydrodynamic fluctuations. For example, the effects on the two particle correlations in the rapidity direction can be investigated. The hydrodynamic fluctuations have a short correlation length in the rapidity direction unlike the initial-state fluctuations. This characteristics can be utilized to separate the effects of the hydrodynamic fluctuations contained in the event-by-event fluctuations. Also, it turned out that the effects of the hydrodynamic fluctuations on the elliptic flow are changed by the initial geometry origin of the elliptic component. Thus, the interplay of the hydrodynamic fluctuations and the genuine initial-state fluctuations can be investigated in the ultra-central collisions where the initial geometry origin of the elliptic flow vanishes,

- The coarse graining of the smeared fluctuating hydrodynamics is a remaining subject to be studied. Analyzing the results of the event-by-event calculations, we can investigate the coarse-graining

scale dependence of the observables as well as the difference between the smearing methods such as the Gaussian smearing and the wavelength cutoff. The coarse-graining scale dependence of the fluctuating hydrodynamics would contain rich physics. Due to the non-linear terms of the hydrodynamic equations, the global behavior of the matter changes with the hydrodynamic fluctuations. Not to change the real physics, the equation of state and the transport coefficients should be renormalized at each coarse-graining scale. The Cooper-Frye formula, which is used in the switching of the description from the fluid to the hadrons, should also have corrections by the hydrodynamic fluctuations.

By taking account the hydrodynamic fluctuations in the dynamical models, we can perform quantitative analyses of the transport properties of the created matter. However, the hydrodynamic fluctuations are not just the noise of the analysis. By considering the above points, we can reach the deeper understanding of the processes of the high-energy nuclear collisions. In the collision processes, the microscopic scale and the macroscopic scale are not separated enough to ignore the thermal fluctuations. Thus the understanding of the hydrodynamics fluctuations, namely the thermal fluctuations of the dissipative hydrodynamics, is an inevitable topic in future studies of the high-energy nuclear collisions.

Acknowledgments

I have made my work and written this thesis with the help of many people. Here I would like to acknowledge each of them. First I have to acknowledge the comments on my work and my thesis by my supervisor, Prof. Tetsuo Hatsuda from RIKEN Nishina Center and the University of Tokyo. He spent much of his time to read thoroughly my thesis and gave me thousands of comments. Without his advice and encouragement I could not complete this thesis. I would like to express my greatest appreciation to him. I also have to acknowledge the powerful support by my collaborator and the former supervisor for my master's degree, Prof. Tetsufumi Hirano from Sophia University. He introduced the physics of high-energy nuclear collisions to me, and lead me to this profound topic on the thermal fluctuations of the hydrodynamics in high-energy nuclear collisions. He always has new interesting problems and topics, which deepened my knowledge. I also thank to the members of Hirano group, Yuji Hirono, Yasuki Tachibana, Masaru Hongo, Ryuichi Kurita, Shiori Takeuchi, Kenichi Nagai, Hiromi Hinohara, and Koshi Kawaguchi for fruitful discussions. I am also grateful to Dr. Clint Young and Prof. Joseph Kapusta for their kind hospitality and fruitful discussions with them during my stay at University of Minnesota.

My study was also supported financially by JSPS KAKENHI Grant Number 12J08554 and others. Prof. Tetsufumi Hirano and Prof. Tomi Otsuki from Sophia University provide me the opportunity to use powerful cluster machines of Sophia University. I am grateful to them and Dr. Koji Kobayashi from Sophia University for the generous and tolerant understanding on my exhausting calculations and the allocation of the computational resources for me.

I would like to acknowledge the environment of my study too. I thank to K. Kamikado, Y. Hirono, K. Suzuki, R. Kurita, K. Masuda, and K. Kawaguchi for taking time for desultory conversations with me. I am also grateful to my family: my mother, my father and my brother Mitsuru. They were always by my side and supported me when I experienced hard times.

Appendix A

Appendix: High-energy nuclear collisions

A.1 Centrality determination

In experiments the charged particle multiplicity $N_{\rm ch}^{\rm raw}$, the total energy E_T, and other amplitudes in various detectors (without the correction of the acceptance and the efficiency of the detectors) are used for the event-by-event centrality determination. In the following table, the major observables to determine the centrality are shown:

Observable	Pseudorapidity range	Detector
$N_{\rm ch}$	$3.0 < \lvert\eta_p\rvert < 4.5$	PHOBOS Paddle Counters [102–104]
$N_{\rm ch}$	$\lvert\eta_p\rvert < 0.5$	STAR TPC [44, 69]
BBC-ZDC correlations	$3.1 < \lvert\eta_p\rvert < 3.9$ (BBC)	PHENIX BBC and ZDC
$N_{\rm ch}$	$\lvert\eta_p\rvert < 0.8$	ALICE TPC [105]
$N_{\rm ch}$	$\lvert\eta_p\rvert < 2.0$ (inner layer)	ALICE SPD [106]
	$\lvert\eta_p\rvert < 1.4$ (outer layer)	
VZERO amplitudes	$2.8 < \eta_p < 5.1$ (V0A)	ALICE VZERO detectors [106]
	$-3.7 < \eta_p < -1.7$ (V0C)	
ZDC-ZEM correlations	$4.8 < \eta_p < 5.7$ (ZEM)	ALICE ZDC and ZEM [106, 107]
E_T	$3.2 < \lvert\eta_p\rvert < 4.9$	ATLAS FCal [100, 108]
E_T	$3 < \lvert\eta_p\rvert < 5$	CMS HF [109]

The symbol $N_{\rm ch}$ denotes the charged particle multiplicity, and E_T the total energy deposition. The full detector names are Time Projection Chamber (TPC), Beam-Beam Counter (BBC), Zero Degree Calorimeters (ZDC), Reaction Plane Detector (RxP), Silicon Pixel Detector (SPD), Vertex-0 Detector (VZERO), the electromagnetic calorimeter close to zero-degree (ZEM), Forward Calorimeters (FCal), and the forward hadron calorimeters (HF). To determine the centrality in PHENIX experiments, ZDC in the forward and backward beam direction, which detect the spectators, are combined with the charged particle multiplicity in BBC to consider a two-dimensional multiplicity distribution called BBC-ZDC correlations.

A.2 Initialization models

Optical Glauber model

In the optical Glauber model, the thickness functions are calculated by integrating the continuous nucleon distribution $\rho_{\rm A}(\boldsymbol{x} - \boldsymbol{b}/2)$ and $\rho_{\rm B}(\boldsymbol{x} + \boldsymbol{b}/2)$ in the z-direction:

$$T^{\rm A}(\boldsymbol{x}_T) = \frac{dN^{\rm A}}{d^2x_T} = A\int_{-\infty}^{\infty} dz \rho_{\rm A}(\boldsymbol{x} - \boldsymbol{b}/2), \tag{A.1}$$

$$T^{\rm B}(\boldsymbol{x}_T) = \frac{dN^{\rm B}}{d^2x_T} = B\int_{-\infty}^{\infty} dz \rho_{\rm B}(\boldsymbol{x} + \boldsymbol{b}/2), \tag{A.2}$$

where A and B are the mass numbers of the nuclei A and B, and $\boldsymbol{b}$ is the impact parameter vector. The coordinate origin is chosen so that the nuclei A and B are centered at symmetric positions: $\boldsymbol{b}/2$

and $-\boldsymbol{b}/2$, respectively. The nucleon distributions are given by the profile of each nucleon $\Delta(\boldsymbol{x})$ and the Woods-Saxon distribution function $\rho_{\rm WS}(\boldsymbol{x})$:

$$\rho_{\rm A/B}(\boldsymbol{x}) = \int d^3\boldsymbol{x}'\Delta(\boldsymbol{x}-\boldsymbol{x}')\rho_{\rm WS}(\boldsymbol{x}'), \tag{A.3}$$

$$\rho_{\rm WS}(\boldsymbol{x}) = \frac{\rho_0}{\exp\frac{|\boldsymbol{x}|-r_{\rm WS}}{d_{\rm WS}}+1}, \tag{A.4}$$

where ρ_0, $r_{\rm WS}$, and $d_{\rm WS}$ are the parameters depending on each nucleus species. The nucleon profile can be set, for example, to a ball: $\Delta(\boldsymbol{x}) = \theta(r_N - |\boldsymbol{x}|)/V_N$ where the normalization is $V_N = 4\pi r_N^3/3$. The radius r_N is determined so that the inelastic nucleon-nucleon scattering cross section is $\sigma_{NN}^{\rm in}(\sqrt{s_{\rm NN}}) = \pi r_N^2$. It should be noticed here that the experimentally measured Woods-Saxon parameters correspond to the density $\rho_{\rm A/B}$ but not to the nucleon position distribution $\rho_{\rm WS}$. In fact the input shape of $\rho_{\rm WS}$ is diffused in $\rho_{\rm A/B}$ due to the finite size nucleon profile, so that the input Woods-Saxon parameters should be chosen to reproduce the experimental nuclear density $\rho_{\rm A/B}$ [160]. The initial entropy density in the transverse plane is written as

$$\frac{dS(\boldsymbol{x}_T)}{\tau_0 d\eta_s d^2x_T} = \frac{C}{\tau_0}\left\{\frac{1-\delta}{2}[T_{\rm part}^{\rm A}(\boldsymbol{x}_T)+T_{\rm part}^{\rm B}(\boldsymbol{x}_T)]+\delta\cdot T_{\rm coll}^{\rm AB}(\boldsymbol{x}_T)\right\}, \tag{A.5}$$

where the local density of the participant nucleons and binary collisions are calculated as

$$T_{\rm part}^{\rm A}(\boldsymbol{x}_T) \equiv \frac{dN_{\rm part}^{\rm A}}{d^2x_T} = T^{\rm A}(\boldsymbol{x}_T)[1-(1-\sigma_{NN}^{\rm in}T^{\rm B}(\boldsymbol{x}_T)/B)^B], \tag{A.6}$$

$$T_{\rm part}^{\rm B}(\boldsymbol{x}_T) \equiv \frac{dN_{\rm part}^{\rm B}}{d^2x_T} = T^{\rm B}(\boldsymbol{x}_T)[1-(1-\sigma_{NN}^{\rm in}T^{\rm A}(\boldsymbol{x}_T)/A)^A], \tag{A.7}$$

$$T_{\rm coll}^{\rm AB}(\boldsymbol{x}_T) \equiv \frac{dN_{\rm coll}}{d^2x_T} = \sigma_{NN}^{\rm in}T^{\rm A}(\boldsymbol{x}_T)T^{\rm B}(\boldsymbol{x}_T). \tag{A.8}$$

The overall scaling factor C and the hard fraction parameter δ are determined for each collision energy $\sqrt{s_{\rm NN}}$ to reproduce the experimental centrality dependence of the charged particle multiplicity at the midrapidity.

Modified BGK model

In the above Glauber modeling, the entropy density profile in the transverse plane is considered. In (2+1)-dimensional hydrodynamic calculations in the transverse plane, the expression (A.5) is sufficient to generate initial conditions at the midrapidity. On the other hand, in calculating the fully (3+1)-dimensional hydrodynamics to discuss the rapidity dependence of observables, the entropy density distribution in the longitudinal direction should be considered, which requires additional modeling. In the modified Brodsky-Gunion-Kuhn (modified BGK) model [119, 161, 162], the initial condition is extended to the rapidity direction as

$$\begin{aligned}\frac{dS(\boldsymbol{x}_T)}{\tau_0 d\eta_s d^2x_T} =& \frac{C}{\tau_0}f^{pp}(\eta_s)\theta(Y_b-|\eta_s|)\\ &\times\left\{(1-\delta)\left[\frac{Y_b+\eta_s}{2Y_b}T_{\rm part}^{\rm A}(\boldsymbol{x}_T)+\frac{Y_b-\eta_s}{2Y_b}T_{\rm part}^{\rm B}(\boldsymbol{x}_T)\right]+\delta\cdot T_{\rm coll}^{\rm AB}(\boldsymbol{x}_T)\right\},\end{aligned} \tag{A.9}$$

where the beam rapidity Y_b is defined so that $\cosh Y_b = \sqrt{s_{\rm NN}}/2m_N$ with the nucleon mass $m_N = 0.939$GeV. The outline of the rapidity distribution is given by the parametrized function $f^{pp}(\eta_s)$ to explain the distribution in pp collisions:

$$f^{pp}(\eta_s) = \exp\left[-\theta(|\eta_s|-\Delta\eta)\frac{(|\eta_s|-\Delta\eta)^2}{\sigma_\eta^2}\right], \tag{A.10}$$

where the parameters $\Delta\eta$ and σ_η are adjusted for each collision energy $\sqrt{s_{\rm NN}}$ to reproduce the measured rapidity distribution of the charged particle multiplicity. The local imbalance of the numbers of the participant nucleons from the nuclei A and B is reflected in the rapidity triangle shapes $(Y_b \pm \eta_s)/2Y_b$ observed in d+A collisions compared to $pp/p\bar{p}$ collisions [163, 164]. At the midrapidity $\eta_s = 0$ the initial condition (A.9) reduces to the original two-dimensional profile (A.5).

Monte-Carlo Glauber model

So far the event-by-event distributions of the nucleons are not considered. Instead the smooth initial condition corresponding the event averaged picture of the initial state is obtained. On the other hand, the effect of the event-by-event distribution is measured through the experimental observables such as two particle correlations, and plays an important role in studying the matter properties. The Monte-Carlo version of the Glauber model (MC-Glauber model) [165] considers this event-by-event distribution of the wounded nucleon positions. First the positions of the nucleons, $\boldsymbol{x}^{(\mathrm{A},i)}$ and $\boldsymbol{x}^{(\mathrm{B},j)}$ $(1 \leq i \leq A, 1 \leq j \leq B)$, are sampled randomly with the probability density function being the Woods-Saxon distribution (A.4) displaced with the impact parameters $\pm\boldsymbol{b}/2$ for the nuclei A/B, respectively. Then the collision detection is performed on each pair of a nucleon from the nucleus A, and another from the nucleus B. The resulting binary-collision list is constructed as $\mathrm{Coll} \equiv \{(i,j) : |\boldsymbol{x}_T^{(\mathrm{A},i)} - \boldsymbol{x}_T^{(\mathrm{B},j)}| < r_N\}$ where $|\boldsymbol{x}_T^{(\mathrm{A},i)} - \boldsymbol{x}_T^{(\mathrm{B},j)}|$ is the projected distance of two nucleons in the transverse plane. The participant nucleons in each nucleus are ones which participate in at least one binary collision: $\mathrm{PartA} \equiv \{i : (i,j) \in \mathrm{Coll}\}$, and $\mathrm{PartB} \equiv \{j : (i,j) \in \mathrm{Coll}\}$. Now the Monte-Carlo version of the thickness functions and the overlap function is calculated as superpositions of the two-dimensional participant/collision profiles $\Delta_T^{\mathrm{part/coll}}(\boldsymbol{x}_T)$:

$$T_{\mathrm{part}}^{\mathrm{A/B}}(\boldsymbol{x}_T) = \sum_{i \in \mathrm{PartA/B}} \Delta_T^{\mathrm{part}}(\boldsymbol{x}_T - \boldsymbol{x}_T^{(\mathrm{A/B},i)}), \tag{A.11}$$

$$T_{\mathrm{coll}}^{\mathrm{AB}}(\boldsymbol{x}_T) = \sum_{(i,j) \in \mathrm{Coll}} \Delta_T^{\mathrm{coll}}(\boldsymbol{x}_T - (\boldsymbol{x}_T^{(\mathrm{A},i)} + \boldsymbol{x}_T^{(\mathrm{B},j)})/2), \tag{A.12}$$

where the two-dimensional profiles are, for example, disks: $\Delta_T^{\mathrm{part/coll}}(\boldsymbol{x}_T) = \theta(r_N - |\boldsymbol{x}_T|)/\sigma_{NN}^{\mathrm{in}}$ where $\sigma_{NN}^{\mathrm{in}}$ is the normalization.

Monte-Carlo KLN model

In the KLN model, the k_T-factorization formula [176] is applied at each point of the transverse plane to generate the three dimensional initial condition:

$$\frac{dS(\eta_s, \boldsymbol{x}_T)}{\tau_0 d\eta_s d^2x_T} = \frac{C}{\tau_0} \frac{dN_g(\eta_s, \boldsymbol{x}_T)}{d\eta_s d^2x_T} \tag{A.13}$$

$$\begin{aligned} &= C\frac{2\pi^2}{C_{\mathrm{F}}} \int^{p_T^{\max}} \frac{d^2p_T}{p_T^2} \int^{p_T} \frac{d^2k_T}{4} \alpha_s(Q^2_{\max}(\boldsymbol{p}_T, \boldsymbol{k}_T)) \\ &\quad \times \phi(x_+(p_T,\eta_s), (\boldsymbol{p}_T + \boldsymbol{k}_T)^2/4; Q^2_{s,\mathrm{A}}(\boldsymbol{x}_T)) \\ &\quad \times \phi(x_-(p_T,\eta_s), (\boldsymbol{p}_T - \boldsymbol{k}_T)^2/4; Q^2_{s,\mathrm{B}}(\boldsymbol{x}_T)), \end{aligned} \tag{A.14}$$

where $C_{\mathrm{F}} = (N_c^2 - 1)/2N_c = 4/3$, $Q^2_{\max} = \max\{(\boldsymbol{p}_T + \boldsymbol{k}_T)^2/4, (\boldsymbol{p}_T - \boldsymbol{k}_T)^2/4\}$, $\alpha_s(Q^2)$ is the running coupling constant of QCD, and the unintegrated gluon distribution $\phi(x, k_T^2; Q_s^2)$ is given by

$$\phi(x, k_T^2; Q_s^2) = \kappa \frac{C_{\mathrm{F}}}{2\pi^3} \frac{(1-x)^4}{\alpha_s(Q_s^2)} \frac{Q_s^2}{\max\{Q_s^2, k_T^2\}}. \tag{A.15}$$

The rapidity dependence enters the Bjorken x as $x_\pm = p_T \exp(\pm\eta_s)/\sqrt{s_{\mathrm{NN}}}$. The distribution in the transverse plane is generated through the transverse-position-dependent saturation scales $Q^2_{s,\mathrm{A/B}}(\boldsymbol{x}_T)^2$ written by the wounded nucleon thickness functions:

$$Q^2_{s,\mathrm{A/B}}(\boldsymbol{x}_T)^2 = Q^2_{s,0} \frac{T_{\mathrm{part}}^{\mathrm{A/B}}(\boldsymbol{x}_T)}{T_0} \left(\frac{x_0}{x}\right)^\lambda. \tag{A.16}$$

The model parameters are $CC_{\mathrm{F}}\kappa^2/\tau_0$, $Q^2_{s,0}x_0^\lambda/T_0$, λ, and $p_T^{\max}$ in these combinations.

Appendix B

Appendix: Relativistic hydrodynamics

B.1 The non-equilibrium part of the entropy current in the first-order case

To ensure the positivity of the dissipative function (3.97), the term linear in the thermodynamic forces should vanish:

$$\partial_\mu \left(\sigma^\mu - \frac{W^\mu - \sum_{i=1}^n \mu_i \nu_i^\mu}{T} \right) = 0. \tag{B.1}$$

Thus, the operand of the above divergence can be written with an antisymmetric potential $\phi^{[\mu\nu]}$:

$$\sigma^\mu - \frac{W^\mu - \sum_{i=1}^n \mu_i \nu_i^\mu}{T} = \partial_\alpha \phi^{[\alpha\mu]}. \tag{B.2}$$

From the assumption of the first-order case, the right hand side should be first-order in derivatives. Therefore the potential $\phi^{[\mu\nu]}$ should be zeroth-order in derivatives and should be constructed only with u^μ. However, an antisymmetric tensor cannot be constructed only with u^μ. As a result, $\phi^{[\mu\nu]}$ always vanishes.

Finally we obtain an expression for the non-equilibrium part of the entropy current:

$$\sigma^\mu = \frac{W^\mu - \sum_{i=1}^n \mu_i \nu_i^\mu}{T}. \tag{B.3}$$

The above equation has a similar from with the thermodynamic relation:

$$s = \frac{e + P - \sum_{i=1}^n \mu_i n_i}{T}. \tag{B.4}$$

In addition the total entropy current S^μ can be written as

$$\begin{aligned} S^\mu &= s u^\mu + \sigma^\mu && \text{(B.5)} \\ &= \frac{1}{T}[(e+P)u^\mu + W^\mu] - \sum \frac{\mu_i}{T}(n_i u^\mu + \nu_i^\mu) && \text{(B.6)} \\ &= \beta_\nu T^{\mu\nu} - \sum_{i=1}^n \alpha_i N_i^\mu + \beta^\mu P, && \text{(B.7)} \end{aligned}$$

where $\beta^\mu = u^\mu/T$, and $\alpha_i = \mu_i/T$.

Appendix C

Appendix: Causal hydrodynamic fluctuations

C.1 Fluctuation-dissipation relation and Kubo formula

For example, the Green-Kubo formula for hydrodynamic system is obtained by the linear-response theory of a non-equilibrium statistical operator [240, 241]

$$\langle\hat{\Pi}\rangle = \int d^4x'\Theta(x^0 - x'^0)(\hat{\Pi}(x), \hat{\Pi}(x'))\beta(x')\theta(x'), \tag{C.1}$$

$$\langle\hat{\pi}^{\mu\nu}\rangle = \int d^4x'\Theta(x^0 - x'^0)(\hat{\pi}^{\mu\nu}(x), \hat{\pi}^{\alpha\beta}(x'))\beta(x')\sigma_{\alpha\beta}(x'), \tag{C.2}$$

$$\langle\hat{\nu}_i^{\mu}\rangle = \int d^4x'\Theta(x^0 - x'^0)\sum_{j=1}^{n}(\hat{\nu}_i^{\mu}(x), \hat{\nu}_j^{\alpha}(x'))\nabla^{\alpha}(\beta(x')\mu_j(x')). \tag{C.3}$$

Here $\beta(x) = 1/T(x)$, $u^{\mu}(x)$, and $\mu_i(x)$ are the thermodynamic fields. The dissipative components are defined as $\hat{\pi}^{\mu\nu}(x) \equiv \Delta^{\mu\nu}{}_{\alpha\beta}(x)\hat{T}^{\alpha\beta}(x)$, $\hat{\Pi}(x) \equiv -\frac{1}{3}\Delta_{\alpha\beta}(x)(\hat{T}^{\alpha\beta}(x) - \langle\hat{T}^{\alpha\beta}(x)\rangle_l)$, and $\hat{\nu}_i^{\mu}(x) \equiv \Delta^{\mu}{}_{\alpha}(x)\hat{N}_i^{\alpha}(x)$. The brackets $\langle\cdots\rangle$ and $\langle\cdots\rangle_l$ denote ensemble averages with a non-equilibrium statistical operator $\hat{\rho}$ and a local-equilibrium statistical operator $\hat{\rho}_l$, respectively:

$$\hat{\rho}_l[\beta(x), u^{\mu}(x), \mu_i(x)] = \exp(-A), \tag{C.4}$$

$$\hat{\rho}[\beta(x), u^{\mu}(x), \mu_i(x)] = \exp(-A + B), \tag{C.5}$$

$$A(t) = \int d^3x'\beta(t, \boldsymbol{x}')\left(u_{\mu}(t, \boldsymbol{x}')\hat{T}^{\mu 0}(t, \boldsymbol{x}') + \sum_{i=1}^{n}\mu_i(t, \boldsymbol{x}')\hat{N}_i^0(t, \boldsymbol{x}')\right), \tag{C.6}$$

$$B(t) = \int_{t>t'} d^4x' e^{-\epsilon(t-t')}\beta(x)\left(u_{\mu}(x')\hat{T}^{\mu 0}(x') + \sum_{i=1}^{n}\mu_i(x')\hat{N}_i^0(x')\right). \tag{C.7}$$

The correlator $(\cdots, \cdots)$ is defined as

$$(\hat{\Gamma}(x), \hat{\Gamma}(x')) \equiv \int d\tau\langle\hat{\Gamma}(x)(e^{-A\tau}\hat{\Gamma}(x')e^{A\tau} - \langle\hat{\Gamma}(x')\rangle_l)\rangle_l, \tag{C.8}$$

where $\hat{\Gamma}(x)$ is an operator in Heisenberg picture. Note that the expressions (C.1)-(C.3) are actually the expansion to the linear order in $B(t)$, and the higher order contributions are neglected in this linear-response regime.

In usual cases the Kubo formula for the Onsager coefficients are obtained by moving thermodynamics forces to outside of the integrals. This procedure can be justified in most cases because the variations of the hydrodynamic fields, such as $\beta(x)$, are slow enough compared to the time scale of microscopic correlations $(\Gamma(x), \Gamma(x'))$.

However, we here do not perform such approximation and just observe the original equations (C.1)-

(C.3). We can then read the expressions of memory functions from those equations:

$$G_\Pi(x,x')\zeta(x') = \Theta(x^0 - x'^0)(\hat{\Pi}(x), \hat{\Pi}(x'))\beta(x'), \tag{C.9}$$

$$G_\pi^{\mu\nu\alpha\beta}(x,x')2\eta(x') = \Theta(x^0 - x'^0)(\hat{\pi}^{\mu\nu}(x), \hat{\pi}^{\alpha\beta}(x'))\beta(x'), \tag{C.10}$$

$$\sum_{j=1}^{k} G_{ij}^{\mu\alpha}(x,x')\kappa_{jk}(x') = \Theta(x^0 - x'^0)(\hat{\nu}_i^\mu(x), \hat{\nu}_k^\alpha(x'))\beta(x'). \tag{C.11}$$

They can be rewritten in the following explicit form in the correlators:

$$(\hat{\Pi}(x), \hat{\Pi}(x')) = T(x')\zeta(x')G_\Pi(x,x') + T(x)\zeta(x)G_\Pi(x',x), \tag{C.12}$$

$$(\hat{\pi}^{\mu\nu}(x), \hat{\pi}^{\alpha\beta}(x')) = 2T(x')\eta(x')G_\pi^{\mu\nu\alpha\beta}(x,x') + 2T(x)\eta(x)G_\pi^{\alpha\beta\mu\nu}(x',x), \tag{C.13}$$

$$(\hat{\nu}_i^\mu(x), \hat{\nu}_k^\alpha(x')) = \sum_{j=1}^{k}[\kappa_{jk}(x')T(x')G_{ij}^{\mu\alpha}(x,x') + \kappa_{kj}(x)T(x)G_{ji}^{\alpha\mu}(x',x)]. \tag{C.14}$$

The left hand sides implies the autocorrelation of the fluctuations of dissipative currents around the local-equilibrium state. Those equations have the form of fluctuation-dissipation relations.

C.2 Proofs of properties of pathline projectors

In this section, we give a proof to the local uniform convergence of the limits in the definition of the pathline projectors, and the properties of the pathline projectors (4.25)-(4.34).

The proof will be made in the following steps: First, we define the function sequences indexed by N which will converge to the pathline projectors, and see the properties of the sequence terms in the subsection C.2.1. In the way of this step, it is already seen that the sequence terms have the properties similar to those to be proved. The later part of the proof treats convergences of the sequences, the commutativity of limits and differential operators, and the properties (4.25)-(4.34) rigorously. In the subsection C.2.2, we show the boundedness of the function sequences. Next, in the subsection C.2.3, we show their pointwise convergence to the pathline projectors. Finally, in the subsection C.2.4, we will show that the derivatives of the function sequences with respect to τ is compactly convergent, and the limits and the differential operators commute. Each step is straightforward but requires tedious calculations due to the complicated structure of the definition of the pathline projectors.

To prove the convergences, we assume the existence of $u(\tau)^\mu$, $\mathrm{D}u(\tau)^\mu$ and $\mathrm{D}^2u(\tau)^\mu$ and their boundedness:

$$M_0 \equiv \sup_{\mu,\tau}|u^\mu(\tau)| < \infty, \qquad M_1 \equiv \sup_{\mu,\tau}|\mathrm{D}u^\mu(\tau)| < \infty, \qquad M_2 \equiv \sup_{\mu,\tau}|\mathrm{D}^2u^\mu(\tau)| < \infty. \tag{C.15}$$

Also, we notice in advance that we repeatedly use the mean-value theorem and the Taylor's theorem: for any function $f(x)$ which is continuously differentiable for two times, there exist $\xi, \xi' \in I(x_0, x_1)$ such that

$$f(x_1) = f(x_0) + (x_1 - x_0)f'(\xi), \tag{C.16}$$

$$f(x_1) = f(x_0) + (x_1 - x_0)f'(x_0) + \frac{(x_1 - x_0)^2}{2}f''(\xi'), \tag{C.17}$$

where the interval $I(x,y)$ is defined as $I(x,y) \equiv \{z \mid \min\{x,y\} \le z \le \max\{x,y\}\}$.

C.2.1 Function sequences $\{\Delta_N(\tau_\mathrm{f};\tau_\mathrm{i})^\mu{}_\alpha\}_N$ and $\{\Delta_N(\tau_\mathrm{f};\tau_\mathrm{i})^{\mu\nu}{}_{\alpha\beta}\}_N$

First, we define function sequences $\{\Delta_N(\tau_\mathrm{f};\tau_\mathrm{i})^\mu{}_\alpha\}_N$ and $\{\Delta_N(\tau_\mathrm{f};\tau_\mathrm{i})^{\mu\nu}{}_{\alpha\beta}\}_N$ to be the inside of the limits in the definition:

$$\Delta_N(\tau_\mathrm{f};\tau_\mathrm{i})^\mu{}_\nu \equiv \begin{cases} g^\mu{}_\nu & (N<0), \\ \Delta(\tau_\mathrm{i})^\mu{}_\nu & (N=0), \\ g^\mu{}_{\alpha_0}\left[\prod_{k=0}^{N-1}\Delta(\tau_k)^{\alpha_k}{}_{\alpha_{k+1}}\right]\Delta(\tau_\mathrm{i})^{\alpha_N}{}_\nu & (N>0), \end{cases} \tag{C.18}$$

$$\Delta_N(\tau_\mathrm{f};\tau_\mathrm{i})^{\mu\mu'}{}_{\nu\nu'} \equiv \begin{cases} g^{\mu}{}_{\nu} g^{\mu'}{}_{\nu'} & (N<0), \\ \Delta(\tau_\mathrm{i})^{\mu\mu'}{}_{\nu\nu'} & (N=0), \\ g^{\mu}{}_{\alpha_0} g^{\mu'}{}_{\alpha_0'} \left[\prod_{k=0}^{N-1} \Delta(\tau_k)^{\alpha_k\alpha_k'}{}_{\alpha_{k+1}\alpha_{k+1}'}\right] \Delta(\tau_\mathrm{i})^{\alpha_N\alpha_N'}{}_{\nu\nu'} & (N>0). \end{cases} \tag{C.19}$$

Here, we defined the $\Delta\tau \equiv \tau_\mathrm{f} - \tau_\mathrm{i}$ and $\tau_k \equiv \tau_\mathrm{f} - \frac{\Delta\tau}{N}k$ for convenience.

The sequence terms hold the following equations for $N, N' \geq 1$:

$$\Delta_N(\tau_\mathrm{f};\tau_\mathrm{i})^{\mu}{}_{\alpha} = \Delta_N(\tau_\mathrm{f};\tau_\mathrm{i})^{\mu}{}_{\kappa}\Delta(\tau_\mathrm{i})^{\kappa}{}_{\alpha} = \Delta(\tau_\mathrm{f})^{\mu}{}_{\kappa}\Delta_N(\tau_\mathrm{f};\tau_\mathrm{i})^{\kappa}{}_{\alpha}, \tag{C.20}$$

$$\Delta_N(\tau_\mathrm{f};\tau_\mathrm{i})^{\mu\nu}{}_{\alpha\beta} = \Delta_N(\tau_\mathrm{f};\tau_\mathrm{i})^{\mu\nu}{}_{\kappa\lambda}\Delta(\tau_\mathrm{i})^{\kappa\lambda}{}_{\alpha\beta} = \Delta(\tau_\mathrm{f})^{\mu\nu}{}_{\kappa\lambda}\Delta_N(\tau_\mathrm{f};\tau_\mathrm{i})^{\kappa\lambda}{}_{\alpha\beta}, \tag{C.21}$$

$$\Delta_N(\tau_\mathrm{i};\tau_\mathrm{i})^{\mu}{}_{\alpha} = \Delta_N(\tau_\mathrm{i})^{\mu}{}_{\alpha}, \tag{C.22}$$

$$\Delta_N(\tau_\mathrm{i};\tau_\mathrm{i})^{\mu\nu}{}_{\alpha\beta} = \Delta_N(\tau_\mathrm{i})^{\mu\nu}{}_{\alpha\beta}, \tag{C.23}$$

$$\Delta_N(\tau_\mathrm{f};\tau_\mathrm{i})^{\mu}{}_{\alpha} = \Delta_N(\tau_\mathrm{i};\tau_\mathrm{f})_{\alpha}{}^{\mu}, \tag{C.24}$$

$$\Delta_N(\tau_\mathrm{f};\tau_\mathrm{i})^{\mu\nu}{}_{\alpha\beta} = \Delta_N(\tau_\mathrm{i};\tau_\mathrm{f})_{\alpha\beta}{}^{\mu\nu}. \tag{C.25}$$

Next, let us look at the derivatives of the sequence. The derivative D_f of a single projector can be written as itself contracted with some tensor from left and right:

$$\mathrm{D}_\mathrm{f}\Delta(\tau_k)^{\mu}{}_{\nu} = -(1-\tfrac{k}{N})(\Delta(\tau_k)^{\mu}{}_{\alpha}\mathrm{D}u^{\alpha}(\tau_k)u_{\nu}(\tau_k) + u^{\mu}(\tau_k)\mathrm{D}u_{\alpha}(\tau_k)\Delta(\tau_k)^{\alpha}{}_{\nu}), \tag{C.26}$$

$$\begin{aligned}\mathrm{D}_\mathrm{f}\Delta(\tau_k)^{\mu\mu'}{}_{\nu\nu'} =& -(1-\tfrac{k}{N})\Delta(\tau_k)^{\mu\mu'}{}_{\alpha\alpha'}[\mathrm{D}u^{\alpha}(\tau_k)u_{\nu}(\tau_k)g^{\alpha'}{}_{\nu'} + g^{\alpha}{}_{\nu}\mathrm{D}u^{\alpha'}(\tau_k)u_{\nu'}(\tau_k)] \\ & -(1-\tfrac{k}{N})[u^{\mu}(\tau_k)\mathrm{D}u_{\alpha}(\tau_k)g^{\mu'}{}_{\alpha'} + g^{\mu}{}_{\alpha}u^{\mu'}(\tau_k)\mathrm{D}u_{\alpha'}(\tau_k)]\Delta(\tau_k)^{\alpha\alpha'}{}_{\nu\nu'}.\end{aligned} \tag{C.27}$$

The derivatives of the sequence terms become the following:

$$\begin{aligned}&\mathrm{D}_\mathrm{f}\Delta_N(\tau_\mathrm{f};\tau_\mathrm{i})^{\mu}{}_{\nu} \\ &= -\sum_{k=0}^{N-1}(1-\tfrac{k}{N})\Delta_k(\tau_\mathrm{f};\tau_k)^{\mu}{}_{\alpha}\mathrm{D}u^{\alpha}(\tau_k)u_{\beta}(\tau_k)\Delta_{N-k-1}(\tau_{k+1};\tau_\mathrm{i})^{\beta}{}_{\nu} \\ &\quad -\sum_{k=0}^{N-1}(1-\tfrac{k}{N})\Delta_{k-1}(\tau_\mathrm{f};\tau_{k-1})^{\mu}{}_{\alpha}u^{\alpha}(\tau_k)\mathrm{D}u_{\beta}(\tau_k)\Delta_{N-k}(\tau_k;\tau_\mathrm{i})^{\beta}{}_{\nu}\end{aligned} \tag{C.28}$$

$$\begin{aligned}&= -\sum_{k=1}^{N-1}\Delta_{k-1}(\tau_\mathrm{f};\tau_{k-1})^{\mu}{}_{\alpha}[(1-\tfrac{k-1}{N})\mathrm{D}u^{\alpha}(\tau_{k-1})u_{\beta}(\tau_{k-1}) \\ &\quad +(1-\tfrac{k}{N})u^{\alpha}(\tau_k)\mathrm{D}u_{\beta}(\tau_k)]\Delta_{N-k}(\tau_k;\tau_\mathrm{i})^{\beta}{}_{\nu} \\ &\quad -\tfrac{1}{N}\Delta_{N-1}(\tau_\mathrm{f};\tau_{N-1})^{\mu}{}_{\alpha}\mathrm{D}u^{\alpha}(\tau_{N-1})u_{\beta}(\tau_{N-1})\Delta(\tau_\mathrm{i})^{\beta}{}_{\nu} \\ &\quad -u^{\mu}(\tau_\mathrm{f})\mathrm{D}u_{\alpha}(\tau_\mathrm{f})\Delta_N(\tau_\mathrm{f};\tau_\mathrm{i})^{\alpha}{}_{\nu},\end{aligned} \tag{C.29}$$

$$\begin{aligned}&\mathrm{D}_\mathrm{f}\Delta_N(\tau_\mathrm{f};\tau_\mathrm{i})^{\mu\mu'}{}_{\nu\nu'} \\ &= -\sum_{k=0}^{N-1}(1-\tfrac{k}{N})\Delta_k(\tau_\mathrm{f};\tau_k)^{\mu\mu'}{}_{\alpha\alpha'}[\mathrm{D}u^{\alpha}(\tau_k)u_{\beta}(\tau_k)g^{\alpha'}{}_{\beta'} + g^{\alpha}{}_{\beta}\mathrm{D}u^{\alpha'}(\tau_k)u_{\beta'}(\tau_k)]\Delta_{N-k-1}(\tau_{k+1};\tau_\mathrm{i})^{\beta\beta'}{}_{\nu\nu'} \\ &\quad -\sum_{k=0}^{N-1}(1-\tfrac{k}{N})\Delta_{k-1}(\tau_\mathrm{f};\tau_{k-1})^{\mu\mu'}{}_{\alpha\alpha'}[u^{\alpha}(\tau_k)\mathrm{D}u_{\beta}(\tau_k)g^{\alpha'}{}_{\beta'} + g^{\alpha}{}_{\beta}u^{\alpha'}(\tau_k)\mathrm{D}u_{\beta'}(\tau_k)]\Delta_{N-k}(\tau_k;\tau_\mathrm{i})^{\beta\beta'}{}_{\nu\nu'},\end{aligned} \tag{C.30}$$

$$\begin{aligned}&= -\sum_{k=1}^{N-1}\Delta_{k-1}(\tau_\mathrm{f};\tau_{k-1})^{\mu\mu'}{}_{\alpha\alpha'}\big((1-\tfrac{k-1}{N})[\mathrm{D}u^{\alpha}(\tau_{k-1})u_{\beta}(\tau_{k-1})g^{\alpha'}{}_{\beta'} + g^{\alpha}{}_{\beta}\mathrm{D}u^{\alpha'}(\tau_{k-1})u_{\beta'}(\tau_{k-1})] \\ &\quad +(1-\tfrac{k}{N})[u^{\alpha}(\tau_k)\mathrm{D}u_{\beta}(\tau_k)g^{\alpha'}{}_{\beta'} + g^{\alpha}{}_{\beta}u^{\alpha'}(\tau_k)\mathrm{D}u_{\beta'}(\tau_k)]\big)\Delta_{N-k}(\tau_k;\tau_\mathrm{i})^{\beta\beta'}{}_{\nu\nu'} \\ &\quad -\tfrac{1}{N}\Delta_{N-1}(\tau_\mathrm{f};\tau_{N-1})^{\mu\mu'}{}_{\alpha\alpha'}[\mathrm{D}u^{\alpha}(\tau_{N-1})u_{\beta}(\tau_{N-1})g^{\alpha'}{}_{\beta'} + g^{\alpha}{}_{\beta}\mathrm{D}u^{\alpha'}(\tau_{N-1})u_{\beta'}(\tau_{N-1})]\Delta(\tau_\mathrm{i})^{\beta\beta'}{}_{\nu\nu'} \\ &\quad -[u^{\mu}(\tau_\mathrm{f})\mathrm{D}u_{\alpha}(\tau_\mathrm{f})g^{\mu'}{}_{\alpha'} + g^{\mu}{}_{\alpha}u^{\mu'}(\tau_\mathrm{f})\mathrm{D}u_{\alpha'}(\tau_\mathrm{f})]\Delta_N(\tau_\mathrm{f};\tau_\mathrm{i})^{\alpha\alpha'}{}_{\nu\nu'}.\end{aligned} \tag{C.31}$$

To obtain (C.29) and (C.31), we shifted the index of the first summation in (C.28) and (C.30) and combined with the second summation.

From the Taylor's theorem, there exist $\xi^{(1)}_{k\beta}, \xi^{(2)}_{k\alpha} \in I(\tau_k, \tau_{k-1})$, such that

$$u_\beta(\tau_{k-1}) = u_\beta(\tau_k) + \tfrac{\Delta\tau}{N}\mathrm{D}u_\beta(\tau_k) + \tfrac{\Delta\tau^2}{2N^2}\mathrm{D}^2u_\beta(\xi^{(1)}_{k\beta}), \tag{C.32}$$

$$u^\alpha(\tau_k) = u^\alpha(\tau_{k-1}) - \tfrac{\Delta\tau}{N}\mathrm{D}u^\alpha(\tau_{k-1}) + \tfrac{\Delta\tau^2}{2N^2}\mathrm{D}^2u^\alpha(\xi^{(2)}_{k\alpha}). \tag{C.33}$$

After substituting the above equations in (C.29) and (C.31), the first terms in the above equations vanish due to the property (C.20)-(C.21). Also, the contribution from the second terms of the above equations almost cancel with each other and the order of the remaining contribution becomes $1/N^2$. Finally, we obtain the following expression for the derivatives:

$$\mathrm{D}_\mathrm{f}\Delta_N(\tau_\mathrm{f};\tau_\mathrm{i})^\mu{}_\nu = -\frac{1}{N}R_N(\tau_\mathrm{f};\tau_\mathrm{i})^\mu{}_\nu + \mathrm{D}\Delta(\tau_\mathrm{f})^\mu{}_\alpha\Delta_N(\tau_\mathrm{f};\tau_\mathrm{i})^\alpha{}_\nu, \tag{C.34}$$

$$\mathrm{D}_\mathrm{f}\Delta_N(\tau_\mathrm{f};\tau_\mathrm{i})^{\mu\mu'}{}_{\nu\nu'} = -\frac{1}{N}R_N(\tau_\mathrm{f};\tau_\mathrm{i})^{\mu\mu'}{}_{\nu\nu'} + \mathrm{D}\Delta(\tau_\mathrm{f})^{\mu\mu'}{}_{\alpha\alpha'}\Delta_N(\tau_\mathrm{f};\tau_\mathrm{i})^{\alpha\alpha'}{}_{\nu\nu'}, \tag{C.35}$$

$$\begin{aligned} R_N(\tau_\mathrm{f};\tau_\mathrm{i})^\mu{}_\nu \equiv & \tfrac{\Delta\tau}{N}\sum_{k=1}^{N-1}\Delta_{k-1}(\tau_\mathrm{f};\tau_{k-1})^\mu{}_\alpha\Big[\tfrac{\Delta\tau}{2}(1-\tfrac{k-1}{N})\mathrm{D}u^\alpha(\tau_{k-1})\mathrm{D}^2u_\beta(\xi^{(1)}_{k\beta}) \\ & + \tfrac{\Delta\tau}{2}(1-\tfrac{k}{N})\mathrm{D}^2u^\alpha(\xi^{(2)}_{k\alpha})\mathrm{D}u_\beta(\tau_k) + \mathrm{D}u^\alpha(\tau_{k-1})\mathrm{D}u_\beta(\tau_k)\Big]\Delta_{N-k}(\tau_k;\tau_\mathrm{i})^\beta{}_\nu \\ & + \tfrac{\Delta\tau}{N}\Delta_{N-1}(\tau_\mathrm{f};\tau_{N-1})^\mu{}_\alpha\mathrm{D}u^\alpha(\tau_{N-1})[\mathrm{D}u_\beta(\tau_\mathrm{i}) + \tfrac{\Delta\tau}{2N}\mathrm{D}^2u_\beta(\xi^{(1)}_{N\beta})]\Delta(\tau_\mathrm{i})^\beta{}_\nu, \end{aligned} \tag{C.36}$$

$$\begin{aligned} R_N(\tau_\mathrm{f};\tau_\mathrm{i})^{\mu\mu'}{}_{\nu\nu'} \equiv & \frac{\Delta\tau}{N}\sum_{k=1}^{N-1}\Delta_{k-1}(\tau_\mathrm{f};\tau_{k-1})^{\mu\mu'}{}_{\alpha\alpha'} \\ & \times\Big((1-\tfrac{k-1}{N})\tfrac{\Delta\tau}{2}[\mathrm{D}u^\alpha(\tau_{k-1})\mathrm{D}^2u_\beta(\xi^{(1)}_{k\beta})g^{\alpha'}{}_{\beta'} + g^\alpha{}_\beta\mathrm{D}u^{\alpha'}(\tau_{k-1})\mathrm{D}^2u_{\beta'}(\xi^{(1)}_{k\beta'})] \\ & + (1-\tfrac{k}{N})\tfrac{\Delta\tau}{2}[\mathrm{D}^2u^\alpha(\xi^{(2)}_{k\alpha})\mathrm{D}u_\beta(\tau_k)g^{\alpha'}{}_{\beta'} + g^\alpha{}_\beta\mathrm{D}^2u^{\alpha'}(\xi^{(2)}_{k\alpha'})\mathrm{D}u_{\beta'}(\tau_k)] \\ & + \mathrm{D}u^\alpha(\tau_{k-1})\mathrm{D}u_\beta(\tau_k)g^{\alpha'}{}_{\beta'} + g^\alpha{}_\beta\mathrm{D}u^{\alpha'}(\tau_{k-1})\mathrm{D}u_{\beta'}(\tau_k)\Big)\Delta_{N-k}(\tau_k;\tau_\mathrm{i})^{\beta\beta'}{}_{\nu\nu'} \\ & + \frac{\Delta\tau}{N}\Delta_{N-1}(\tau_\mathrm{f};\tau_{N-1})^{\mu\mu'}{}_{\alpha\alpha'}\Big(\mathrm{D}u^\alpha(\tau_{N-1})[\mathrm{D}u_\beta(\tau_\mathrm{i}) + \tfrac{\Delta\tau}{2N}\mathrm{D}^2u_\beta(\xi^{(1)}_{N\beta})]g^{\alpha'}{}_{\beta'} \\ & + g^\alpha{}_\beta\mathrm{D}u^{\alpha'}(\tau_{N-1})[\mathrm{D}u_{\beta'}(\tau_\mathrm{i}) + \tfrac{\Delta\tau}{2N}\mathrm{D}^2u_{\beta'}(\xi^{(1)}_{N\beta'})]\Big)\Delta(\tau_\mathrm{i})^{\beta\beta'}{}_{\nu\nu'}. \end{aligned} \tag{C.37}$$

The residue terms $R_N(\tau_\mathrm{f};\tau_\mathrm{i})^\mu{}_\nu$ and $R_N(\tau_\mathrm{f};\tau_\mathrm{i})^{\mu\mu'}{}_{\nu\nu'}$ contain N terms in the summations, but they have a factor of $1/N$ on their head. It will be shown that the terms $R_N(\tau_\mathrm{f};\tau_\mathrm{i})^\mu{}_\nu$ and $R_N(\tau_\mathrm{f};\tau_\mathrm{i})^{\mu\mu'}{}_{\nu\nu'}$ are bounded in the next subsection. Thus, the first terms of (C.34) and (C.35) vanish in the limit of $N\to\infty$, which is also treated in later subsections.

C.2.2 The boundedness of the sequences $\{\Delta_N(\tau_\mathrm{f};\tau_\mathrm{i})\}_N$ and $\{R_N(\tau_\mathrm{f};\tau_\mathrm{i})\}_N$

In this section, to show the boundedness of $\{\Delta_N(\tau_\mathrm{f};\tau_\mathrm{i})\}_N$ and $\{R_N(\tau_\mathrm{f};\tau_\mathrm{i})\}_N$, we find an upper bound of the absolute value of sequence terms which is independent from N. It should be noticed that there are many ways of finding an upper bound depending on the way of making inequalities and here we show only an instance of upper bounds.

Since $u(\tau)^\mu$ and its derivatives are bounded as (C.15), the projectors $\Delta(\tau)^\mu{}_\nu$ and $\Delta(\tau)^{\mu\mu'}{}_{\nu\nu'}$ and their derivatives are also bounded:

$$\sup_{\mu,\nu,\tau}|\Delta(\tau)^\mu{}_\nu| \le 1 + M_0^2, \tag{C.38}$$

$$\sup_{\mu,\nu,\tau}|\mathrm{D}\Delta(\tau)^\mu{}_\nu| \le 2M_0M_1, \tag{C.39}$$

$$\sup_{\mu,\nu,\tau}|\mathrm{D}^2\Delta(\tau)^\mu{}_\nu| \le 2(M_0M_2 + M_1^2), \tag{C.40}$$

$$\sup_{\mu,\mu',\nu,\nu',\tau}|\Delta(\tau)^{\mu\mu'}{}_{\nu\nu'}| \le \tfrac{4}{3}(1+M_0^2)^2, \tag{C.41}$$

$$\sup_{\mu,\mu',\nu,\nu',\tau} |\mathrm{D}\Delta(\tau)^{\mu\mu'}{}_{\nu\nu'}| \le \tfrac{16}{3} M_0 M_1 (1+M_0^2), \tag{C.42}$$

$$\sup_{\mu,\mu',\nu,\nu',\tau} |\mathrm{D}^2\Delta(\tau)^{\mu\mu'}{}_{\nu\nu'}| \le \tfrac{16}{3} [(M_0 M_2 + M_1^2)(1+M_0^2) + 2M_0^2 M_1^2]. \tag{C.43}$$

From the mean-value theorem, for any integer k, l such that $0 \le k < l \le N$, there exist $\xi^{(3)}_{k\mu\alpha}, \xi^{(3)}_{k\mu\mu'\alpha\alpha'} \in I(\tau_{k+1}, \tau_k)$ such that

$$\Delta_{l-k}(\tau_k;\tau_l)^{\mu}{}_{\nu} = \Delta(\tau_k)^{\mu}{}_{\alpha}\Delta_{l-k-1}(\tau_{k+1};\tau_l)^{\alpha}{}_{\nu} \tag{C.44}$$

$$= [\Delta(\tau_{k+1})^{\mu}{}_{\alpha} + \tfrac{\Delta\tau}{N}\mathrm{D}\Delta(\xi^{(3)}_{k\mu\alpha})^{\mu}{}_{\alpha}]\Delta_{l-k-1}(\tau_{k+1};\tau_l)^{\alpha}{}_{\nu} \tag{C.45}$$

$$= \sum_{\alpha=0}^{3} [g^{\mu}{}_{\alpha} + \tfrac{\Delta\tau}{N}\mathrm{D}\Delta(\xi^{(3)}_{k\mu\alpha})^{\mu}{}_{\alpha}]\Delta_{l-k-1}(\tau_{k+1};\tau_l)^{\alpha}{}_{\nu}, \tag{C.46}$$

$$\Delta_{l-k}(\tau_k;\tau_l)^{\mu\mu'}{}_{\nu\nu'} = \Delta(\tau_k)^{\mu\mu'}{}_{\alpha\alpha'}\Delta_{l-k-1}(\tau_{k+1};\tau_l)^{\alpha\alpha'}{}_{\nu\nu'} \tag{C.47}$$

$$= [\Delta(\tau_{k+1})^{\mu\mu'}{}_{\alpha\alpha'} + \tfrac{\Delta\tau}{N}\mathrm{D}\Delta(\xi^{(3)}_{k\mu\mu'\alpha\alpha'})^{\mu\mu'}{}_{\alpha\alpha'}]\Delta_{l-k-1}(\tau_{k+1};\tau_l)^{\alpha}{}_{\nu} \tag{C.48}$$

$$= \sum_{\alpha,\alpha'=0}^{3} [g^{\mu}{}_{\alpha} g^{\mu'}{}_{\alpha'} + \tfrac{\Delta\tau}{N}\mathrm{D}\Delta(\xi^{(3)}_{k\mu\mu'\alpha\alpha'})^{\mu\mu'}{}_{\alpha\alpha'}]\Delta_{l-k-1}(\tau_{k+1};\tau_l)^{\alpha\alpha'}{}_{\nu\nu'}, \tag{C.49}$$

$$\sup_{\mu,\nu} |\Delta_{l-k}(\tau_k;\tau_l)^{\mu}{}_{\nu}| \le (1+\tfrac{M'}{N}) \cdot \sup_{\alpha,\nu} |\Delta_{l-k-1}(\tau_{k+1};\tau_l)^{\alpha}{}_{\nu}|, \tag{C.50}$$

$$\sup_{\mu,\nu} |\Delta_{l-k}(\tau_k;\tau_l)^{\mu\mu'}{}_{\nu\nu'}| \le (1+\tfrac{M''}{N}) \cdot \sup_{\alpha,\nu} |\Delta_{l-k-1}(\tau_{k+1};\tau_l)^{\alpha\alpha'}{}_{\nu\nu'}|. \tag{C.51}$$

Here, we defined the constants, M' and M'', as $M' \equiv 8|\Delta\tau|M_0M_1$ and $M'' \equiv \frac{256}{3}|\Delta\tau|M_0M_1(1+M_0^2)$. By recursively applying the above inequalities, the following equations are obtained:

$$\sup_{\mu,\nu} |\Delta_{l-k}(\tau_k;\tau_l)^{\mu}{}_{\nu}| \le \cdots \le (1+\tfrac{M'}{N})^{l-k} \cdot \sup_{\alpha,\nu} |\Delta(\tau_l)^{\alpha}{}_{\nu}| \tag{C.52}$$

$$\le e^{M'(l-k)/N}(1+M_0^2) \le e^{M'}(1+M_0^2), \tag{C.53}$$

$$\sup_{\mu,\nu} |\Delta_{l-k}(\tau_k;\tau_l)^{\mu\mu'}{}_{\nu\nu'}| \le \cdots \le (1+\tfrac{M''}{N})^{l-k} \cdot \sup_{\alpha,\nu} |\Delta(\tau_l)^{\alpha\alpha'}{}_{\nu\nu'}| \tag{C.54}$$

$$\le e^{M''(l-k)/N}\tfrac{4}{3}(1+M_0^2)^2 \le e^{M''}\tfrac{4}{3}(1+M_0^2)^2. \tag{C.55}$$

Therefore, each term of the sequence, $\Delta_N(\tau_\mathrm{f};\tau_\mathrm{i})^{\mu}{}_{\nu}$ and $\Delta_N(\tau_\mathrm{f};\tau_\mathrm{i})^{\mu\mu'}{}_{\nu\nu'}$, is bounded.

Using (C.53) and (C.55), it can also be shown that $R_N(\tau_\mathrm{f};\tau_\mathrm{i})^{\mu}{}_{\nu}$ and $R_N(\tau_\mathrm{f};\tau_\mathrm{i})^{\mu\mu'}{}_{\nu\nu'}$ are bounded: for $N \ge 1$,

$$\begin{aligned}|R_N(\tau_\mathrm{f};\tau_\mathrm{i})^{\mu}{}_{\nu}| \le \sum_{\alpha,\beta=0}^{3} \Bigg[&\tfrac{|\Delta\tau|}{N} \sum_{k=1}^{N-1} |\Delta_{k-1}(\tau_\mathrm{f};\tau_{k-1})^{\mu}{}_{\alpha}| \Big[\tfrac{|\Delta\tau|}{2}|1-\tfrac{k-1}{N}| \cdot |\mathrm{D}u^{\alpha}(\tau_{k-1})| \cdot |\mathrm{D}^2 u_{\beta}(\xi^{(1)}_k)| \\ &+ \tfrac{|\Delta\tau|}{2}|1-\tfrac{k}{N}| \cdot |\mathrm{D}^2 u^{\alpha}(\xi^{(2)}_k)| \cdot |\mathrm{D}u_{\beta}(\tau_k)| + |\mathrm{D}u^{\alpha}(\tau_{k-1})| \cdot |\mathrm{D}u_{\beta}(\tau_k)| \Big] |\Delta_{N-k}(\tau_k;\tau_\mathrm{i})^{\beta}{}_{\nu}| \\ &+ \tfrac{|\Delta\tau|}{N}|\Delta_{N-1}(\tau_\mathrm{f};\tau_{N-1})^{\mu}{}_{\alpha}| \cdot |\mathrm{D}u^{\alpha}(\tau_{N-1})| \cdot \Big[|\mathrm{D}u_{\beta}(\tau_\mathrm{i})| + \tfrac{|\Delta\tau|}{2N}|\mathrm{D}^2 u_{\beta}(\xi^{(1)}_N)| \Big] \cdot |\Delta(\tau_\mathrm{i})^{\beta}{}_{\nu}| \Bigg]\end{aligned} \tag{C.56}$$

$$\begin{aligned}\le 16 \Big[&\tfrac{|\Delta\tau|}{N} \sum_{k=1}^{N-1} (1+M_0^2) e^{M'(k-1)/N} \big[\tfrac{|\Delta\tau|}{2} M_1 M_2 + \tfrac{|\Delta\tau|}{2} M_2 M_1 + M_1^2 \big] (1+M_0^2) e^{M'(N-k)/N} \\ &+ \tfrac{|\Delta\tau|}{N}(1+M_0^2) e^{M'(N-1)/N} M_1 [M_1 + \tfrac{|\Delta\tau|}{2N} M_2](1+M_0^2) \Big]\end{aligned} \tag{C.57}$$

$$\le 16|\Delta\tau|(1+M_0^2)^2 e^{M'(N-1)/N}[|\Delta\tau|M_1M_2 + M_1^2] =: M_R(\Delta\tau), \tag{C.58}$$

$$
\begin{aligned}
|R_N(\tau_{\rm f};\tau_{\rm i})^{\mu\mu'}{}_{\nu\nu'}| \le\ & \frac{|\Delta\tau|}{N}\sum_{k=1}^{N-1} 64\cdot\tfrac{4}{3}(1+M_0^2)^2 e^{M''(k-1)/N} && \text{(C.59)}\\
& \times\Big(\tfrac{|\Delta\tau|}{2}\cdot 4M_1M_2+2M_1^2\Big)\tfrac{4}{3}(1+M_0^2)^2e^{M''(N-k)/N}\\
& +\frac{|\Delta\tau|}{N}64\cdot\tfrac{4}{3}(1+M_0^2)^2e^{M''(N-1)/N}\cdot 2M_1[M_1+\tfrac{|\Delta\tau|}{2N}M_2]\tfrac{4}{3}(1+M_0^2)^2\\
\le\ & \frac{|\Delta\tau|}{N}\sum_{k=1}^{N-1}\tfrac{2048}{9}(1+M_0^2)^4e^{M''}(M_1^2+|\Delta\tau|M_1M_2) && \text{(C.60)}\\
& +\frac{|\Delta\tau|}{N}\cdot\tfrac{2048}{9}(1+M_0^2)^4e^{M''}(M_1^2+|\Delta\tau|M_1M_2)\\
\le\ & |\Delta\tau|\cdot\tfrac{2048}{9}(1+M_0^2)^4e^{M''}(M_1^2+|\Delta\tau|M_1M_2)=:M_R'(\Delta\tau). && \text{(C.61)}
\end{aligned}
$$

C.2.3 The convergence of $\{\Delta_N(\tau_{\rm f};\tau_{\rm i})^{\mu}{}_{\nu}\}_N$ and $\{\Delta_N(\tau_{\rm f};\tau_{\rm i})^{\mu\mu'}{}_{\nu\nu'}\}_N$

First, we consider the difference $|\Delta_N(\tau_{\rm f};\tau_{\rm i})^{\mu}{}_{\nu}-\Delta_{N-1}(\tau_{\rm f};\tau_{\rm i})^{\mu}{}_{\nu}|$ and $|\Delta_N(\tau_{\rm f};\tau_{\rm i})^{\mu\mu'}{}_{\nu\nu'}-\Delta_{N-1}(\tau_{\rm f};\tau_{\rm i})^{\mu\mu'}{}_{\nu\nu'}|$ for $N\ge 2$.

$$
\begin{aligned}
&\Delta_N(\tau_{\rm f};\tau_{\rm i})^{\mu}{}_{\nu}-\Delta_{N-1}(\tau_{\rm f};\tau_{\rm i})^{\mu}{}_{\nu}\\
&=[\Delta_N(\tau_{\rm f};\tau_{\rm i})^{\mu}{}_{\nu}-\Delta_{N-1}(\tau_1;\tau_{\rm i})^{\mu}{}_{\nu}]-[\Delta_{N-1}(\tau_{\rm f};\tau_{\rm i})^{\mu}{}_{\nu}-\Delta_{N-1}(\tau_1;\tau_{\rm i})^{\mu}{}_{\nu}] && \text{(C.62)}\\
&=[\tfrac{\Delta\tau}{N}{\rm D}\Delta(\tau_1)^{\mu}{}_{\alpha}+\tfrac{\Delta\tau^2}{2N^2}{\rm D}^2\Delta(\xi^{(4)}_{0\mu\alpha})^{\mu}{}_{\alpha}]\Delta_{N-1}(\tau_1;\tau_{\rm i})^{\alpha}{}_{\nu} && \text{(C.63)}\\
&\quad-\tfrac{\Delta\tau}{N}{\rm D}\Delta(\xi^{(5)}_{\mu\nu})^{\mu}{}_{\alpha}\Delta_N(\xi^{(5)}_{\mu\nu};\tau_{\rm i})^{\alpha}{}_{\nu}+\tfrac{\Delta\tau}{N(N-1)}R_{N-1}(\xi^{(5)}_{\mu\nu};\tau_{\rm i})^{\mu}{}_{\nu}\\
&=\tfrac{\Delta\tau^2}{2N^2}{\rm D}^2\Delta(\xi^{(4)}_{0\mu\alpha})^{\mu}{}_{\alpha}\Delta_{N-1}(\tau_1;\tau_{\rm i})^{\alpha}{}_{\nu}\\
&\quad-\tfrac{\Delta\tau(\xi^{(5)}_{\mu\nu}-\tau_1)}{N}{\rm D}[{\rm D}\Delta(\tau)^{\mu}{}_{\alpha}\Delta_{N-1}(\tau;\tau_{\rm i})^{\alpha}{}_{\nu}]|_{\tau=\xi^{(6)}_{\mu\nu}}+\tfrac{\Delta\tau}{N(N-1)}R_{N-1}(\xi^{(5)}_{\mu\nu};\tau_{\rm i})^{\mu}{}_{\nu}, && \text{(C.64)}\\
&\Delta_N(\tau_{\rm f};\tau_{\rm i})^{\mu\mu'}{}_{\nu\nu'}-\Delta_{N-1}(\tau_{\rm f};\tau_{\rm i})^{\mu\mu'}{}_{\nu\nu'}\\
&=[\Delta_N(\tau_{\rm f};\tau_{\rm i})^{\mu\mu'}{}_{\nu\nu'}-\Delta_{N-1}(\tau_1;\tau_{\rm i})^{\mu\mu'}{}_{\nu\nu'}]-[\Delta_{N-1}(\tau_{\rm f};\tau_{\rm i})^{\mu\mu'}{}_{\nu\nu'}-\Delta_{N-1}(\tau_1;\tau_{\rm i})^{\mu\mu'}{}_{\nu\nu'}] && \text{(C.65)}\\
&=[\tfrac{\Delta\tau}{N}{\rm D}\Delta(\tau_1)^{\mu\mu'}{}_{\alpha\alpha'}+\tfrac{\Delta\tau^2}{2N^2}{\rm D}^2\Delta(\xi^{(4)}_{0\mu\mu'\alpha\alpha'})^{\mu\mu'}{}_{\alpha\alpha'}]\Delta_{N-1}(\tau_1;\tau_{\rm i})^{\alpha\alpha'}{}_{\nu\nu'} && \text{(C.66)}\\
&\quad-\tfrac{\Delta\tau}{N}{\rm D}\Delta(\xi^{(5)}_{\mu\mu'\nu\nu'})^{\mu\mu'}{}_{\alpha\alpha'}\Delta_N(\xi^{(5)}_{\mu\mu'\nu\nu'};\tau_{\rm i})^{\alpha\alpha'}{}_{\nu\nu'}+\tfrac{\Delta\tau}{N(N-1)}R_{N-1}(\xi^{(5)}_{\mu\mu'\nu\nu'};\tau_{\rm i})^{\mu\mu'}{}_{\nu\nu'}\\
&=\tfrac{\Delta\tau^2}{2N^2}{\rm D}^2\Delta(\xi^{(4)}_{0\mu\mu'\alpha\alpha'})^{\mu\mu'}{}_{\alpha\alpha'}\Delta_{N-1}(\tau_1;\tau_{\rm i})^{\alpha\alpha'}{}_{\nu\nu'} && \text{(C.67)}\\
&\quad-\tfrac{\Delta\tau(\xi^{(5)}_{\mu\mu'\nu\nu'}-\tau_1)}{N}{\rm D}[{\rm D}\Delta(\tau)^{\mu\mu'}{}_{\alpha\alpha'}\Delta_{N-1}(\tau;\tau_{\rm i})^{\alpha\alpha'}{}_{\nu\nu'}]|_{\tau=\xi^{(6)}_{\mu\mu'\nu\nu'}}+\tfrac{\Delta\tau}{N(N-1)}R_{N-1}(\xi^{(5)}_{\mu\nu};\tau_{\rm i})^{\mu\mu'}{}_{\nu\nu'}.
\end{aligned}
$$

Here, we used the Taylor's theorem and the mean-value theorem: there exist $\xi^{(4)}_{0\mu\nu}$, $\xi^{(4)}_{0\mu\mu'\nu\nu'}$, $\xi^{(5)}_{\mu\nu}$, $\xi^{(5)}_{\mu\mu'\nu\nu'}\in I(\tau_1,\tau_{\rm f})$, $\xi^{(6)}_{\mu\nu}\in I(\tau_1,\xi^{(5)}_{\mu\nu})$, and $\xi^{(6)}_{\mu\mu'\nu\nu'}\in I(\tau_1,\xi^{(5)}_{\mu\mu'\nu\nu'})$ such that

$$
\begin{aligned}
\Delta(\tau_{\rm f})^{\mu}{}_{\nu}&=\Delta(\tau_1)^{\mu}{}_{\nu}+\tfrac{\Delta\tau}{N}{\rm D}\Delta(\tau_1)^{\mu}{}_{\nu}+\tfrac{\Delta\tau^2}{2N^2}{\rm D}^2\Delta(\xi^{(4)}_{0\mu\nu})^{\mu}{}_{\nu}, && \text{(C.68)}\\
\Delta(\tau_{\rm f})^{\mu\mu'}{}_{\nu\nu'}&=\Delta(\tau_1)^{\mu\mu'}{}_{\nu\nu'}+\tfrac{\Delta\tau}{N}{\rm D}\Delta(\tau_1)^{\mu\mu'}{}_{\nu\nu'}+\tfrac{\Delta\tau^2}{2N^2}{\rm D}^2\Delta(\xi^{(4)}_{0\mu\mu'\nu\nu'})^{\mu\mu'}{}_{\nu\nu'}, && \text{(C.69)}\\
\Delta_{N-1}(\tau_{\rm f};\tau_{\rm i})^{\mu}{}_{\nu}&=\Delta_{N-1}(\tau_1;\tau_{\rm i})^{\mu}{}_{\nu}+\tfrac{\Delta\tau}{N}{\rm D}_{\rm f}\Delta_{N-1}(\xi^{(5)}_{\mu\nu};\tau_{\rm i})^{\mu}{}_{\nu}, && \text{(C.70)}\\
\Delta_{N-1}(\tau_{\rm f};\tau_{\rm i})^{\mu\mu'}{}_{\nu\nu'}&=\Delta_{N-1}(\tau_1;\tau_{\rm i})^{\mu\mu'}{}_{\nu\nu'}+\tfrac{\Delta\tau}{N}{\rm D}_{\rm f}\Delta_{N-1}(\xi^{(5)}_{\mu\nu};\tau_{\rm i})^{\mu\mu'}{}_{\nu\nu'}, && \text{(C.71)}\\
{\rm D}\Delta(\xi^{(5)}_{\mu\nu})^{\mu}{}_{\alpha}\Delta_{N-1}(\xi^{(5)}_{\mu\nu};\tau_{\rm i})^{\alpha}{}_{\nu}&={\rm D}\Delta(\tau_1)^{\mu}{}_{\alpha}\Delta_{N-1}(\tau_1;\tau_{\rm i})^{\alpha}{}_{\nu} && \text{(C.72)}\\
&\quad+(\xi^{(5)}_{\mu\nu}-\tau_1){\rm D}[{\rm D}\Delta(\tau)^{\mu}{}_{\alpha}\Delta_{N-1}(\tau;\tau_{\rm i})^{\alpha}{}_{\nu}]|_{\tau=\xi^{(6)}_{\mu\nu}},\\
{\rm D}\Delta(\xi^{(5)}_{\mu\mu'\nu\nu'})^{\mu\mu'}{}_{\alpha\alpha'}\Delta_{N-1}(\xi^{(5)}_{\mu\mu'\nu\nu'};\tau_{\rm i})^{\alpha\alpha'}{}_{\nu\nu'}&={\rm D}\Delta(\tau_1)^{\mu\mu'}{}_{\alpha\alpha'}\Delta_{N-1}(\tau_1;\tau_{\rm i})^{\alpha\alpha'}{}_{\nu\nu'}\\
&\quad+(\xi^{(5)}_{\mu\mu'\nu\nu'}-\tau_1){\rm D}[{\rm D}\Delta(\tau)^{\mu\mu'}{}_{\alpha\alpha'}\Delta_{N-1}(\tau;\tau_{\rm i})^{\alpha\alpha'}{}_{\nu\nu'}]|_{\tau=\xi^{(6)}_{\mu\mu'\nu\nu'}}. && \text{(C.73)}
\end{aligned}
$$

Then, we find upper bounds of the differences:

$$
\begin{aligned}
&|\mathrm{D}[\mathrm{D}\Delta(\tau)^{\mu}{}_{\alpha}\Delta_{N-1}(\tau;\tau_{\mathrm{i}})^{\alpha}{}_{\nu}]| \\
&= \left|\left[\mathrm{D}^2\Delta(\tau)^{\mu}{}_{\beta} + \mathrm{D}\Delta(\tau)^{\mu}{}_{\alpha}\mathrm{D}\Delta(\tau)^{\alpha}{}_{\beta}\right]\Delta_{N-1}(\tau;\tau_{\mathrm{i}})^{\beta}{}_{\nu} - \tfrac{1}{N-1}\mathrm{D}\Delta(\tau)^{\mu}{}_{\alpha}R_{N-1}(\tau;\tau_{\mathrm{i}})^{\alpha}{}_{\nu}\right| && \text{(C.74)} \\
&\leq [2(M_0M_2+M_1^2)+(2M_0M_1)\cdot 4\cdot(2M_0M_1)]\cdot 4\cdot(1+M_0^2)e^{M'} + \tfrac{1}{N-1}2M_0M_1\cdot 4\cdot M_R(\tau-\tau_{\mathrm{i}}) && \text{(C.75)} \\
&\leq 8[M_0M_2+M_1^2+8M_0^2M_1^2](1+M_0^2)e^{M'} + 8M_0M_1M_R(\Delta\tau) =: M^{(1)}(\Delta\tau). && \text{(C.76)} \\
&|\Delta_N(\tau_{\mathrm{f}};\tau_{\mathrm{i}})^{\mu}{}_{\nu} - \Delta_{N-1}(\tau_{\mathrm{f}};\tau_{\mathrm{i}})^{\mu}{}_{\nu}| \\
&\leq \tfrac{|\Delta\tau|^2}{2N^2}\cdot 2(M_0M_2+M_1^2)\cdot 4\cdot(1+M_0^2)e^{M'} + \tfrac{|\Delta\tau(\xi^{(5)}_{\mu\nu}-\tau_1)|}{N}M^{(1)}(\Delta\tau) + \tfrac{|\Delta\tau|}{N(N-1)}M_R(\xi^{(5)}_{\mu\nu}-\tau_{\mathrm{i}}) && \text{(C.77)} \\
&\leq \tfrac{|\Delta\tau|^2}{2N^2}\cdot 2(M_0M_2+M_1^2)\cdot 4\cdot(1+M_0^2)e^{M'} + \tfrac{|\Delta\tau|^2}{N^2}M^{(1)}(\Delta\tau) + \tfrac{|\Delta\tau|}{N(N-1)}M_R(\Delta\tau) && \text{(C.78)} \\
&\leq \tfrac{1}{N(N-1)}[\tfrac{|\Delta\tau|^2}{2}\cdot 2(M_0M_2+M_1^2)\cdot 4\cdot(1+M_0^2)e^{M'} + |\Delta\tau|^2M^{(1)}(\Delta\tau) + |\Delta\tau|M_R(\Delta\tau)] && \text{(C.79)} \\
&=: \tfrac{1}{N(N-1)}M^{(2)}(\Delta\tau). && \text{(C.80)} \\
&|\mathrm{D}[\mathrm{D}\Delta(\tau)^{\mu\mu'}{}_{\alpha\alpha'}\Delta_{N-1}(\tau;\tau_{\mathrm{i}})^{\alpha\alpha'}{}_{\nu\nu'}]| \\
&= \left|\left[\mathrm{D}^2\Delta(\tau)^{\mu\mu'}{}_{\beta\beta'} + \mathrm{D}\Delta(\tau)^{\mu\mu'}{}_{\alpha\alpha'}\mathrm{D}\Delta(\tau)^{\alpha\alpha'}{}_{\beta\beta'}\right]\Delta_{N-1}(\tau;\tau_{\mathrm{i}})^{\beta\beta'}{}_{\nu\nu'} - \tfrac{1}{N-1}\mathrm{D}\Delta(\tau)^{\mu\mu'}{}_{\alpha\alpha'}R_{N-1}(\tau;\tau_{\mathrm{i}})^{\alpha\alpha'}{}_{\nu\nu'}\right| && \text{(C.81)} \\
&\leq \left[\tfrac{16}{3}[(M_0M_2+M_1^2)(1+M_0^2)+2M_0^2M_1^2]+16[\tfrac{16}{3}M_0M_1(1+M_0^2)]^2\right]\cdot 16\cdot\tfrac{4}{3}(1+M_0^2)^2e^{M''} \\
&+ 16\tfrac{16}{3(N-1)}M_0M_1(1+M_0^2)M_R'(\tau-\tau_{\mathrm{i}}) && \text{(C.82)} \\
&\leq \tfrac{1024}{9}(1+M_0^2)^2\left[(M_0M_2+M_1^2)(1+M_0^2)+2M_0^2M_1^2+\tfrac{256}{3}M_0^2M_1^2(1+M_0^2)^2\right]e^{M''} \\
&+ \tfrac{256}{3}M_0M_1(1+M_0^2)M_R'(\Delta\tau) =: M'^{(1)}(\Delta\tau). && \text{(C.83)} \\
&|\Delta_N(\tau_{\mathrm{f}};\tau_{\mathrm{i}})^{\mu\mu'}{}_{\nu\nu'} - \Delta_{N-1}(\tau_{\mathrm{f}};\tau_{\mathrm{i}})^{\mu\mu'}{}_{\nu\nu'}| \\
&\leq \tfrac{|\Delta\tau|^2}{2N^2}\cdot\tfrac{16}{3}[(M_0M_2+M_1^2)(1+M_0^2)+2M_0^2M_1^2]\cdot 16\cdot\tfrac{4}{3}(1+M_0^2)^2e^{M''} \\
&+ \tfrac{|\Delta\tau(\xi^{(5)}_{\mu\mu'\nu\nu'}-\tau_1)|}{N}M'^{(1)}(\Delta\tau) + \tfrac{|\Delta\tau|}{N(N-1)}M_R'(\xi^{(5)}_{\mu\mu'\nu\nu'}-\tau_{\mathrm{i}}) && \text{(C.84)} \\
&\leq \tfrac{1}{N(N-1)}\left[\tfrac{512|\Delta\tau|^2}{9}[(M_0M_2+M_1^2)(1+M_0^2)+2M_0^2M_1^2](1+M_0^2)^2e^{M''}\right. \\
&\left.+|\Delta\tau|^2M'^{(1)}(\Delta\tau) + |\Delta\tau|M_R'(\xi^{(5)}_{\mu\mu'\nu\nu'}-\tau_{\mathrm{i}})\right] && \text{(C.85)} \\
&=: \tfrac{1}{N(N-1)}M'^{(2)}(\Delta\tau). && \text{(C.86)}
\end{aligned}
$$

For integers N_1, N_2 such that $N_2 > N_1 \geq 1$,

$$
\begin{aligned}
0 &\leq |\Delta_{N_2}(\tau_{\mathrm{f}};\tau_{\mathrm{i}})^{\mu}{}_{\nu} - \Delta_{N_1}(\tau_{\mathrm{f}};\tau_{\mathrm{i}})^{\mu}{}_{\nu}| && \text{(C.87)} \\
&\leq \sum_{N=N_1+1}^{N_2}|\Delta_N(\tau_{\mathrm{f}};\tau_{\mathrm{i}})^{\mu}{}_{\nu} - \Delta_{N-1}(\tau_{\mathrm{f}};\tau_{\mathrm{i}})^{\mu}{}_{\nu}| && \text{(C.88)} \\
&\leq \sum_{N=N_1+1}^{N_2}\frac{1}{N(N-1)}M^{(2)}(\Delta\tau) = \left(\frac{1}{N_1}-\frac{1}{N_2}\right)M^{(2)}(\Delta\tau), && \text{(C.89)} \\
0 &\leq |\Delta_{N_2}(\tau_{\mathrm{f}};\tau_{\mathrm{i}})^{\mu\mu'}{}_{\nu\nu'} - \Delta_{N_1}(\tau_{\mathrm{f}};\tau_{\mathrm{i}})^{\mu\mu'}{}_{\nu\nu'}| \\
&\leq \sum_{N=N_1+1}^{N_2}|\Delta_N(\tau_{\mathrm{f}};\tau_{\mathrm{i}})^{\mu\mu'}{}_{\nu\nu'} - \Delta_{N-1}(\tau_{\mathrm{f}};\tau_{\mathrm{i}})^{\mu\mu'}{}_{\nu\nu'}| && \text{(C.90)} \\
&\leq \sum_{N=N_1+1}^{N_2}\frac{1}{N(N-1)}M'^{(2)}(\Delta\tau) = \left(\frac{1}{N_1}-\frac{1}{N_2}\right)M'^{(2)}(\Delta\tau). && \text{(C.91)}
\end{aligned}
$$

Therefore the sequences are Cauchy sequences and they are pointwise convergent:

$$
\lim_{\substack{N_2\to\infty\\N_1\to\infty}}|\Delta_{N_2}(\tau_{\mathrm{f}};\tau_{\mathrm{i}})^{\mu}{}_{\nu} - \Delta_{N_1}(\tau_{\mathrm{f}};\tau_{\mathrm{i}})^{\mu}{}_{\nu}| = 0, \qquad \text{(C.92)}
$$

$$\lim_{\substack{N_2\to\infty\\N_1\to\infty}} |\Delta_{N_2}(\tau_\mathrm{f};\tau_\mathrm{i})^{\mu\mu'}{}_{\nu\nu'} - \Delta_{N_1}(\tau_\mathrm{f};\tau_\mathrm{i})^{\mu\mu'}{}_{\nu\nu'}| = 0. \tag{C.93}$$

Here, we can define a pathline projector as the limit value of the sequence:

$$\Delta(\tau_\mathrm{f};\tau_\mathrm{i})^{\mu}{}_{\nu} \equiv \lim_{N\to\infty} \Delta_N(\tau_\mathrm{f};\tau_\mathrm{i})^{\mu}{}_{\nu}, \tag{C.94}$$

$$\Delta(\tau_\mathrm{f};\tau_\mathrm{i})^{\mu\mu'}{}_{\nu\nu'} \equiv \lim_{N\to\infty} \Delta_N(\tau_\mathrm{f};\tau_\mathrm{i})^{\mu\mu'}{}_{\nu\nu'}. \tag{C.95}$$

Then, it follows that

$$|\Delta(\tau_\mathrm{f};\tau_\mathrm{i})^{\mu}{}_{\nu} - \Delta_{N_1}(\tau_\mathrm{f};\tau_\mathrm{i})^{\mu}{}_{\nu}| \leq \frac{M^{(2)}(\Delta\tau)}{N_1}, \tag{C.96}$$

$$|\Delta(\tau_\mathrm{f};\tau_\mathrm{i})^{\mu\mu'}{}_{\nu\nu'} - \Delta_{N_1}(\tau_\mathrm{f};\tau_\mathrm{i})^{\mu\mu'}{}_{\nu\nu'}| \leq \frac{M'^{(2)}(\Delta\tau)}{N_1}. \tag{C.97}$$

By taking the limit $N\to\infty$ for (C.20)-(C.25), we obtain (4.25)-(4.30) which were to be proved.

It can even be shown that the sequences are compactly convergent. For any compact closed interval $[\tau_\mathrm{A},\tau_\mathrm{B}]$, and for any $\tau_\mathrm{f},\tau_\mathrm{i}\in[\tau_\mathrm{A},\tau_\mathrm{B}]$,

$$0 \leq |\Delta_N(\tau_\mathrm{f};\tau_\mathrm{i})^{\mu}{}_{\nu} - \Delta(\tau_\mathrm{f};\tau_\mathrm{i})^{\mu}{}_{\nu}| \leq \frac{M^{(2)}(\Delta\tau)}{N} \leq \frac{M^{(2)}(|\tau_\mathrm{B}-\tau_\mathrm{A}|)}{N}, \tag{C.98}$$

$$0 \leq |\Delta_N(\tau_\mathrm{f};\tau_\mathrm{i})^{\mu\mu'}{}_{\nu\nu'} - \Delta(\tau_\mathrm{f};\tau_\mathrm{i})^{\mu\mu'}{}_{\nu\nu'}| \leq \frac{M'^{(2)}(\Delta\tau)}{N} \leq \frac{M'^{(2)}(|\tau_\mathrm{B}-\tau_\mathrm{A}|)}{N}. \tag{C.99}$$

Therefore the sequences are uniformly convergent in the interval $[\tau_\mathrm{A},\tau_\mathrm{B}]$:

$$\lim_{N\to\infty} \sup_{\tau_\mathrm{f},\tau_\mathrm{i}\in[\tau_\mathrm{A},\tau_\mathrm{B}]} |\Delta_N(\tau_\mathrm{f};\tau_\mathrm{i})^{\mu}{}_{\nu} - \Delta(\tau_\mathrm{f};\tau_\mathrm{i})^{\mu}{}_{\nu}| = 0, \tag{C.100}$$

$$\lim_{N\to\infty} \sup_{\tau_\mathrm{f},\tau_\mathrm{i}\in[\tau_\mathrm{A},\tau_\mathrm{B}]} |\Delta_N(\tau_\mathrm{f};\tau_\mathrm{i})^{\mu\mu'}{}_{\nu\nu'} - \Delta(\tau_\mathrm{f};\tau_\mathrm{i})^{\mu\mu'}{}_{\nu\nu'}| = 0. \tag{C.101}$$

C.2.4 The compact convergence of $\{\mathrm{D_f}\Delta_N(\tau_\mathrm{f};\tau_\mathrm{i})^{\mu}{}_{\nu}\}_N$ and $\{\mathrm{D_f}\Delta_N(\tau_\mathrm{f};\tau_\mathrm{i})^{\mu\mu'}{}_{\nu\nu'}\}_N$

For any compact closed interval $[\tau_\mathrm{A},\tau_\mathrm{B}]$, and for any $\tau_\mathrm{f},\tau_\mathrm{i}\in[\tau_\mathrm{A},\tau_\mathrm{B}]$,

$$0 \leq |\mathrm{D_f}\Delta_N(\tau_\mathrm{f};\tau_\mathrm{i})^{\mu}{}_{\nu} - \mathrm{D}\Delta(\tau_\mathrm{f})^{\mu}{}_{\alpha}\Delta(\tau_\mathrm{f};\tau_\mathrm{i})^{\alpha}{}_{\nu}| \tag{C.102}$$

$$\leq \frac{1}{N}|R_N(\tau_\mathrm{f};\tau_\mathrm{i})^{\mu}{}_{\nu}| + |\mathrm{D}\Delta(\tau_\mathrm{f})^{\mu}{}_{\alpha}| \cdot |\Delta_N(\tau_\mathrm{f};\tau_\mathrm{i})^{\alpha}{}_{\nu} - \Delta(\tau_\mathrm{f};\tau_\mathrm{i})^{\alpha}{}_{\nu}| \tag{C.103}$$

$$\leq \frac{1}{N}[M_R(\Delta\tau) + 8M_0M_1M^{(2)}(\Delta\tau)] \tag{C.104}$$

$$\leq \frac{1}{N}[M_R(\tau_\mathrm{B}-\tau_\mathrm{A}) + 8M_0M_1M^{(2)}(\tau_\mathrm{B}-\tau_\mathrm{A})] =: \frac{1}{N}M^{(3)}(\tau_\mathrm{B}-\tau_\mathrm{A}), \tag{C.105}$$

$$0 \leq |\mathrm{D_f}\Delta_N(\tau_\mathrm{f};\tau_\mathrm{i})^{\mu\mu'}{}_{\nu\nu'} - \mathrm{D}\Delta(\tau_\mathrm{f})^{\mu\mu'}{}_{\alpha\alpha'}\Delta(\tau_\mathrm{f};\tau_\mathrm{i})^{\alpha\alpha'}{}_{\nu\nu'}| \tag{C.106}$$

$$\leq \frac{1}{N}|R_N(\tau_\mathrm{f};\tau_\mathrm{i})^{\mu\mu'}{}_{\nu\nu'}| + |\mathrm{D}\Delta(\tau_\mathrm{f})^{\mu\mu'}{}_{\alpha\alpha'}| \cdot |\Delta_N(\tau_\mathrm{f};\tau_\mathrm{i})^{\alpha\alpha'}{}_{\nu\nu'} - \Delta(\tau_\mathrm{f};\tau_\mathrm{i})^{\alpha\alpha'}{}_{\nu\nu'}| \tag{C.107}$$

$$\leq \frac{1}{N}[M_R(\Delta\tau) + \tfrac{256}{3}M_0M_1(1+M_0^2)M^{(2)}(\Delta\tau)] \tag{C.108}$$

$$\leq \frac{1}{N}[M_R(\tau_\mathrm{B}-\tau_\mathrm{A}) + \tfrac{256}{3}M_0M_1(1+M_0^2)M^{(2)}(\tau_\mathrm{B}-\tau_\mathrm{A})] \tag{C.109}$$

$$=: \frac{1}{N}M'^{(3)}(\tau_\mathrm{B}-\tau_\mathrm{A}), \tag{C.110}$$

Therefore the derivatives of the sequences are also uniformly convergent in the interval:

$$\lim_{N\to\infty} \sup_{\tau_\mathrm{f},\tau_\mathrm{i}\in I} |\mathrm{D_f}\Delta_N(\tau_\mathrm{f};\tau_\mathrm{i})^{\mu}{}_{\nu} - \mathrm{D}\Delta(\tau_\mathrm{f})^{\mu}{}_{\alpha}\Delta(\tau_\mathrm{f};\tau_\mathrm{i})^{\alpha}{}_{\nu}| = 0, \tag{C.111}$$

$$\lim_{N\to\infty} \sup_{\tau_\mathrm{f},\tau_\mathrm{i}\in I} |\mathrm{D_f}\Delta_N(\tau_\mathrm{f};\tau_\mathrm{i})^{\mu\mu'}{}_{\nu\nu'} - \mathrm{D}\Delta(\tau_\mathrm{f})^{\mu\mu'}{}_{\alpha\alpha'}\Delta(\tau_\mathrm{f};\tau_\mathrm{i})^{\alpha\alpha'}{}_{\nu\nu'}| = 0. \tag{C.112}$$

That is, the derivatives $\{\mathrm{D_f}\Delta_N(\tau_\mathrm{f};\tau_\mathrm{i})^\mu{}_\nu\}_N$ and $\{\mathrm{D_f}\Delta_N(\tau_\mathrm{f};\tau_\mathrm{i})^{\mu\mu'}{}_{\nu\nu'}\}_N$ are compactly convergent, and it means that the limit and the derivative commute:

$$\mathrm{D_f}\Delta(\tau_\mathrm{f};\tau_\mathrm{i})^\mu{}_\nu = \mathrm{D_f}\lim_{N\to\infty}\Delta_N(\tau_\mathrm{f};\tau_\mathrm{i})^\mu{}_\nu \tag{C.113}$$

$$= \lim_{N\to\infty}\mathrm{D_f}\Delta_N(\tau_\mathrm{f};\tau_\mathrm{i})^\mu{}_\nu \tag{C.114}$$

$$= \mathrm{D}\Delta(\tau_\mathrm{f})^\mu{}_\alpha\Delta(\tau_\mathrm{f};\tau_\mathrm{i})^\alpha{}_\nu, \tag{C.115}$$

$$\mathrm{D_f}\Delta(\tau_\mathrm{f};\tau_\mathrm{i})^{\mu\mu'}{}_{\nu\nu'} = \mathrm{D_f}\lim_{N\to\infty}\Delta_N(\tau_\mathrm{f};\tau_\mathrm{i})^{\mu\mu'}{}_{\nu\nu'} \tag{C.116}$$

$$= \lim_{N\to\infty}\mathrm{D_f}\Delta_N(\tau_\mathrm{f};\tau_\mathrm{i})^{\mu\mu'}{}_{\nu\nu'} \tag{C.117}$$

$$= \mathrm{D}\Delta(\tau_\mathrm{f})^{\mu\mu'}{}_{\alpha\alpha'}\Delta(\tau_\mathrm{f};\tau_\mathrm{i})^{\alpha\alpha'}{}_{\nu\nu'}. \tag{C.118}$$

Here, (4.33) and (4.34) are proved. In consequence, (4.35) is obtained from (4.34) with (C.26), (C.27) and (4.26).

Finally, we show (4.31) and (4.32). Let us consider the derivatives of the product of two pathline projectors:

$$\mathrm{D}[\Delta(\tau_\mathrm{f};\tau)^\mu{}_\alpha\Delta(\tau;\tau_\mathrm{i})^\alpha{}_\nu] = 2\Delta(\tau_\mathrm{f};\tau)^\mu{}_\alpha[\mathrm{D}\Delta(\tau)^\alpha{}_\beta]\Delta(\tau;\tau_\mathrm{i})^\beta{}_\nu \tag{C.119}$$

$$= 0, \tag{C.120}$$

$$\mathrm{D}[\Delta(\tau_\mathrm{f};\tau)^{\mu\mu'}{}_{\alpha\alpha'}\Delta(\tau;\tau_\mathrm{i})^{\alpha\alpha'}{}_{\nu\nu'}] = 2\Delta(\tau_\mathrm{f};\tau)^{\mu\mu'}{}_{\alpha\alpha'}[\mathrm{D}\Delta(\tau)^{\alpha\alpha'}{}_{\beta\beta'}]\Delta(\tau;\tau_\mathrm{i})^{\beta\beta'}{}_{\nu\nu'} \tag{C.121}$$

$$= 0. \tag{C.122}$$

We used (4.33) in the first line, and (C.26) to obtain the next line. Thus, the expression $\Delta(\tau_\mathrm{f};\tau)^\mu{}_\alpha\Delta(\tau;\tau_\mathrm{i})^\alpha{}_\nu$ and $\Delta(\tau_\mathrm{f};\tau)^{\mu\mu'}{}_{\alpha\alpha'}\Delta(\tau;\tau_\mathrm{i})^{\alpha\alpha'}{}_{\nu\nu'}$ are unchanged even if τ is changed. By choosing τ_f as τ, (4.31) and (4.32) are obtained:

$$\Delta(\tau_\mathrm{f};\tau)^\mu{}_\alpha\Delta(\tau;\tau_\mathrm{i})^\alpha{}_\nu = \Delta(\tau_\mathrm{f};\tau_\mathrm{f})^\mu{}_\alpha\Delta(\tau_\mathrm{f};\tau_\mathrm{i})^\alpha{}_\nu \tag{C.123}$$

$$= \Delta(\tau_\mathrm{f};\tau_\mathrm{i})^\mu{}_\nu, \tag{C.124}$$

$$\Delta(\tau_\mathrm{f};\tau)^{\mu\mu'}{}_{\alpha\alpha'}\Delta(\tau;\tau_\mathrm{i})^{\alpha\alpha'}{}_{\nu\nu'} = \Delta(\tau_\mathrm{f};\tau_\mathrm{f})^{\mu\mu'}{}_{\alpha\alpha'}\Delta(\tau_\mathrm{f};\tau_\mathrm{i})^{\alpha\alpha'}{}_{\nu\nu'} \tag{C.125}$$

$$= \Delta(\tau_\mathrm{f};\tau_\mathrm{i})^{\mu\mu'}{}_{\nu\nu'}. \tag{C.126}$$

Appendix D

Appendix: New numerical scheme

D.1 Conservation law in a curved coordinate system

The conservation law in the flat coordinates is

$$\partial_{\bar{\alpha}} T^{\bar{\alpha}\bar{\beta}} = 0, \qquad \partial_{\bar{\alpha}} N_i^{\bar{\alpha}} = 0. \tag{D.1}$$

where $T^{\mu\nu}$ is the energy-stress tensor of the fluid, and N_i^μ $(i = 1, \ldots, n)$ are other conserved currents. They have the form of the continuity equation $\partial_t U = -\boldsymbol{\partial} \cdot \boldsymbol{F}$, where U is a conserved density and $\boldsymbol{F}$ is its flux. There are many conservative schemes for this form of equations used in various fields. In relativistic hydrodynamic model for high-energy nuclear collisions, several schemes categorized in finite volume method (FVM) is used.

In general coordinates, the conservation laws have a somewhat different form:

$$0 = \bar{\partial}_\mu T^{\mu\nu} = \frac{1}{\sqrt{-g}} \partial_\mu (\sqrt{-g} T^{\mu\nu}) + \Gamma^\nu{}_{\xi\mu} T^{\mu\xi}, \tag{D.2}$$

$$0 = \bar{\partial}_\mu N_i^\mu = \frac{1}{\sqrt{-g}} \partial_\mu (\sqrt{-g} N_i^\mu), \tag{D.3}$$

where $\sqrt{-g(x)} \equiv \sqrt{-\det g_{\mu\nu}} = |\det g^{\bar{\alpha}}{}_\mu|$ is the Jacobian of the coordinate transformation. They can be rewritten using the tensor densities $\mathfrak{T}^{\mu\nu}(x) \equiv \sqrt{-g} T^{\mu\nu}$ and $\mathfrak{N}_i^\mu(x) \equiv \sqrt{-g} N_i^\mu$:

$$\partial_\mu \mathfrak{T}^{\mu\nu} + \Gamma^\nu{}_{\xi\mu} \mathfrak{T}^{\mu\xi} = 0, \qquad \partial_\mu \mathfrak{N}_i^\mu = 0. \tag{D.4}$$

The conservation law for the conserved current densities $\mathfrak{N}_i^\mu$ still has the form of the continuity equation. Accordingly, the existing conservative schemes can be directly applied to these conserved currents. In this case, the conserved quantity is $U = \mathfrak{N}_i^0$. While, the conservation law has a different form for the energy-stress tensor. Although the conserved four-momentum density seems to be $\mathfrak{T}^{0\nu}$, the density has an apparent source term $\Gamma^\nu{}_{\xi\mu} \mathfrak{T}^{\mu\xi}$ in its continuity equation. This equation for the energy-stress tensor can be solved with an ordinary finite volume method with a source term. Such naive solution, however, breaks the conservation law with discretization error.

To appropriately treat the apparent source term, let us recall the origin of the term. The term comes from the spacetime dependence of the basis of the second index of $T^{\mu\nu}$. Here, we can think about the conservation law for the mixed tensor density $\mathfrak{T}^{\mu\bar{\alpha}} \equiv \sqrt{-g} T^{\mu\bar{\alpha}}$:

$$\partial_\mu \mathfrak{T}^{\mu\bar{\alpha}} = 0. \tag{D.5}$$

In the above equation, the apparent source term disappeared since the second-index basis of the energy-stress tensor density is now that of the flat coordinate. This equation has the form of the continuity equation and the conserved four-momentum density $\mathfrak{T}^{0\bar{\alpha}}$ can be solved with an ordinary finite volume method without discretization errors in conservation. The basis of the first index of the energy-stress tensor density is fixed to the grid basis since the differential ∂_μ should be evaluated in the direction of the simulation grid. In contrast, the second index is a free index and its basis can be chosen freely. It is natural to choose the laboratory basis for the second index because the energy and the momentum are

the conserved quantity related to the translational symmetry in the directions of Minkowski basis $\partial_{\bar{\alpha}}$, but not in the directions of a curved basis ∂_μ. The total four momentum is

$$\mathcal{P}^{\bar{\alpha}} = \int d^3x \mathfrak{T}^{0\bar{\alpha}} \tag{D.6}$$

and they are conserved quantities. They can be used to check the conservation of the scheme.

As we have seen so far, solving the hydrodynamic equations using the mixed tensor components is one conservative way. However, this can break other symmetries of the system. The reason to use the curved coordinates is typically that the system – including initial condition, boundary conditions, etc. – has some symmetry and the coordinates should be chosen not to break the symmetry. In such cases, it can cause discretization errors in the symmetry to use the mixed tensor component $\mathfrak{T}^{0\bar{\alpha}}$ for time evolution. Therefore, we still use the ordinary contravariant tensor density $\mathfrak{T}^{\mu\nu}$ for time evolution, but apply the FVM discretization to the mixed-tensor equation (D.5). The conservation law (D.5) is discretized as follows in a regular grid:

$$\mathfrak{T}^{0\bar{\alpha}}(x + \hat{0}/2) = \mathfrak{T}^{0\bar{\alpha}}(x - \hat{0}/2) - \sum_i \frac{\Delta x^0}{\Delta x^i}[\mathfrak{T}^{i\bar{\alpha}}(x + \hat{i}/2) - \mathfrak{T}^{i\bar{\alpha}}(x - \hat{i}/2)]. \tag{D.7}$$

Here, Δx^i is the mesh size of the grid in the direction of i and Δx^0 is the stride between time steps. The vectors $\hat{\mu}$ are the primitive lattice vectors with the direction of the coordinate μ and the length of $|\Delta x^\mu|$. $\mathfrak{T}^{0\bar{\alpha}}(x - \hat{0}/2)$ are the conserved densities of a cell x in the current step, and $\mathfrak{T}^{0\bar{\alpha}}(x + \hat{0}/2)$ are those in the next step. The averaged flux densities on each surface of the cell $\mathfrak{T}^{i\bar{\alpha}}(x \pm \hat{i}/2)$ are evaluated using the conserved densities $\mathfrak{T}^{0\bar{\alpha}}(x - \hat{0}/2)$ and other quantities. By plugging the transformation $T^{\mu\bar{\alpha}} = g^{\bar{\alpha}}{}_\nu T^{\mu\nu}$ in the above equation, the expression for the evolution of the ordinary tensor $\mathfrak{T}^{0\mu}$ is obtained. The result is

$$\begin{aligned}\mathfrak{T}^{0\mu}(x + \hat{0}/2) = g^\mu{}_\nu(x + \hat{0}/2; x)[&g^\nu{}_\xi(x; x - \hat{0}/2)\mathfrak{T}^{0\xi}(x - \hat{0}/2) \\ &- \frac{1}{\Delta V}\sum_i \Delta x^0 \Delta S_i (g^\nu{}_\xi(x; x + \hat{i}/2)\mathfrak{T}^{i\xi}(x + \hat{i}/2) - g^\nu{}_\xi(x; x - \hat{i}/2)\mathfrak{T}^{i\xi}(x - \hat{i}/2))],\end{aligned} \tag{D.8}$$

where $\Delta V \equiv \prod_i \Delta x^i$ is the cell volume and $\Delta S_i \equiv \Delta V / \Delta x^i$ is surface areas. The "parallel transporter" $g^\mu{}_\nu(x; y) \equiv g^\mu{}_{\bar{\alpha}}(x) g^{\bar{\alpha}}{}_\nu(y)$ parallelly transports a vector of the point y to the point x. The left index of the parallel transporter corresponds to the point x and the right index to the point y. The time evolution with the above equation can be made in the following way: First, parallelly transport the conserved densities to $\Delta x^0/2$ away in the forward time direction. Next, evaluate the fluxes on the surfaces, parallelly transport them to the cell center x, and add them to the conserved densities. Finally, again parallelly transport the conserved densities to $\Delta x^0/2$ away. This procedure can also be applied to an unstructured grid. During the procedure, the total four momentum

$$\mathcal{P}^{\bar{\alpha}} = \sum_{x_i \in \mathrm{Cells}} \Delta V_i \, g^{\bar{\alpha}}{}_\mu(x_i) \mathfrak{T}^{0\mu}(x_i) \tag{D.9}$$

is explicitly conserved.

Finally, let us compare the result with the naive FVM with the apparent source term. Using the relation $a_1 b_1 - a_2 b_2 = \frac{a_1 + a_2}{2}(b_1 - b_2) + (a_1 - a_2)\frac{b_1 + b_2}{2}$, the equation (D.8) can be transformed into the following form:

$$0 = \sum_\mu \frac{g^\nu{}_\xi(x; x + \hat{\mu}/2)\mathfrak{T}^{\mu\xi}(x + \hat{\mu}/2) - g^\nu{}_\xi(x; x - \hat{\mu}/2)\mathfrak{T}^{\mu\xi}(x - \hat{\mu}/2)}{\Delta x^\mu} \tag{D.10}$$

$$= \sum_\mu \delta^{(\mu)\nu}{}_\xi \frac{\mathfrak{T}^{\mu\xi}(x + \hat{\mu}/2) - \mathfrak{T}^{\mu\xi}(x - \hat{\mu}/2)}{\Delta x^\mu} + \sum_\mu \Gamma^{(\mu)\nu}{}_{\xi\mu} \frac{\mathfrak{T}^{\mu\xi}(x + \hat{\mu}/2) + \mathfrak{T}^{\mu\xi}(x - \hat{\mu}/2)}{2}. \tag{D.11}$$

We defined $\delta^{(\mu)\nu}{}_\xi \equiv [g^\nu{}_\xi(x; x + \hat{\mu}/2) + g^\nu{}_\xi(x; x - \hat{\mu}/2)]/2 = \delta^\nu{}_\xi + \mathcal{O}((\Delta x^\mu)^2)$, which is almost the Kronecker delta $\delta^\nu{}_\xi$, and a discretized expression of the Christoffel symbols $\Gamma^{(\mu)\nu}{}_{\xi\mu}$:

$$\Gamma^{(\mu)\nu}{}_{\xi\mu} \equiv \frac{g^\nu{}_\xi(x; x + \hat{\mu}/2) - g^\nu{}_\xi(x; x - \hat{\mu}/2)}{\Delta x^\mu} = g^\nu{}_{\bar{\alpha}}(x) \frac{g^{\bar{\alpha}}{}_\xi(x + \hat{\mu}/2) - g^{\bar{\alpha}}{}_\xi(x - \hat{\mu}/2)}{\Delta x^\mu} \tag{D.12}$$

$$= g^\nu{}_{\bar{\alpha}} \partial_\mu g^{\bar{\alpha}}{}_\xi + \mathcal{O}((\Delta x^\mu)^2) = \Gamma^\nu{}_{\xi\mu} + \mathcal{O}((\Delta x^\mu)^2). \tag{D.13}$$

While, the naive FVM with the apparent source term can be written in the comparable form:

$$0 = \sum_{\mu} \delta^{\nu}{}_{\xi} \frac{\mathfrak{T}^{\mu\xi}(x + \hat{\mu}/2) - \mathfrak{T}^{\mu\xi}(x - \hat{\mu}/2)}{\Delta x^{\mu}} + \sum_{\mu} \Gamma^{\nu}{}_{\xi\mu} \mathfrak{T}^{\mu\xi}(x - \hat{\mu}/2). \tag{D.14}$$

Hence, the equation (D.8), which is equivalent to (D.11), can be seen as a special conservative version of the discretized conservation law of (D.4), which is slightly different from naive one (D.14). Note that the Christoffel symbols are discretized although its analytic expression can be obtained from the given coordinate transformation. While the analytic expression is the cell-center value of the Christoffel symbols, the finite difference of parallel transporter, $\Gamma^{(\mu)\nu}{}_{\xi\mu}$, is the cell-averaged value of the Christoffel symbols, so it is natural to use the finite difference rather than the analytic differential expression.

Appendix E

Appendix: Noise Integration

E.1 Itô integral and Stratonovich integral

Here we give an explicit definition of the fields with the Itô integral (6.60) and the Stratonovich integral (6.61). First we consider the case that the coefficient of dB is a function of time:

$$dX_l^{\mathrm{I}} \equiv f_l(t)dt + \sum_m g_{lm}(t) \cdot dB_m(t), \tag{E.1}$$

$$dX_l^{\mathrm{S}} \equiv f_l(t)dt + \sum_m g_{lm}(t) \circ dB_m(t), \tag{E.2}$$

where t is a time, and X is a variable to solve, and $f_l(t)$ and $g_{lm}(t)$ are functions of time. The noise terms $B_m(t)$ are independent Brownian motions which satisfy $\langle B_l(t_1)B_m(t_2)\rangle = \delta_{lm}\min\{t_1, t_2\}$. Those integrals are defined as follows:

$$X_l^{\mathrm{I}}(t) = X(0) + \int_0^t dt f_l(t) + \sum_m \int_0^t g_{lm}(t) \cdot dB_m(t), \tag{E.3}$$

$$X_l^{\mathrm{S}}(t) = X(0) + \int_0^t dt f_l(t) + \sum_m \int_0^t g_{lm}(t) \circ dB_m(t), \tag{E.4}$$

$$\int_0^t g_{lm}(t) \cdot dB_m(t) \equiv \lim_{N\to\infty} \sum_{i=0}^{N-1} g_{lm}(t_i^{(N)})[B_m(t_{i+1}^{(N)}) - B_m(t_i^{(N)})], \tag{E.5}$$

$$\int_0^t g_{lm}(t) \circ dB_m(t) \equiv \lim_{N\to\infty} \sum_{i=0}^{N-1} g_{lm}\left(\frac{t_{i+1}^{(N)} + t_i^{(N)}}{2}\right)[B_m(t_{i+1}^{(N)}) - B_m(t_i^{(N)})] \tag{E.6}$$

$$= \lim_{N\to\infty} \sum_{i=0}^{N-1} \frac{g_{lm}(t_{i+1}^{(N)}) + g_{lm}(t_i^{(N)})}{2}[B_m(t_{i+1}^{(N)}) - B_m(t_i^{(N)})], \tag{E.7}$$

where $t_i^{(N)} \equiv (i/N)t$.

If the functions f_l and g_{lm} are dependent on the integrals X_l themselves, the differential form of the integrals can be written in the following form:

$$dX_l^{\mathrm{I}} \equiv f_l(X^{\mathrm{I}}, t)dt + \sum_m g_{lm}(X^{\mathrm{I}}, t) \cdot dB_m(t), \tag{E.8}$$

$$dX_l^{\mathrm{S}} \equiv f_l(X^{\mathrm{S}}, t)dt + \sum_m g_{lm}(X^{\mathrm{S}}, t) \circ dB_m(t). \tag{E.9}$$

The hydrodynamic equations for fluctuating hydrodynamics have this form. The equations above can be seen as a dynamical equation of the variable $X_l(t)$. In this case the definition (E.3)-(E.7) can be

extended. The definition with the Itô integral becomes

$$X_l^{\mathrm{I}}(t_0^{(N)};t) = X_l(0), \tag{E.10}$$

$$\begin{aligned} X_l^{\mathrm{I}}(t_{i+1}^{(N)};t) =& X_l^{\mathrm{I}}(t_i^{(N)};t) + f_l(X^{\mathrm{I}}(t_i^{(N)};t),t_l)(t_{i+1}^{(N)} - t_i^{(N)}) \\ &+ \sum_m g_{lm}(X^{\mathrm{I}}(t_i^{(N)};t),t)[B_m(t_{i+1}^{(N)}) - B_m(t_i^{(N)})], \quad (i = 0,\ldots,N-1), \end{aligned} \tag{E.11}$$

$$X_l^{\mathrm{I}}(t) \equiv \lim_{N\to\infty} X_l^{\mathrm{I}}(t_N^{(N)};t). \tag{E.12}$$

The Stratonovich version becomes

$$X_l^{\mathrm{S}}(t_0^{(N)};t) = X_l(0), \tag{E.13}$$

$$\begin{aligned} X_l^{\mathrm{S}}(t_{i+1}^{(N)};t) =& X_l^{\mathrm{S}}(t_i^{(N)};t) + f_l(X^{\mathrm{S}}(t_i^{(N)};t),t_l)(t_{i+1}^{(N)} - t_i^{(N)}) \\ &+ \sum_m \frac{g_{lm}(X^{\mathrm{S}}(t_{i+1}^{(N)};t),t) + g_{lm}(X^{\mathrm{S}}(t_i^{(N)};t),t)}{2}[B_m(t_{i+1}^{(N)}) - B_m(t_i^{(N)})], \\ &(i = 0,\ldots,N-1), \end{aligned} \tag{E.14}$$

$$X_l^{\mathrm{S}}(t) \equiv \lim_{N\to\infty} X_l^{\mathrm{S}}(t_N^{(N)};t). \tag{E.15}$$

A difference of two integrals can be found in recurrence relations (E.11), and (E.14). While the recurrence relation in the Itô integral has an explicit form with respect to the next time step $X^{\mathrm{I}}(t_{i+1}^{(N)};t)$, the relation in the Stratonovich integral does not have an explicit form since the next time step $X^{\mathrm{S}}(t_{i+1}^{(N)};t)$ is contained also in the right hand side. Nevertheless, the next time step $X^{\mathrm{S}}(t_{i+1}^{(N)};t)$ can be solved to fulfill the relation.

Appendix F

Appendix: Integrated dynamical model

F.1 Cooper-Frye sampling with viscous effects

Here we describe the details of the effective procedure of the Cooper-Frye sampling used in our numerical calculations.

The input of the sampling is the hypersurface information including data of each hypersurface element which are obtained as an output of hydrodynamics. The data for a hypersurface element consist of the fluid fields on its position, such as temperature, fluid velocity, and dissipative currents, as well as the size, direction, and spacetime position of the hypersurface element itself. Then the whole hypersurface can be expressed with a sequence of such data of hypersurface elements.

The outermost loop of the sampling procedure would be the loop over the hypersurface elements. The hypersurface for an event consists of millions of hypersurface elements and it is unfavorable to load entire data with such large size on memory at once. Therefore the sampling is performed for each hypersurface element by reading the data of one hypersurface element at once, and all the process for the hypersurface element is completed before reading the information of the next element.

The next loop is the one over the species of the resonances. In a loop step for a resonance, first we calculate a mean number of the particles, $\Delta N_i'$, using numerical integration with the isotropic distribution function $f_{\max}(p)$, and determine an actual number of the particles using Poisson random number generator with the calculated mean number $\Delta N_i'$. We then randomly sample the momentum and its direction of each particle with the isotropic version of the probability density function $f_{\max}(p, \boldsymbol{x})$. Finally we accept or reject each generated particle with the anisotropic probability $P_{\text{aniso}}(p)$.

The integral to obtain the mean value $\Delta N_i'$ can be transformed into a sum of two one-dimensional integrals:

$$\Delta N_i' = g_i \int \frac{d^3p}{(2\pi)^3 E} [\Delta\sigma_\mu p^\mu]^+ f_{\max}(p, \boldsymbol{x}) \tag{F.1}$$

$$= \frac{g_i T^3}{8\pi^2} [4(\Delta\sigma^0)^+ I_B + |\Delta\boldsymbol{\sigma}|\Theta(1 - v_\sigma) I_S], \tag{F.2}$$

$$I_B \equiv \int_{\beta m_i}^{\infty} dx f_{\max}(x) x\sqrt{x^2 - (\beta m_i)^2}, \tag{F.3}$$

$$I_S \equiv \int_{x_\sigma}^{\infty} dx f_{\max}(x)(x v_\sigma - \sqrt{x^2 - (\beta m_i)^2})^2, \tag{F.4}$$

$$f_{\max}(x) \equiv \frac{1}{e^x/\lambda_i - \epsilon} \left[1 + \frac{\pi_{\max}}{2(e+P)} \frac{(x^2 - (\beta m_i)^2) e^x/\lambda_i}{e^x/\lambda_i - \epsilon}\right], \tag{F.5}$$

where $\Delta\sigma_0 \equiv \Delta\sigma_\mu u^\mu$, and $|\Delta\boldsymbol{\sigma}| \equiv \sqrt{-\Delta^{\mu\nu}\Delta\boldsymbol{\sigma}_\mu\Delta\boldsymbol{\sigma}_\nu}$ are hypersurface components seen in the local rest frame. The dimensionless parameters v_σ, and x_σ are defined as $v_\sigma \equiv |\Delta\sigma_0|/|\Delta\boldsymbol{\sigma}|$, and $x_\sigma \equiv \beta m_i/\sqrt{1 - v_\sigma^2}$. The first integral I_B is the bulk contribution, which is related to the number of particles inside a fluid element whose temperature got lower than the switching temperature. The second integral I_S is the surface contribution, which is related to the number of particles moved from a fluid element with temperature higher than the switching temperature to another with temperature lower. In order to

obtain the above result, it should be noticed that the angular integration can be performed as follows:

$$\int d\Omega[\Delta\sigma_\mu p^\mu]^+ = 2\pi \int_{-1}^{1} d\cos\theta[\Delta\sigma_0 E + |\Delta\boldsymbol{\sigma}| \cdot |\boldsymbol{p}| \cos\theta]^+ \tag{F.6}$$

$$= \pi \left[4\Delta\sigma_0 E \Theta(\Delta\sigma_0) + \frac{(|\Delta\sigma_0| E - |\Delta\boldsymbol{\sigma}| \cdot |\boldsymbol{p}|)^2}{|\Delta\boldsymbol{\sigma}| \cdot |\boldsymbol{p}|} \Theta(|\Delta\boldsymbol{\sigma}| \cdot |\boldsymbol{p}| - |\Delta\sigma_0| E) \right]. \tag{F.7}$$

In addition the integration with respect to the absolute value of the momentum $|\boldsymbol{p}|$ is replaced by a dimensionless energy $x \equiv \beta E = \beta\sqrt{|\boldsymbol{p}|^2 + m_i^2}$ to have a simpler expression. The dimensionless quantities v_σ, and x_σ are interpreted as the velocity of the hypersurface, and the dimensionless energy of the particles sharing the same velocity with the hypersurface, respectively.

The one-dimensional integrations over the unbounded intervals (F.3), (F.4) can be numerically performed, for example, using the Gauss-Laguerre quadrature. However, we substitute the integration variable with bounded intervals to make it simple to evaluate and control numerical errors. We chose a specific integration variable t, such that $x - x_0 = \tan t^2$ where $x_0 = \beta m_i, x_\sigma$ is the lower bound of the interval. The choice is used to reduce the singular behavior of the light boson distribution function $f_0(x)$ at lower energy region. The integral interval of the substituted variable, $t \in [0, \sqrt{\pi/2}]$, is bounded, and thus we adopt the Gauss-Legendre quadrature for the numerical integrations.

Bibliography

[1] C. N. Yang and R. L. Mills, Phys. Rev. **96**, 191 (1954).

[2] Y. Nambu, "A systematics of hadrons in subnuclear physics," Preludes In Theoretical Physics (1966) 133-142.

[3] H. D. Politzer, Phys. Rev. Lett. **30**, 1346 (1973).

[4] D. J. Gross and F. Wilczek, Phys. Rev. Lett. **30**, 1343 (1973).

[5] J. C. Collins and M. J. Perry, Phys. Rev. Lett. **34**, 1353 (1975).

[6] N. Cabibbo and G. Parisi, Phys. Lett. B **59**, 67 (1975).

[7] G. Baym and S. A. Chin, Phys. Lett. B **62**, 241 (1976).

[8] J. I. Kapusta, Nucl. Phys. B **148**, 461 (1979).

[9] E. V. Shuryak, Sov. Phys. JETP **47**, 212 (1978) [Zh. Eksp. Teor. Fiz. **74**, 408 (1978)].

[10] P. de Forcrand, PoS LAT **2009**, 010 (2009) [arXiv:1005.0539 [hep-lat]].

[11] K. Fukushima and T. Hatsuda, Rept. Prog. Phys. **74**, 014001 (2011) [arXiv:1005.4814 [hep-ph]].

[12] "The Frontiers of Nuclear Science," 2007 NSAC Long Range Plan, Nuclear Science Advisory Committee (NSAC), Office of Science, U. S. Department of Energy.

[13] F. R. Brown, F. P. Butler, H. Chen, N. H. Christ, Z. h. Dong, W. Schaffer, L. I. Unger and A. Vaccarino, Phys. Rev. Lett. **65**, 2491 (1990).

[14] Y. Aoki, Z. Fodor, S. D. Katz and K. K. Szabo, JHEP **0601**, 089 (2006) [hep-lat/0510084].

[15] Y. Aoki, G. Endrodi, Z. Fodor, S. D. Katz and K. K. Szabo, Nature **443**, 675 (2006) [hep-lat/0611014].

[16] A. Bazavov, T. Bhattacharya, M. Cheng, N. H. Christ, C. DeTar, S. Ejiri, S. Gottlieb and R. Gupta *et al.*, Phys. Rev. D **80**, 014504 (2009) [arXiv:0903.4379 [hep-lat]].

[17] C. DeTar and U. M. Heller, Eur. Phys. J. A **41**, 405 (2009) [arXiv:0905.2949 [hep-lat]].

[18] A. Bazavov, T. Bhattacharya, M. Cheng, C. DeTar, H. T. Ding, S. Gottlieb, R. Gupta and P. Hegde *et al.*, Phys. Rev. D **85**, 054503 (2012) [arXiv:1111.1710 [hep-lat]].

[19] S. Borsanyi, Z. Fodor, C. Hoelbling, S. D. Katz, S. Krieg and K. K. Szabo, Phys. Lett. B **730**, 99 (2014) [arXiv:1309.5258 [hep-lat]].

[20] M. Asakawa and K. Yazaki, Nucl. Phys. A **504**, 668 (1989).

[21] A. Barducci, R. Casalbuoni, S. De Curtis, R. Gatto and G. Pettini, Phys. Lett. B **231**, 463 (1989).

[22] A. Barducci, R. Casalbuoni, S. De Curtis, R. Gatto and G. Pettini, Phys. Rev. D **41**, 1610 (1990).

[23] F. Wilczek, Int. J. Mod. Phys. A **7**, 3911 (1992) [Int. J. Mod. Phys. A **7**, 6951 (1992)].

[24] J. Berges and K. Rajagopal, Nucl. Phys. B **538**, 215 (1999) [hep-ph/9804233].

[25] B. C. Barrois, Nucl. Phys. B **129**, 390 (1977).

[26] D. Bailin and A. Love, Phys. Rept. **107**, 325 (1984).

[27] K. Rajagopal and F. Wilczek, In *Shifman, M. (ed.): At the frontier of particle physics, vol. 3* 2061-2151 [hep-ph/0011333].

[28] M. G. Alford, A. Schmitt, K. Rajagopal and T. Schäfer, Rev. Mod. Phys. **80**, 1455 (2008) [arXiv:0709.4635 [hep-ph]].

[29] C. Fabjan and J. Schukraft, 'The Large Hadron Collider: A marvel technology', EPFL-Press Lausanne, Switzerland, 2009 (Editor: L. Evans), chapter 5.4 [arXiv:1101.1257 [physics.ins-det]].

[30] The event display images of the STAR experiment is taken from the web page at http://www.star.bnl.gov/public/imagelib/collisions2001/ in the site of the STAR of BNL.

[31] J. Y. Ollitrault, Phys. Rev. D **46**, 229 (1992).

[32] W. Reisdorf and H. G. Ritter, Ann. Rev. Nucl. Part. Sci. **47**, 663 (1997).

[33] P. F. Kolb, J. Sollfrank and U. W. Heinz, Phys. Rev. C **62**, 054909 (2000) [hep-ph/0006129].

[34] P. F. Kolb, P. Huovinen, U. W. Heinz and H. Heiselberg, Phys. Lett. B **500**, 232 (2001) [hep-ph/0012137].

[35] D. Teaney, J. Lauret and E. V. Shuryak, nucl-th/0110037.

[36] D. Teaney, J. Lauret and E. V. Shuryak, Phys. Rev. Lett. **86** (2001) 4783 [nucl-th/0011058].

[37] P. Huovinen, P. F. Kolb, U. W. Heinz, P. V. Ruuskanen and S. A. Voloshin, Phys. Lett. B **503**, 58 (2001) [hep-ph/0101136].

[38] T. Hirano, Phys. Rev. C **65**, 011901 (2002) [nucl-th/0108004].

[39] T. Hirano and K. Tsuda, Phys. Rev. C **66**, 054905 (2002) [nucl-th/0205043].

[40] P. Huovinen, Nucl. Phys. A **761**, 296 (2005) [nucl-th/0505036].

[41] C. Nonaka and S. A. Bass, Phys. Rev. C **75**, 014902 (2007) [nucl-th/0607018].

[42] B. Schenke, S. Jeon and C. Gale, Phys. Rev. C **82**, 014903 (2010) [arXiv:1004.1408 [hep-ph]].

[43] H. Niemi, K. J. Eskola and P. V. Ruuskanen, Phys. Rev. C **79**, 024903 (2009) [arXiv:0806.1116 [hep-ph]].

[44] C. Adler *et al.* [STAR Collaboration], Phys. Rev. Lett. **87**, 182301 (2001) [nucl-ex/0107003].

[45] C. Adler *et al.* [STAR Collaboration], Phys. Rev. C **66**, 034904 (2002) [nucl-ex/0206001].

[46] K. Adcox *et al.* [PHENIX Collaboration], Phys. Rev. Lett. **89**, 212301 (2002) [nucl-ex/0204005].

[47] S. S. Adler *et al.* [PHENIX Collaboration], Phys. Rev. Lett. **91**, 182301 (2003) [nucl-ex/0305013].

[48] B. B. Back *et al.* [PHOBOS Collaboration], Phys. Rev. Lett. **89**, 222301 (2002) [nucl-ex/0205021].

[49] B. B. Back *et al.* [PHOBOS Collaboration], Phys. Rev. Lett. **94**, 122303 (2005) [nucl-ex/0406021].

[50] B. B. Back *et al.* [PHOBOS Collaboration], Phys. Rev. C **72**, 051901 (2005) [nucl-ex/0407012].

[51] U. W. Heinz and M. Jacob, nucl-th/0002042.

[52] U. W. Heinz and P. F. Kolb, Nucl. Phys. A **702**, 269 (2002) [hep-ph/0111075].

[53] M. Gyulassy, nucl-th/0403032.

[54] M. Gyulassy and L. McLerran, Nucl. Phys. A **750**, 30 (2005) [nucl-th/0405013].

[55] B. Muller and J. L. Nagle, Ann. Rev. Nucl. Part. Sci. **56**, 93 (2006) [nucl-th/0602029].

[56] L. D. McLerran and T. Toimela, Phys. Rev. D **31**, 545 (1985).

[57] J. I. Kapusta, P. Lichard and D. Seibert, Phys. Rev. D **44**, 2774 (1991) [Phys. Rev. D **47**, 4171 (1993)].

[58] C. Gale and K. L. Haglin, In *Hwa, R.C. (ed.) et al.: Quark gluon plasma* 364-429 [hep-ph/0306098].

[59] S. Turbide, C. Gale, E. Frodermann and U. Heinz, Phys. Rev. C **77**, 024909 (2008) [arXiv:0712.0732 [hep-ph]].

[60] S. S. Adler *et al.* [PHENIX Collaboration], Phys. Rev. Lett. **94**, 232301 (2005) [nucl-ex/0503003].

[61] A. Adare *et al.* [PHENIX Collaboration], Phys. Rev. Lett. **104**, 132301 (2010) [arXiv:0804.4168 [nucl-ex]].

[62] S. Afanasiev *et al.* [PHENIX Collaboration], arXiv:0706.3034 [nucl-ex].

[63] J. Zhao [STAR Collaboration], J. Phys. G **38**, 124134 (2011) [arXiv:1106.6146 [nucl-ex]].

[64] T. Matsui and H. Satz, Phys. Lett. B **178**, 416 (1986).

[65] S. S. Adler *et al.* [PHENIX Collaboration], Phys. Rev. C **69**, 014901 (2004) [nucl-ex/0305030].

[66] A. Adare *et al.* [PHENIX Collaboration], Phys. Rev. Lett. **98**, 232301 (2007) [nucl-ex/0611020].

[67] A. Adare *et al.* [PHENIX Collaboration], Phys. Rev. Lett. **101**, 122301 (2008) [arXiv:0801.0220 [nucl-ex]].

[68] B. I. Abelev *et al.* [STAR Collaboration], Phys. Rev. C **80**, 041902 (2009) [arXiv:0904.0439 [nucl-ex]].

[69] C. Adler *et al.* [STAR Collaboration], Phys. Rev. Lett. **89**, 202301 (2002) [nucl-ex/0206011].

[70] S. S. Adler *et al.* [PHENIX Collaboration], Phys. Rev. Lett. **91**, 072301 (2003) [nucl-ex/0304022].

[71] J. Adams *et al.* [STAR Collaboration], Phys. Rev. Lett. **91**, 172302 (2003) [nucl-ex/0305015].

[72] M. Gyulassy and M. Plumer, Phys. Lett. B **243**, 432 (1990).

[73] X. N. Wang and M. Gyulassy, Phys. Rev. Lett. **68**, 1480 (1992).

[74] J. Adams *et al.* [STAR Collaboration], Phys. Rev. Lett. **91**, 072304 (2003) [nucl-ex/0306024].

[75] J. Adams *et al.* [STAR Collaboration], Phys. Rev. Lett. **95**, 152301 (2005) [nucl-ex/0501016].

[76] A. Adare *et al.* [PHENIX Collaboration], Phys. Rev. C **78**, 014901 (2008) [arXiv:0801.4545 [nucl-ex]].

[77] S. S. Adler *et al.* [PHENIX Collaboration], Phys. Rev. Lett. **97**, 052301 (2006) [nucl-ex/0507004].

[78] J. Rafelski and B. Muller, Phys. Rev. Lett. **48**, 1066 (1982) [Phys. Rev. Lett. **56**, 2334 (1986)].

[79] J. Sollfrank and U. W. Heinz, In *Hwa, R.C. (ed.): Quark-gluon plasma, vol.2* 555-634, and Helsinki U. - HU-TFT-95-27 (95,rec.May) 81 p [nucl-th/9505004].

[80] A. Andronic, P. Braun-Munzinger and J. Stachel, Nucl. Phys. A **772**, 167 (2006) [nucl-th/0511071].

[81] F. Antinori *et al.* [NA57 Collaboration], J. Phys. G **32**, 427 (2006) [nucl-ex/0601021].

[82] C. Alt *et al.* [NA49 Collaboration], Phys. Rev. C **77**, 024903 (2008) [arXiv:0710.0118 [nucl-ex]].

[83] P. Kovtun, D. T. Son and A. O. Starinets, Phys. Rev. Lett. **94**, 111601 (2005) [hep-th/0405231].

[84] B. Alver *et al.* [PHOBOS Collaboration], Phys. Rev. Lett. **98**, 242302 (2007) [nucl-ex/0610037].

[85] A. M. Poskanzer and S. A. Voloshin, Phys. Rev. C **58**, 1671 (1998) [nucl-ex/9805001].

[86] B. Alver and G. Roland, Phys. Rev. C **81**, 054905 (2010) [Phys. Rev. C **82**, 039903 (2010)] [arXiv:1003.0194 [nucl-th]].

[87] K. Aamodt *et al.* [ALICE Collaboration], Phys. Lett. B **708**, 249 (2012) [arXiv:1109.2501 [nucl-ex]].

[88] K. Aamodt *et al.* [ALICE Collaboration], Phys. Rev. Lett. **107**, 032301 (2011) [arXiv:1105.3865 [nucl-ex]].

[89] G. Aad *et al.* [ATLAS Collaboration], Phys. Rev. C **86**, 014907 (2012) [arXiv:1203.3087 [hep-ex]].

[90] [CMS Collaboration], CMS-PAS-HIN-11-005.

[91] A. Adare *et al.* [PHENIX Collaboration], Phys. Rev. Lett. **107**, 252301 (2011) [arXiv:1105.3928 [nucl-ex]].

[92] J. I. Kapusta, B. Muller and M. Stephanov, Phys. Rev. C **85**, 054906 (2012) [arXiv:1112.6405 [nucl-th]].

[93] B. Schenke, P. Tribedy and R. Venugopalan, Phys. Rev. Lett. **108**, 252301 (2012) [arXiv:1202.6646 [nucl-th]].

[94] C. Gale, S. Jeon, B. Schenke, P. Tribedy and R. Venugopalan, Phys. Rev. Lett. **110**, no. 1, 012302 (2013) [arXiv:1209.6330 [nucl-th]].

[95] H. Kowalski and D. Teaney, Phys. Rev. D **68**, 114005 (2003) [hep-ph/0304189].

[96] J. Bartels, K. J. Golec-Biernat and H. Kowalski, Phys. Rev. D **66**, 014001 (2002) [hep-ph/0203258].

[97] F. Gelis, T. Lappi and L. McLerran, Nucl. Phys. A **828**, 149 (2009) [arXiv:0905.3234 [hep-ph]].

[98] J. Jia [ATLAS Collaboration], Nucl. Phys. A **904-905**, 421c (2013) [arXiv:1209.4232 [nucl-ex]].

[99] J. Jia and S. Mohapatra, Phys. Rev. C **88**, no. 1, 014907 (2013) [arXiv:1304.1471 [nucl-ex]].

[100] G. Aad *et al.* [ATLAS Collaboration], JHEP **1311**, 183 (2013) [arXiv:1305.2942 [hep-ex]].

[101] Y. Tachibana and T. Hirano, Phys. Rev. C **90**, no. 2, 021902 (2014) [arXiv:1402.6469 [nucl-th]].

[102] B. B. Back *et al.* [PHOBOS Collaboration], Phys. Rev. Lett. **85**, 3100 (2000) [hep-ex/0007036].

[103] B. B. Back *et al.* [PHOBOS Collaboration], Phys. Rev. C **65**, 061901 (2002) [nucl-ex/0201005].

[104] B. B. Back, M. D. Baker, M. Ballintijn, D. S. Barton, B. Becker, R. R. Betts, A. A. Bickley and R. Bindel *et al.*, Nucl. Phys. A **757**, 28 (2005) [nucl-ex/0410022].

[105] K. Aamodt *et al.* [ALICE Collaboration], Phys. Rev. Lett. **105**, 252302 (2010) [arXiv:1011.3914 [nucl-ex]].

[106] B. Abelev *et al.* [ALICE Collaboration], Phys. Rev. C **88**, no. 4, 044909 (2013) [arXiv:1301.4361 [nucl-ex]].

[107] K. Aamodt *et al.* [ALICE Collaboration], JINST **3**, S08002 (2008).

[108] G. Aad *et al.* [ATLAS Collaboration], Phys. Lett. B **707** (2012) 330 [arXiv:1108.6018 [hep-ex]].

[109] S. Chatrchyan *et al.* [CMS Collaboration], Phys. Rev. C **87**, no. 1, 014902 (2013) [arXiv:1204.1409 [nucl-ex]].

[110] T. W. Ludlam, A. Pfoh and A. Shor, IN *BROOKHAVEN 1985, PROCEEDINGS, EXPERIMENTS FOR A RELATIVISTIC HEAVY ION COLLIDER*, 373-381.

[111] A. Shor and R. S. Longacre, Phys. Lett. B **218**, 100 (1989).

[112] B. Alver, M. Baker, C. Loizides and P. Steinberg, arXiv:0805.4411 [nucl-ex].

[113] T. Hirano, P. Huovinen, K. Murase and Y. Nara, Prog. Part. Nucl. Phys. **70**, 108 (2013) [arXiv:1204.5814 [nucl-th]].

[114] S. S. Adler *et al.* [PHENIX Collaboration], Phys. Rev. C **69**, 034909 (2004) [nucl-ex/0307022].

[115] B. Schenke, S. Jeon and C. Gale, Phys. Lett. B **702**, 59 (2011) [arXiv:1102.0575 [hep-ph]].

[116] A. Dumitru, S. A. Bass, M. Bleicher, H. Stoecker and W. Greiner, Phys. Lett. B **460**, 411 (1999) [nucl-th/9901046].

[117] S. A. Bass, A. Dumitru, M. Bleicher, L. Bravina, E. Zabrodin, H. Stoecker and W. Greiner, Phys. Rev. C **60**, 021902 (1999) [nucl-th/9902062].

[118] S. A. Bass and A. Dumitru, Phys. Rev. C **61**, 064909 (2000) [nucl-th/0001033].

[119] T. Hirano, U. W. Heinz, D. Kharzeev, R. Lacey and Y. Nara, Phys. Lett. B **636**, 299 (2006) [nucl-th/0511046].

[120] T. Hirano, U. W. Heinz, D. Kharzeev, R. Lacey and Y. Nara, Phys. Rev. C **77**, 044909 (2008) [arXiv:0710.5795 [nucl-th]].

[121] H. Petersen, J. Steinheimer, G. Burau, M. Bleicher and H. Stocker, Phys. Rev. C **78**, 044901 (2008) [arXiv:0806.1695 [nucl-th]].

[122] H. Petersen and M. Bleicher, Phys. Rev. C **79**, 054904 (2009) [arXiv:0901.3821 [nucl-th]].

[123] H. Petersen and M. Bleicher, Phys. Rev. C **81**, 044906 (2010) [arXiv:1002.1003 [nucl-th]].

[124] G. Y. Qin, H. Petersen, S. A. Bass and B. Muller, Phys. Rev. C **82**, 064903 (2010) [arXiv:1009.1847 [nucl-th]].

[125] H. Petersen, G. Y. Qin, S. A. Bass and B. Muller, Phys. Rev. C **82**, 041901 (2010) [arXiv:1008.0625 [nucl-th]].

[126] H. Petersen, V. Bhattacharya, S. A. Bass and C. Greiner, Phys. Rev. C **84**, 054908 (2011) [arXiv:1105.0340 [nucl-th]].

[127] H. Petersen, Phys. Rev. C **84**, 034912 (2011) [arXiv:1105.1766 [nucl-th]].

[128] S. Pratt and J. Vredevoogd, Phys. Rev. C **78**, 054906 (2008) [Phys. Rev. C **79**, 069901 (2009)] [arXiv:0809.0516 [nucl-th]].

[129] K. Werner, I. Karpenko, T. Pierog, M. Bleicher and K. Mikhailov, Phys. Rev. C **82**, 044904 (2010) [arXiv:1004.0805 [nucl-th]].

[130] K. Werner, I. Karpenko, T. Pierog, M. Bleicher and K. Mikhailov, Phys. Rev. C **83**, 044915 (2011) [arXiv:1010.0400 [nucl-th]].

[131] K. Werner, I. Karpenko and T. Pierog, Phys. Rev. Lett. **106**, 122004 (2011) [arXiv:1011.0375 [hep-ph]].

[132] K. Werner, I. Karpenko, M. Bleicher, T. Pierog and S. Porteboeuf-Houssais, Phys. Rev. C **85**, 064907 (2012) [arXiv:1203.5704 [nucl-th]].

[133] H. Song, S. A. Bass, U. Heinz, T. Hirano and C. Shen, Phys. Rev. Lett. **106**, 192301 (2011) [Phys. Rev. Lett. **109**, 139904 (2012)] [arXiv:1011.2783 [nucl-th]].

[134] H. Song, S. A. Bass and U. Heinz, Phys. Rev. C **83**, 024912 (2011) [arXiv:1012.0555 [nucl-th]].

[135] H. Song, S. A. Bass and U. Heinz, Phys. Rev. C **83**, 054912 (2011) [Phys. Rev. C **87**, no. 1, 019902 (2013)] [arXiv:1103.2380 [nucl-th]].

[136] R. A. Soltz, I. Garishvili, M. Cheng, B. Abelev, A. Glenn, J. Newby, L. A. Linden Levy and S. Pratt, Phys. Rev. C **87**, no. 4, 044901 (2013) [arXiv:1208.0897 [nucl-th]].

[137] S. Ryu, S. Jeon, C. Gale, B. Schenke and C. Young, Nucl. Phys. A **904-905**, 389c (2013) [arXiv:1210.4588 [hep-ph]].

[138] M. Gyulassy, D. H. Rischke and B. Zhang, Nucl. Phys. A **613**, 397 (1997) [nucl-th/9609030].

[139] C. E. Aguiar, Y. Hama, T. Kodama and T. Osada, Nucl. Phys. A **698**, 639 (2002) [hep-ph/0106266].

[140] Y. Hama, T. Kodama and O. Socolowski, Jr., Braz. J. Phys. **35**, 24 (2005) [hep-ph/0407264].

[141] R. Andrade, F. Grassi, Y. Hama, T. Kodama and O. Socolowski, Jr., Phys. Rev. Lett. **97**, 202302 (2006) [nucl-th/0608067].

[142] R. P. G. Andrade, F. Grassi, Y. Hama, T. Kodama and W. L. Qian, Phys. Rev. Lett. **101**, 112301 (2008) [arXiv:0805.0018 [hep-ph]].

[143] J. Takahashi, B. M. Tavares, W. L. Qian, R. Andrade, F. Grassi, Y. Hama, T. Kodama and N. Xu, Phys. Rev. Lett. **103**, 242301 (2009) [arXiv:0902.4870 [nucl-th]].

[144] F. G. Gardim, F. Grassi, Y. Hama, M. Luzum and J. Y. Ollitrault, Phys. Rev. C **83**, 064901 (2011) [arXiv:1103.4605 [nucl-th]].

[145] Y. Y. Ren, W. N. Zhang and J. L. Liu, Phys. Lett. B **669**, 317 (2008) [arXiv:0810.0316 [hep-ph]].

[146] H. Holopainen, H. Niemi and K. J. Eskola, Phys. Rev. C **83**, 034901 (2011) [arXiv:1007.0368 [hep-ph]].

[147] R. Chatterjee, H. Holopainen, T. Renk and K. J. Eskola, Phys. Rev. C **83**, 054908 (2011) [arXiv:1102.4706 [hep-ph]].

[148] T. Renk, H. Holopainen, J. Auvinen and K. J. Eskola, Phys. Rev. C **85**, 044915 (2012) [arXiv:1105.2647 [hep-ph]].

[149] Z. Qiu and U. W. Heinz, Phys. Rev. C **84**, 024911 (2011) [arXiv:1104.0650 [nucl-th]].

[150] B. H. Alver, C. Gombeaud, M. Luzum and J. Y. Ollitrault, Phys. Rev. C **82**, 034913 (2010) [arXiv:1007.5469 [nucl-th]].

[151] B. Schenke, S. Jeon and C. Gale, Phys. Rev. Lett. **106**, 042301 (2011) [arXiv:1009.3244 [hep-ph]].

[152] B. Schenke, S. Jeon and C. Gale, Phys. Rev. C **85**, 024901 (2012) [arXiv:1109.6289 [hep-ph]].

[153] A. K. Chaudhuri, Phys. Lett. B **710**, 339 (2012) [arXiv:1108.5552 [nucl-th]].

[154] M. Rihan Haque, V. Roy and A. K. Chaudhuri, Phys. Rev. C **86**, 037901 (2012) [arXiv:1204.2986 [nucl-ex]].

[155] P. Bozek and W. Broniowski, Phys. Rev. C **85**, 044910 (2012) [arXiv:1203.1810 [nucl-th]].

[156] L. Pang, Q. Wang and X. N. Wang, Phys. Rev. C **86**, 024911 (2012) [arXiv:1205.5019 [nucl-th]].

[157] H. Zhang, T. Song and C. M. Ko, Phys. Rev. C **87**, no. 5, 054902 (2013) [arXiv:1208.2980 [hep-ph]].

[158] R. J. Glauber and G. Matthiae, Nucl. Phys. B **21**, 135 (1970).

[159] A. Bialas, M. Bleszynski and W. Czyz, Nucl. Phys. B **111**, 461 (1976).

[160] T. Hirano and Y. Nara, Phys. Rev. C **79**, 064904 (2009) [arXiv:0904.4080 [nucl-th]].

[161] A. Adil and M. Gyulassy, Phys. Rev. C **72**, 034907 (2005) [nucl-th/0505004].

[162] S. J. Brodsky, J. F. Gunion and J. H. Kuhn, Phys. Rev. Lett. **39**, 1120 (1977).

[163] B. B. Back *et al.* [PHOBOS Collaboration], Phys. Rev. C **72**, 031901 (2005) [nucl-ex/0409021].

[164] G. J. Alner *et al.* [UA5 Collaboration], Z. Phys. C **33**, 1 (1986).

[165] M. L. Miller, K. Reygers, S. J. Sanders and P. Steinberg, Ann. Rev. Nucl. Part. Sci. **57**, 205 (2007) [nucl-ex/0701025].

[166] L. D. McLerran and R. Venugopalan, Phys. Rev. D **50**, 2225 (1994) [hep-ph/9402335].

[167] L. D. McLerran and R. Venugopalan, Phys. Rev. D **49**, 3352 (1994) [hep-ph/9311205].

[168] L. D. McLerran and R. Venugopalan, Phys. Rev. D **49**, 2233 (1994) [hep-ph/9309289].

[169] T. Hirano and Y. Nara, Nucl. Phys. A **743**, 305 (2004) [nucl-th/0404039].

[170] H. J. Drescher and Y. Nara, Phys. Rev. C **76**, 041903 (2007) [arXiv:0707.0249 [nucl-th]].

[171] H.-J. Drescher and Y. Nara, Phys. Rev. C **75**, 034905 (2007) [nucl-th/0611017].

[172] D. Kharzeev and M. Nardi, Phys. Lett. B **507**, 121 (2001) [nucl-th/0012025].

[173] D. Kharzeev and E. Levin, Phys. Lett. B **523**, 79 (2001) [nucl-th/0108006].

[174] D. Kharzeev, E. Levin and M. Nardi, Phys. Rev. C **71**, 054903 (2005) [hep-ph/0111315].

[175] D. Kharzeev, E. Levin and M. Nardi, Nucl. Phys. A **730**, 448 (2004) [Nucl. Phys. A **743**, 329 (2004)] [hep-ph/0212316].

[176] L. V. Gribov, E. M. Levin and M. G. Ryskin, Phys. Rept. **100**, 1 (1983).

[177] J. D. Bjorken, Phys. Rev. D **27**, 140 (1983).

[178] P. Petreczky, J. Phys. G **39**, 093002 (2012) [arXiv:1203.5320 [hep-lat]].

[179] M. Cheng, N. H. Christ, S. Datta, J. van der Heide, C. Jung, F. Karsch, O. Kaczmarek and E. Laermann *et al.*, Phys. Rev. D **77**, 014511 (2008) [arXiv:0710.0354 [hep-lat]].

[180] P. Huovinen and P. Petreczky, Nucl. Phys. A **837**, 26 (2010) [arXiv:0912.2541 [hep-ph]].

[181] M. Luzum and J. Y. Ollitrault, Nucl. Phys. A **904-905**, 377c (2013) [Nucl. Phys. A **904**, 377c (2013)] [arXiv:1210.6010 [nucl-th]].

[182] H. Song, S. A. Bass, U. Heinz, T. Hirano and C. Shen, Phys. Rev. C **83**, 054910 (2011) [Phys. Rev. C **86**, 059903 (2012)] [arXiv:1101.4638 [nucl-th]].

[183] H. Niemi, G. S. Denicol, P. Huovinen, E. Molnar and D. H. Rischke, Phys. Rev. Lett. **106**, 212302 (2011) [arXiv:1101.2442 [nucl-th]].

[184] H. Niemi, G. S. Denicol, P. Huovinen, E. Molnar and D. H. Rischke, Phys. Rev. C **86**, 014909 (2012) [arXiv:1203.2452 [nucl-th]].

[185] S. Ryu, J.-F. Paquet, C. Shen, G. S. Denicol, B. Schenke, S. Jeon and C. Gale, arXiv:1502.01675 [nucl-th].

[186] A. Monnai, J. Phys. Conf. Ser. **432**, 012011 (2013) [arXiv:1301.2713 [nucl-th]].

[187] F. Cooper and G. Frye, Phys. Rev. D **10**, 186 (1974).

[188] D. Teaney, Phys. Rev. C **68**, 034913 (2003) [nucl-th/0301099].

[189] A. Monnai and T. Hirano, Phys. Rev. C **80**, 054906 (2009) [arXiv:0903.4436 [nucl-th]].

[190] H. Sorge, H. Stoecker and W. Greiner, Annals Phys. **192**, 266 (1989).

[191] H. Sorge, A. von Keitz, R. Mattiello, H. Stoecker and W. Greiner, Z. Phys. C **47**, 629 (1990).

[192] H. Sorge, L. Winckelmann, H. Stoecker and W. Greiner, Z. Phys. C **59**, 85 (1993).

[193] H. Sorge, Phys. Rev. C **52**, 3291 (1995) [nucl-th/9509007].

[194] L. A. Winckelmann, S. A. Bass, M. Bleicher, M. Brandstetter, A. Dumitru, C. Ernst, L. Gerland and J. Konopka *et al.*, Nucl. Phys. A **610**, 116C (1996) [nucl-th/9610033].

[195] S. A. Bass, M. Belkacem, M. Bleicher, M. Brandstetter, L. Bravina, C. Ernst, L. Gerland and M. Hofmann *et al.*, Prog. Part. Nucl. Phys. **41**, 255 (1998) [Prog. Part. Nucl. Phys. **41**, 225 (1998)] [nucl-th/9803035].

[196] M. Bleicher, E. Zabrodin, C. Spieles, S. A. Bass, C. Ernst, S. Soff, L. Bravina and M. Belkacem *et al.*, J. Phys. G **25**, 1859 (1999) [hep-ph/9909407].

[197] Y. Nara, N. Otuka, A. Ohnishi, K. Niita and S. Chiba, Phys. Rev. C **61**, 024901 (2000) [nucl-th/9904059].

[198] M. Isse, A. Ohnishi, N. Otuka, P. K. Sahu and Y. Nara, Phys. Rev. C **72**, 064908 (2005) [nucl-th/0502058].

[199] E. Andersen, F. Antinori, N. Armenise, H. Bakke, J. Ban, D. Barberis, H. Beker and W. Beusch *et al.*, Phys. Lett. B **433**, 209 (1998).

[200] H. Appelshauser *et al.* [NA49 Collaboration], Phys. Lett. B **444**, 523 (1998) [nucl-ex/9810005].

[201] M. Nasim [STAR Collaboration], Nucl. Phys. A **904-905**, 413c (2013) [Nucl. Phys. A **904**, 413c (2013)] [arXiv:1210.5045 [nucl-ex]].

[202] E. V. Shuryak, Nucl. Phys. A **750**, 64 (2005) [hep-ph/0405066].

[203] L. D. Landau and E. M. Lifshitz, *Fluid Mechanics*, (Pergamon Press, New York, 1959), Secs. 133-136.

[204] C. Segre, Memorie della R. Accademia dei Lincei **3a** 127 (1884).

[205] G. S. Hall, Diff. Geom. **12**, 53 (1984).

[206] J. Santos, M. J. Reboucas, and A. F. F. Teixeira, Gen. Rel. Grav. **27** 989-999 (1995)

[207] C. Eckart, Phys. Rev. **58**, 919 (1940).

[208] A. Kandus and C. G. Tsagas, Mon. Not. Roy. Astron. Soc. **385**, 883 (2008) [arXiv:0711.3573 [astro-ph]].

[209] D. H. Rischke, Lect. Notes Phys. **516**, 21 (1999) [nucl-th/9809044].

[210] T. Tsumura, T. Kunihiro and K. Ohnishi, Phys. Lett. B **646**, 134 (2007).

[211] K. Tsumura and T. Kunihiro, Phys. Lett. B **690**, 255 (2010) [arXiv:0906.0079 [hep-ph]].

[212] A. Monnai and T. Hirano, Nucl. Phys. A **847**, 283 (2010) [arXiv:1003.3087 [nucl-th]].

[213] T. Osada, Phys. Rev. C **85**, 014906 (2012) [arXiv:1111.1276 [nucl-th]].

[214] T. Osada, Eur. Phys. J. A **48**, 167 (2012) [arXiv:1204.1124 [nucl-th]].

[215] I. Prigogine, "Etude thermodynamique des phnomnes irrversibles," Desoer, Liége, (1947).

[216] W. A. Hiscock and L. Lindblom, Annals Phys. **151**, 466 (1983).

[217] W. A. Hiscock and L. Lindblom, Phys. Rev. D **31**, 725 (1985).

[218] W. A. Hiscock and L. Lindblom, Phys. Rev. D **35**, 3723 (1987).

[219] C. R. Cattaneo Comptes Rendus **247**, 431 (1958).

[220] P. Vernotte, Comptes Rendus **246**, 3154 (1958).

[221] M. Chester, Phys. Rev. **131**, 2003 (1963).

[222] J. Masoliver, J. M. Porrà, and G. H. Weiss, Phys. Rev. E, **48**, 939 (1993)

[223] T. Prüstel, M. Meier-Schellersheim, arXiv:1301.7139 [math-th].

[224] W. Israel, Annals Phys. **100**, 310 (1976).

[225] W. Israel and J. M. Stewart, Annals Phys. **118**, 341 (1979).

[226] I. Muller, Z. Phys. **198**, 329 (1967).

[227] D. Jou, J. Casas Vazquez and G. Lebon G, Rep. Prog. Phys **51**, 1105-1179 (1988).

[228] D. Jou, G. Leblon and J. Casas Vasquez, *Extended thermodynamics* (Springer, New York, 1993); *Extended thermodynamics* (2nd edition, Springer, Heidelberg, 1996, second edition).

[229] I. Müller, T. Ruggeri, *Rational Extended Thermodynamics* (Springer, New York, 1998, second edition)

[230] D. Jou, J. Casas Vazquez and G. Lebon G, Rep. Prog. Phys. **62**, 1035-1142 (1999).

[231] K. Murase and T. Hirano, arXiv:1304.3243 [nucl-th].

[232] L. D. Landau and E. M. Lifshitz, *Fluid Mechanics*, (Pergamon Press, New York, 1959), Sec.

[233] E. Calzetta, Class. Quant. Grav. **15**, 653 (1998) [gr-qc/9708048].

[234] S. Jennings, J. Aerosol Sci. **19**, 159 (1988).

[235] J. Kapusta, B. Muller and M. Stephanov, Acta Phys. Polon. B **43**, 781 (2012) [arXiv:1201.3405 [nucl-th]].

[236] J. I. Kapusta, B. Mueller and M. Stephanov, Nucl. Phys. A **904-905**, 499c (2013) [arXiv:1211.3370 [nucl-th]].

[237] J. I. Kapusta and J. M. Torres-Rincon, Nucl. Phys. A **904-905**, 887c (2013) [arXiv:1306.3932 [nucl-th]].

[238] C. Young, J. I. Kapusta, C. Gale, S. Jeon and B. Schenke, Phys. Rev. C **91**, no. 4, 044901 (2015) [arXiv:1407.1077 [nucl-th]].

[239] G. S. Denicol, T. Kodama, T. Koide and P. Mota, Braz. J. Phys. **37**, 776 (2007).

[240] D. N. Zubarev, *Nonequilibrium Statistical Thermodynamics*, (Plenum, New York, 1974).

[241] A. Hosoya, M. a. Sakagami and M. Takao, Annals Phys. **154**, 229 (1984).

[242] H. Mori, Phys. Rev. **112**, 1829 (1958).

[243] H. Mori, Phys. Rev. **115**, 298 (1959).

[244] G. S. Denicol, J. Noronha, H. Niemi and D. H. Rischke, Phys. Rev. D **83**, 074019 (2011) [arXiv:1102.4780 [hep-th]].

[245] G. S. Denicol, H. Niemi, J. Noronha and D. H. Rischke, arXiv:1103.2476 [hep-th].

[246] Y. Minami and Y. Hidaka, arXiv:1401.0006 [hep-ph].

[247] H. Petersen, C. Coleman-Smith, S. A. Bass and R. Wolpert, J. Phys. G **38**, 045102 (2011) [arXiv:1012.4629 [nucl-th]].

[248] T. Kodama and T. Koide, J. Phys. Conf. Ser. **509**, 012016 (2014) [arXiv:1310.3872 [nucl-th]].

[249] E. Wong and M. Zakai, Ann. Math. Statist., **36**, 1560-1564 (1965)

[250] E. Wong and M. Zakai, Int. J. Eng. Sci., **3**, 213-229 (1965)

[251] E. Wong and M. Zakai, Proceedings of the Third International Conference IFAC, London, 3B.1-3B.8 (1966) .

[252] Martin Hairer, Étienne Pardoux, arXiv:1409.3138 [math.PR] (2014).

[253] J. L. Albacete, A. Dumitru and Y. Nara, J. Phys. Conf. Ser. **316**, 012011 (2011) [arXiv:1106.0978 [nucl-th]].

[254] T. Hirano and Y. Nara, PTEP **2012**, 01A203 (2012) [arXiv:1203.4418 [nucl-th]].

[255] P. Colella and P. R. Woodward, J. Comput. Phys. **54**, 174 (1984).

[256] A. Harten, P.D. Lax and B. van Leer, SIAM Rev. **25**, 35-61, (1983).

[257] B. Einfeldt, SIAM J. Numer. Anal. **25**, 294-318, (1988).

[258] S. Afanasiev *et al.* [PHENIX Collaboration], Phys. Rev. C **80**, 024909 (2009) [arXiv:0905.1070 [nucl-ex]].